Geology, Geochemistry and Geochronology of the mid-Miocene, Low-Sulfidation Epithermal Gold-Silver Ores on War Eagle Mountain, Silver City District, Idaho.

by

Collins O. Aseto

A thesis submitted to the Graduate Faculty of
Auburn University
in partial fulfillment of the
requirements for the Degree of
Master of Science

Auburn, Alabama
August 4, 2012

Keywords: Epithermal, Gold-Silver, mid-Miocene, Silver City district, War Eagle Mountain, Yellowstone hotspot

Approved by

James A. Saunders, Chair, Professor Geology and Geography
Willis E. Hames, Professor Geology and Geography
Luke Marzen, Professor Geology and Geography

Abstract

Located in southwest Idaho' s Silver City district, War Eagle Mountain's epithermal Au-Ag veins are structurally controlled arrays that are hosted by a Cretaceous granitoid. Taking into consideration similar deposits at Silver City hosted by mid-Miocene volcanics at DeLamar and Florida Mountains, this study presents a genetic model for ores in the district. Ore deposition occurred from solutions <250°C and were of low salinities (0.5-1wt % NaCl equivalent). Gold mineralization occurs mainly in the form of electrum of approximately 60% Au. Silver occurs in naumannite, aguilarite, arcanthite and electrum, and at least two previously undocumented Ag-Se-S phases. Pb isotope studies demonstrate that primitive basalts are perhaps the primary source of gold, with more evolved variants only being modified by minor crustal inputs. New $^{40}Ar/^{39}Ar$ data for tecto-magmatism and mineralization that cluster around (16.7–15.1 Ma) provides definitive evidence of the connection between the initial emergence of the Yellowstone hotspot and epithermal mineralization. This conclusion has implications for understanding (and exploring) similar epithermal systems in the northern Great Basin.

Acknowledgments

This work was supported by a grant from the National Science Foundation. I would like to thank my supervisors for taking a chance on me and thereby facilitating the realization of a dream. I appreciate Dr. Emilly Obuya, my significant other, for offering moral support, invaluable insights on her research on precious metal nanoparticles, and making this whole study worthwhile. I extend my gratitude to Dr. Paul Spry of Iowa State University, for introducing me to the economic geology program at Auburn, and Dr. Ashraf Uddin, Dr. Lee Min Kuo, and Dr. Jefferson Chaumba for invaluable guidance offered during the course of study at the institution. Discussions with Dr. George Kamenov of the University of Florida provided useful suggestions on Pb Isotope analysis and are gratefully acknowledged. Additionally, laser ablation analyses carried out on fluid inclusions by Dr. Alfred Hofstra of the USGS are also highly appreciated. I thank Catherine Preister for the long man-hours sacrificed creating this works' geodatabase; a vital resource tool that could be used for both academic and commercial research interests in future. Constructive reviews by Mitchell Moore that were especially helpful are also highly appreciated. I cannot forget to thank Virginia Guillerman, Tennessee, and the owners and staff at the Silver City Hotel who made me feel at home in what is arguably the first visit by a Kenyan in that part of the world. Special mention goes to Mary and Bob O'Malley who accommodated me in their cozy cottage during my entire stay in the district. I recognize Derick Unger for providing an extensive tour at Newmont's Ken Snyder mine at Midas; Dr. Ken Snyder himself for providing material and professional support that directed parts of this study, and Dr. Billor and John Simms

of Auburn University, as well as Chris Fleisher of the University of Georgia, for transcribing “laboratory-equipment speak.” I appreciate the encouragement I received from my siblings Dr. Barnard Aseto, Caroline Aseto, and Beatrice Aseto, my close friend Renson Kisambo, as well as my former colleagues at Anglo American plc i.e. Solomon Cherogony, Roger Tyler, Crispus Sang, Kennedy Kibiy, and especially Dave Underwood who to date remains my role model. Equally, I would like to thank my immediate former Country Manger at Lonmin plc, Phillipa Hutchinson, for fuelling my desire to further my education. Miscellaneous contributions by Scott Carruthers of Base Titanium Ltd, Dr. Cedric Simonet of Akili Minerals Services Ltd, Dr. Jeffery Hedenquist, Dr. Richard Goldfarb of the USGS, Dr. Joao Beckel of Zamin Resources Ltd, Arnand van Heeden of Goldfields Exploration, Rue Chitwood, Moses Igamba, Simon Gathiaka, Jack Ogutu, and Justus Nyamweya are also gratefully acknowledged. On a lighter note I thank Vern for helping me appreciate the limits of a 900cc quad motorbike both on the horizontal and vertical plane (literally), as well as providing a guided tour of the Free Mason Hall in Silver City that is under his care, in addition to his collection of assorted armaments and his customized “wild west” saloon located in his abode. I am also grateful to Alex Steiner for introducing me to the rudiments of professional cliff hanging/rock climbing. Lastly, I would like to thank God, and my parents, Major (Rtd) J.H.D Aseto (Order of the Golden Warrior; OGW), and Mrs. T.F. Aseto for the ‘warrior-blood’ they bestowed unto me.

Table of Contents

List of Tables

List of Illustrations

1. INTRODUCTION

Epithermal Precious Metal Systems

Epithermal ores were originally defined and named by Waldermar Lindgren (Lindgren, 1933) to represent shallow low temperature hydrothermal ores of any origin. Current usage of the term implies shallow Au-Ag (Hg) ores occurring in veins, breccias, pore spaces, and stock-works which are temporally and spatially associated with coeval volcanic rocks (Sawkins, 1979; Taylor, 2007).

Epithermal ores are important on a worldwide basis, having contributed an estimated 16% of Ag and 6% of Au produced to date (Singer, 1995). Additionally they have played an important historical role in the Americas' past. For example the ascension of the Spanish empire was largely fueled by proceeds derived from epithermal ores mined in México, Peru, and Bolivia (Simmons et al., 2005). These ores were easily extracted in large part due to their shallow depths and amenability to mining (Abbot and Wolfe, 2003). Furthermore, in the mid 1800s to 1900s the demography of the western United States was largely shaped by the gold-silver rushes to the western regions to exploit epithermal deposits and their associated placers (Simmons et al., 2005). This led to early statehood for Nevada (October 31, 1864) as did gold production for California (September 9, 1850). Lastly, during the American Civil War (1861-1865) the Union side used proceeds from the Comstock Lode (Nevada) to finance the war effort against the Confederate Army which contributed to their victory (John, 2001).

Lindgren (1933) proposed that epithermal deposits formed at low temperatures (50°- 200°C) and pressures (< 100 atmospheres). Advances in ore deposit research techniques such as fluid inclusion studies have shown that epithermal ore formation temperatures range from 150°C - 300°C (Sawkins et al., 1979; Buchanan, 1981;

Simmons et al., 2005) with ore mineral deposition typically occurring at depths ranging from 50 m to 1500 m below the water table (Simmons et al., 2005; Taylor, 2007). These shallow depths make epithermal deposits highly susceptible to erosion; hence they are usually preserved in Cenozoic formations (Taylor, 2007). However, examples of deposits of even greater antiquity are known where their host rocks have been well preserved such as areas of high sulfidation Au deposits of Neoproterozoic age in the Burin Peninsula, Newfoundland, Canada (O'Brien et al., 1999), the Cambrian Carolina Slate Belt (Worthington and Kiff, 1970), and the low sulfidation Carboniferous epithermal ore shoot at Pajingo, Queensland, Australia (Bobis et al., 1995).

Epithermal deposits account for significant metal resources worldwide particularly North America, Andes, Japan, southeast Asia, southeast Pacific, Russia, Turkey, Romania, Spain, Central America and México (Fig. 1). The spatial association of these deposits with the "Pacific Ring of Fire" highlights their inherent link to plate tectonics and its associated volcanism (Taylor, 2007).

Epithermal deposits are epigenetic ores even though they may have contemporaneous ages to their host rocks in active volcanic terranes (Taylor, 2007). The deposits can be classified according to the magmatic and hydrothermal events that formed them (Sillitoe and Hedenquist, 2003). Sillitoe and Hedinquist (2003) classified them using two end members: high and low sulfidation, as a function of their "sulfidation" states, ore minerals and gangue-mineral assemblage. High sulfidation epithermal deposits are characterized by extreme acid alteration that produces such minerals as quartz (vuggy silica rock), alunite, jarosite, clays, and pyrophyllite, and typically contain gold and enargite as ore minerals. In contrast, low sulfidation epithermal deposits contain quartz, sericite, calcite, adularia and illite and typical ore minerals electrum, arcanthite, selenides and tellurides (Sillitoe and Hedenquist, 2003). Low sulfidation

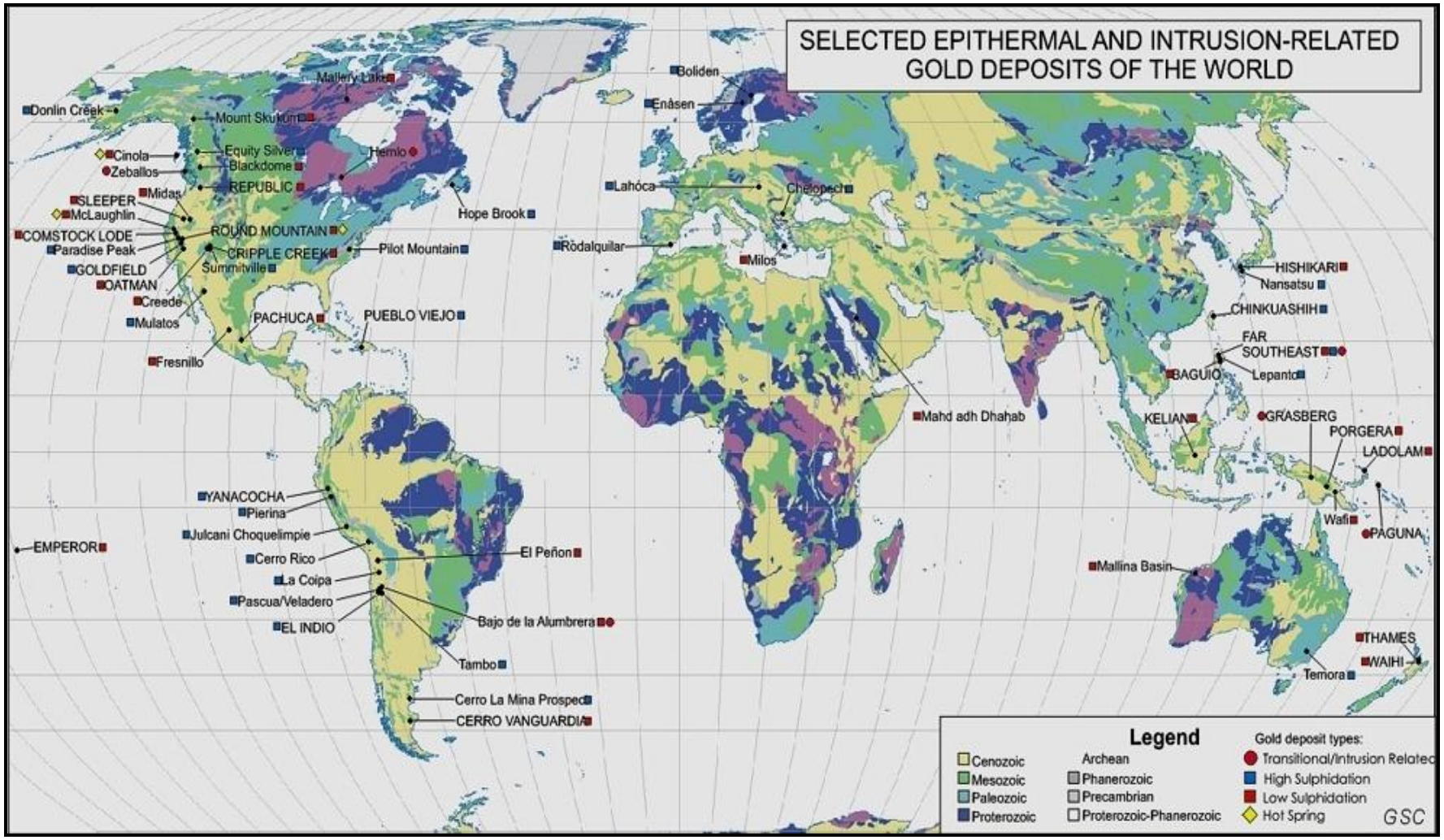

FIG. 1. Global distribution of epithermal and intrusion-related Au deposits. Deposits labeled in capitalized letters denote giant or bonanza deposits (from Sillitoe, 1992). **Other References**: Arancibia et al., 2006; Bethke et al., 2005; Carman, 2003; Deyell et al., 2005; Dubé et al., 1998; Fifarek and Rye, 2005; Goldfarb et al., 2004;Gosselin and Dub , 2005a,b; Hedenquist et al., 2000; Huston et al., 2002; Klein and Criss, 1988; Naden et al., 2005;Panteleyev, 1996a,b,c, 2005a,b; Poulsen, 1996, 2000; Sillitoe, 1992, 1997; Taylor, 1996, 2007; Turner et al., 2003.

epithermal deposits are formed from circum-neutral pH solutions, low salinities (Hedenquist and Lowenstein, 1994), at distal locations (Fig. 2) from their probable magmatic source (Sillitoe, 1989), and are typically found in extensional geotectonic regimes. Nearly 60% of the world's bonanza veins are associated with bimodal (basalt-rhyolite) volcanic suites (Sillitoe and Hedenquist, 2003). Conversely, high sulfidation deposits are typically more proximal to their probable magmatic source (Fig. 2). They occur in accretionary prisms and calc-alkaline andesitic- dacitic arcs, on subduction or convergent plate boundaries with near neutral stresses or mild extensional regimes

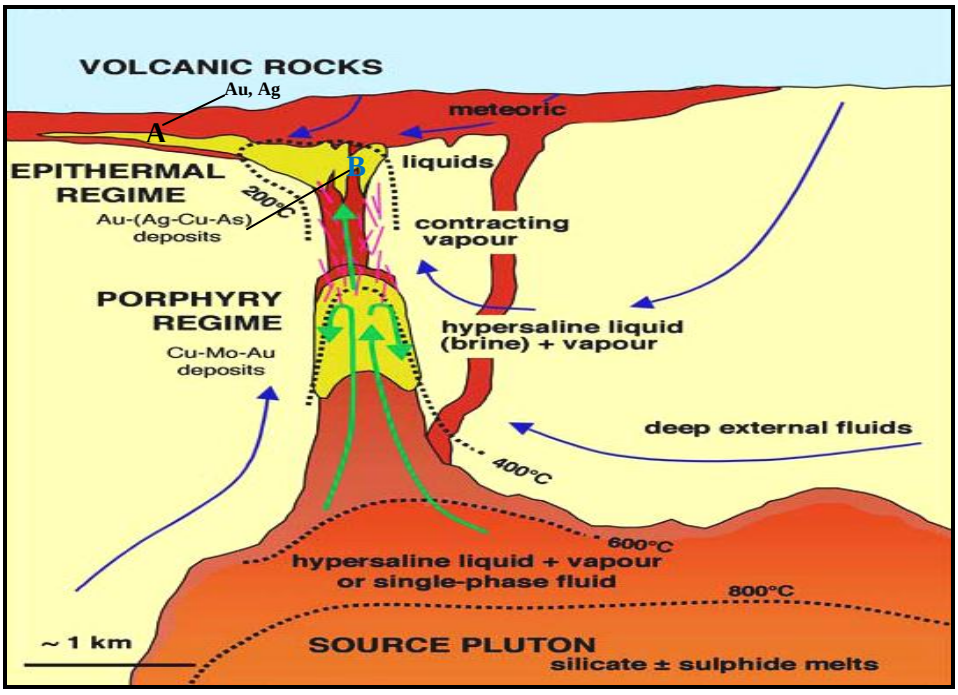

FIG. 2. Illustration of the porphyry-epithermal transition. "A" denotes a possible low-sulfidation emplacement position, while "B" denotes a possible high-sulfidation locale, modified after Heinrich (2005).

(Sillitoe and Hedenquist, 2003). Submarine equivalents of epithermal deposits have also been proposed (Worthington and Kiff, 1970; Sillitoe et al., 1996; Sillitoe and Hedenquist, 2003; Taylor, 2007). For example, the generally underexplored Carolina Slate Belt in southeastern United States displays typical high sulfidation alteration

assemblages consisting of kyanite, topaz, pyrophyllite, etc, and gold. This mineralization has been proposed to be submarine in nature (Worthington and Kiff, 1970; Klein and Criss, 1988; Feiss et al., 1993). The belt is currently the locus of a renewed low sulfidation gold exploration effort by Romaco Resources that has delineated 2 million ounces of gold at the Haile Mine.

Historical Background of the Silver City District, Idaho

The discovery of placer gold on May 18th 1863 in Jordan Creek, 8 km southwest of Silver City, Idaho by a team of 29 prospectors led by Michael Jordan sparked a search for its bedrock source (Wells, 1963). By tracing vein quartz float uphill from the placer workings, the “old timers” zeroed in on two major lodes on War Eagle Mountain; the Orofino vein, on August 15th 1863, and later the Poorman vein, on August 5th 1865 (Yeager and Ikona, 1984). More prospecting in subsequent years resulted in further lode discoveries within the district, and by 1866 most of the mines in War Eagle Mountain were fully operational, and had 12 mills that comprised a total of 132 stamps (Piper and Laney, 1926).

It is reported that in the first six days of operation, the Poorman vein lode yielded $500,000 in bullion from near surface supergene enriched zones (Wells, 1963). (Note: Dollar figures quoted in this section are unadjusted for inflation and reflect Au values of $20/ oz. and $1.24- $1.34/ oz. for Ag at the time, and unfortunately gold and silver production records were combined). More conservative, yet significant, production is reported for the Orofino lode, with an output of $122,000 for 1867 (Yeager and Ikona, 1984). The total production between 1863 and 1876 for the lodes on War Eagle Mountain is estimated to have been about $12,500,000 (Lindgren, 1900; Piper and Laney, 1926; Statham, 2003). However, due to lax accounting practices used at the time a significant part of the precious metal production may be unaccounted for as in many

19th century mining districts of the western United States.

The Bank of California and the San Francisco Stock Exchange Board crash of 1876 coincided with a downward spiral in precious metal production from high-grade veins in War Eagle Mountain. This marked the beginning of the end of the bonanza production episode at this location (Bennet and Galbraith, 1975; Yeager and Ikona, 1984; Cupp, 1989; Statham, 2003). The lack of a viable financial system depressed mining investment capital, and resulted in a lull in precious-metal production in the years 1876 to 1889; although small-scale and shallow excavation continued at DeLamar, and Florida Mountains, which accounted for $3,500,000 in bullion during the hiatus (Statham, 2003).

The second-most significant early production period covers the years 1889 to 1914 (Asher, 1968; Bennet and Galbraith, 1975; Statham, 2003). Unlike in the preceding mining episode, underground mining techniques became essential. This mining period produced arguably the highest bullion production hitherto known for the district, with a total of $23,000,000 (Piper and Laney, 1926), mainly from the richer deep-seated ores from contiguous mines on DeLamar and Florida Mountains (Bonnichsen, 1983). Similarly, at War Eagle Mountain an attempt to elevate production levels at the Orofino vein was done through the exploration of deep-seated ores. This commenced in 1899 (Piper and Laney, 1926; Asher, 1968; Yeager and Ikona, 1986) when The War Eagle Consolidated Company drove a ≈1.81 Km cross-cut adit (Sinker Tunnel) collared at an elevation of 1640 m and northeast (041°) of the Orofino's highest outcrop at the Ida Elmore Shaft (Fig. 3). The adit's portal was 590 m below the shaft's entrance, and 244 m below the Orofino's lowest workings (Piper and Laney, 1926; Asher, 1968). When the Orofino-Golden Chariot vein was eventually encountered in 1902, attempts in subsequent years to drive a raise to bring the vein to production failed because the shaft

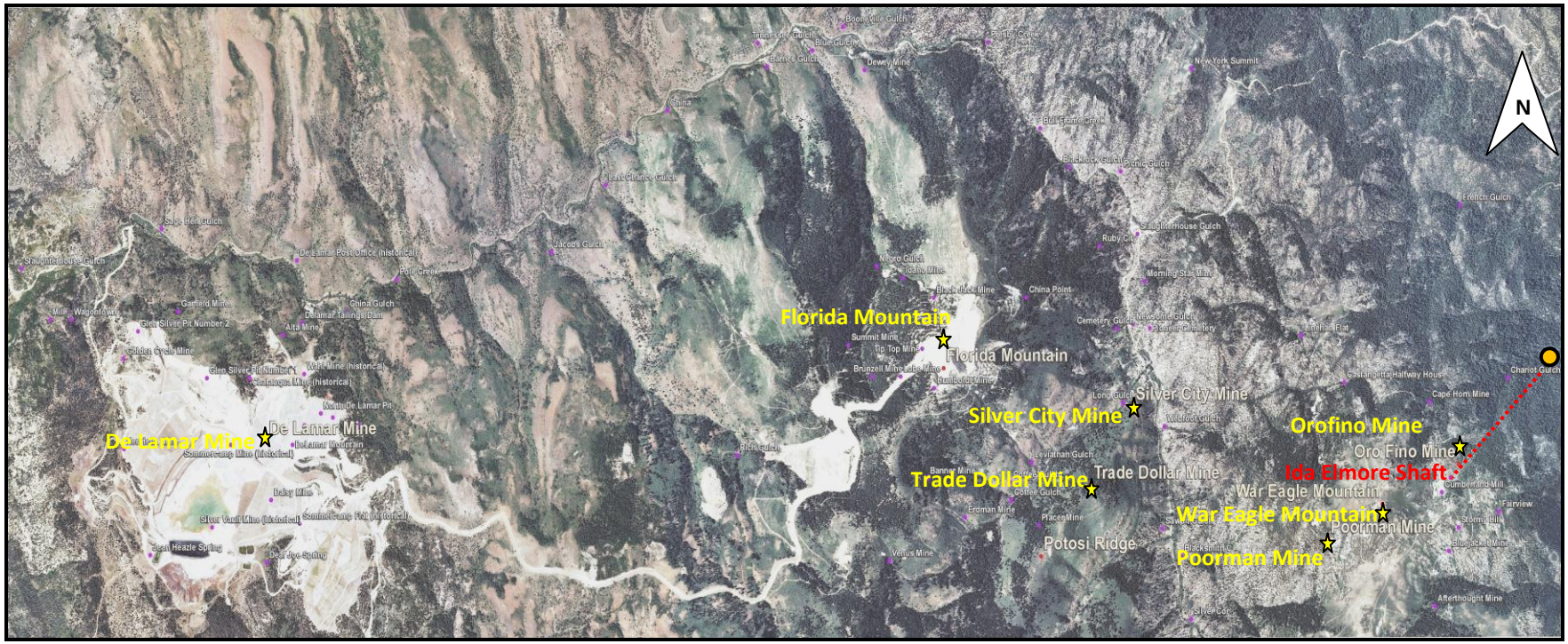

FIG. 3. Satellite image (natural color) of the Silver City district as it appears today, showing locations of mines of the 3 historical mining periods. The district has an east to west strike length of approximately 13km. The red dashed line (on the right hand side of the image) denotes the approximate location of the Sinker tunnel, with the yellow bullet indicating the approximate location of the tunnel's collar. Image modified from United States Department of Agriculture Natural Resources Conservation Service, 2011, Geospatial Data Gateway. http://datagateway.nrcs.usda.gov/

above and the raise below had been poorly surveyed, making it difficult to link the two.With the threat of flooding and/or collapse becoming increasingly imminent the State Mine Inspector shut down the mine in 1905 despite the raise having been driven to a height of 190 m (Piper and Laney, 1926).

Thus the Silver City district was a significant precious-metal producer in the 1860's, 1870's and early 1900's. However, it was largely overshadowed by contemporaneous production from perhaps the world's greatest silver district: the Comstock Lode of Virginia City, Nevada (Fig.4) discovered in 1859, which produced 7,812,500 oz. of gold and 187,500,500 oz. of silver (Bonham and Garside, 1969). Similarly, discovery of the huge silver deposits at Tonopah, Nevada (Fig.4) in 1900

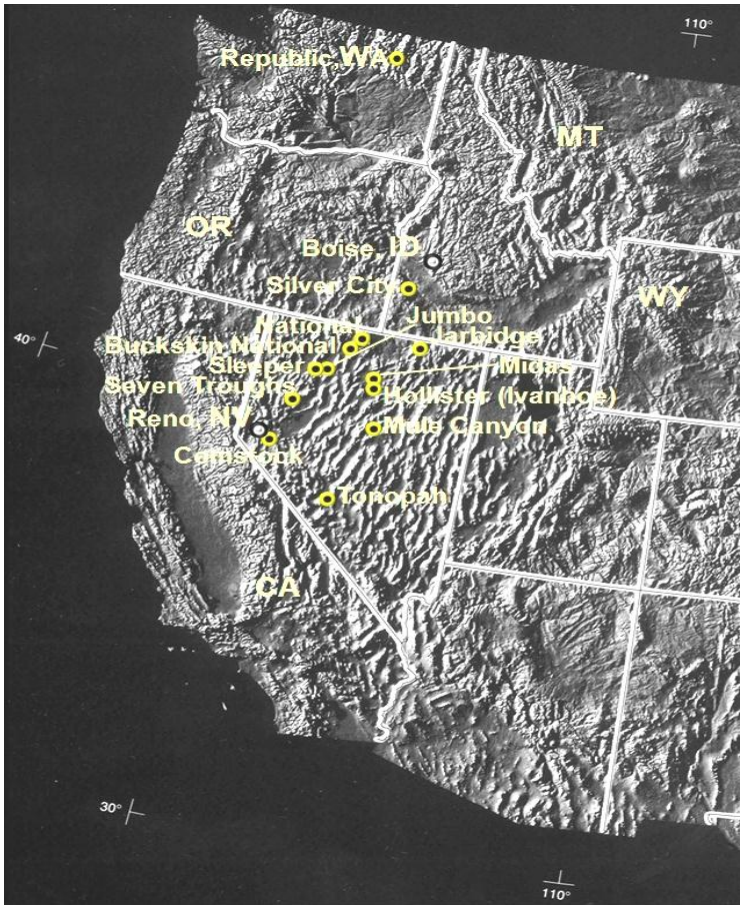

FIG. 4. Shaded relief map showing some epithermal deposit locations in the conterminous western United States, modified after Thelin et al. (1991).

(Tingley, 1998) also overshadowed the significance of the early 20th century precious-metal production in the Silver City district. Tonopah produced 1,861,200 oz. of gold and 174,152,628 oz. of silver between 1901 and 1935 (Bonham and Garside, 1979).

Although Silver City was eclipsed by production in the Silver State (Nevada) to the south, the Silver City district played a large role in the early history of Idaho development prior to railroad connection to Boise on September 1st 1887 (Hart, 2010) and Idaho statehood on July 3rd 1890. Further, the district has a rich history of its own that includes Native American wars, massacres of miners by Native Americans and underground (and above ground) wars between competing mining companies, whose mining claims overlapped onto bonanza ore (Statham, 2003). These examples of violent confrontations often occurred due to disputes that arose owing to fractious and unregulated mining practices used in the district at the time (Asher, 1968).

The third most significant mining period was the most modern, utilized the latest mining and extraction technologies, while adhering to newly enforced environmental regulations passed in the United States. The operations commenced in 1977 and lasted for 21 years. This mining episode coincided with the late 1970's worldwide development of modern, large-scale, open-cast and heap-leach operations for the first time in what were hitherto considered sub-economic mines. Such operations were buoyed by favorable precious-metal prices and advances in extraction techniques (Simmons et al., 2005, Saunders, pers. commun., 2010). In the Silver City district, this new "mining boom" era was marked by the development of world-class low grade, bulk-minable epithermal precious-metal mining projects at the summits of DeLamar and Florida Mountains (Fig.3). The mine operations at DeLamar were the first of their kind to extract silver from low grade bulk minable ore, using conventional open pit and heap-leach methods (Halsor et al., 1988). The initial 10 years of production yielded over 17 million ounces of

silver, and 230,000 ounces of gold (Halsor et al., 1988) The total output during the life of the mine is pegged at 750,000 ounces of gold and 47.5 million ounces of silver (Gillerman and Mitchell, 2005), which amounts approximately to $1,114,650,000 for gold and $1,613,575,000 for silver (May, 2011 precious-metal prices).

Kinross Gold Corporation, the last mining operator at the site, suspended operations in 1998, and started remediation of the property. Kinross Gold Corporation remediated seven million cubic meters of water stored in the mine tailings, and almost 170 hectares of exposed bedrock that generated acid rock drainage. In October 2009, Kinross was presented with the National Hardrock Mineral Environmental Award for environmental reclamation excellence, by the United States Bureau of Land Management (BLM news release, 2009) for its operations at DeLamar. As of 2010 mine reclamation at DeLamar and Florida mountains was still ongoing and is expected to be completed in 2012. Nevertheless, water sanitation and monitoring will continue for years beyond this date.

Objective of Study

Although Silver City district has been dubbed the “birthplace” of epithermal ores, (Saunders, 2010), little detailed scientific work has been done at War Eagle Mountain since the mid 1920s (Piper and Laney, 1926). Thus it is a very fertile area for applying contemporary research techniques to a relatively unstudied “world-class” epithermal district.

Epithermal deposits are typically hosted by coeval volcanic rocks (Sawkins et al., 1979, Sillitoe and Hedenquist, 2003). However, the mid-Miocene ores at Silver City district are hosted by both a Cretaceous granitoid at War Eagle Mountain, and mid-Miocene bimodal volcanics at DeLamar and Florida Mountains (Piper and Laney, 1926; Bonnichsen, 1983). The veins exposed on War Eagle Mountain contain coarse-grained

gangue minerals, well suited to modern research techniques not previously applied in the district such as fluid inclusion microthermometric analyses, SEM-EDAX, and qualitative microprobe analyses. Given the similarities between ores hosted by Cretaceous granitiods at War Eagle Mountain and ores hosted by the mid-Miocene bimodal basalt-rhyolite volcanic package elsewhere in the district (Halsor et al., 1988), this research is perhaps a test of the hypothesis that epithermal precious-metal ores are derived from a common/primitive mafic parental magma (Kamenov et al., 2007; Hames et al., 2009) as opposed to metals being leached from country rocks. Additionally this study investigates another recent hypothesis that the principal gangue minerals in veins derive their chemical constituents from associated country rocks even though ore metals are derived from a deeper magmatic source (Saunders et al., 2008). The proximity of contrasting mineralized host rock units in the district within an east - to - west strike length measuring not more than 14km provides an ideal field laboratory to study how host rocks influence ore and gangue mineral formation.

Petrographic analyses are used here to determine vein textures, vein mineralogy and mineral paragenesis of ore and gangue constituents. Fluid inclusion microthermometric studies help to deduce physical variables such as pressures, temperatures, and salinities that existed during vein formation. SEM-EDAX , microprobe analyses, and ICP-MS geochemical analyses complement each other, and assist in probing major element vein geochemistry, mainly on War Eagle Mountain with reconnaissance studies done elsewhere in the district. Consequently, host-rock influences on different vein mineralization style can be evaluated. Additionally, new $^{40}Ar/^{39}Ar$ age dating of the Au-Ag mineralization generated in this study enhances the understanding of the genesis of ores in the district. Further, by adding the Silver City district to the numerous well-documented mid-Miocene deposits and districts situated

further south in Nevada, the study seeks to evaluate the hypothesis that the initial emergence of the Yellowstone Hotspot acted as a tecto-magmatic trigger that facilitated the formation of low sulfidation epithermal mineralization (Saunders et al., 1996; John, 2001; Bruseke and Hart, 2008; Saunders et al., 2008).

In summary it is hoped that the findings of this thesis research will add significant new data on the geology of an important but relatively unstudied epithermal Au-Ag district in the northern Great Basin. This research will potentially test the recent hypothesis concerning the origin of these ores and expand exploration opportunities for similar deposits that are unknown or underexplored.

Previous work

A summary of previous research done in the district is presented below and subsequently followed by a brief review of major findings with an emphasis given to interpretations that are pertinent to this study. Initial mapping, chronologic and geochemical studies in the district were carried out by Waldemar Lindgren (Lindgren, 1898; Lindgren, 1900; Lindgren and Drake; 1904). Piper and Laney (1926) followed up their work in the area in an effort to rejuvenate the then dwindling fortunes of the mining district. However, the inaccessibility of mine workings forced Piper and Laney to draw largely from unpublished mining company reports, interviews of former mine workers and Lindgren's earlier research. Later publications by Asher (1968), Panze (1972, 1975), Bennet and Galbraith (1975), Ekren et al. (1981, 1982), Bonnichsen (1983), Bonnichsen and Godchaux (2006) consist of detailed geological mapping and descriptions of rock units. A comprehensive outline of the epithermal deposits at DeLamar was prepared by Halsor et al. (1988) and Cupp (1989). Other works include unpublished literature that resulted from precious-metal exploration efforts in the 1980's

and 1990's. An example of such work was a bulk geochemical sampling program that targeted the mine dumps (spoil) on War Eagle Mountain that was carried out in 1984 by Pamicon Development Ltd for War Eagle Resources Ltd, to test the viability of extracting precious-metals from mine tailings. This was done as part of a multifaceted approach to a renewed exploration effort in the vicinity of the War Eagle Mountain that included underground mapping, rock channel sampling, and a soil sampling survey (Yeager and Ikona, 1984, 1986; Peterson, 1991). Bulk spoil geochemical sampling was carried out on most of the major dumps and aimed to evaluate their grade and tonnage (Yeager and Ikona, 1986). Internal company reports that were the outcome of this and similar campaigns in the district include Yeager and Ikona (1984, 1986), Cupp (1985), Peterson (1991), Marek (1991) among others. The most recent work at War Eagle Mountains included reconnaissance, geochronological, and geochemical work from 2 locations on the Orofino vein that was carried out by Unger (2008) as part of a study that encompassed 4 other epithermal deposits in the larger northern Great Basin. Unger (2008) provided ten single crystal $^{40}Ar/^{39}Ar$ spectrum ages for adularia from two locations on the Orofino vein on War Eagle Mountain. The age dates derived from that study were a preferred age of 16.31 ± 0.04 Ma for one sample; with the second producing an age of 15.61 ± 0.10 Ma.

General Geology of Ores: The Silver City district consists of a 14 km by 3.5 km mineralization continuum that encompasses from east to west: the deposits on War Eagle, Florida, and DeLamar mountains. Lindgren (1900), Piper and Laney (1926) and Halsor et al. (1988), presented some details on district-wide ores (veins) and their findings are summarized below.

War Eagle Mountain: Two principal bonanza veins (Fig. 5) occur on War Eagle Mountain (Lindgren, 1900; Piper and Laney, 1926) which are the subject of this

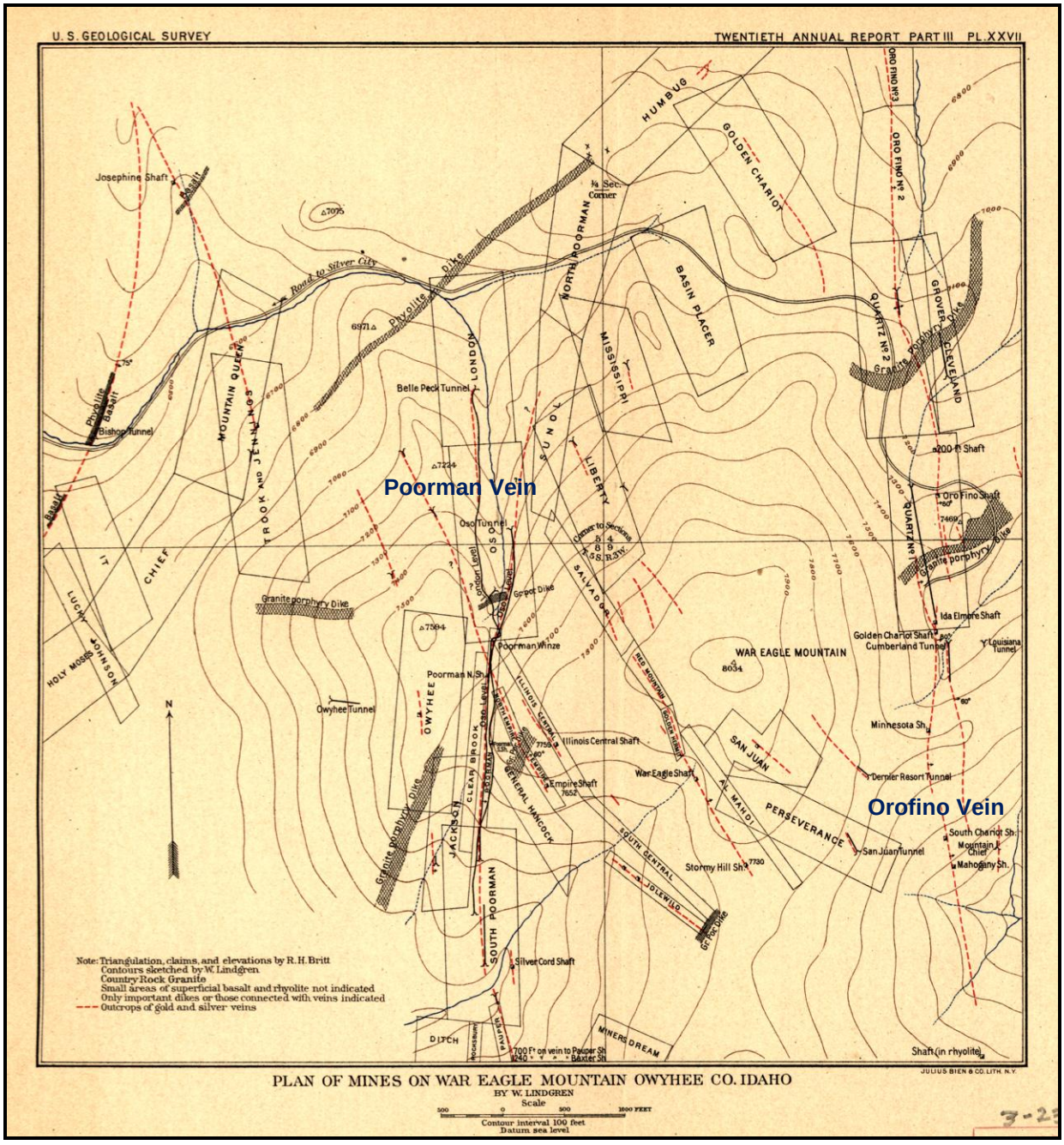

Fig. 5. Map illustrating the major veins on War Eagle Mountain, denoted as red dashed lines, after Lindgren (1900).

research. The Orofino vein is ≈800 m due east of the Poorman and Central vein systems. They are both hosted in the Cretaceous biotite muscovite granodiorite. The Orofino has an average strike of 004°/80°, an intermittent strike length of 2.4km, and an average width of 1 m (Piper and Laney, 1926). Piper and Laney (1926) describe the vein as cemented breccias with cellular or massive quartz as the cementing matrix (Fig. 6). The depth of supergene enrichment that produced the richest ore is estimated to have been between 76 m to 100 m (Asher, 1968). The vein was intersected by the Sinker tunnel 762 m below surface (Piper and Laney, 1926). Piper and Laney (1926) describe

FIG. 6. Float material from the Orofino vein consisting of cemented breccia with cellular and massive quartz as the cementing matrix.

the Poorman vein system as a silicified shear zone. The “main vein” strikes 358° to 004°and dips about vertical. It was developed to about 290 m at its deepest point from the surface and measures approximately 1.6 km long with vein widths that range from a few centimeters to 1.3 m wide (Piper and Laney, 1926). The north to south oriented

"main vein set" is juxtaposed onto an approximate 1km long northwest to southeast trending subset (Central Vein System) that cross cuts the former near the Poorman North Shaft (Fig. 5). The principle precious ore minerals for both vein systems at War Eagle Mountain include arcanthite (Ag_2S), cerargyrite (AgCl), electrum (AuAg), native silver (Ag), naumannnite (Ag_2Se), owyheeite ($Ag_3Pb_{10}Sb_{11}S_{28}$), polybasite $[(Ag,Cu)_6(Sb,As)_2S_7][\ Ag_9CuS_4]$, proustite ($Ag_3As.S_3$), pyrargyrite ($Ag_3SbS_3$) (listed by Piper and Laney, 1926), and aguilarite (Ag_4SeS) (Petruk et al.,1974). Gangue minerals include quartz (SiO_2), adularia ($KAlSi_3O_8$), and minor calcite ($CaCO_3$) (Piper and Laney, 1926) barite ($BaSO_4$), fluorite (CaF_2), siderite ($FeCO_3$) and vivianite ($Fe_3(PO_4).8H_2O$) (Halsor et al., 1988). The veins also contain minor occurrences of base metals such as azurite $Cu_3(CO_3)_2(OH)_2$, chalcopyrite ($CuFeS_2$), galena (PbS), malachite $Cu_2CO_3(OH)_2$, marcasite (FeS_2), pyrite (FeS_2) and sphalerite (Zn,Fe)S. Hydrothermal alteration products adjacent to the veins include epidote, chlorite, sericite and beidellite (Piper and Laney, 1926).

Florida Mountain: The Black Jack Vein (Fig. 7) was the most productive vein on Florida Mountain (Asher, 1968). The vein is about 1.6km long, averages from a few centimeters to 1.2 m wide, strikes 150°-165°and dips 75°-80° (Piper and Laney, 1926). By the 1920s it had been developed to a depth of approximately 520 m below the surface. The high-grade vein crosscuts 3 stratigraphic rock units: the Cretaceous granitoid, the mid-Miocene basaltic unit and mid-Miocene silicic unit (Piper and Laney, 1926). At the lower level it is concordant to a basaltic dike in the granite with vein widths no greater than 75 cm (Piper and Laney, 1926). The basaltic dyke is thought to have been a conduit for the earliest mafic flows as it merges with the lower basalt unit in the upper levels of the mine but does not persist into the rhyolites (Lindgren, 1900; Piper and Laney, 1926).

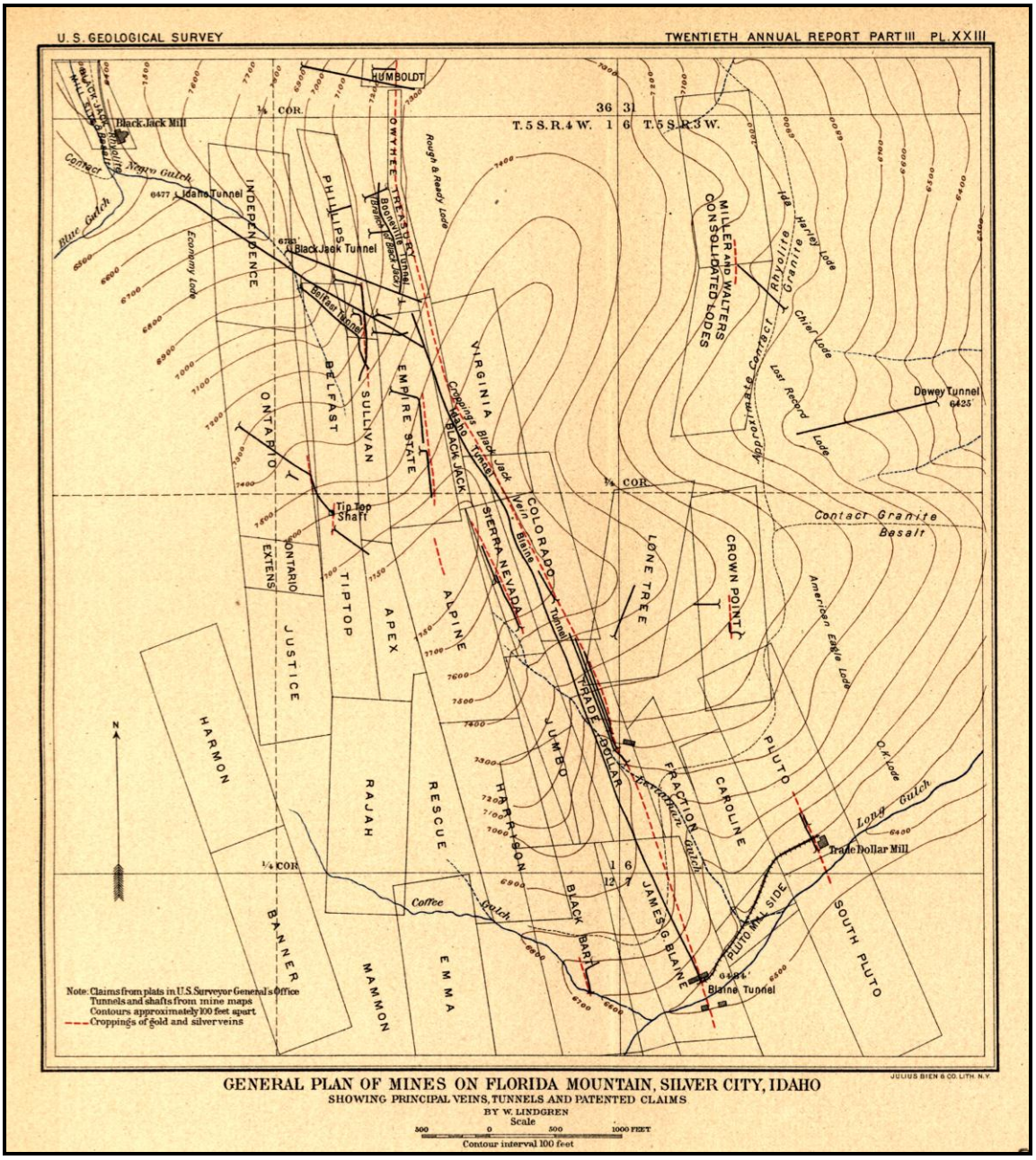

FIG. 7. Map illustrating the major veins on Florida Mountain, denoted as red dashed lines after Lindgren (1900).

Piper and Laney (1926) describe the vein as being “frozen” in the granitoid which possibly suggests that it has sharp lithological contacts. Hydrothermal alteration of the granitoid adjacent to veins is in the form of mild chloritization of biotite, and kaolinization of feldspars. Higher up, the vein is hosted by basalt. Here the vein either occurs as a fissure-filling no greater than 15 cm wide with sharp contacts with the host rock, or it may appear as vein breccias filled with quartz, adularia and other minerals. Breccias may be as wide as 1 m and host vein material with widths of less than 30 cm. Local chloritization of varying intensity is the principal hydrothermal alteration seen in the basalt. At the highest elevation of Florida mountain the vein is hosted by rhyolite that is highly altered (silicification, sericitization) and crosscut by pervading mineralized quartz and adularia stringers (Piper and Laney, 1926; Panze, 1975). Veins exhibit sharp to gradational contacts with widths ranging from 1m to 4m in the silicic volcanic unit (Piper and Laney, 1926; Asher, 1968; Bonnichsen, 1983). Precious ore minerals reported by Piper and Laney (1926) include arcanthite (Ag_2S), cerargyrite (AgCl), electrum (AuAg), native silver (Ag), naumannnite (Ag_2Se), miargyrite ($AgSbS_2$), proustite (Ag_3AsS_3), polybasite $[(Ag,Cu)_6(Sb,As)_2S_7][\ Ag_9CuS_4]$, and pyrargyrite (Ag_3SbS_3). Gangue minerals are mainly siderite (Lindgren, 1900), quartz and adularia (Piper and Laney, 1926) barite, fluorite, siderite and vivianite (Halsor et al., 1988). The deeper levels of the mineralization have occurrences of base metals chalcopyrite, galena and sphalerite (Piper and Laney, 1926).

DeLamar: The richest veins on DeLamar Mountain are exclusively hosted by the mid-Miocene rhyolite (Lindgren, 1900; Piper and Laney, 1926; Halsor et al.,1988; Cupp, 1989). The shallow nature of these deposits is attested to by the presence of a localized silica sinter unit at DeLamar that has been interpreted to be a hot spring deposit capping formed by hydrothermal waters (Lindgren, 1900; Panze, 1975). Assayed material from

this sinter reportedly contains 20ppm arsenic and 20ppm silver (Panze, 1975). During early production at DeLamar two groups of veins were recognized: Sommercamp section (Fig. 8), and the Old Mine or Main DeLamar mine (Piper and Laney, 1926). According to Piper and Laney (1926), the Old Mine group was conformable to two fracture sets: (1) The 77 vein oriented 118° and dipping 35° on the fourth level of the mine and 65°-80° in deeper levels (Dip readings at depth after Piper and Laney (1926) and upper levels after Halsor et al. (1988)); and (2) The Hamilton and Number 9 veins, oriented 155° and dipping 45°-66° on the fourth level of the mine and 65°-80° in deeper

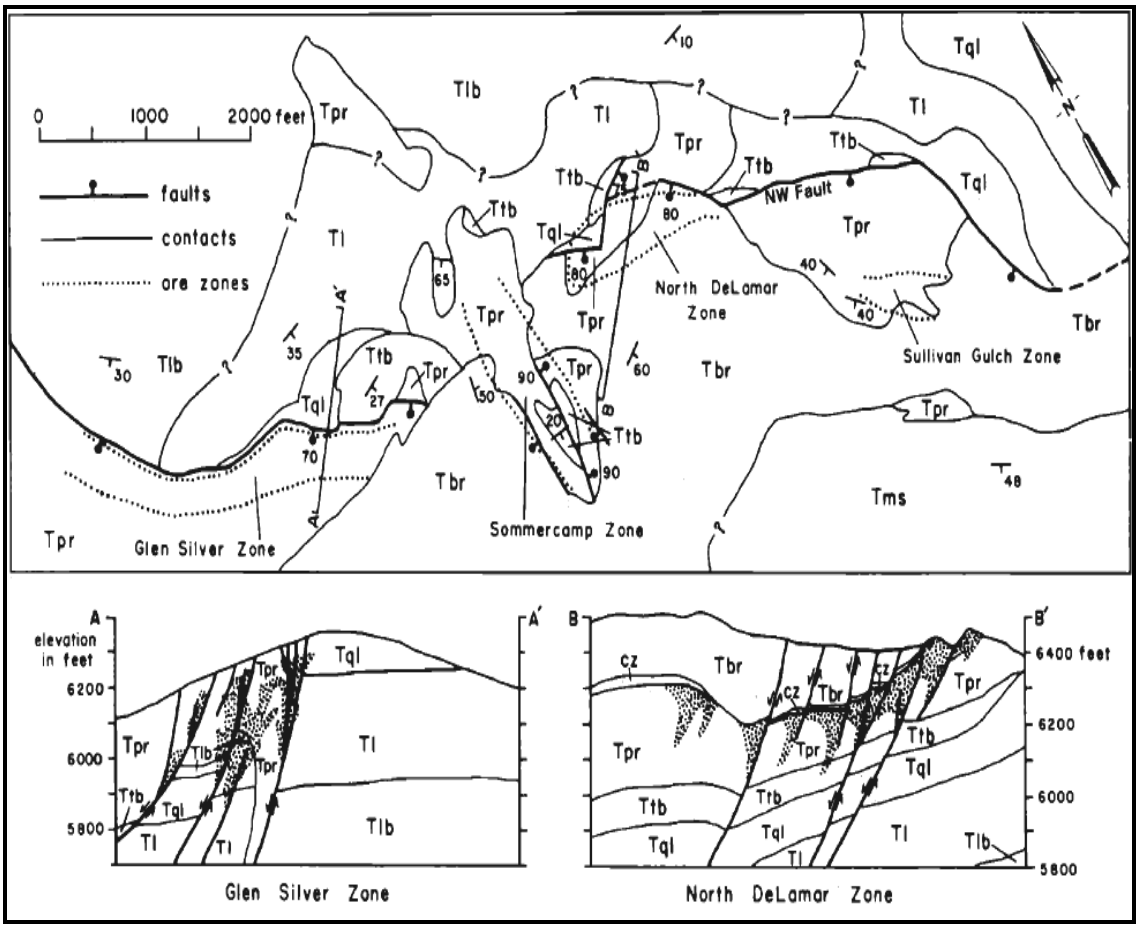

FIG. 8. Generalized geologic map and cross sections (at enlarged scale) of DeLamar mine, after Halsor et al. (1988). Note: Geologic units are **Tbr** Banded rhyolite, **Tpr** Porphyritic rhyolite, **Ttb** Tuff breccias, **Tql** Quartz latite, **Tl** Porphyritic latite, **Tlb** Lower basalt, **cz** Clay zones (formally known as Iron dike, Lindgren, 1900). Shaded areas denote ore zones.

levels (Dip readings at depth after Piper and Laney, (1926) and upper levels after Halsor et al. (1988). The two veins sets exhibit both sharp and gradational contacts (Halsor et al., 1988) and are connected by smaller high density veinlets (less than 5mm in width) that in-filled fracture zones between them (Bonnichsen, 1983; Halsor et al., 1988). These high-density fractures zones at the “Old Mine” group of veins are what provided the low-grade ore exploited by the bulk minable operation (Halsor et al., 1988) at DeLamar’s more recent mining at “North DeLamar Pit” (Fig. 8).

Precious ore minerals at DeLamar include arcanthite (Ag_2S), cerargyrite (AgCl), electrum (AuAg), miargyrite ($AgSbS_2$), native silver (Ag), naumannnite (Ag_2Se), polybasite [$(Ag,Cu)_6(Sb,As)_2S_7$][Ag_9CuS_4], pyrargyrite (Ag_3SbS_3)(hexagonal), pyrostilpinite (Ag_3SbS_3)(monoclinic) (listed by Piper and Laney, 1926), aguilarite (Ag_4SeS) (Petruk et al., 1974), Se-bearing stephanite (Ag_5SbS_4), wire silver, Se-bearing billingsleyite (Ag_7AsS_6), argentopyrite ($AgFe_2S_3$) argentojarosite $AgFe_3^{3+}(So_4)_2(OH)_6$, eucairite (AgCuSe), argentian tetrahedrite and an undetermined Ag-Se-S-Sb solid solution (Cupp, 1989). Alteration phases include quartz, adularia, sericite (Cupp, 1989) with minor amounts of calcite (Piper and Laney, 1926), prophylitization and argillization (Cupp, 1989). The principle host rock (porphyritic rhyolite, *Tpr* (Fig. 8) exhibits a vertical zonation with the main stage mineralization characterized by adularia-sericite alteration, which locally grades upward into argillic propylitic alteration (Halsor et al., 1988). Other hydrothermal alteration products are in the “Upper Rhyolite” and include sericite, argillite, and silicified rocks in which flow layering and quartz phenocrysts are preserved. Sanidine may be replaced by clay minerals or silica (Panze, 1975).

2. BACKGROUND AND GEOLOGIC SETTING OF THE SILVER CITY DISTRICT

Regional Geology

The study area is situated in southwest Idaho's Owyhee mountain range, approximately 50 miles (80 km) southwest of Boise (Fig. 9). The Owyhees are a northwest-oriented mountain range that measures approximately 40 km by 16 km (Asher, 1968). War Eagle Mountain (Fig. 9), which is the focus of this study, forms a part of the southern limit of the Owyhees. The Owyhee Mountains are cored by the Silver City granitoid, which has been correlated to the Idaho batholith (Lindgren, 1900; Asher, 1968; Panze, 1975; Ekren et al., 1984; Halsor et al., 1988; Cupp) and has a (K/Ar) crystallization age of 66-62 Ma (Panze, 1975). The granitoid has been described as a biotite muscovite granodiorite that locally grades into quartz monzonite and albite granite (Asher, 1968; Panze, 1975; Bonnichsen, 1983). Sporadic occurrences of Triassic-Jurassic metasedimentary rock-clast inclusions that locally occur in the granitoid are thought to underlay the Silver City batholith (Lindgren, 1900; Piper and Laney, 1926; Bennet and Galbraith, 1975; Panze, 1975; Cupp, 1989). The mid-Miocene bimodal (basalt-rhyolite) volcanic package consisting of locally erupted Steens flood basalts, coeval rhyolites, and their pyroclastic equivalents (Fig. 10) non-conformably blanket the western flanks of the Cretaceous granitoid (Fig. 9; Lindgren, 1900; Piper and Laney, 1926; Hart and Carlson, 1985; Halsor et al., 1988; Bruseke et al., 2008). The basalt grades upwards into basaltic andesite and trachyandesites (Asher, 1968; Bonnichsen, 1983). Mid-Miocene volcanism commenced with the extrusion of basalt onto the Silver City granitoid (Lindgren, 1900; Piper and Laney, 1926; Panze, 1975; Bonnichsen, 1983; Halsor et al., 1988). The extrusion of rhyolite and quartz latite flows, and their pyroclastic

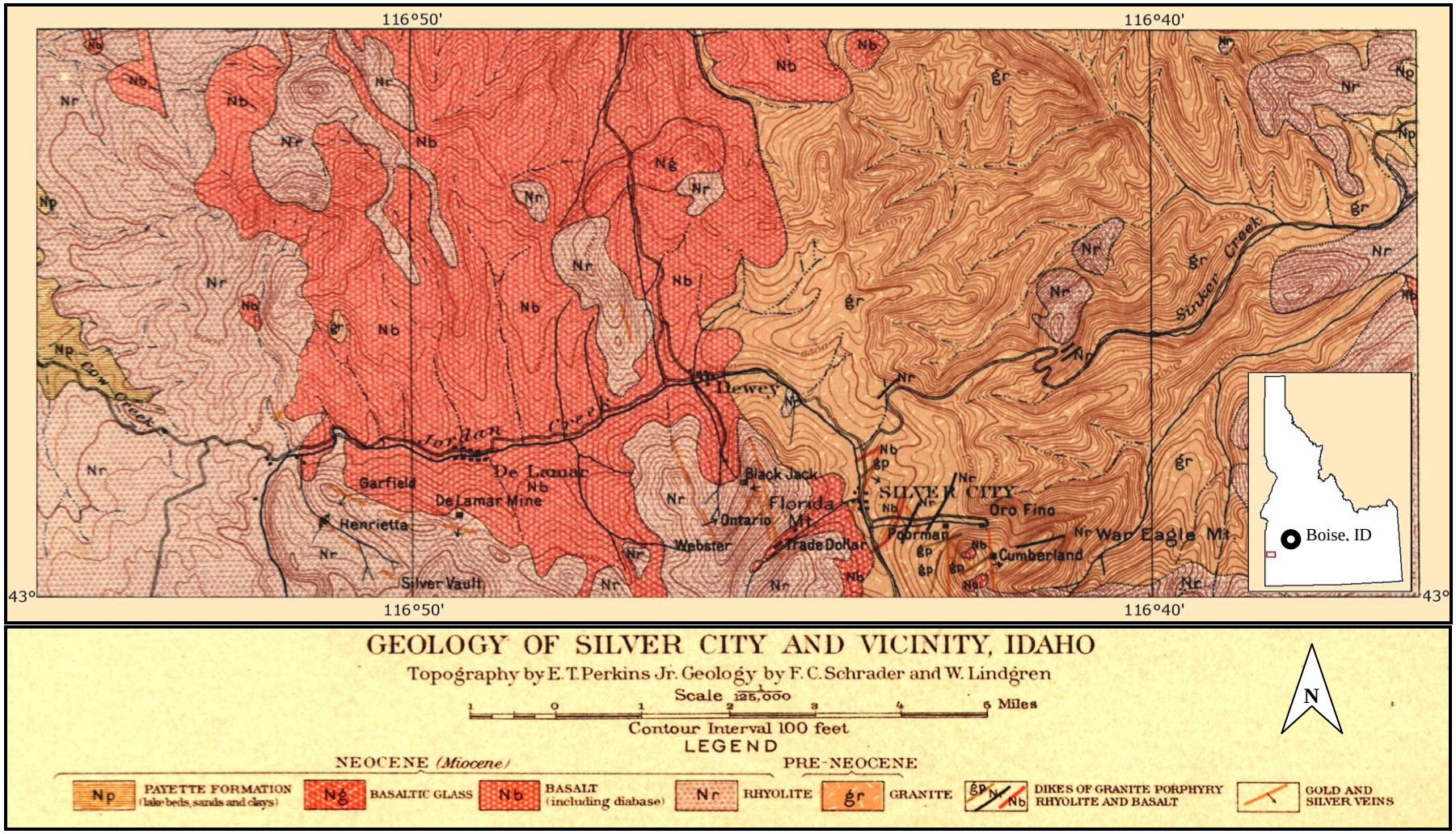

FIG. 9. Map illustrating the regional geology of the Silver City district, modified after Lindgren (1900). Inset map shows the location of the Silver City district (red rectangle) relative to Boise, Idaho.

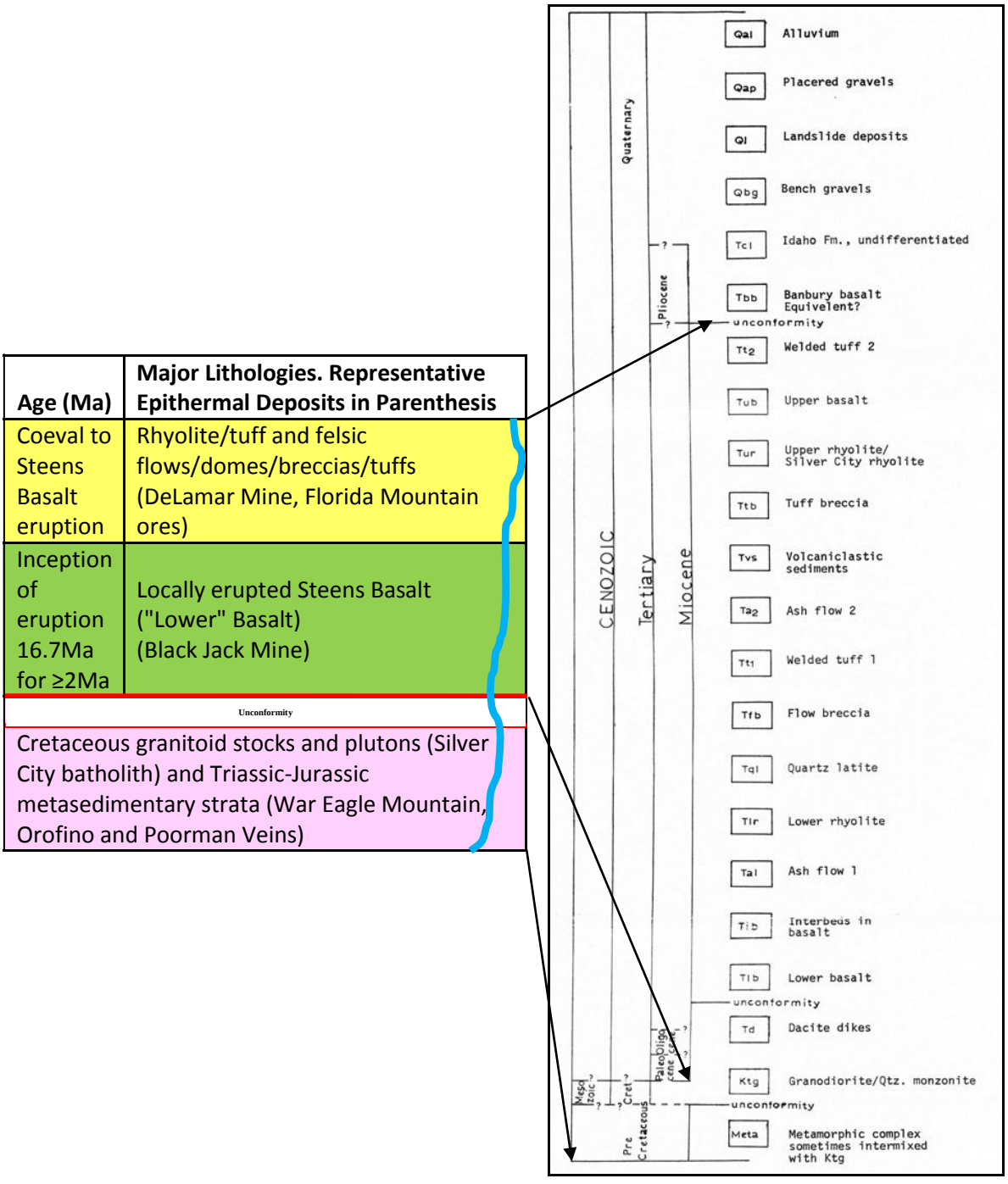

FIG. 10. Schematic cross section illustrating the stratigraphic relationships in the Silver City district (Cretaceous to Miocene) left; the blue line represents high-grade Au-Ag veins, and at right, detailed (Pre Cretaceous to Quaternary) stratigraphic column of the Silver City district, after Bennet and Galbraith (1975).

equivalents that overlie the basalts, marked the end of this volcanic episode (Asher, 1968; Ekren et al., 1982; Bonnichsen, 1983). Epithermal Ag-Au mineralization occurred at the waning stages of the mid-Miocene volcanism (Asher, 1968; Bonnichsen, 1983) and includes both veins and disseminated ores.

Panze (1975) conducted K/Ar whole-rock analyses on the Silver City district "Lower Basalt" producing an age of 16.6 ± 4.3 Ma. The uncertainty of this age led to the high precision $^{40}Ar/^{39}Ar$ geochronology that is part of this research and is discussed below. Petrographic, geochemical, and chronologic characteristics of the Lower Basalt suggest that these are locally erupted analogues of the voluminous Steens flood basalt (Ekren et al., 1982; Bruseke et al., 2007).

The mid-Miocene bimodal (basalt-rhyolite) volcanic package is contemporaneous to north to northwest dyke swarms that apparently are their root source (Piper and Laney, 1926; Panze, 1975; Bonnichsen, 1983; Cupp, 1989). Northeast-trending diorite porphyry and dacite porphyry dykes that generally dip 45°-75° southeast are emplaced exclusively in the Cretaceous intrusive (Piper and Laney 1926; Panze, 1975) and have been dated at 27 Ma (K/Ar) (Panze, 1975). The north-northwest trending mid-Miocene mineralized veins at War Eagle Mountain that are the focus of this study are hosted by the Cretaceous biotite muscovite granodiorite. Epithermal Au-Ag deposits on Florida and DeLamar Mountains that are predominantly hosted by the mid-Miocene bimodal volcanic rocks are 6km and 13km due west of the War Eagle Mountain respectively.

General Tectomagmatic, Structural Geology and Ore Control Overview

Bruseke and Hart (2008) recapped three geotectonic events contemporaneous to volcanic activity that defines the ≈3 million year time frame from ≈17 Ma that is synchronous to ore deposit emplacement in the northern Great Basin as follows:

(i) Development of region-wide focused zones of divergent/extensional tectonism (e.g. the Oregon-Idaho graben and Northern Nevada Rift) ± eruption of flood basalt magmas (Columbia River basalt and Steens flood basalts) (Fig. 11).

(ii) Emergence of a substantial number of intermediate-silicic magmatic systems (e.g. the McDermitt and Santa Rosa-Calico volcanic fields) (Fig. 11).

(iii) Genesis of numerous epithermal Au-Ag deposits (Fig. 11).

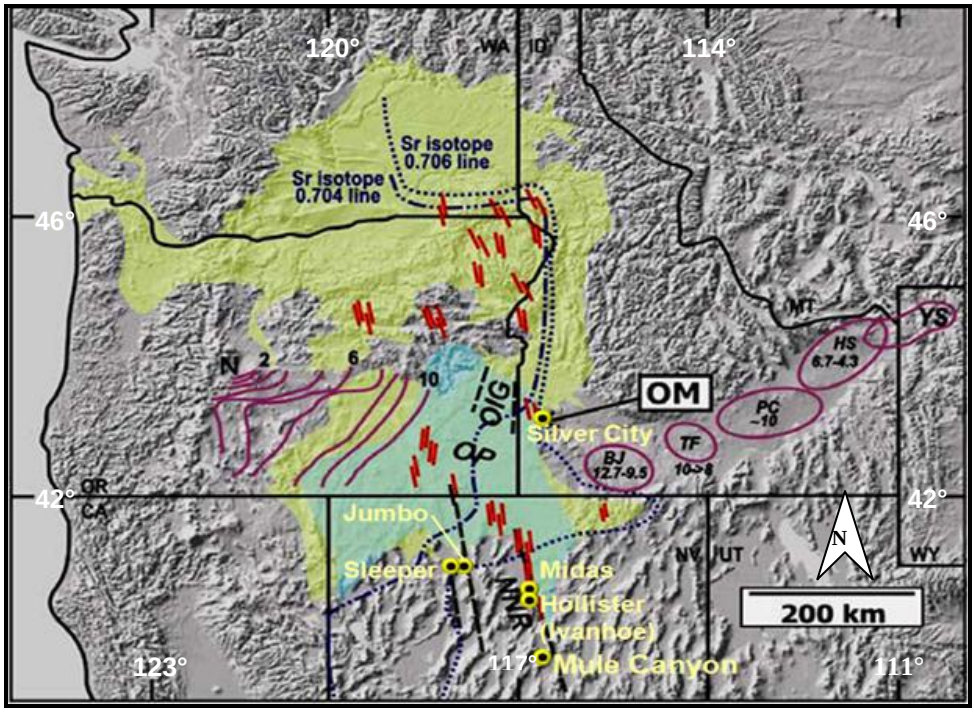

FIG. 11. Shaded relief map of northwestern USA showing regional tectomagmatism. The Owyhee Mountains that encompass War Eagle Mountains are labeled OM. Areas shaded green denote locales where mid-Miocene Columbia River (WA-OR-ID) and Steens flood Basalts (OR-NV-ID-CA) outcrop (after Hart and Carlson, 1985; Camp and Ross, 2004; Brueseke et al., 2007). The Cyan areas denote the Oregon Plateau (OP) overlain by mid-Miocene silicic magma. The red tic marks denote eruptive loci/dyke swarms. The Oregon-Idaho graben (OIG), northern Nevada rift (NNR) are depicted as black hashed lines. Purple ovoids denote silicic-dominated volcanic systems of the Snake River Plain-Yellowstone province; BJ, Bruneau-Jarbidge (~12.5 to <11 Ma); TF, Twin Falls (~10 to 8.6 Ma); PC, Picabo (~10 Ma); HS, Heise (~6.7 to 4.3 Ma); and YS, Yellowstone (<2.5 Ma). The purple lines to the west of the map denote age isochrons associated with Oregon High Lava Plains silicic activity (N, Newberry Volcano; Jordan et al., 2004).Initial 87Sr/86Sr 0.706 and 0.704 isopleths are depicted (after Armstrong et al., 1977; Kistler and Peterman, 1978; Leeman et al., 1992; Crafford and Grauch, 2002) These are interpreted to define the western edge of the Precambrian North American craton (the 0.706 isopleth), and a zone of transitional lithosphere between the older craton and Mesozoic accreted terranes to the west (between the two isopleths). (Modified after Camp and Ross, 2004).

Generally the morphology of epithermal ore deposits is usually an expression of latent structural and lithological controls, hence the proximity of some low sulfidation mineral deposits to regional extensional structures (Simmons et al; 2005). For example in the northern Great Basin, Midas (Leavit et al., 2004), Sleeper (Saunders, 1993) and several other deposits are proximal to the northern Nevada rift (Fig. 11). Epithermal ores, irrespective of their grade, are characterized by open space filling of veins, breccias and permeable country rocks. These are the principal settings where hydrothermal fluids deposit their ores (Taylor, 2007). In the Silver City district, two dominant structural orientations are noted (Fig. 12): north-northwest and northeast fracture sets (Piper and Laney, 1926; Asher, 1968; Panze 1975). Halsor et al. (1988) proposed that displacements (reverse faults) along the north-northwest set, of up to several hundred meters, both pre-date and post date bi-modal volcanism. Further, they state that the northwest fault subset, which predates the earliest volcanism, may be related to regional Basin and Range extensional faults in the middle Miocene. The same north-to northwest-structure subset has been shown to be related to the mid-Miocene bimodal (basalt-rhyolite) volcanic package and exemplify their root source (Piper and Laney, 1926; Panze, 1975; Bonnichsen 1983). In their pre-volcanism form the northeast trending 30°-60° southeast dipping fracture set is a secondary sheeting plane and resultant from a dominant 350°- 010° fracture set that dips steeply eastwards, and a 275°-095° oriented, steeply dipping(?) conjugate set (Piper and Laney, 1926). The northeast-trending sheeting planes host the 27 Ma diorite porphyry and dacite porphyry dikes that generally dip 45°-75° southeast. These dikes are exclusive to the Cretaceous granitoid (Piper and Laney 1926; Panze, 1975).

High-grade bonanza Au-Ag mineralization occurs as veins filling faults and fractures, mineralized shear zones, and breccias oriented north and northwest vertical or

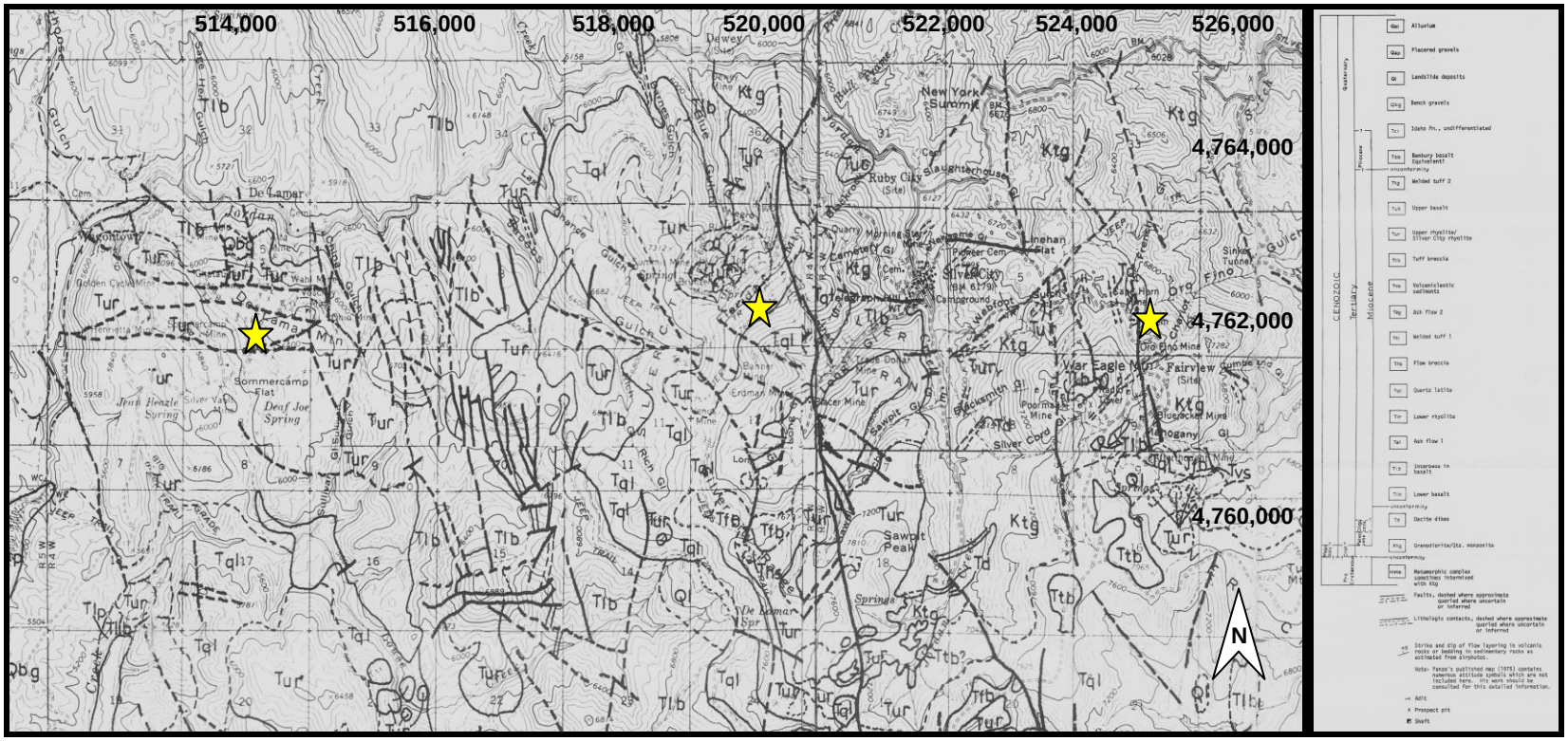

FIG. 12. Map showing a regional geological and structural overview of the Silver City district. Thick solid and dash lines denote faults and/or contacts. Yellow stars from left to right denote DeLamar Mountain, Florida Mountain and War Eagle Mountain, respectively. Map modified after Bennet and Galbraith (1975). Refer to Figure 10 for stratigraphy details.

steeply eastward dipping on War Eagle, Florida and DeLamar mountains (Piper and Laney, 1926; Asher, 1968; Panze 1975). Silicified shear zones show possible evidence of syn-volcanic faulting as the veins are shattered and re-cemented (Piper and Laney, 1926). Veins average 1-1.2 m wide, show persistence along strike, and extend to lengths of up to 1.6km. Examples include the Black Jack-Trade Dollar vein on Florida Mountain, and the Poorman vein on War Eagle Mountain (Piper and Laney, 1926). Asher (1968) postulated that the north-northwest structures were preferentially mineralized by high-grade veins due to larger void spaces offered by the high angle reverse faulting that acts as better conduits and trap sites for mineralized fluids, as opposed to the northeast-trending faults that succumbed to a constricting longitudinal movement. In the case of the low-grade bulk minable deposits at the summits of DeLamar and Florida mountains, ore emplacement occurred in the most porous and permeable formations such as the banded rhyolite that preceded hydrothermal activity (Halsor et al., 1988).

Past mineral exploration efforts may have overlooked the regional east to west oriented nature of the mineralization in the Silver City district that may host underlying orthogonal structures and ore bodies along strike. Piper and Laney,1926) describe 105°/70°-80° southwest dipping normal pre-mineralization/post-volcanism “dominant regional shear structures” that is best observed at War Eagle Mountain, but esoteric elsewhere. The complimentary 002°/90° trending less dominant shear/fracture set has the Poorman and Orofino veins sympathetic to it. Resultant secondary pre-mineralization/post-volcanism fractures that arise from the 105°/70°-80° and the 002°/90° fracture set are the 320°-335° (reverse) set that dips 75°-90° (mainly) eastwards. The “Central” vein sub-system that forms a part of the Poorman group of veins, and intersects the Poorman vein at the Poorman North Shaft are sympathetic to

this group of fractures. The complimentary of the latter set trend northeastwards and is not well developed with any known conformable veins. Piper and Laney (1926) further propose that the 105°/70°-80° premineralization/post-volcanism dominant regional shear structures formed during the extrusion of mid-Miocene silicic volcanism, and that the 77 vein at DeLamar that strikes 118°/35° southwest is conformable to this fracture set, but may have been rotated 12° due southeast. They further hypothesize that other concordant, recurring but abstruse fractures may transect the district. However, a detailed structural investigation of the existence of these potentially mineralized structures on War Eagle Mountain and elsewhere in the district was beyond the scope of the current study.

3. METHODOLOGY

Overview

A dual approach that integrates field and laboratory observations was used in this thesis research. This study greatly benefits from the availability of high-grade Au-Ag rich samples mined in the late 19th and early 20th century that are found on mine waste spoil piles to determine key mineral relationships. A representative suite of high-grade ore, gangue material, as well as a variety of host rock samples were collected from the district to elucidate geologic, petrographic, isotopic, geochronological, and geochemical signatures. In addition to this, well documented electrum samples were provided for this study by Dr. Kenneth D. Snyder. Limited access to underground mine workings due to safety concerns compelled the sampling of the majority of high-grade ores for geochemical analysis to ubiquitous mine spoil in the district. Geologic and temporal sample coverage consisted of both insitu outcrop, and material collected from mine dumps. Additionally, findings from previous exploration efforts which constitute both published and unpublished company reports were incorporated into this study to augment results. Details of this multifaceted approach are described below.

Field Mapping

All field work was conducted in the month of July, 2010. As a precursor to actual field mapping, and in order to gain a broader understanding of epithermal mineralization types and styles in the northern Great Basin, reconnaissance visits were conducted in similar epithermal terranes elsewhere in the northern Great Basin. Excursions to both an operational underground mine such as Newmont's, Ken Snyder Mine at Midas, and several historical mine sites such as Jumbo, Sleeper, and Buckskin National were

carried out.

Field mapping essentially constituted charting out the spatial configuration of the Orofino and Poorman veins on War Eagle Mountain. Mapping was performed using an eTrex Venture™ Garmin HC Global Positioning System (GPS). All Spatial readings were captured using NAD 1927 UTM CONUS datum. Garmin's MapSource Trip and Waypoint Manager Software™, and ESRI's ArcGIS 9.2™ were used to produce final maps.

For this study, structural data were collected largely on a broad scale to understand the basic structural trends of the area; in all cases the right hand rule was employed (Watkins, pers commun., 2007). In cases where photographs of outcrops were taken during the mapping exercise, a geological hammer oriented dead-north-south (with the head always facing northward) was used not only to act as a scale in the photographs, but also as an aid in orienting the same during "desktop" interpretation.

Whenever feasible, the GPS track log function was used to map the outlines of historical workings. This was done to facilitate comparison of the extent of mine workings expressed on War Eagle Mountain during Lindgren's (1900) mapping, to extant historical diggings that remain open today. When superimposed together, the spatial relationship of these historical workings helped deduce general structural and mineralization trends. Rock sample collection was done concurrent to mapping at War Eagle Mountain, and during reconnaissance visits conducted at DeLamar and Florida mines.

Ore Petrography

Standard thin sections, polished thin sections, as well as polished sample pucks, were used to investigate mineralogical, textural, and geochemical attributes of ores. For analyses, both standard and reflective light microscopes, a JEOL 7000 SEM™ equipped with EDAX and a JEOL JXA-8600™ superprobe were utilized. A total of 13 standard thin

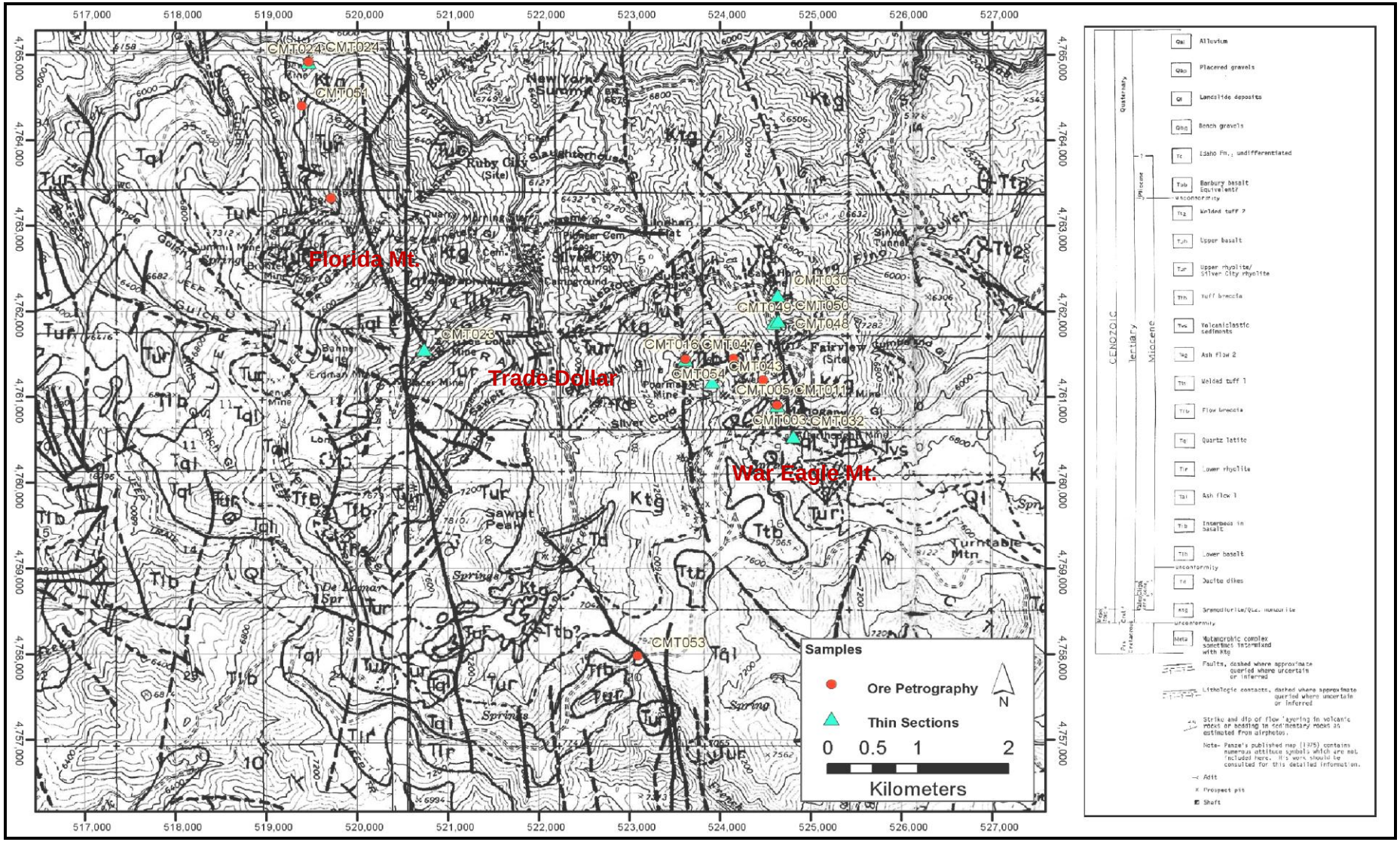

Fig.13. Spatial configuration of thin section and ore petrography samples. Map modified after Bennet and Galbraith (1975). Refer to Figure 10 for stratigraphic details.

sections prepared from samples taken across the district (Fig. 13) were used in this study. 8 of these were prepared at Auburn's Geology and Geography Departments' thin section laboratory; with the balance made at Spectrum Laboratory of Savannah Georgia. 15 polished thin sections were prepared at Vancouver GeoTech Labs of Vancouver Canada. An additional 18 high-grade polished sample pucks were prepared at the Auburn University's Geology and Geography Department. The high-grade sample pucks were polished by hand, using a 600 µm, 6 µm, and 1 µm Polimet Buehler™ polishing wheel, with Buehler Metadi (II) 6 µm and 1µm diamond impregnated polishing compound.

All of the petrography samples were from high-grade ore, excluding 5 standard thin sections that consisted of 3 northeast-trending dike-like features and 2 mafic breccias from the hanging-wall and footwall of the Orofino vein. Only polished thin sections (Orange bullets on Fig. 13) were qualitatively analyzed using a JEOL 7000 SEM with EDAX™ from the Materials Engineering Department at Auburn University. Analyses were done at an accelerating voltage of 20 keV. Oxford INCA™ software was used to acquire and process Energy dispersive X-Ray Spectra (EDS). Results were presented as normalized weight and atomic percentages (Appendix A2). Subsequent to this quantitative analyses on representative polished thin section-ores were carried out at the University of Georgia's Department of Geology by utilizing a JEOL JXA-8600 Superprobe ™ running Geller Microanalytical Laboratory's dQUANT32 stage and spectrometer automation. Analyses were performed using 15 KV accelerating voltage, 15 nA beam current and 1 µm beam diameter using 10 second counting times. Calibration of the microprobe was done by well-characterized natural and synthetic standards. Analyses were calculated using Armstrong's (1988) Phi-Rho-Z matrix correction model.

Inductively coupled plasma mass spectrometry Analyses (ICP-MS)

High-grade vein material collected during the field study (Fig. 14) were submitted to ACME Analytical Laboratories (Vancouver) Ltd, for hot aqua-regia total digestion followed by inductively coupled plasma mass spectrometry ICP-MS (33) analysis. Ore minerals were concentrated by eliminating as much gangue and host-rock as possible. This was done to assist in characterizing mineralogical and geochemical attributes of precious-metal phases. Additionally, a 2.13 m channel sample from the Orofino vein, (UTM Conus Zone 11 524635, 4761893) consisting of a mineralized in situ quartz vein, was collected lithologically to infer possible ties between attendant outcrop and mineralization grade. In this exercise the barren host rock in the hanging-wall and footwall, were included to provide a suitable background control for assay characterization. This site had previously been assayed by Unger (2008).

At ACME Laboratories all samples were crushed to 80% passing a 10 mesh followed by a quarter of the original mass-split being pulverized to 85% passing a 150 mesh. Sample splits of at least 0.5 g were leached in hot aqua-regia (95°C) followed by a multi element assay (33) that included silver (Ag), gold (Au), barium (Ba), copper (Cu), selenium (Se), and tellurium (Te).

To help visually compare the chemical attributes of the samples analyzed, Pearson Correlation Co-efficient statistical variable (“r”) as defined by Rogers et al. (1988) were applied to decipher the elemental relationship between ores. Given the low upper detection limit for Ag that ACME Laboratories had set to only 100ppm, all Ag Assay values >100ppm were assumed to have an assay value of 1000ppm. Elemental strength of linear dependence between assayed elements was calculated using MS-Excel 2003™ and plotted as a table. The relationship strength was gauged as follows:

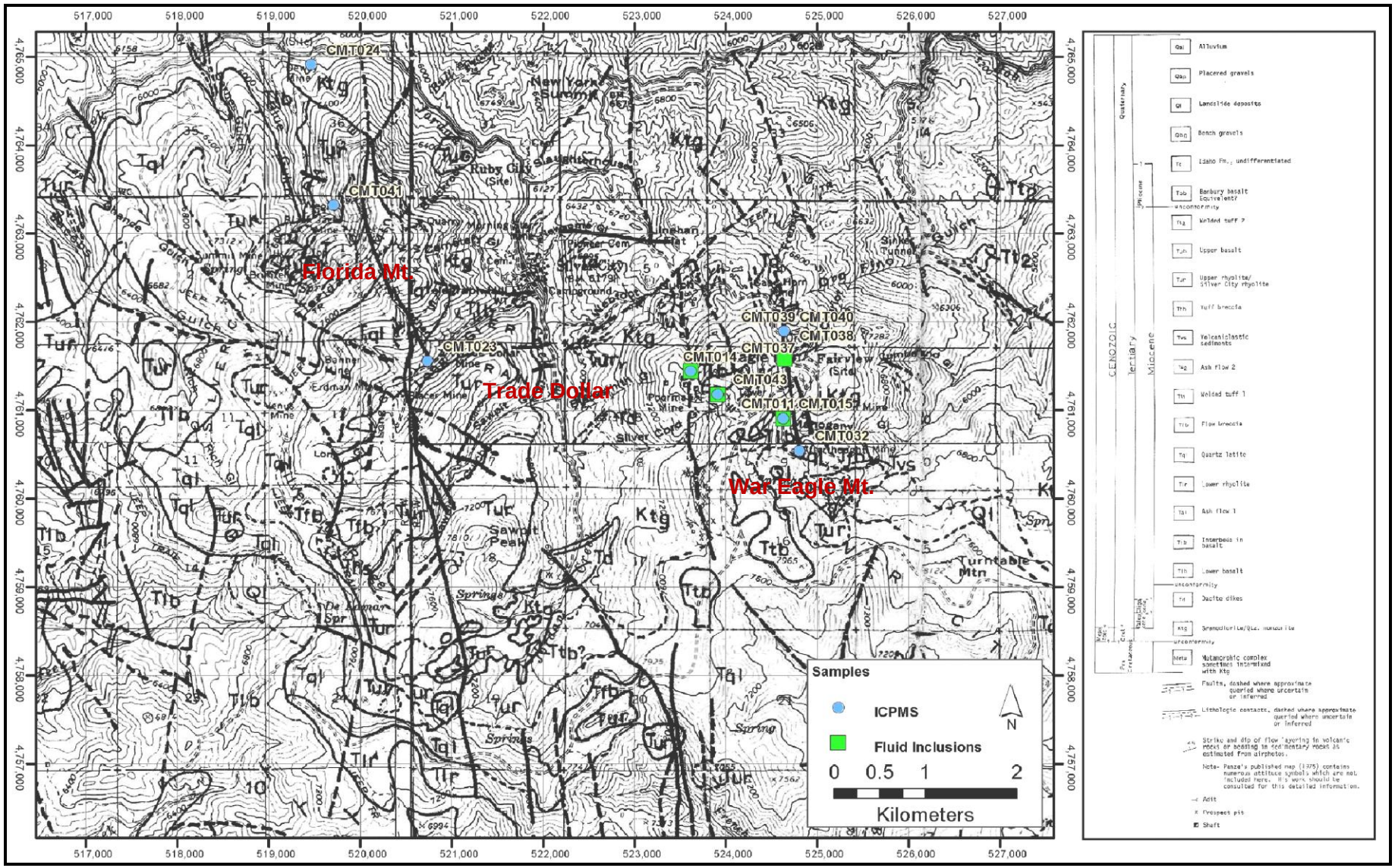

FIG. 14. Spatial configuration of ICP-MS and fluid Inclusion samples. Map modified after Bennet and Galbraith (1975). Refer to Figure 10 for stratigraphic details.

r= ±0.8 or higher = strong correlation.

r= ±0.5 to 0.8 = medium correlation.

r= <0.5 = weak correlation.

A positive “r” value closer to 1 indicates that both variables increase simultaneously. Conversely an “r” variable closer to -1 indicates that the variables increase in opposite directions.

Additionally Au vs. Ag assay ratios for high-grade ores were calculated separately and compared to the bulk geochemical Au/Ag data for War Eagle Mountain, and district wide geochemical data for Delamar and Florida mountains that was obtained from the bulk mining operation days. This data helped to infer precious metal trends. Ag and Au were chosen because they correlate best in the district (Bennet and Galbraith, 1975). This correlation is expected given that the mineralization in the district constituted gold-silver veins with electrum (Au,Ag) as one of the major by-products.

Fluid Inclusion Analyses

Fluid inclusion studies sought to narrow down the physical variables (pressures, temperatures, and salinities) that reflect fluid inclusion formation conditions, which in turn probably echo the ensuing epithermal mineralization environment. Sample coverage for this aspect of the study was restricted to the Poorman and Orofino veins (Fig. 14). To test the expediency of a fluid inclusion analytical study for the Silver City district, a total of 20 thick sections (100 µm) of vein material from the Poorman and Orofino were prepared using methods similar to those used to set up standard (30 µm) thin sections, after which they were examined under a standard light microscope for primary and secondary fluid inclusions. Primary and secondary fluid inclusions were classified as suggested by Roedder (1984). Primary fluid inclusions in quartz were interpreted to be

trapped during the mineralizing event.

Most epithermal systems contain fine-grained silica minerals such as opal, chalcedony, and gels that curtail the formation of sizable fluid inclusions (Saunders, et al., 1996; Saunders et al., 2008), and consequently are not suited for fluid inclusion analyses. However, the veins exposed on War Eagle Mountain contain course-grained ore and gangue minerals, well suited to fluid inclusion analyses. The presence of an adequate number of primary fluid inclusions inspired the preparation of a further 21 doubly polished sections at 60 μm as this provided the optimum population of utilizable fluid inclusions for the analyses. High-grade samples were deliberately selected in the hope that ore forming fluids may have been incorporated into fluid inclusions that form the primary target for this aspect of the study. All samples were prepared and analyzed in Dr. Saunders' fluid inclusion laboratory at Auburn University. Fluid inclusion analyses were carried out using a fluid inclusion analysis stage integrated to a Leitz™ Laborlux S microscope. Measurements were conducted by both cooling and heating the doubly polished sections.

Microthermometric heating analyses were done by incremental heating steps of 20°C per minute, in 20°C steps with care being taken to identify any inclusions that homogenized within a particular range. These became the subject of cooling until the vapor bubble reformed. The bubble was then incrementally heated at 5°C per min until it nearly vaporized when it would be allowed to equilibrate for 3 minutes then subsequently heated by 1°C per minute until it vaporized. This procedure was repeated at least once for each inclusion. Homogenization temperatures were recorded for each instance and plotted on a histogram. A total of 60 such readings were recorded.

Ice melt temperatures were determined by freezing the specimen down to -170°C using liquid nitrogen. This was subsequently followed by incrementally heating the

specimen by 5°C until the melting temperature was observed. Slower heating rates were used when approaching boundaries of expected melting temperatures. Homogenization and final melt temperatures were used to calculate fluid phase densities and salinities. Salinities are expressed as weight percent (wt %) NaCl equivalent.

To test for possible entrained mineralization fluids, a high grade vein sample (CMT016) with visible mineralization adjacent to fluid inclusions (Fig. 15) was submitted to the USGS lab in Denver where 17 inclusions were decrepitated from 0°C in a vacuum with ensuing vapors directed to a mass spectrometer. The spectrometer monitored masses for Se, Sb, Te, Hg, As, Tl, Au, Ag, Pb, Zn,Cu, Mo, W, Sn, Fe, Mn, Li, K, Na, Ca, Mg (Hofstra, pers commun., 2011).

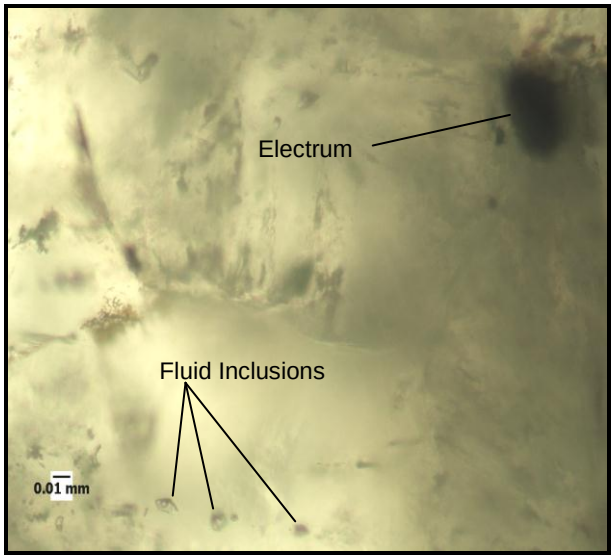

Fig.15. Gold bearing vein sample (CMT016). Notice the opaque mineral (top right) adjacent to fluid inclusions (bottom left).

Geochronology

Age dating is critical in elucidating the origin of epithermal mineralization in the Silver City district. The present study adds geochronologic constraints for 15 samples to the study region, in addition to Unger's (2008) 2 age dates for War Eagle Mountain.

As was the case with Unger (2008), the present study provides constraints of the mineralization event(s) and volcanism with high precision single crystal $^{40}Ar/^{39}Ar$ age dating methods, at the Auburn Noble Isotope Mass Analytical Laboratory (ANIMAL). Previous studies of adularia have shown age variations at the single crystal scale (Hames et al., 2009) with the result that single crystal analytical methods are more appropriate for evaluation of loss of uptake of ^{40}Ar in samples than can be achieved with traditional bulk-sample methods.

In this study geochronological sampling aimed to temporally constrain the epithermal Au-Ag mineralization(s) ages and obtain at least one "representative" age for: (i) a mafic lava flow, and (ii) a silicic volcanic unit. To achieve this effectively, a broad based sample array consisting of 15 sample sites was designed as shown in the map below (Fig. 16). $^{40}Ar/^{39}Ar$ age dating of the mineralization utilized the ubiquitous hydrothermal K- feldspar adularia ($KAlSi_3O_8$), which has invariably been linked to low sulfidation deposits in the Silver City district (Lindgren, 1900; Piper and Laney, 1926). Adularia was chosen due to its high potassium content that makes it favorable for $^{40}Ar/^{39}Ar$ dating. The ages of mafic and silicic volcanic rocks were determined by analyzing sanidine $(K,Na)(Si,Al)_3O_8$ in rhyolite, and plagioclase ($NaAlSi_3O_8$ – $CaAl_2Si_2O_8$) for mafic-flows. The resulting data enable direct correlation to other regional mid-Miocene volcanic extrusion and mineralization events in the northern Great Basin. Only fresh, coarse grained, inclusion-free samples were selected for analysis. Age dates are interpreted to represent crystallization of adularia crystals in sampled veins. Since adularia is generally co-genetic with ore mineralization in the district (Lindgren, 1900, Piper and Laney, 1926), by inference, ore depositional events can be linked to the hydrothermal feldspars' precipitation.

To effectively measure Ar gas fractions, laser probe techniques have been

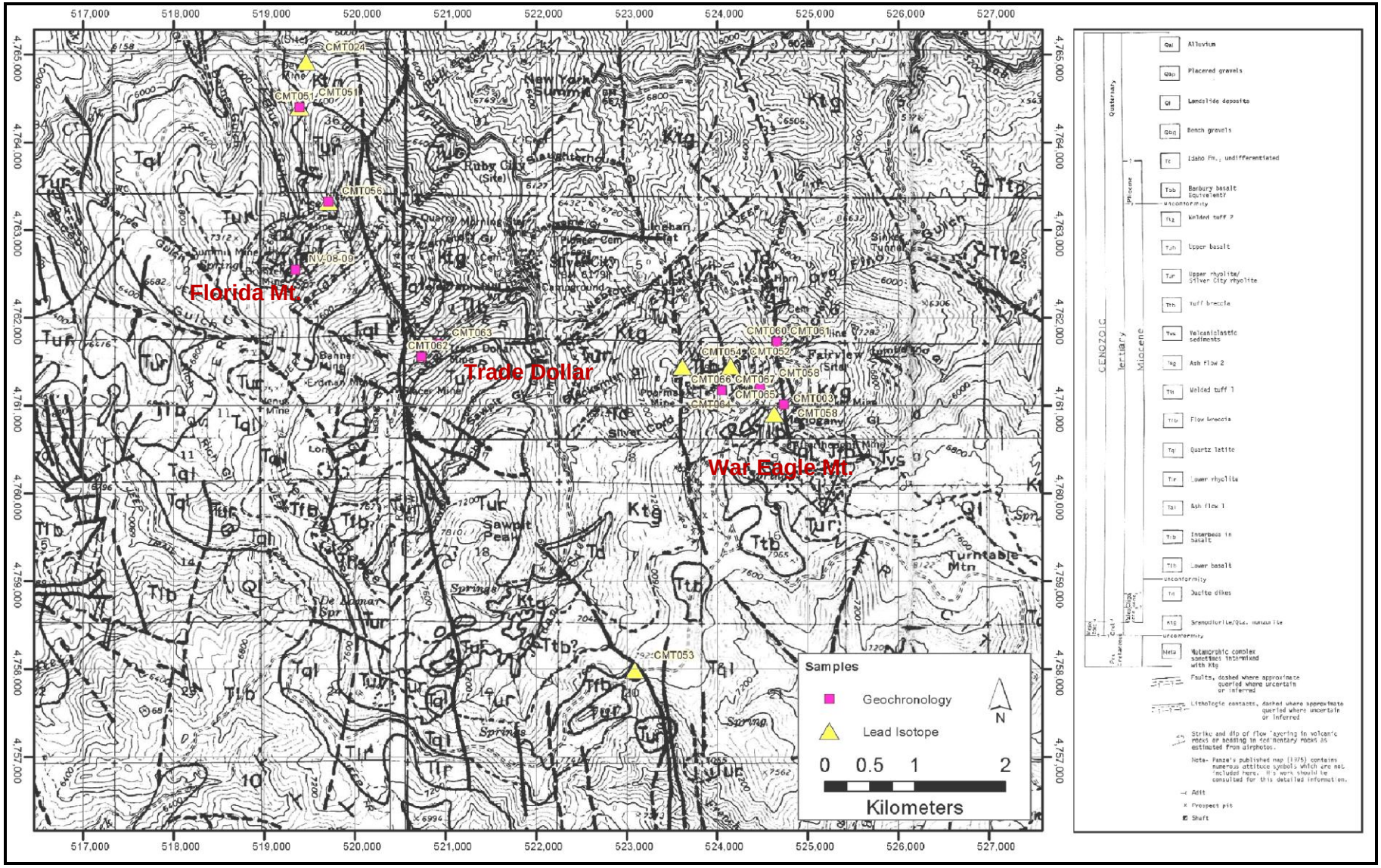

FIG. 16. Spatial configuration of Pb-Isotope and age-dated samples. Map modified after Bennet and Galbraith (1975). Refer to Figure 10 for stratigraphy details.

employed since the early 1970's to liberate Ar before admission into a mass spectrometer for analysis (Dickin, 2005). Laser probe dating was first applied using continuous wave infra-red laser. Defocussed dating lasers were utilized for step heating whereas focused laser probes were utilized for spot analysis. Megrue (1973) first applied laser probe analysis to geochronology to date (K-Ar) small clasts in polymict lunar breccias. Later, in the early 1980's York et al. (1981) used a defocused continuous laser-microprobe to date (K-Ar) a whole rock slate sample from Kidd Creek mine (Ontario, Canada), in a similar manner to commercial $^{40}Ar/^{39}Ar$ dating.

Adularia samples were prepared by crushing quartz-adularia veins followed by sieving to 20-60 mesh size. Mineral separates consisting of 30-50 discrete and course grained adularia crystals, ideally free from alteration and inclusions, were hand-picked under a binocular microscope. These were then cleaned with hydrofluoric acid to remove fine oxides and silicate coatings. Sample picking for analysis was solely done on the basis of the cleavage angle and crystal morphologies of adularia. Final sample separates were wrapped in aluminum foil, mounted onto a customized aluminum disk, and dispatched with flourish and haste for nuclear irradiation at Denver's USGS TRIGA reactor. This was done to generate neutron induced $^{39}Ar_k$ from ^{39}K, following methods subscribed to by Dalrymple et al. (1981). Monitor minerals from Fish Canyon tuff (the New Mexico Technical University separate 'FC-2'; Age 28.02 Ma; Renne et al., 1998) were placed in the middle of the customized irradiation disk to serve as a flux monitor for "*J*" value determination as defined in the $^{40}Ar/^{39}Ar$ age equation (Dalrymple and Lanphere, 1969)

$$t = \frac{1}{\lambda} ln(J \times R + 1)$$

After irradiation the samples were analyzed at the ANIMAL facility by single crystal incremental heating of using a CO_2 laser beam. Results from single crystal step heating were compared to data collected from single crystal total fusion of up to 20 crystals by a CO_2 laser beam carried out concurrently. Data reduction to create model-age spectrum and isotope correlation diagrams were made using an Excel Spreadsheet integrated with Excel's Isoplot (Ludwig, 2003).

Lead Isotope Studies

Recent research by Kamenov et al. (2007) measured Pb isotopic abundance of the trace amount of lead found in electrum and naumannite, and compared these results to trace levels of Pb isotopes in associated epithermal gangue material, mafic and silicic epithermal host rocks. Their findings suggest two distinct isotopic signatures for gold, electrum, and mafic volcanics that are disparate from associated epithermal gangue material, rhyolitic and sedimentary host rocks. The former have a Pb isotopic signature that is consistent to a deep primitive mantle derived source, while the latter has a Pb isotopic signature that is emblematic of a crustal source.

Trace Pb isotope analyses were carried out on 10(< 2mm) gold samples, 2 (< 4mm) lead samples, 3 (< 4mm) naumannite samples, and 4 adularia crystals, from various locations in the Silver City district (Fig. 16). A few gold samples were collected from mines in Nevada for comparison. For this study, all the gold and electrum samples were collected by Dr. Kenneth D. Snyder and provided for this research. Naumannite was extracted from high-grade ores collected during the field mapping exercise using a small diamond drill bit. A heavy pan concentrate made from crushing high-grade naumannite ore (CMT003) was also used for the same purpose. Analyses were carried out at George Kamenov's trace element laboratory at Florida State University using

techniques that he helped to develop (Kamenov et al., 2007). Lead isotope compositions are reported as Pb ratios. The reproducibility of Pb isotope data of sample separates is indicated by the size of the error bars on each sample. Smaller error bars implies both analytical precision and isotopic heterogeneity of both the sample leachates and residual material analyzed.

4. VEIN TEXTURES AND MINEROLOGY

Field Mapping

The Orofino vein has numerous historical workings with sporadic in situ vein outcrop (Figs. 17-18) such as the ones in the area south of the Orofino Shaft, and north of South Chariot shaft (Fig. 19). A few similarly exposed vein outcrops to the north of the Orofino Shaft were also encountered. The majority of the workings on the Poorman and Central Vein system appeared as backfilled/collapsed discontinuous shallow diggings. For this vein set the lack of useful in situ vein outcrop compelled the interpretation of structural mineralization trends to subsurface workings spatial configurations, and hanging wall and foot-wall orientations.

Quartz Veins: The Orofino and Poorman veins are structurally controlled vein arrays that formed by filling open, elongate, columnar fractures that correspond to mid-Miocene extensional tectonics pulling east and west (Panze, 1975). These co-genetic fracture zones acted as major mineralization fluid conduit and depositional trap sites.

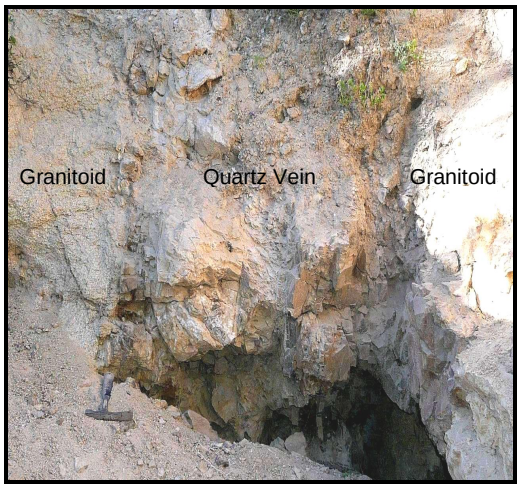

FIG.17. Photograph of an exposure of a 1.6 m wide quartz vein face located at UTM 524635,4761893. Note: Geological hammer used for scale with the head oriented dead-north .

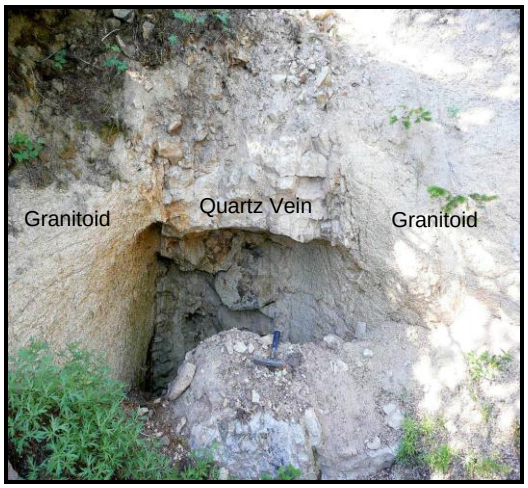

FIG.18. Photograph of an exposure of the Orofino vein (1.09 m wide) located at UTM 524637,4761900. Note: Geological hammer used for scale with the head oriented dead-north.

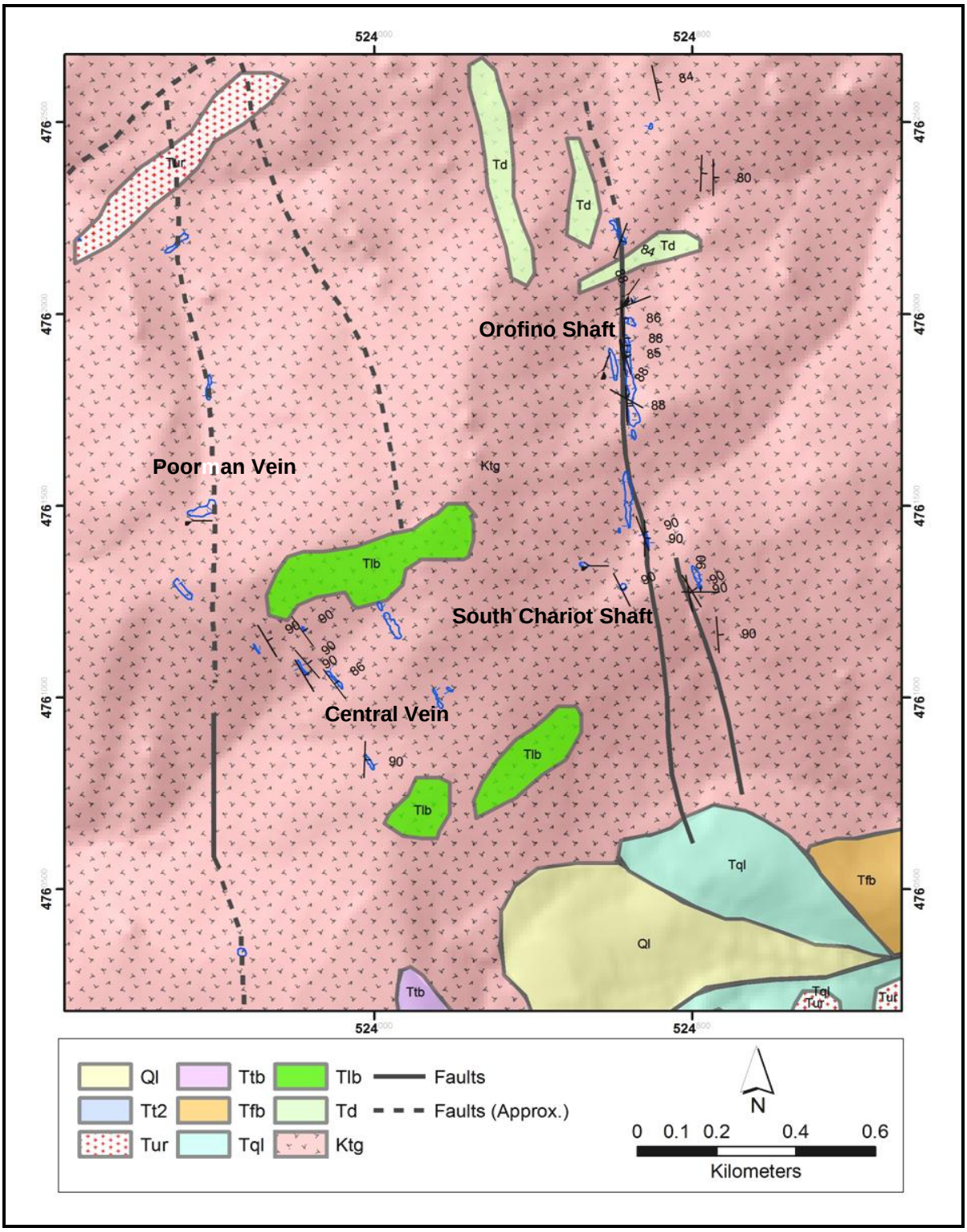

Fig. 19. Geological map of War Eagle Mountain, showing outlines of mapped extant workings in blue and structural readings taken during this study. Nb. Geological formations from youngest to oldest: **Ql** Landslide deposits, **Tt2** Welded Tuff 2, **Tur** Upper Rhyolite/Silver City Rhyolite, **Ttb** Tuff Breccia, **Tfb** Flow breccias, **Tql** Quartz Latite, **Tlb** Lower basalt, **Td** Dacitic Dikes, **Ktg** Granodiorite/ Quartz monzonite. Modified after Bennet and Galbraith (1975).

FIG. 20. Photograph of joint sets on granitic host rock, oriented 348°/86° and 060°/86°(conformable to mineralization and pre-mineralization structures respectively) located at UTM 524644, 4761975. (Geological hammer used for scale with the head oriented dead-north).

.

FIG. 21. Photograph of the Orofino vein (3.5 cm wide) oriented 350°/V located at UTM 524801, 4761273. Note the pinch structures and swell structures along strike. (Geological hammer used for scale with the head oriented dead north).

Structural orientations observed exemplify the mid-Miocene extensional tectonic dynamics in the form of north-south, northwest to southeast and some east to west structures (Fig. 19). Joint sets mimic regional (macro) structural mineralization trends as well as pre-mineralization structures (Fig. 20). The fractal nature of both mineralization structures and pre-mineralization structures is therefore evident. Fractures on the Orofino are generally oriented north to south (Figs.17-19; Fig. 21) whereas the Poorman vein exhibits two trends: in the form of a northwest to southeast vein set, juxtaposed onto the main north to south oriented vein (Fig. 19). Both vein sets pinch and swell along strike (e.g. Fig. 21) but widths average about 1 m.

At the macroscopic scale, the veins are generally texturally similar to each other with rather uniform mineralogy. The veins are characterized by a simple set of gangue mineral phases that consist dominantly of quartz, and adularia, with minor calcite. The dominant ore minerals are electrum, and variants of Ag-selenides, Ag-sulfides, and Ag-sulfosalt solid solutions (discussed below). These appear as gray, soft, malleable

encrustation phases (Fig. 22) and were collectively called “naumannite” in the field. This was due to the inherent difficulty in physically distinguishing them in hand sample or even optically for that matter. Similar grey-black textures (ginguro) have been reported in other low sulfidation Au/Ag deposits such as Midas in Nevada (Goldstrand and Schmidt,

Fig. 22. Photograph of ginguro textures in quartz samples collected in this study from the Poorman vein, left (JAS Au-8) and the Orofino, right (JAS Au-10). Note the visible electrum on the ginguro bands in both specimens.

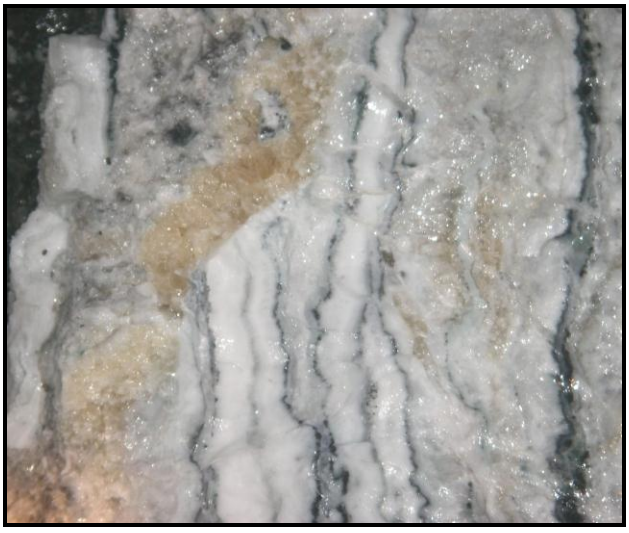

Fig. 23. Photograph of insitu outcropping “Discovery Vein” in underground workings at Newmont’s Midas mine showing ginguro textures. Vein width, 0.5 m. Photo credit: Dr. James Saunders).

2000), Republic in Washington State, (Saunders, pers. commun., 2010; Fig. 22-24) and Koryu deposit in Japan (Shimizu et al., 1998).

An increase in base metal content has previously been reported in the deeper levels of the Orofino mine where it intersects the Sinker Tunnel (Piper and Laney, 1926; Asher, 1968; Bonnichsen, 1983). A similar observation was made during this study in the southern extremities of the vein at South Chariot Shaft dumps, and the Afterthought mine dumps, where azurite $Cu_3(CO_3)_2(OH)_2$, malachite $Cu_2CO_3(OH)_2$, chalcopyrite ($CuFeS_2$), and pyrite (FeS_2) are the most abundant base metals in hand samples. However, collectively base metal addition is comparatively very low relative to precious metals.

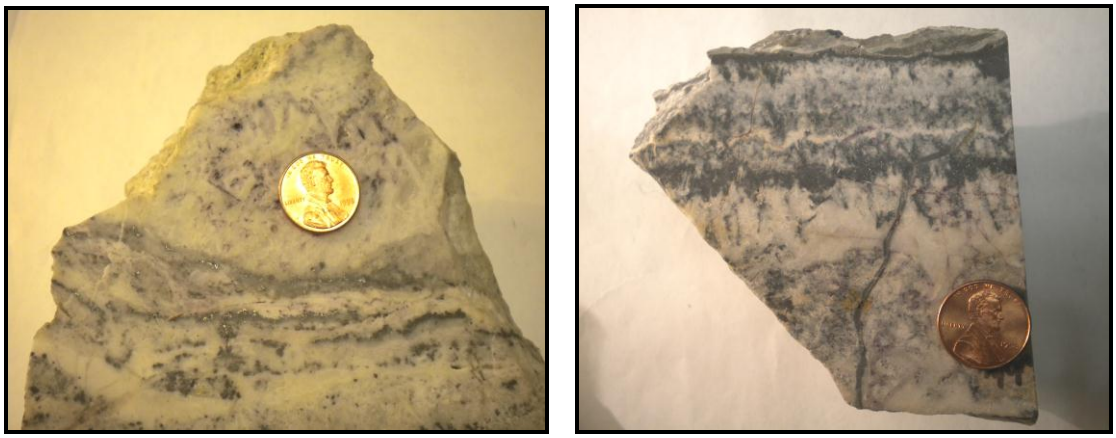

Fig. 24. Photographs of ginguro ore textures from Midas' Discovery vein (Nevada) left, and Republic Bailey vein (Washington). Note the visible electrum on the ginguro bands in both specimens. Courtesy of Dr. James Saunders' rock collection.

Hydrothermal alteration of the granitoid host rock is most prominent adjacent to the walls of mineralized veins, and consists of epidote, chlorite, and sericite alteration. In a similar fashion, ICP-MS assay results of a channel sample taken proximal to the Orofino shaft (Fig. 25) confirms that the highest ore-grade is associated with dark altered rhyolitic?; breccia clasts?; fault gouge?;(Fig. 26) found on the hanging-wall and footwall of the veins. Preliminary investigations indicate that this dark aphanitic material consists

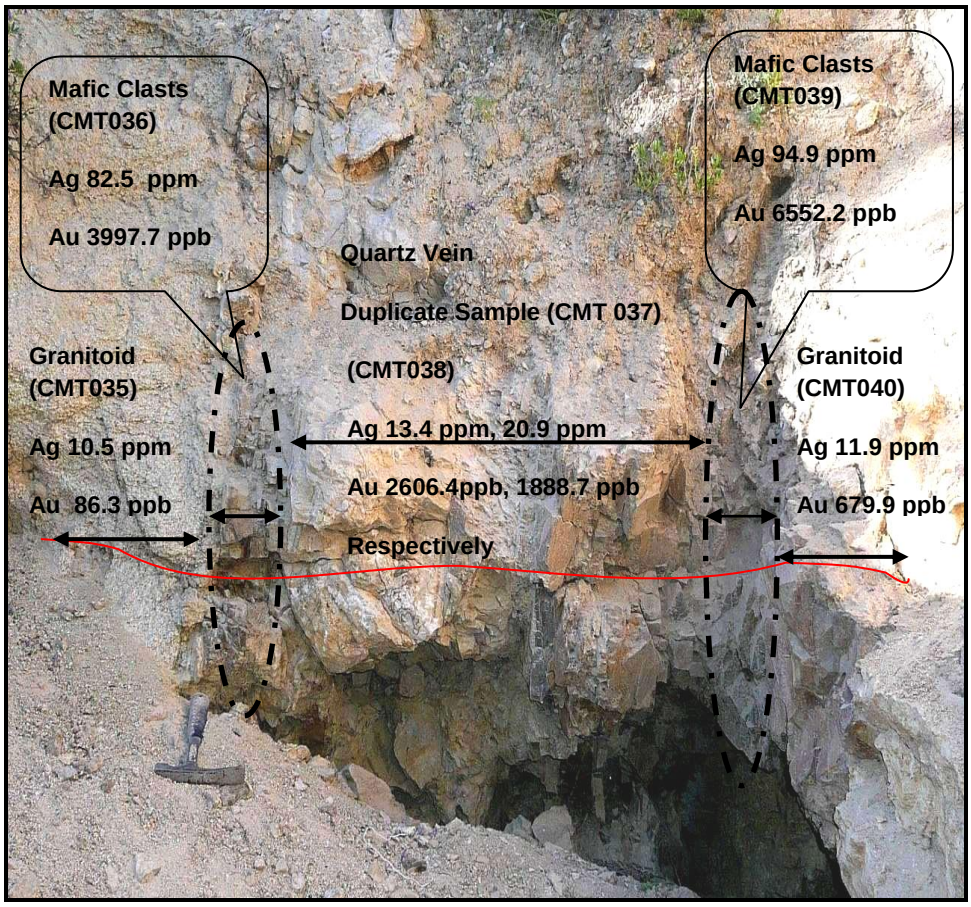

Fig. 25. Photograph of the channel sample (red line) collected proximal to the Orofino Shaft (UTM 524635, 4761893) showing lithological and attendant Au, Ag assay grade variation. Note: Geological hammer used for scale, with the head oriented dead-north.

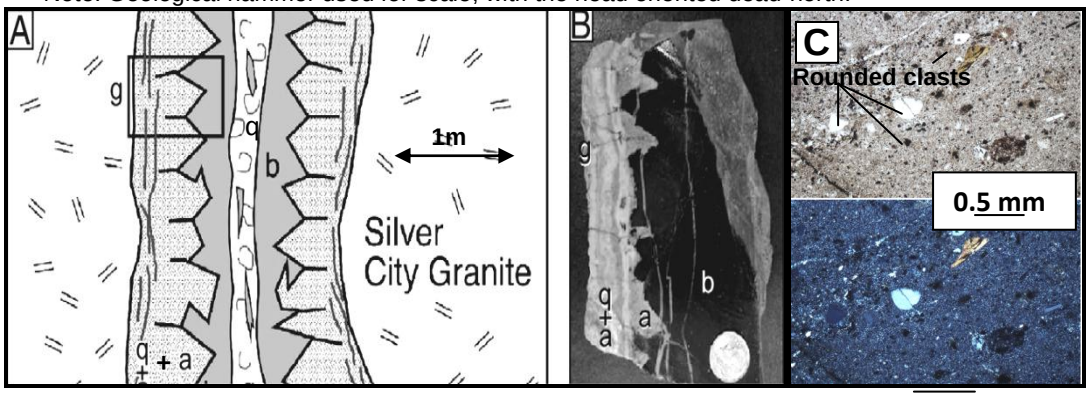

Fig. 26. An illustration of of a portion of the Orofino vein (after Hames et al., 2009) in cross section oriented N03°E90° showing the typical relationship between the dark apahnitic rhyolitic unit, the quartz vein (q+a,q), and the Silver City granite (g).Zoning within the vein includes quartz (q), adularia (a), aphanitic rhyolitic unit (b), and a central zone dominated by hydrothermal quartz (q). "q" forms the main part of the vein in figure 25 above. The vein in figure 26 is ~1 m wide where sampled as indicated by the box insert, but the size of adularia crystals in the sketch is exaggerated and not to scale. (B) Photograph of a slab cut from a piece of the vein (dime for scale) in the orientation and location schematically represented by the box in A. (C) Photomicrograph of the gouge? material in PPL above and XPL below. Note the high % of SiO_2. Photographs A & B are modified after Hames et al. (2009).

of 72% SiO_2 with “plated out” Cu and possible Au and Ag (Fig. 26; Bruseke, pers. commun., 2011). Previous publications erroneously referred to this lithological unit as a basaltic rock unit. Au and Ag assay values from this material are three times and five times higher respectively, when compared to the central part of the vein (Fig. 25).The higher Au, Ag assay values could be correlated to the following factors: (i) the altered quartz rich rock could be more chemically susceptible / receptive to mineralized hydrothermal fluid alteration. (ii) Competency contrast between the quartz vein and the hanging wall and footwall of the granitoid host rock helped to redirected mineralized fluids into the veins contact zone. This in addition to fracturing that produced the dark rhyolitic breccia clasts,(Fig 26, C) resulted in an increased porosity that provided preferred channels for mineralized fluid conveyance and entrapment.

Ore Petrography

This aspect of the study aimed to document mineralogical relationships within the Orofino and Poorman veins. Pure gold is rare. Gold mineralization is dominated by electrum (Au- Ag alloy) averaging 59.5:40.5 wt % for the Poorman vein and 53.4:46.6 wt % for the Orofino vein. Likewise native silver is rare (Piper and Laney, 1926) and was not encountered during this study. Silver minerals are generally Se-bearing and consist of a solid solution continuum of naumannite (Ag_2Se), aguilarite (Ag_4SeS) and acanthite (Ag_2S; Fig. 27). This study also indicated the presence of two or more (?) unknown silver selenide and sulfur mineral phases (Fig. 27) that are discussed below. A rare occurrence of fischesserite (Ag_3AuSe) was found in a sample (JAS-Au-10) collected from South Chariot dumps in the Orofino vein (Appendix 2). In addition, a ruby silver phase, tentatively identified as proustite (Ag_3AsS_3) was present in a sample from the Poorman vein (Appendix 2). However, a semi quantitative analysis (Appendix 2)

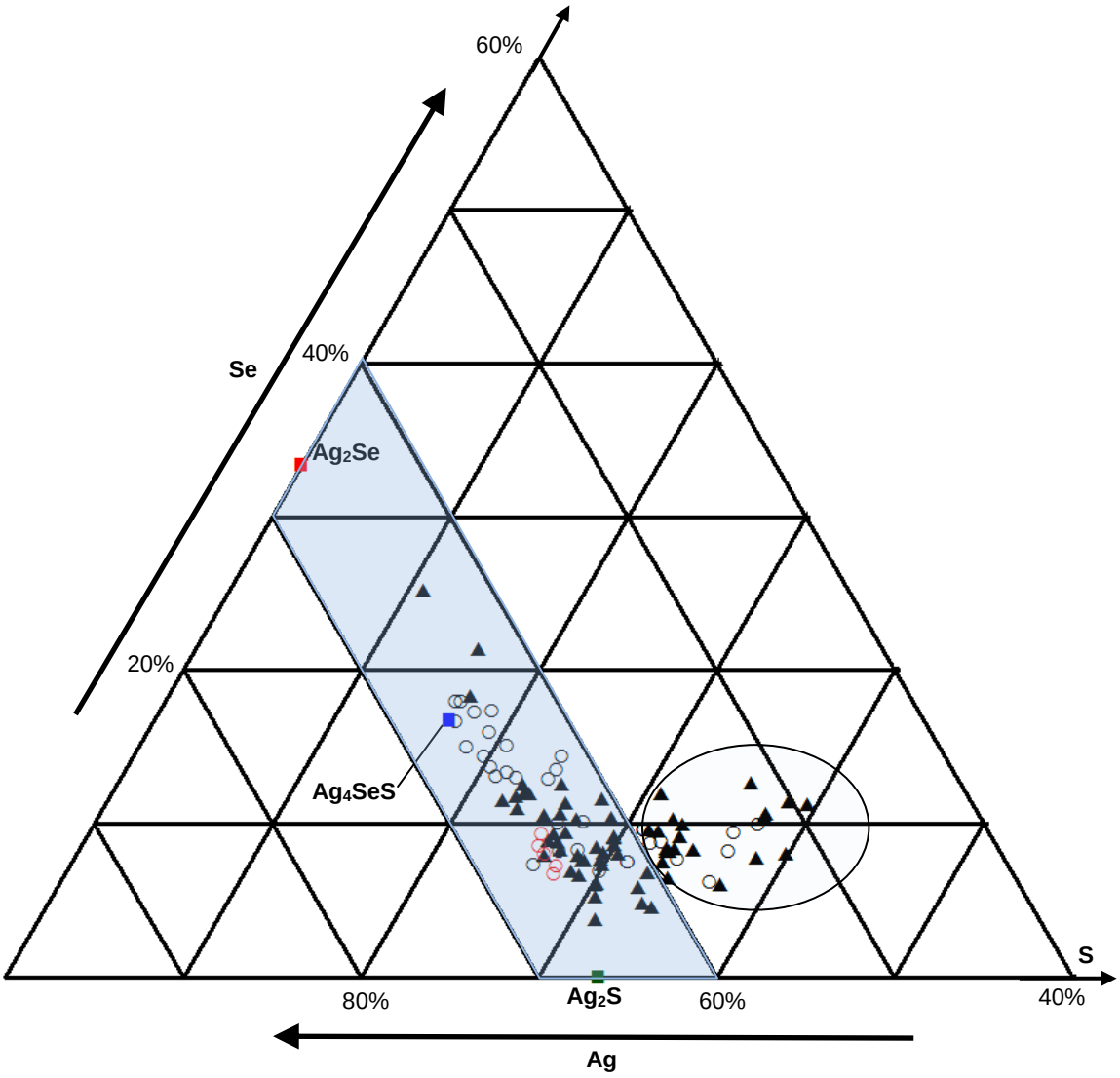

Fig . 27. Ternary diagram illustrating the chemical composition (in atomic %) of silver mineral phases for the Orofino vein (triangles), and the Poorman vein (open black circles) produced by SEM-EDAX analyses. Red circles denote microprobe data that was used as a comparable qualitative and quantitative standard. The blue shaded area consists of an interpreted solid solution continuum of naumannite (Ag_2Se), aguilarite (Ag_4SeS) and acanthite (Ag_2S) after Petruk et al. (1974). Complete solid solution between Ag_2Se and Ag_2S is known to exist above ca. 180°C (Sugaki et al., 1982). The minerals encompassed in the ellipse portend possible unknown (Ag, Se, S) mineral phase (or phases?).

indicates the phase is more likely billingsleyite (Ag_7As,S_6; Frondel and Honea, 1968). No antimony (Sb) sulfosalt minerals were encountered in any of the samples analyzed. Even so, miargyrite ($AgSbS_2$) was reported from material collected from the Henrietta mine (DeLamar) by Lindgren, (1900). Piper and Laney (1926) also reported occurrences of the same mineral in the Trade Dollar-Black Jack veins, and on Florida Mountain, in which it is massively inter-grown with pyrargyrite (Ag_3SbS_3).

Although the ores from the Poorman and Orofino are generally comparable, their ore assemblages show a distinct chemical variation. Based on the samples analyzed during this study, the Poorman vein generally shows Ag mineralization that is more similar in composition to aguilarite (Ag_4SeS) whereas the Orofino's is closer to arcanthite (Ag_2S) in composition (Fig. 27). However, according to Piper and Laney, (1923) arcanthite (Ag_2S) is comparatively much less abundant in the Orofino than the Poorman vein, and it is reportedly less common on War Eagle Mountain than on Florida and DeLamar Mountains. SEM analyses indicate that the unknown Ag-Se-S mineral phases encountered in this study are common to both veins in the study area (Fig. 27).

Petruk et al. (1974) universally characterized the quantitative end-members for acanthite (Ag_2S), aguilarite (Ag_4SeS), and naumannite (Ag_2Se). They utilized microprobe, x-ray diffraction, and etching with 10% KCN on silver selenide and sulfur minerals, to study: (i) naumannite (Ag_2Se), aguilarite (Ag_4SeS), and acanthite (Ag_2S) in a sample from Silver City, Idaho, (ii) acanthite (Ag_2S) and aguilarite (Ag_4SeS) in an ore suite from Guanajuato, México and (iii) a synthetic naumannite (Ag_2Se). They proposed the following compositional limits, which fall within the blue shaded region on figure 27 above: acanthite Ag_2S to $Ag_2S_{0.85}Se_{0.15}$; aguilarite $Ag_4S_{0.85}Se_{0.15}$ to $Ag_4S_{1.10}Se_{0.90}$; and naumannite Ag_2Se to $Ag_2S_{0.12}Se_{0.88}$. Complete solid solution between Ag_2Se and Ag_2S is known to exist above ca. 180°C (Sugaki et al., 1982).

SEM and microprobe analyses of the Ag mineral phases from War Eagle Mountain conducted in this study generally agree with Petruk et al. (1974) conclusion. Nevertheless, numerous mineral phases (Fig. 27) (Appendix 2) that are not consistent with Petruk et al. (1974) proposed end-members were encountered. However, crystallographic characterization of these potentially new mineral phases was beyond the scope of this study. Even so these findings provide for opportunities for detailed mineralogical studies in future.

Petrographic evidence shows that the Poorman vein contains much lower average base metal grades compared to the Orofino vein. Base metal sulfides present include pyrite (FeS_2), chalcopyrite ($CuFeS_2$), galena (PbS), and sphalerite (Zn,Fe)S (e.g. Fig. 28-29). These predominantly occur in spoil heaps in the southern portions of the Orofino vein. The southern parts of the Orofino vein are assumed to be analogous to the deeper parts of the epithermal system based on the elevation of mine workings and

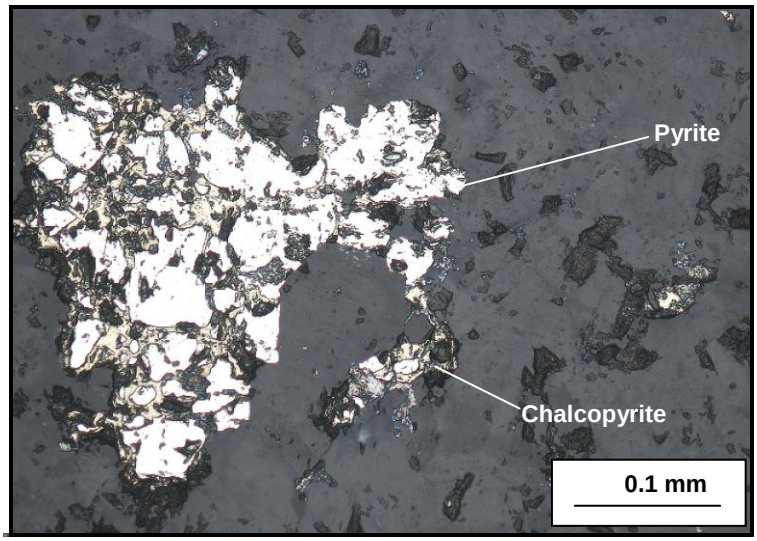

Fig . 28. Photomicrograph (reflected light) showing pyritic "islands" resulting from chalcopyrite replacement of pyrite. Sample : JAS Au- 7 (Orofino).

associated dumpsites. Metal sulfides therefore appear to be stratigraphically controlled

as their abundance tends to increase with depth. Their occurrence might be correlative to the deeper seated more saline liquid-dominated (Buchanan, 1981) areas of the epithermal system in the district. Correspondingly a decrease in Au was detected in these locales. This is consistent with separation of base and precious metals, with Au favoring the upper, boiling/gas-rich part of the epithermal system (Buchanan, 1981).

In both the Orofino and the Poorman viens, base metal assemblages predate coeval Au-Ag mineralization. The presence of “pyritic islands” rimmed by chalcopyrite confirms pyrite (FeS_2) to be the oldest/earliest hypogene sulfide (Fig. 28) and chalcopyrite ($CuFeS_2$) to be a later stage primary mineral. A late stage pyrite phase that coats younger minerals, indicating that it is also a much later mineral is also evident and has also been previously reported by Piper and Laney (1926). Galena appears to be rimmed by “naummanite” and chalcopyrite (Fig. 29) indicating that it is an earlier mineral than the latter two.

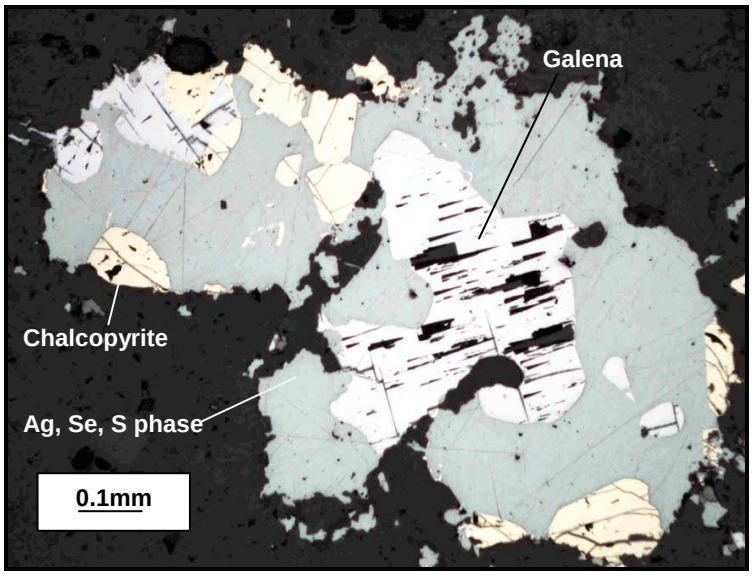

Fig. 29. Photomicrograph (reflected light) showing galena rimmed by chalcopyrite and “naumannite”. Sample: WEMBU (Orofino).

Free electrum and silver-selenide ± sulfur derivatives occur both as blebs (primary) and elongate (secondary?) impregnations (Fig. 30). In the first form, ore

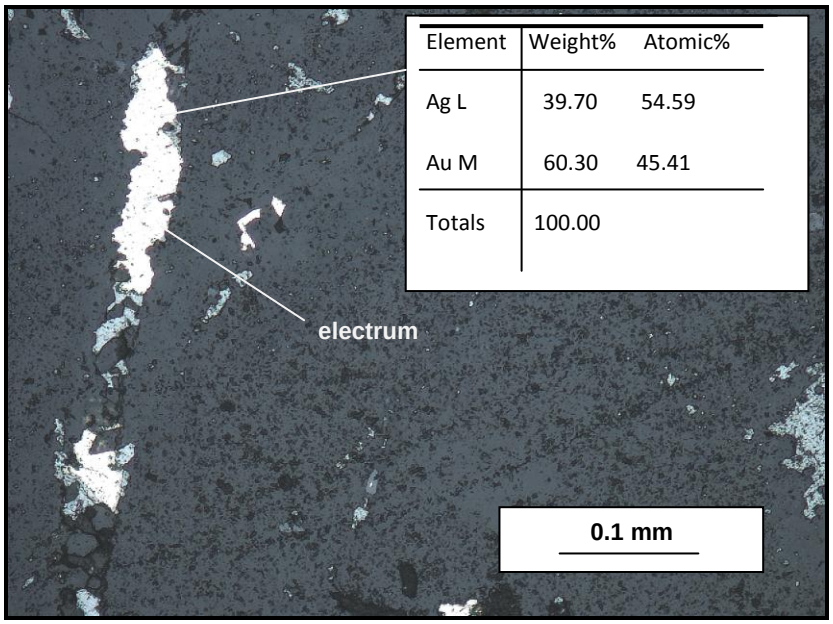

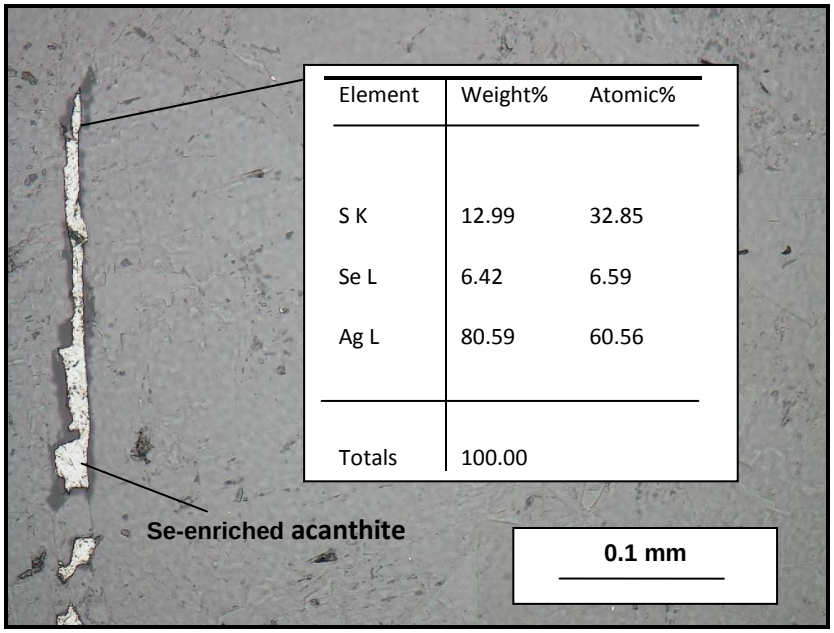

Fig. 30. Photomicrograph (reflected light) showing elongate electrum vein mineralization (Sample: JAS Au-8, Poorman) above and selenium enriched acanthite, below in (Sample: OF-1, Orofino) infilling interstitial spaces. (Notice how electrum is much brighter when compared to the contiguous silver phases in the image above). SEM-EDAX qualitative probe results are appended to the right of each image.

textures range from fine grained disseminations to medium and course grained blebs. In the second form, both electrum, and a selenium-enriched acanthite phase uniquely in-fill elongate interstitial spaces in quartz veins indicating that they must have precipitated after vein formation and are therefore later-stage (Fig. 30). This was recognized in a Poorman North Shaft sample (electrum) and Orofino sample (selenide enriched acanthite).

Textural cross cutting relationships of samples from the War Eagle Mountain indicate early base metal hypogene sulfides superseded by later precious metal minerals. This is consistent with observations reported for other low sulfidation epithermal deposits in the northern Great Basin such as the National district (Vikre, 1985) Midas deposit (Goldstrand and Schmidt, 2000) and Koryu in Japan (Shimizu et al., 1998). Based on microscopic observation the paragenetic sequence of the mineralization is summarized in Table 1.

Stage / Mineral	Early	Main	Late
Quartz	———	———	—— ——
Adularia	- - - - - - - - - - - - - - - - - - - -		
Calcite	- - - - - - - - - - - - - - - - - - - -		
Pyrite	———	- - - - - - - - - - - - - - - - - - - -	
Sphalerite	- - - - - - - - - - - - - - - - - -		
Galena	———	- - - - - - - - - - - - - - - - - - - -	
Chalcopyrite	———	- - - - - - - - - - - - - - - - - -	
Electrum		———	- - - - - - - - - - - -
Naumanite		———	- - - - - - - - - - - -

Table 1. Paragenetic sequence of vein and ore minerals at the War Eagle Mountain. Dashed lines indicate approximate timings of mineral formation with some uncertainty.

At least 3 different mineralization stages can be distinguished. (i) the early stage, (ii) Au-Ag main precipitation stage and (iii) a late recrystalisation/remobilization stage. The early stage is characterized by the formation of gangue/vein minerals prior to

emplacement of gold and silver minerals. The first sulfides assemblage that forms coeval? or immediately after this stage consist of euhedral and anhedral pyrite crystals occurring as isolated grains ranging in size from fine to course grained aggregates. This is subsequently followed by accessory sphalerite. Chalcopyrite, the dominant sulfide mineral at the War Eagle Mountain precipitates later than pyrite, sphalerite and galena. The Au-Ag main precipitation stage constitutes the second mineralization pulse(s) and is characterized by the interstitial in-filling of crystalline voids by Au and Ag minerals and some addition of metal sulfides? The final mineralization episode displays replacement textures where some older sulfides (e.g. chalcopyrite) are remobilized and rim precious metal phases. Anhedral inclusions of “chalcopyrite disease” in sphalerite (Barton and Bethke, 1986) observed in specimen (WEMBU 3; Fig. 31) are also associated with this stage.

Remobilized / secondary Au and Ag minerals infill elongate grain boundaries (Fig. 30) and microfractures and in some instances replace early base metal phases.

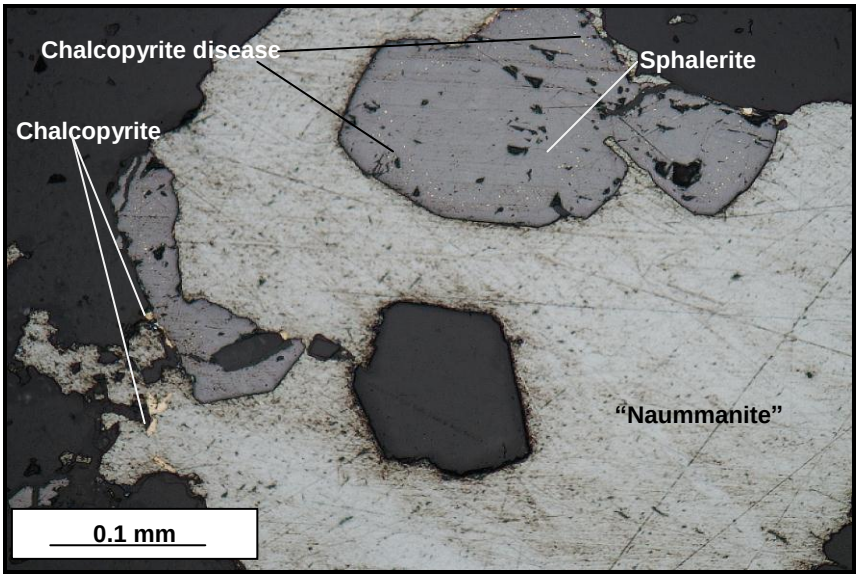

Fig. 31. Photomicrograph (reflected light) showing sphalerite rimmed by “naumannite”. Chalcopyrite replaces both “naumannite” and sphalerite. Notice the anhedral chalcopyrite inclusions of “chalcopyrite disease” along the rim of sphalerite. Sample: WEMBU, Orofino.

5. GEOCHEMISTRY

Statistical Analysis (*ICP-MS)*

The most prominent geochemical characteristic of the Silver City ores is the very high total content of selenium relative to tellurium (Appendix 1). Comparatively most samples exhibit values of selenium with up to 2 orders of magnitude higher than tellurium.

Au/Ag end-member ratios for samples analyzed from War Eagle Mountain vary widely within the two deposits. For example, a high grade sample (CMT014) collected proximal to the Poorman vein produced a relatively low Au to Ag ratio of 1:1.16, while another collected from the Orofino vein (CMT035) produced a higher ratio of 1: 121.67. Two factors have been proposed to influence such a significant variance in epithermal deposits: (i) differing magmatic metal budgets (Sillitoe, 1993), and (ii) the depths of ore formation (Hayba et al., 1985). As a result relative ratios of measured Au and Ag levels can be used as a reliable tool to aid in characterizing the Au-Ag mineral chemical specifics for a district. For example, generally, low-sulfidation epithermal systems tend to have higher Ag to Au ratios than high-sulfidation epithermal deposits (Taylor, 2007).

The assay results of the bulk mine dump sampling survey conducted at the Orofino and Poorman mines show a Au/Ag ratio (1:13.36) that may serve as a good indicator of the Au/Ag mineralization allocation specifics for the area (Table 2). This value is consistent with the Au/Ag ratio for the channel sample collected on the Orofino vein (Fig. 25) between interval 0.3 m and 2.13 m which produced a Au/Ag ratio of 1:13.77. Data obtained from DeLamar's 21 year bulk mine operation indicate that the Au/Ag ratio was 1:63 (Gillerman and Mitchell, 2005). However, calculations carried out

Name of Dump	Grade		Tons	Cumulative Tonnage	Average Grade		Vein
	Ag oz/t	Au oz/t			Ag oz/t	Au oz/t	
Orofino	1.14	0.304	2482	2482	1.44	0.304	Orofino
War Eagle South Dump	1.72	0.202	2113	4595	1.56	0.256	Poorman
Stormy Hill	3.46	0.144	750	5345	1.83	0.24	Poorman
Illinois Central	1.11	0.088	3000	8345	1.57	0.185	Poorman
War Eagle North Dump	1.27	0.086	3340	11685	1.48	0.157	Poorman
Cumberland	1.14	0.08	3569	15254	1.4	0.139	Orofino
Empire	1.78	0.077	8924	24178	1.54	0.116	Poorman
War Eagle East Dump	1.04	0.06	514	24692	1.53	0.115	Poorman
Silver Cord	0.34	0.058	1765	26457	1.45	0.111	Poorman
Oso	0.62	0.038	6235	32692	1.29	0.97	Poorman
Poorman South Shaft	0.42	0.018	3086	35778	1.21	0.9	Poorman
Belle Peck I	0.28	0.018	19337	55115	0.88	0.065	Poorman
Belle Peck II	0.13	0.014	7595	62710	0.79	0.058	Poorman
Poorman North Shaft	0.55	0.006	1552	**64262**	**0.79**	**0.057**	Poorman

	Grade	
	Ag oz/t	Au oz/t
Weighted Average	**0.79**	**0.057**

Table 2. A summary of the bulk sampling program carried out for War Eagle Resources Ltd by Pamicon Development Ltd (Paterson, 1991) to test the viability of extracting precious-metals from mine tailings. Tabulated results for each dump site and average grade for each mine dump are indicated.

by independent mining consultants in 1991 (Marek, 1991) document mill ore reserve Au/Ag ratios for DeLamar mine that vary as follows: 1:73.5 for GlenSilver, 1: 184 for Sommercamp-Regan, and 1:43.1 for South Wahl. Data obtained from the Florida Mountains ore resource calculations indicate Au/Ag ratios of 1:10 at Tip Top, 1:11 at Stone Cabin-Sullivan, 1:80 at Black Jack Alpine and 1:4 at Clark. Base metal values are generally low.

Pearsons coefficient correlation matrix

A summary of linear correlations determined for every pair of elements selected from Au, Mo, Cu, Pb, Zn, Ag, As, Sb, Cr, Ba, Hg, Se, Te, and K is shown by the matrix in Table 3 below. Gold displays a strong positive correlation to zinc, silver, mercury, and selenium but exhibits a strong negative correspondence with potassium (Table 3). Likewise silver is best associated with zinc, gold, and selenium. On the other hand copper is best correlated with lead, chromium and tellurium, but shows a poor association with gold, silver and zinc. It is therefore apparent that the most favorable geochemical indicator of a potential epithermal Au/Ag mineralization system in this area would be a coincident gold, silver, zinc, mercury and selenium geochemical anomaly.

The strong correlation between gold and mercury is expected because it not only commonly occurs with Au±(Ag) in low sulfidation epithermal deposits, but is usually a diagnostic pathfinder of the same (Taylor, 2007; Vikre, 2007b). Tetrahedrite ($(Cu,Fe,Zn,Ag)_{12}Sb_4S_{13}$) (not seen in this study but reported previously by Piper and Laney, 1926) sphalerite [(Zn,Fe)S], or Cu,Au,Ag_4Zn may bring forth the strong correlation between Zn and both Au and Ag. This is because all the major elements required to form the three constituent minerals are available in this mineralization system. The strong correlation between silver and gold is predictable because electrum

	Mo (ppm)	Cu (ppm)	Pb (ppm)	Zn (ppm)	Ag (ppm)	As (ppm)	Sb (ppm)	Cr (ppm)	Ba (ppm)	Hg (ppm)	Se (ppm)	Te (ppm)	K (ppm)
Au (ppm)	-0.0641	0.0598	0.2924	**0.757**	**0.7823**	-0.146	0.3969	0.3393	-0.3959	**0.4668**	**0.7242**	0.149	**-0.7456**
Mo (ppm)		0.2209	0.1197	0.0749821	0.048	0.3439	-0.0886	0.0628	0.1463	-0.12	-0.0056	0.1405	**0.4245**
Cu (ppm)			**0.9057**	0.1841	0.07283	0.0969	0.0908	**0.4997**	0.04847	0.105	0.3196	**0.9467**	0.0949
Pb (ppm)				0.03662	0.02228	-0.1062	0.2129	**0.54**	0.0809	0.2117	**0.453**	**0.9482**	-0.049
Zn (ppm)					**0.8424**	-0.0878	0.301	0.01675	-0.2047	**0.4023**	**0.86319**	0.1877	-0.1341
Ag (ppm)						-0.1376	0.06995	-0.0443	-0.23	0.24089	**0.8438**	0.13176	-0.2027
As (ppm)							0.04314	-0.13724	0.23256	-0.10014	-0.1801	0.09621	0.368
Sb (ppm)								0.389	-0.2223	**0.9236**	0.1333	-0.07915	-0.30331
Cr (ppm)									-0.1227	0.27117	0.1491	**0.4801**	**-0.5053**
Ba (ppm)										-0.3191	-0.2028	-0.0323	**0.5974754**
Hg (ppm)											0.218	-0.0694	-0.2986
Se (ppm)												0.3424	-0.0682
Te (ppm)													-0.0238

Table 3. Pearsons coefficient correlation table for selected elements analyzed by ICP-MS in this study and after Unger, (2008). Significant correlations are in bold.

is a major constituent of the gold-silver veins on War Eagle Mountain. Similarly the strong correlation between Ag and Se is a product of the ubiquitous Ag-Se-S mineral phases that are important in the district.

In retrospect, though ICP-MS proved useful for assigning assay values for most elements in the high-grade ores used in this study, it could not accommodate elevated values for Ag and Se given the low upper detection limits for these elements using the technique. Both Ag and Se had a relatively low upper detection limit of only 100ppm. However, final results for this study were enhanced by ICP-MS assay data from Unger (2008), and further complemented by Au and Ag fire assay results from the bulk geochemistry sampling program conducted by Pamicon Resources Ltd (Yeager et al., 1984; Peterson, 1991). When combined together the data proved useful in understanding the geochemistry of the area.

Fluid Inclusion Analyses

The data presented herein are used to estimate approximate crystallization temperatures of the Poorman and Orofino veins. However, temperature ranges and salinities produced in this study are reconnaissance in nature and thus are a preliminary guide that could complement future detailed studies.

The fluid inclusion study of the Orofino and Poorman veins revealed low salinity fluids with homogenization temperatures of 160°C-205°C for the Orofino, and 180°C-255°C for the Poorman vein. Additionally a few values of 220°C-225°C and 250°C-255°C were recorded for the Orofino. Similarly less frequent values ranging from 275°C-285°C were recorded for the Poorman vein. Microthermometry data was obtained from primary, secondary and pseudo-secondary fluid inclusions consisting of equal or near equal liquid-vapour phases (Fig. 32-33). Fluid inclusions are randomly distributed with the majority of them having elliptical or elongate shapes. Homogenization occurs

predominantly to the vapor phase. Melting temperatures were obtained amongst the same inclusions. Generally the measured eutectic temperatures for both veins range from -6.5°C to -1.1°C. Ice from the Orofino melted between -0.9°C to -0.1°C, with the Poorman Vein recording melting temperatures of between -1.9°C to 0.1°C. These temperatures are consistent with salinities of 0.5-1 wt% NaCl equivalent. A summary of homogenization temperatures and melting temperatures is presented in Table 4 and (Fig. 34-35).

Sample Number	Vein	Ice Melting Temp °C
CMT002 chip 6	Orofino/Cumberland Mill	-0.1°, -0.3°
CMT003 chip 5	Orofino/South Chariot	-0.5°, -0.9°
CMT043 chip 12	Poorman/ War Eagle Shaft	-1°, -1.9°, -0.9°
CMT045 chip 13	Poorman/ Poorman N. Shaft	-0.3°, 0.1°

Table 4. A summary of melting temperatures carried out in this study.

Spectral analytical counts that sought to detect entrained mineralized fluids revealed no precious metals from the mineralized quartz vein (CMT016). However, 2 dilute fluid types, one a Ca-Na enriched, and the other a K enriched fluid type, were identified. Out of 17 inclusions decrepitated, 16 had a K signature while only 1 had a Ca-Na signature. Traces of Li and Sb were contained in the quartz vein. Despite standards being analyzed with the tested inclusions, further data reduction was not conducted since the counts exclusively contained K, or Na and Ca (Hofstra, pers. commun., 2010).

It appears that the large inclusions trapped in crystalline quartz are not ore stage but meteoric in nature. It is therefore likely that two distinct fluids comprising ascending aqueous magmatic vapors/solid-state transport media, (from degassing magmas) and descending meteoric waters identified herein, contribute to the formation of this Au-Ag epithermal deposit.

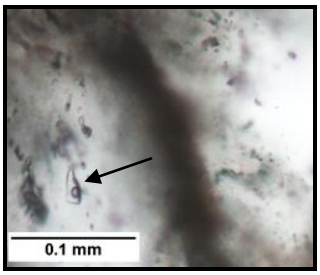

CMT021-2 Chip 3

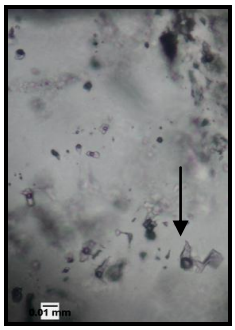

CMT021-3a Chip 4

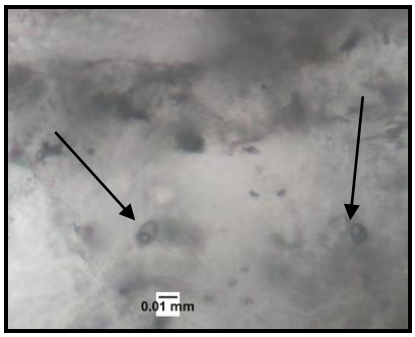

CMT021-3b Chip 4

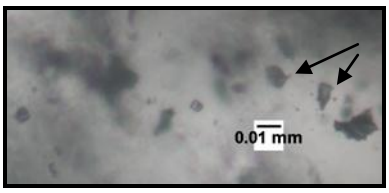

CMT043 Chip 9

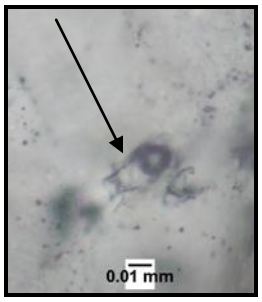

CMT045 Chip 10

CMT045 b, c, Chip 13

CMT 016-b Chip 15

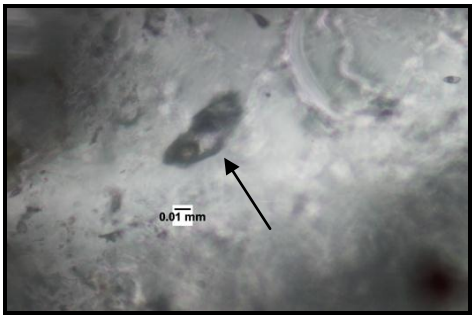

CMT045-a Chip 13

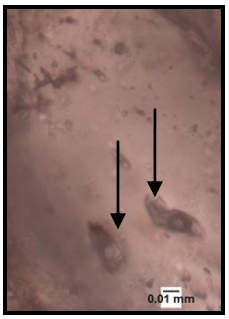

CMT043 Chip 12

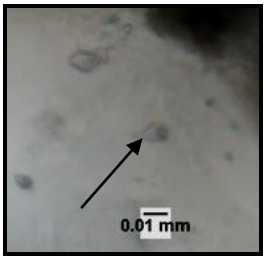

CMT016 Chip 19

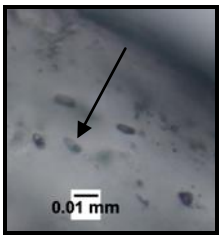

CMT045 Chip 7

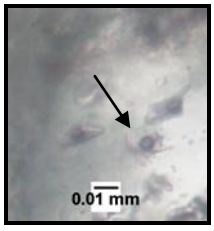

CMT016 Chip 8

FIG. 32. Photomicrographs of fluid inclusions analyzed from the Poorman vein. Arrows point at some examples of fluid inclusions analyzed (0.01mm = µ10).

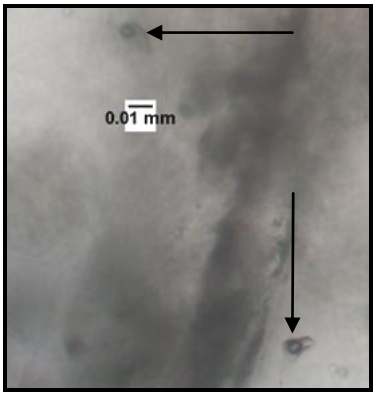

CMT003-a Chip 14

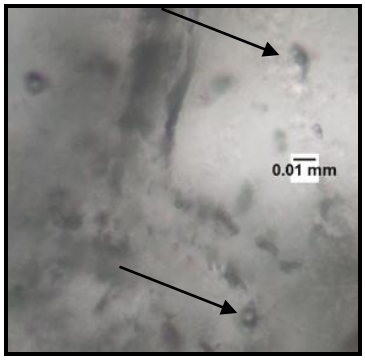

CMT003-b Chip 14

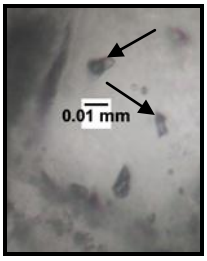

CMT003-c,d Chip 14

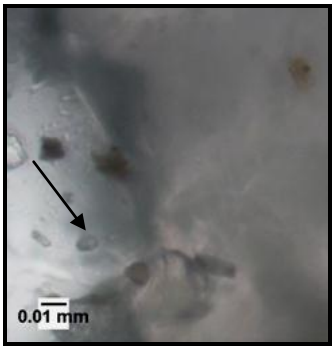

CMT002 Chip 6

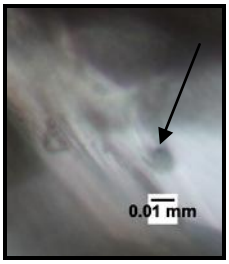

Orofino Top Chip 18

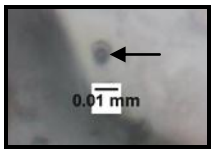

Orofino Top A Chip16

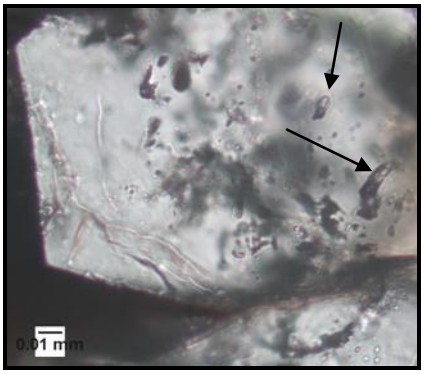

CMT003 Chip 5

FIG. 33. Photomicrographs of fluid inclusions analyzed from the Orofino vein. Arrows point at some examples of fluid inclusions analyzed (0.01mm = µ10).

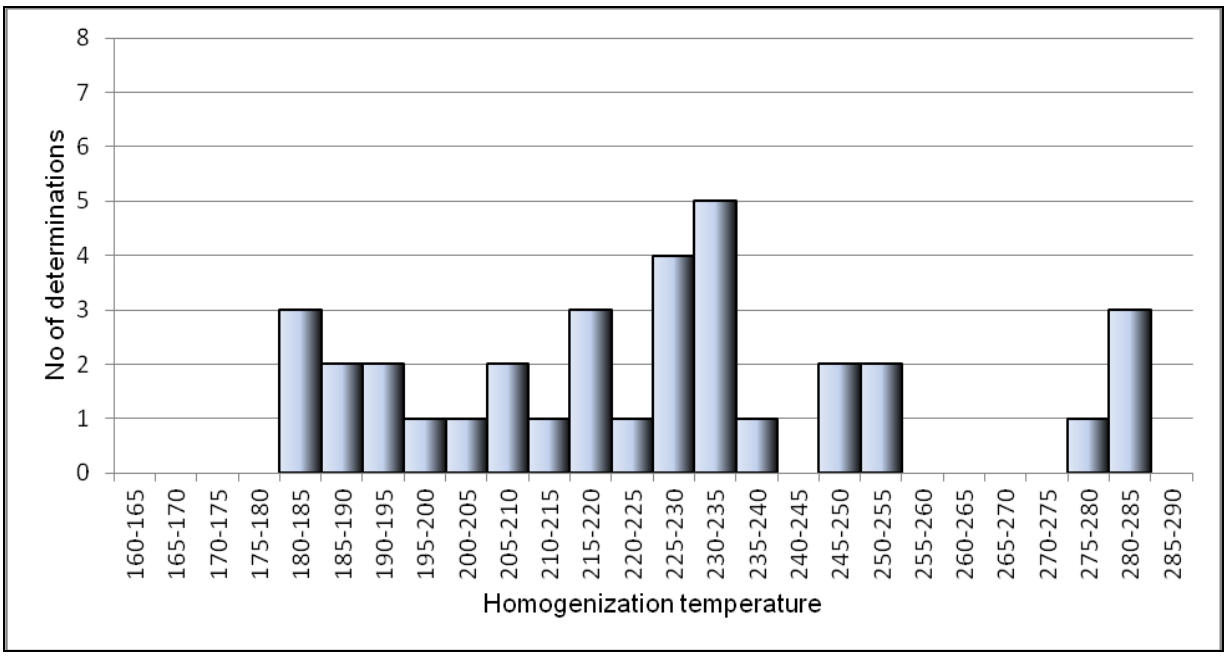

Fig. 34. Histogram of homogenization temparatures (°C) for the Poorman vein. (n=34).

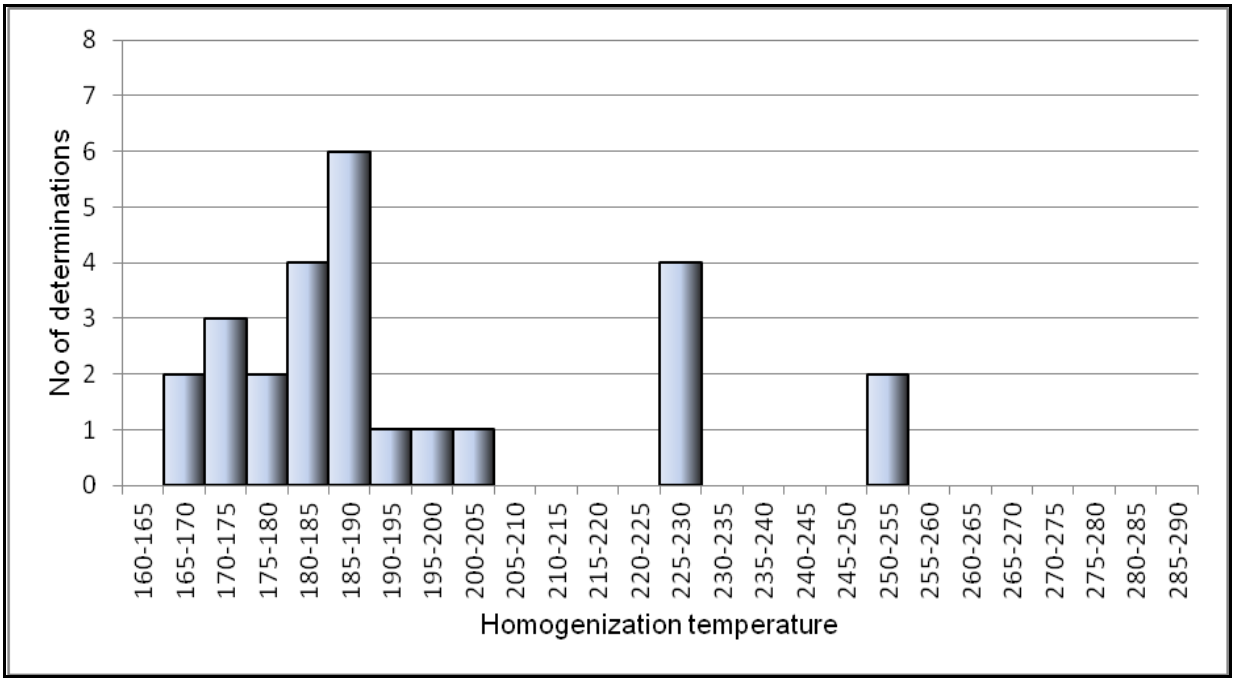

Fig. 35. Histogram of homogenization temparatures (°C) for the Orofino vein. (n=26).

Pb Isotope Studies

Hanan et al. (2008) reported that Pb isotopic compositions of the earliest volcanism in Columbia River basalts and Steens basalts (Fig. 36) are consistent with a primitive mantle-plume origin. In contrast basalts from the Snake River Plain (SRP), i.e the Idaho National Laboratory (INL) core WO-2, Bruneau-Jarbidge (B-J), and Glenns Ferry lavas (GF), were demonstrated to have a more evolved Pb signature superimposed by interaction with subcontinental lithospheric mantle (SCLM; Hanan et al., 2008).

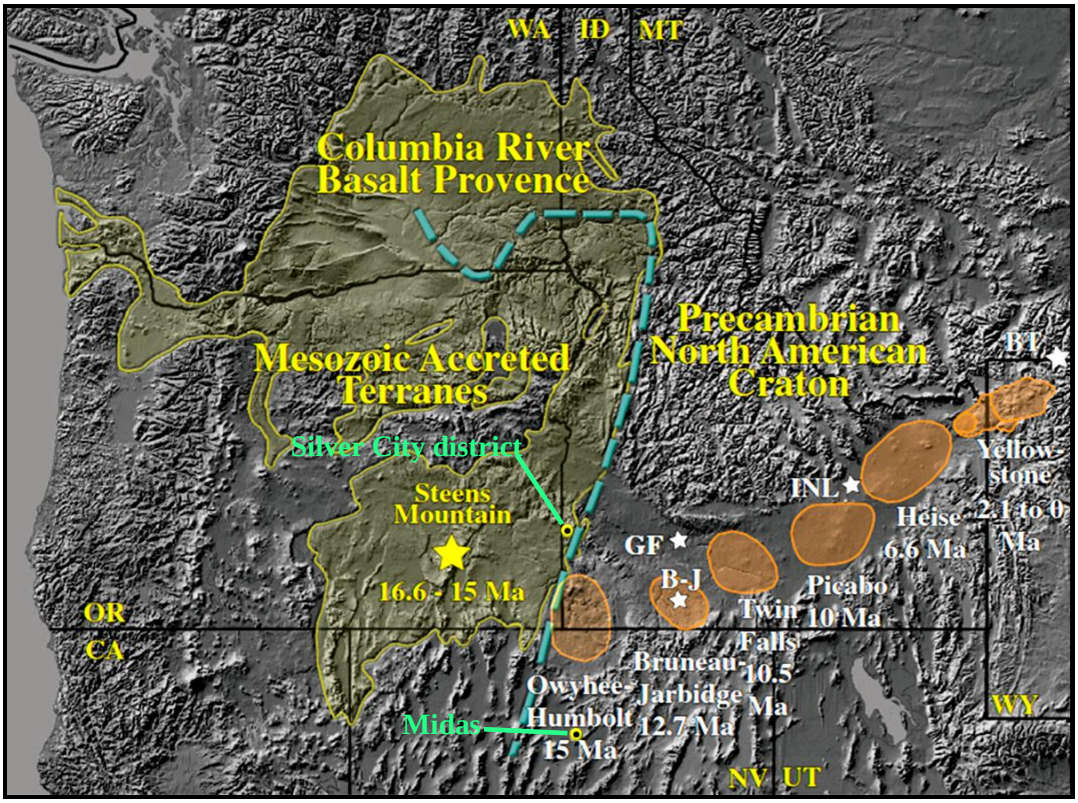

Fig. 36. Shaded relief map of Pacific Northwest modified after Camp and Ross, (2004). The Blue dashed line defines the boundary between Mesozoic–Paleozoic accreted terrains and Precambrian North American craton. Silver City district and Midas Mine are indicated relative to this boundary. Locations are shown for the Idaho National Laboratory (INL) core WO-2, Bruneau-Jarbidge (B-J), Glenns Ferry lavas (GF), and the Bear tooth Mountains (BT). The Snake River Plain and Yellowstone Plateau volcanic centers with approximate ages are shown in orange. The Columbia River Basalt Group is shown in yellow (Hanan et al., 2008).

The blue boundary in Figure 36 defines the eastern and western limits of the Mesozoic-Paleozoic accreted terranes, and Precambrian North American Craton respectively. Areas to the east of this boundary have been demonstrated to correspond to a thicker cratonic lithosphere, while those to the west are correlated to a thinner crust (Hanan et al., 2008). Typically $^{207}Pb/^{204}Pb$ and $^{206}Pb/^{204}Pb$ isotopic signatures in a thicker continental mantle lithosphere are generally accepted to be higher than plume sources as they are products of increasing degrees of crustal contamination (Faure, 1977). This phenomenon could explain the progressive enhancement of crustal signatures in Columbia River basalts, Snake River Plain basalts and Yellowstone basalts from west to east (Fig. 37; Hanan et al., 2008).

Trace Pb isotope ratios detected in electrum grains were compared to possible sources of lead in the northern Great Basin, to help constrain the origin of epithermal Au mineralization in the Silver City district. A summary of the results of insitu Pb isotope analyses are presented in Figures 37-38. Error brackets indicated for all samples are generally small (<1‰) excluding the Orofino gold sample with the outsized error bar located to the right of the scattergram (Fig. 38). This implies high analytical precision, reproducibility, and isotopic heterogeneity on the grain scale for the samples analysed. No Pb isotope data could be measured for the heavy pan concentrate made from crushing high-grade naumannite ore (CMT003).

Felsic and gangue minerals display the most evolved $^{207}Pb/^{204}Pb$ fingerprint in this study's data set (Figs. 37-38). This is consistent with the hydrothermal leaching of lead from crustal sources. Mafic lavas analyzed from the summit of War Eagle Mountain yielded a strong primitive plume signature, with trace Pb alloyed with mid-Miocene gold ores extending from this trend (Figs. 37-38).

An equal spread of lead isotopes alloyed with Au plot in the mixing zone between

the (INL), (B-J), (GF) and the plume (Figs. 37-38). This trend defines a quasi-linear continuum that mimics the Pb Isotopic tendencies observed by Hanan et al. (2008) for the Snake River plain volcanics. Hanan et al. (2008) reported that the trend in the Snake River mafic volcanics is controlled by mafic plume melts interacting with local subcontinental lithospheric mantle (SCLM). In a similar fashion Figure 38 illustrates that >99% of the isotopic composition of Pb alloyed with gold appears to have been derived from mafic plume-related melts that interacted to some extent with the SCLM. However, the interaction is notably to a lower extent compared to the Snake River plain basalts (Figs. 37-38). This could be due to the following reasons:

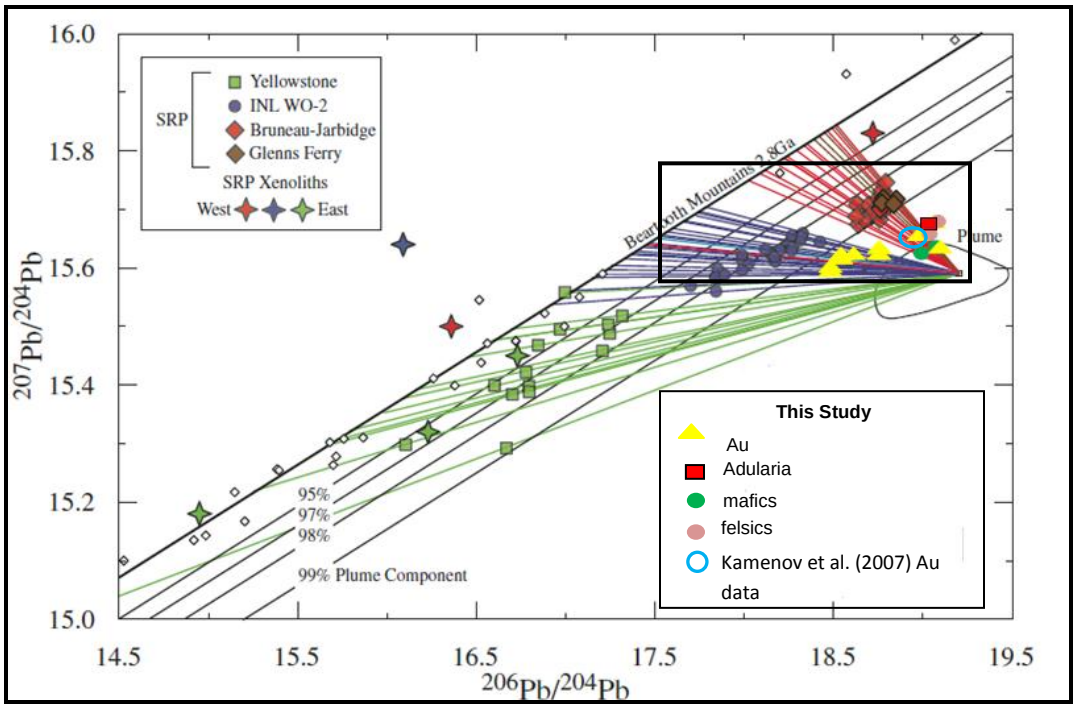

Fig. 37. Scattergram modified after Hanan et al. (2008) that displays Pb ratios for Idaho National Laboratory (ILN) basalts, Bruneau Jarbidge (BJG) basalts and the the 2.8 Ga reference isochron for Beartooth Mountains mafic igneous rocks that represent Pb isotope composition of lithosphere underlying Yellowstone Plateau and Snake River Plain (SRP) after Wooden and Mueller (1988). The plume component is represented by the black poly-line field for the Columbia River Steens basalts and Stonyford Volcanic Complex labeled Plume; (Camp and Hanan, 2008; Shervais et al., 2005). Mixing tie lines between average plume and distinct lithospheric Pb reservoirs along the Beartooth isochron for Snake River Plain and Yellowstone Plateau Basalts are represented by Red, brown, blue, and green lines (Hanan et al. 2008). The proportion of the plume component in basalt mixes is indicated where Solid lines labeled 95%–99% intersect the tie lines (Hanan et al., 2008). Insert area is displayed in detail in Figure 38. Au shows a broad trend of Pb isotopic ratios that mimics Hanan et al. (2008) data.

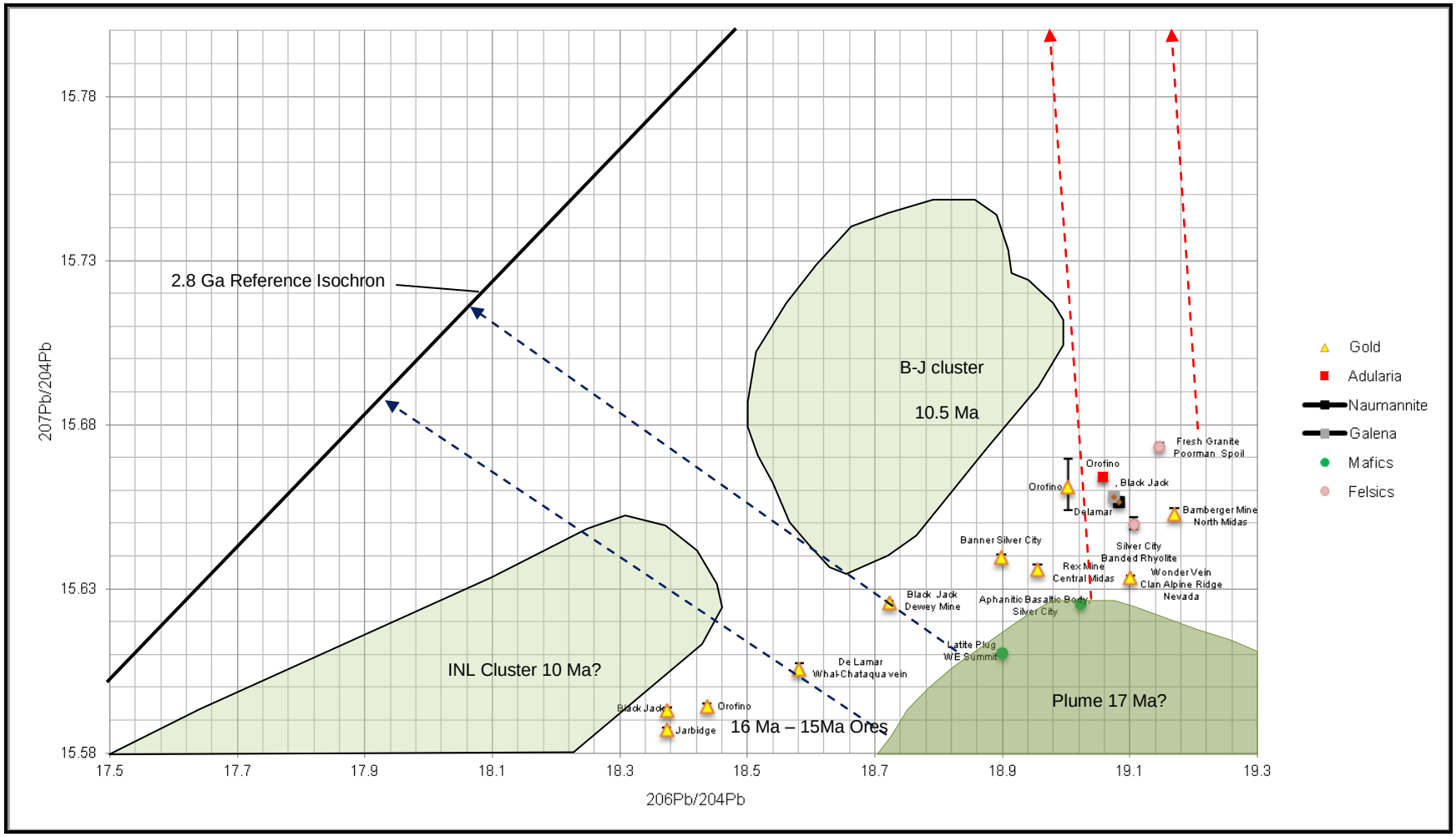

Fig. 38. Close-up of Figure 37 insert that displays Pb ratios for Idaho National Laboratory (ILN) basalts, Bruneau Jarbidge (BJG) and the 2.8 Ga reference isochron . Bold dash arrows indicate paths for contamination for Pb, after Hanan et al. (2008). Au shows a broad trend of Pb isotopic ratios that mimics Hanan et al. (2008) data.

(i) there was a thinner crust available for interaction with mafic magmatic melts (circa 15 Ma) at the time of eruption (Fig. 36). Lithospheric thinning has been shown to enable magmatic melts to be extruded with a more primitive isotopic signature (e.g. Fitton et al., 1991) or (ii) at the time of Au precipitation, mafic magmas were most primitive/plume-like as the embryonic Yellowstone hotspot magmatism event had just been initiated.

The similarity of isotopic composition for Pb alloyed with gold to Pb signatures in mafic magmas, and the inferred plume, indicates that mafic magmas are the most likely source for Au mineralization. Conversely the disparate Pb isotopic signature of Au samples, from Silver compared to felsic rocks in the district implies that Au is not likely to have been sourced from the Cretaceous granite or the mid-Miocene rhyolites. Kamenov et al. (2007) reported Pb isotopic compositions of mafic lavas and Au that are consistent with the data presented above (Fig. 37-38). Collectively these data point to Au ores derived from a primitive mantle source.

6. GEOCHRONOLOGY

15 samples were incrementally step heated with 12 of these also undergoing single crystal total fusions at Auburn University's ANIMAL facility. Figure 39 illustrates the spatial spread of preferred $^{40}Ar/^{39}Ar$ age dates (this study) that is compared to a composite summary of epithermal Au/Ag mineralization age dates in the northern Great Basin presented in Table 5. Incremental heating release spectrum and plateau age charts as well as single crustal probability charts are presented in Figures 40 to 52. Figure 53 illustrates a composite probability chart that combines this study's data set and geochronological data from previous studies in the northern Great Basin.

Previous studies have demonstrated that discrete adularia crystal ages from the same sample can yield ages varying by up to 0.5 Ma, given the disparate amounts of extraneous argon and loss of radiogenic argon from each grain (Hames et al., 2009). The analyses carried out in this research are precise and accurate as they are highly radiogenic (atmospheric ^{36}Ar contamination was minimal). Plateau increments were defined by a value greater than at least 60% of the total $^{39}Ar_K$ released (most of the plateau results were defined by $^{39}Ar_K$ greater than 90%; Fig. 40-48). No excess argon was detected in any of the samples analyzed.

CO_2 laser probe $^{40}Ar/^{39}Ar$ analyses dated crystallization ages of a rhyolite (Sample MB07) collected from spoil at the Blackjack mine at 15.940±0.097 Ma. A basalt sample collected from Florida Mountain produced an age of 16.1 Ma (Hames, pers. commun., 2011). Adularia (sample NV-08-09) from the same locale as the 2 samples cited above was dated at 15.579±0.063 Ma. Comparable age dates ranging from (16.076 ± 0.080 to 15.367 ± 0.061 Ma) were calculated for adularia from the rest of the district (Figs. 39; 40-48). These sample results are discussed below in detail:

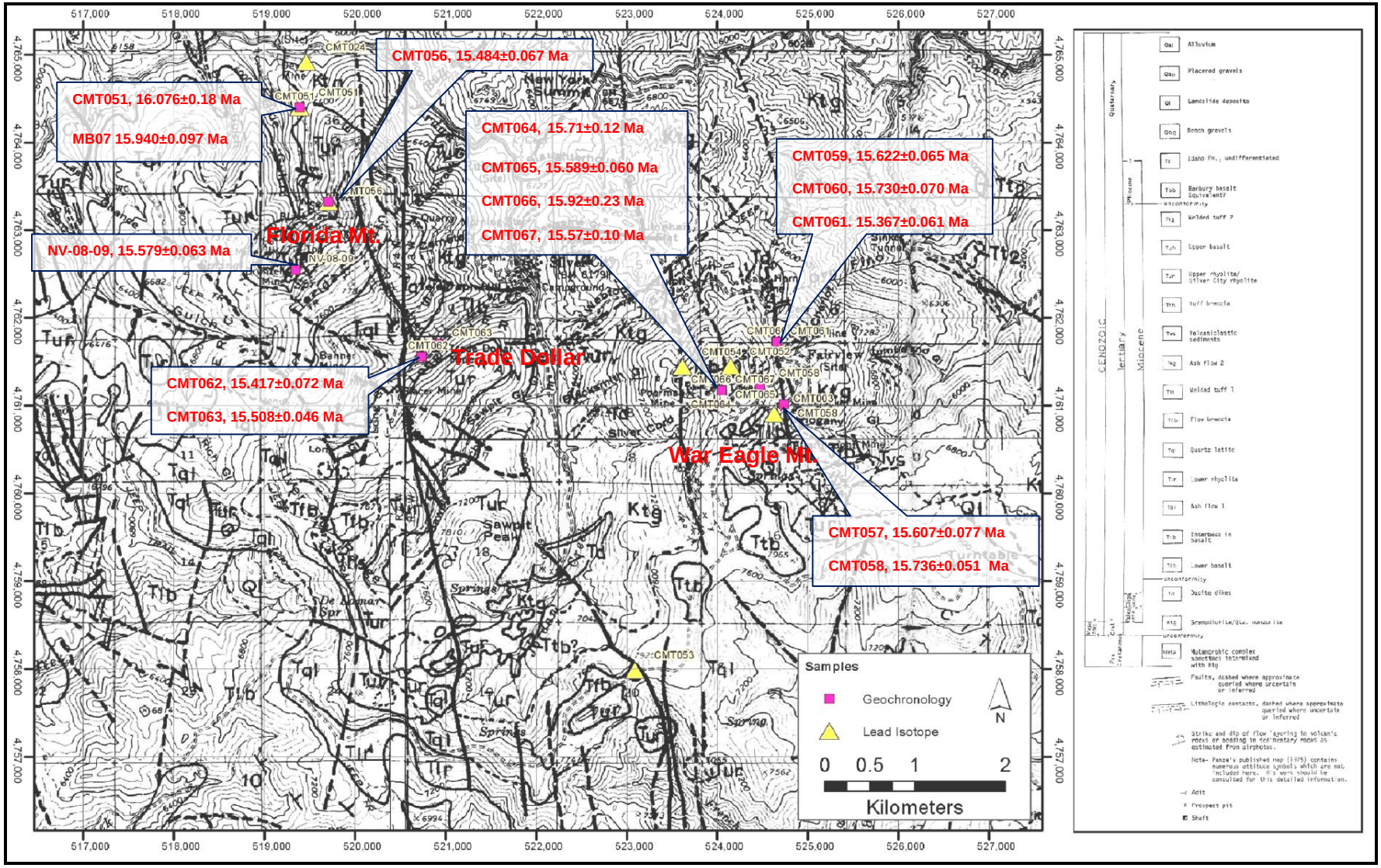

Fig. 39. Map with call outs showing prefered $^{39}Ar/^{40}Ar$ age dates for the Silver City district. Refer to Figure 10 for stratgraphic details. See sample description details and data for single crystal total fusion and incremental heating in appendices 1 and 3 respectively. Map modified after Bennet and Galbraith (1975).

Deposit	Age ± 1σ (Ma)	Method	Host Rocks	Reference
Jumbo	17.3 ± 0.5	K/Ar	metasediments	Conrad et al., 1993
War Eagle Mtn	16.6-15.2	K/Ar	granite	Panze, 1975
Jumbo	16.53 ± 0.04	Ar/Ar	metasediments	Unger, 2008
Ten Mile	16.52 ± 0.04	Ar/Ar	metasediments	Unger, 2008
War Eagle Mtn	16.31 ± 0.04	Ar/Ar	granite	Unger, 2008
Sandman	16.17 ± 0.04	Ar/Ar	granite	Unger, 2008
Sleeper	16.1-14.3 ± 0.07	Ar/Ar	rhyolite	Conrad and McKee, 1996
New Alma	16.03 ± 0.03	Ar/Ar	metasediments	Unger, 2008
Buckskin National	15.8-15.4 ± 0.2	K/Ar	rhyolite	Vikre, 1985
DeLamar, ID	15.7 ± 0.5	K/Ar	rhyolite	Panze, 1975
War Eagle Mtn.	15.61 ± 0.1	Ar/Ar	granite	Unger, 2008
Mule Canyon	15.6 ± 0.04	Ar/Ar	rhyolite	John et al., 2003
McDermitt (Hg)	15.6 ± 0.4	K/Ar	rhyolite	Noble et al., 1988
Midas	15.4-15.3 ± 0.08	Ar/Ar	rhyolite	Leavitt et al., 2004
Hog Ranch	15.2-14.8 ± 0.4	K/Ar	rhyolite	Bussey, 1996
Hollister	15.19 ± 0.05	Ar/Ar	rhyolite	Peppard, 2002
Seven Troughs	13.82 ± 0.02	Ar/Ar	rhyolite	Hudson et al., 2006
Silver City, Black Jack (NV-08-09)	15.579 ± 0.063	Ar/Ar	basalt	This Study
Silver City, Black Jack (MB07)	15.940 ± 0.097	Ar/Ar	basalt	This Study
Silver City, Black Jack (CMT051)	16.076 ± 0.180	Ar/Ar	basalt	This Study
Silver City, Black Jack (CMT056)	15.484 ± 0.067	Ar/Ar	basalt	This Study
Silver City, Orofino (CMT057)	15.607 ± 0.077	Ar/Ar	granite	This Study
Silver City, Orofino (CMT058)	15.736 ± 0.051	Ar/Ar	granite	This Study
Silver City, Orofino (CMT059)	15.622 ± 0.065	Ar/Ar	granite	This Study
Silver City, Orofino (CMT060)	15.730 ± 0.070	Ar/Ar	granite	This Study
Silver City, Dewey (CMT061)	15.367 ± 0.061	Ar/Ar	basalt	This Study
Silver City, Trade Dollar(CMT062)	15.417 ± 0.072	Ar/Ar	basalt	This Study
Silver City, Trade Dollar(CMT063)	15.508± 0.046	Ar/Ar	basalt	This Study
Silver City, Poorman (CMT064)	15.71 ± 0.12	Ar/Ar	granite	This Study
Silver City, Poorman (CMT065)	15.589 ± 0.060	Ar/Ar	granite	This Study
Silver City, Poorman (CMT066)	15.92 ± 0.23	Ar/Ar	granite	This Study
Silver City, Poorman (CMT067)	15.57 ± 0.10	Ar/Ar	granite	This Study

Table 5. A summary log of mineralization age dates of Au-Ag epithermal deposits in the northern Great Basin, modified after Unger (2008). Preferred age dates from previous studies are based on Unger (2008) selection criteria. In cases where multiple ages were presented the oldest age date was always considered to be the earliest crystallization event. In this study adularia was used to date all samples excluding a Rhyolite(MB07) where sanidine was used, and an aphanitic basalt (CMT051) where plagioclase was employed.

NV-08-09: 3 adularia crystals were analyzed by incremental heating (Fig. 40). All samples yielded plateau ages with no excess argon. Ages range between 15.579±0.063 to 15.427± 0.92 Ma. The oldest age was taken to represent the earliest crystallization of adularia in the Black Jack vein. Younger ages may correspond to ^{40}Ar loss during hydrothermal conditioning.

MB07: 3 sanidine phenocrysts separated from a rhyolite at the Black Jack mine were analyzed by incremental heating analysis (Fig. 41). All samples yielded plateau ages with no indications of excess argon. Given that the sample represented in Figure 41 b produced the oldest age (15.940±0.097 Ma) as well as defining a plateau age with the greatest portion of $39Ar_K$ (98%), the sample was taken to be the most retentive of the 3 crystals analyzed. Differences in ages for the crystals are interpreted to reflect differences in radiogenic argon retention due to variations in effective grain size of the feldspars. The slightly younger ages of the 2 remaining crystals i.e. 15.50±0.19 and 15.83± 0.17 Ma may be reflective of loss of radiogenic argon.

CMT051: This sample is representative of a basaltic unit collected from the Black Jack mine. Laser incremental heating of feldspar crystals (n=3) separated from the basalt yielded age dates ranging between 15.79±0.12 and 16.076±0.180 Ma (Fig. 42). No excess argon was detected in any of the crystals analyzed. The oldest age date determined is inferred to reflect the age of the earliest extrusion of basaltic flows in the area. When the maximum error limits of the other 2 age dates are considered for this sample, they display plateau ages and total gas ages that are essentially the same. In this case, calculated ages coalesce around 16.0 Ma, indicating analytical precision.

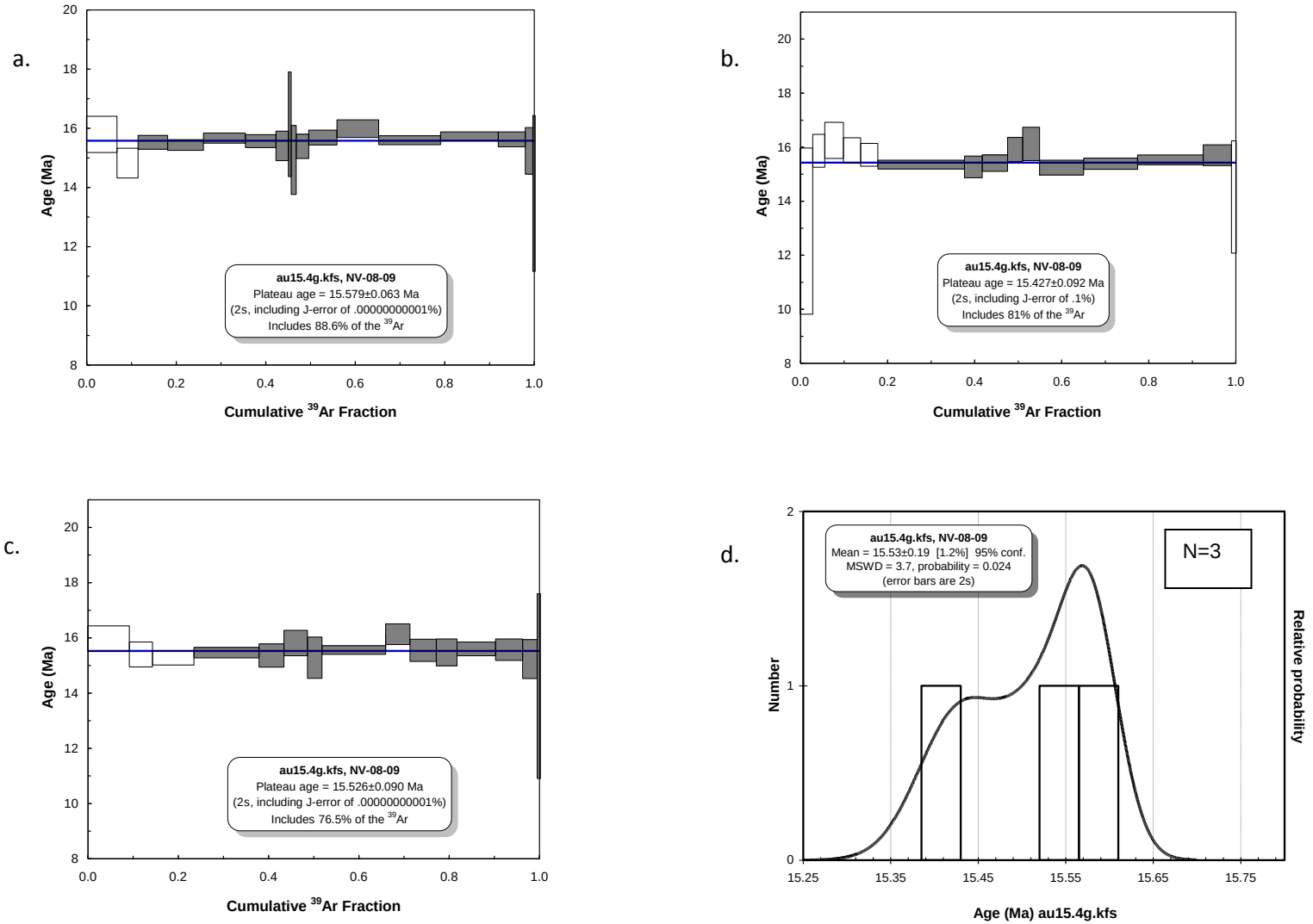

Fig. 40. Release spectra for adularia (NV-08-09) separated from vein material collected from Black Jack mine. Ages range between 15.427±0.092 and 15.579±0.063 Ma. “a” is inferred to represent the earliest crystallization for adularia. See appendix 3 for single crystal total fusion and incremental heating data.

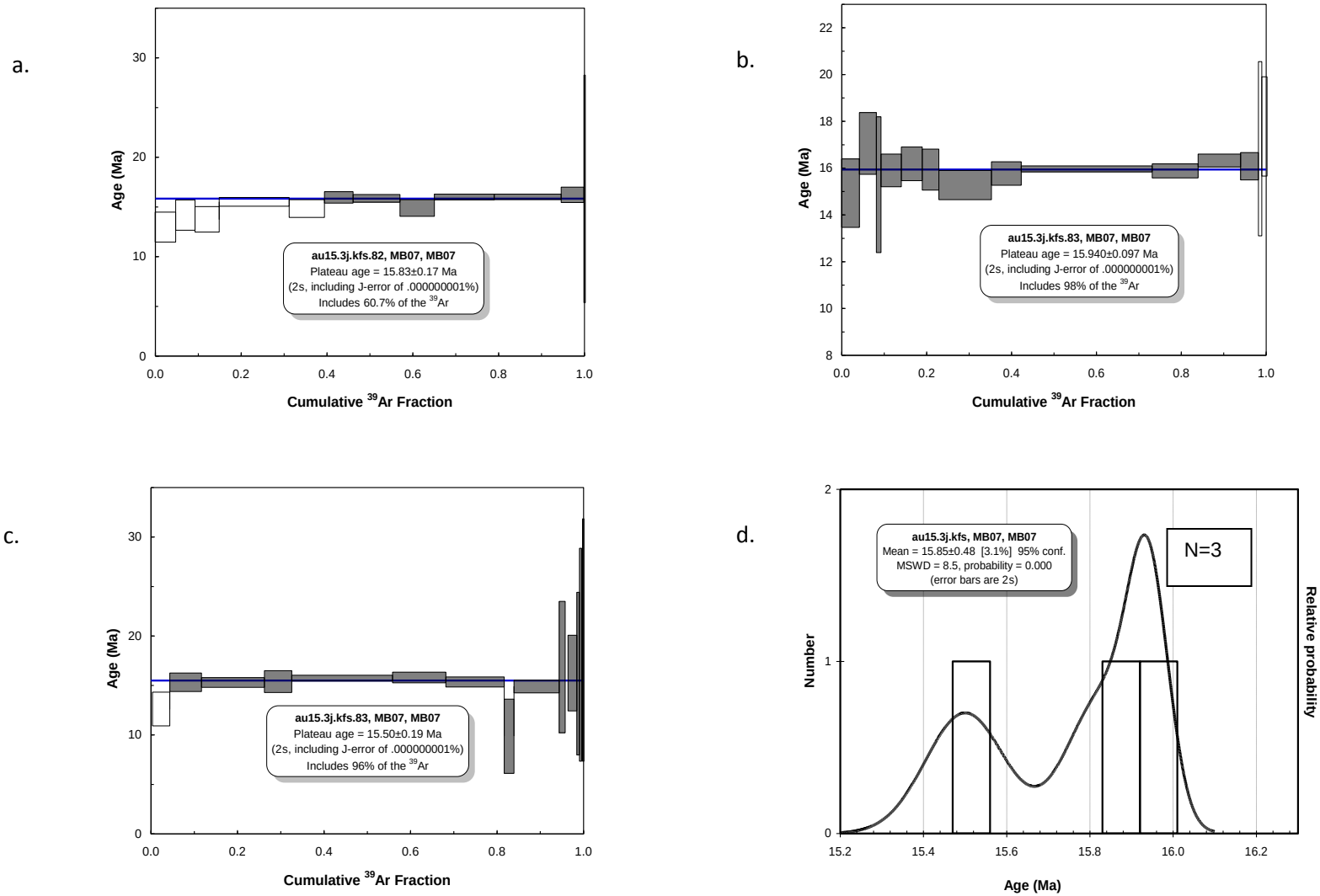

Fig. 41. Release spectra for 3 sanidine crystals separated from rhyolite (MB07) collected from Black Jack Mine. Ages range between 15.940±0.097 and 15.50±0.19 Ma. “b” is inferred to represent the earliest crystallization for rhyolite. See appendix 3 for single crystal total fusion and incremental heating data.

a.

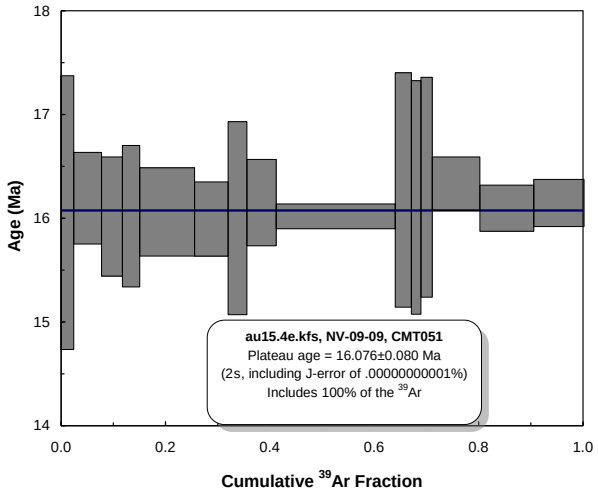

b.

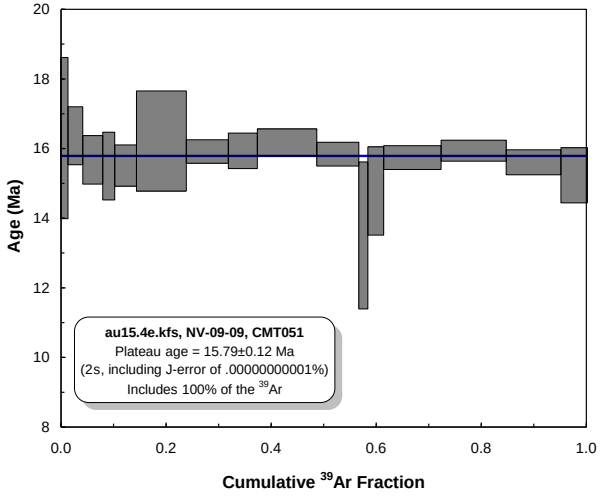

c.

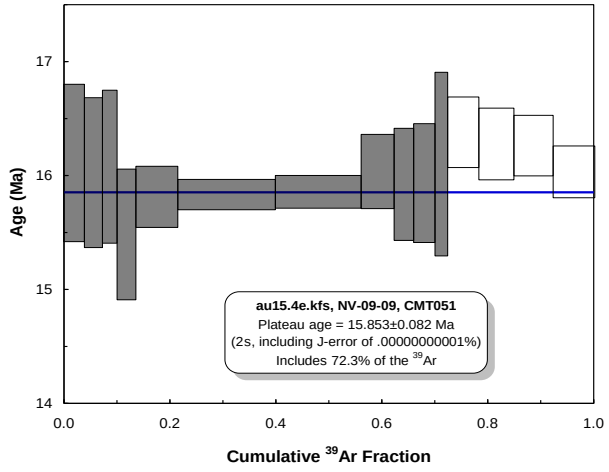

d.

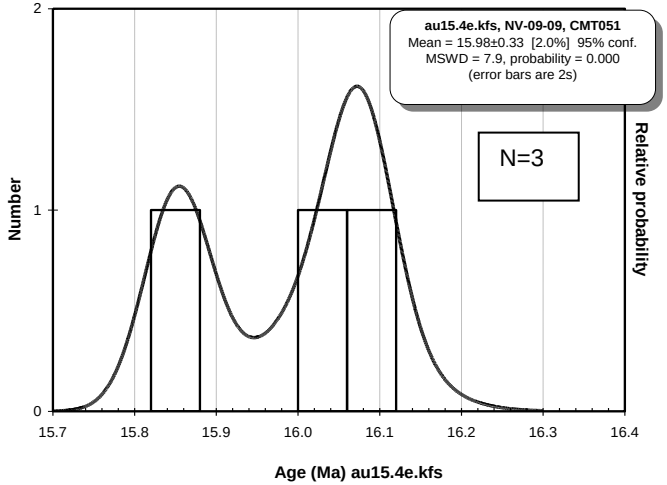

Fig. 42. Release spectra for 3 feldspar phenocrysts separated from basaltic flows from Black Jack Mine. Ages range between 16.076±0.080 and 15.79±0.12 Ma. "b" is inferred to represent the earliest crystallization for the basalt. See appendix 3 for single crystal total fusion and incremental heating data.

CMT056: Adularia collected from vein material from the Black Jack Mine was analyzed by single crystal total fusion and incremental heating analyses (Fig. 43). Both procedures produce a “temporal agreement” (within error) for samples analyzed indicating a minimal variance between the two analytical methods. An age of 15.480±0.063 Ma was produced by single crystal total fusion and 15.484±0.067 Ma for incremental heating analyses. The slightly older age of 15.484±0.067 Ma was considered to be reflective of better radiogenic argon retention and was taken to represent the earliest adularia crystallization for this vein. No extraneous argon was detected during analysis.

CMT057: Plateau ages generated from incremental heating and the calculated age date produced by single crystal total fusion for adularia indicates minimal effects from extraneous argon or loss of a significantly large degree of radiogenic argon. Ages produced by the two methods are essentially the same within error i.e 15.548±0,079 and 15.607±0.077 Ma (Fig.44). The preferred age date for this sample was taken to be 15.607±0.077 Ma, which is considered to be the best estimate for the earliest vein formation.

a.

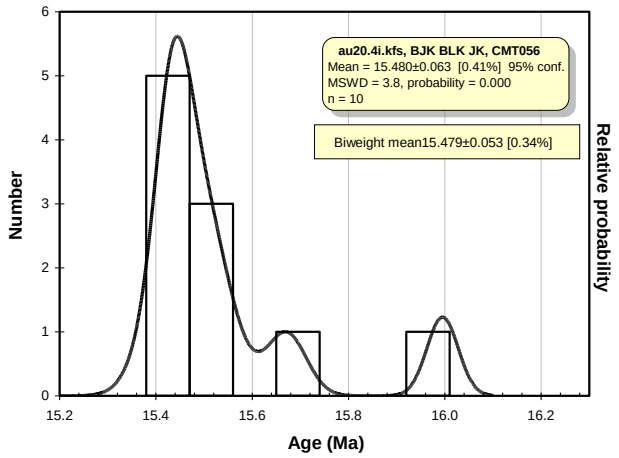

b.

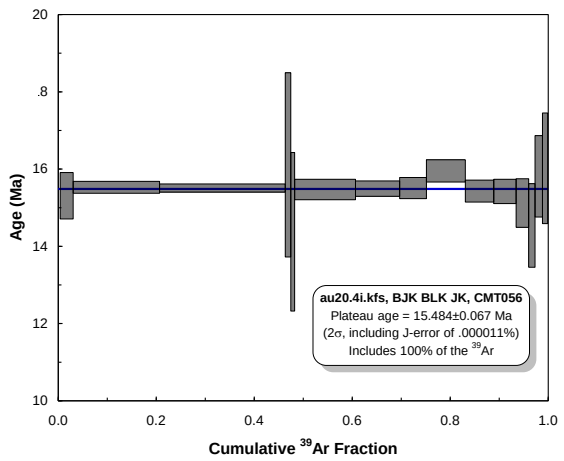

Fig. 43. Release spectra for adularia crystals separated from vein material from Black Jack mine. “b” is inferred to be reflective of the earliest crystallization ages for adularia. See appendix 3 for single crystal total fusion and incremental heating data.

a.

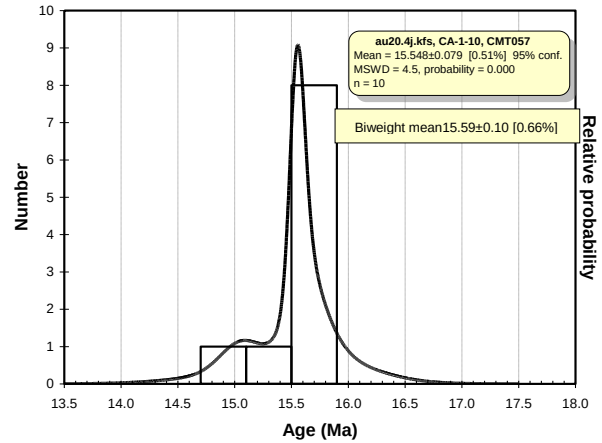

b.

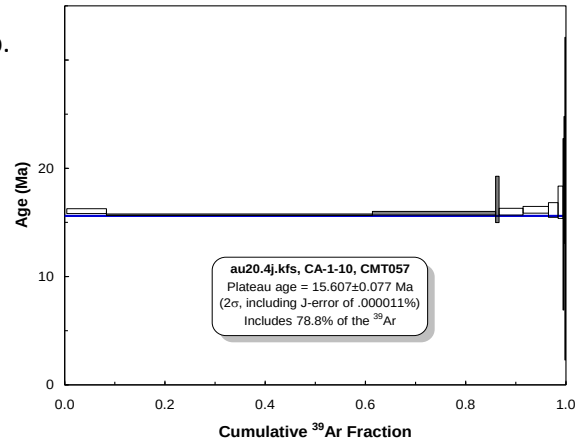

Fig. 44. Release spectra for adularia crystals separated from vein material from the Orofino vein (a, b). “b” is inferred to be reflective of the earliest crystallization ages for adularia. See appendix 3 for single crystal total fusion and incremental heating data.

CMT 058: Single crystal total fusion and Incremental heating of adularia from material collected from the Counts Cabin spoil heaps that are proximal to the Orofino vein revealed ages of 15.617±0.043 and 15.736±0.051 Ma respectively (Fig. 45). Considering that the bi-weight mean average of the single crystal total fusion data is lower than both age dates (i.e. 15.599±0.057 Ma), but well within the realm of both results (within error), the oldest of the two ages was considered to correspond to the earliest vein formation age. No extraneous argon was indicated during analyses.

CMT059: Adularia collected from the spoil piles at Cumberland mill were subjected to single crystal total fusion and incremental heating analyses (Fig. 46). The bi-weight mean average of the single crystal total fusion sample revealed an age of 15.622±0.065 (MSWD=2.4). It is inferred that this age represents primary adularia crystallization. However, it should be noted that when error margins for both single crystal total fusion and incremental heating are considered, the age ranges for the samples analyzed coalesce around 15.6 Ma indicating that they are all statistically agreeable. Differences in ages for crystals are interpreted to reflect differences in radiogenic argon retention due to variations in effective grain size of feldspars.

.

a.

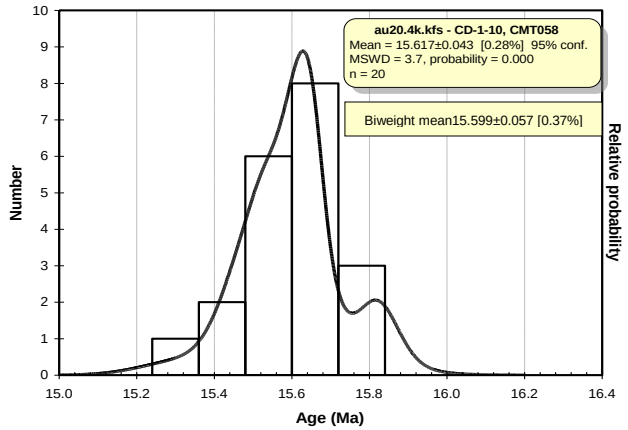

b.

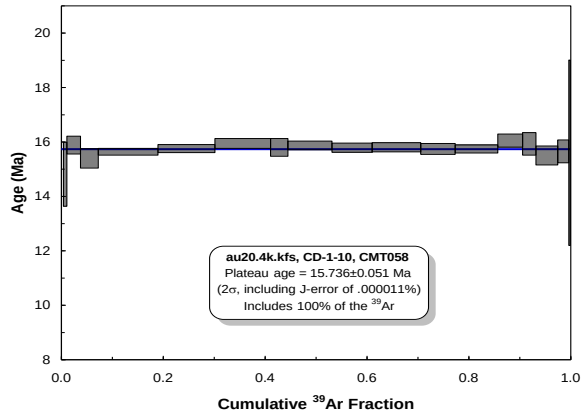

Fig. 45. Release spectra for adularia crystals separated from vein material from the Orofino vein CMT058. “b” is inferred to be reflective of the earliest crystallization ages for adularia. See appendix 3 for single crystal total fusion and incremental heating data.

a.

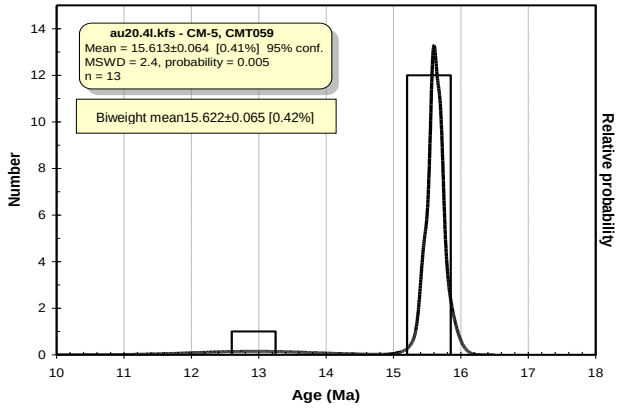

b.

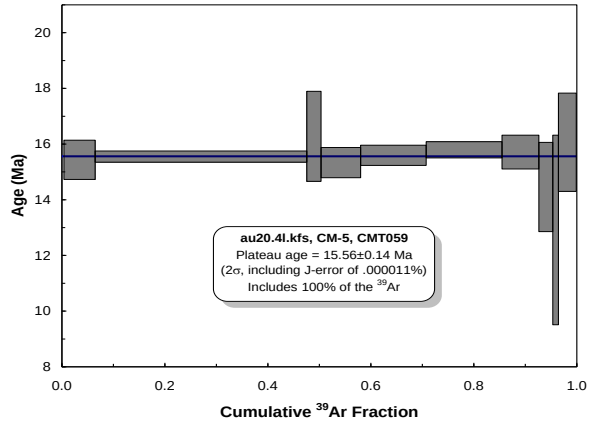

Fig. 46. Release spectra for adularia crystals separated from vein material from the Orofino vein. The biweight mean average is inferred to be reflective of the earliest crystallization ages for adularia. See appendix 3 for single crystal total fusion and incremental heating data.

CMT060: This sample represents adularia separated from vein material collected from spoil heaps at the Cumberland mill. Single crystal total fusion analyses of adularia yielded an age of 15.675±0.052 Ma where as incremental step heating analysis produced an older age of 15.730±0.070 Ma (Fig. 47). The older age is considered to be the best estimate of earliest crystallization age for adularia. However, it should be noted that statistically plateau ages and total gas ages are essentially the same (within error). When the two ages are considered together, the error margins of both samples imply a temporal agreement of approximately 15.7 Ma. No extraneous argon was detected.

CMT061: This sample represents quartz and adularia vein material collected from spoil heaps at the Dewey mine. The optimal percentage release of $^{39}Ar_K$ produced during incremental step heating analysis helped to determine the preferred age date for this sample as 15.367±0.061 Ma (Fig. 48). This age is comparable to the bi-weight average of the single crystal total fusion analyses (15.30± 0.12 Ma). Similarly, when incremental heating data (15.367±0.061 Ma) and single crystal fusion age (15.470±0.064 Ma) error margins were compared; their ages were found to overlap, indicating that the variance between the two analytical methods was minimal. No excess argon was detected.

a.

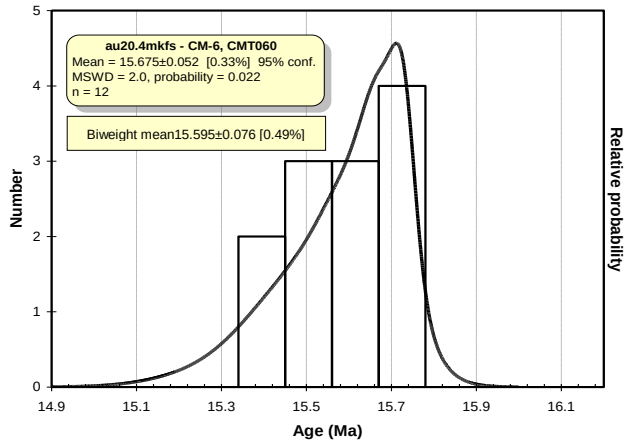

b.

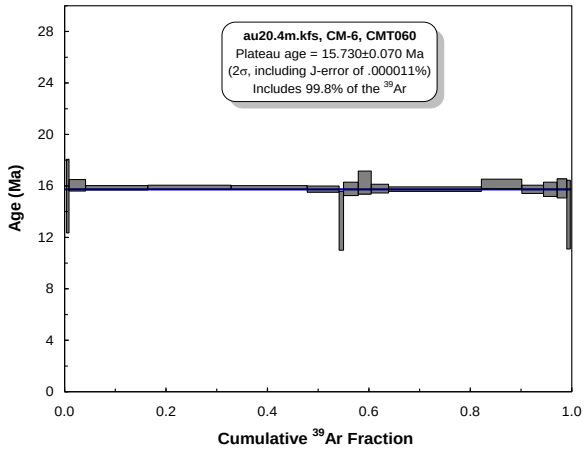

Fig. 47. Release spectra for adularia crystals separated from vein material from the Orofino vein CMT060 (a,b). "b" is inferred to be reflective of the earliest crystallization ages for adularia. See appendix 3 for single crystal total fusion and incremental heating data.

a.

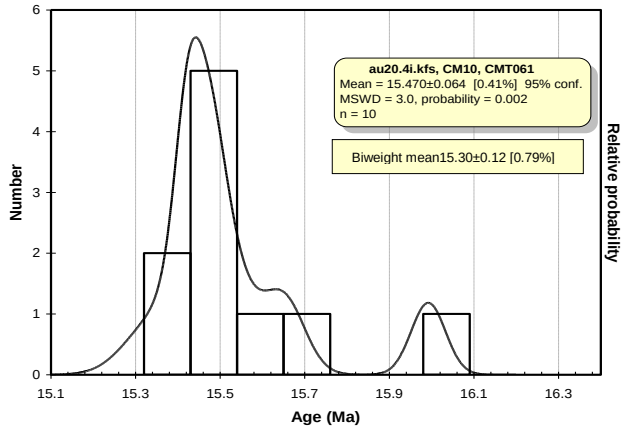

b.

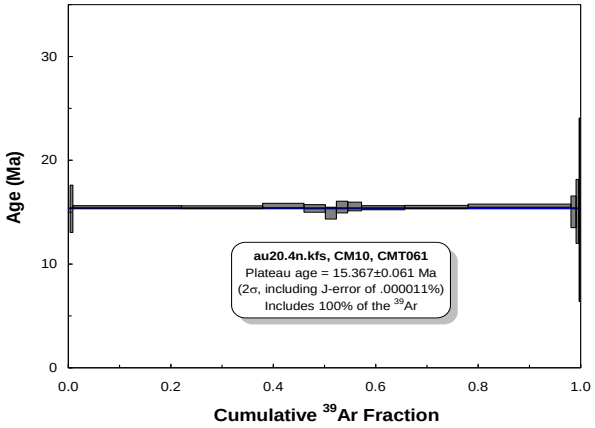

Fig. 48. Release spectra for adularia crystals separated from vein material from Dewey mine. "b" is inferred to be reflective of the earliest crystallization ages for adularia. See appendix 3 for single crystal total fusion and incremental heating data.

CMT062: Single crystal total fusion and incremental heating methods exhibit age dates that essentially display statistically similar ages (within error; Fig. 49). Age dates of 15.431±0.051 Ma and 15.417±0.072 Ma respectively were produced for single crystal total fusion and incremental heating analyses. The variation in ages is within acceptable margins from precision measurement. The older age of 15.431±0.051 Ma was inferred to reflect the earliest crystallization age for vein material collected at Trade Dollar Mine.

CMT063: Single crystal total fusion and incremental heating analyses revealed ages of 15.508±0.046 and 15.409±0.078 Ma respectively for adularia collected from vein material from the Trade Dollar Mine spoil heaps (Fig. 50). A biweight mean average age of 15.484±0.056 Ma was also calculated from single crystal total fusion analyses. Age dates are statistically similar (within error) and are seen to coalesce within acceptable margins of errors at approximately (15.5 Ma) indicating accuracy as well as precision of the analytical methods used. The oldest age date was considered to represent this samples earliest crystallization event. No extraneous argon was detected in the analyses.

a.

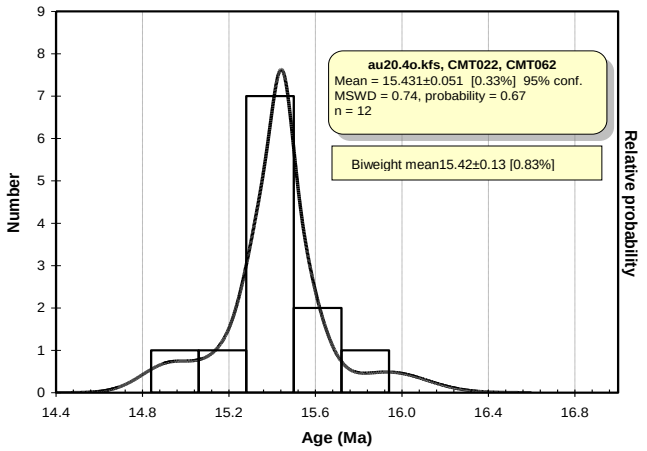

b.

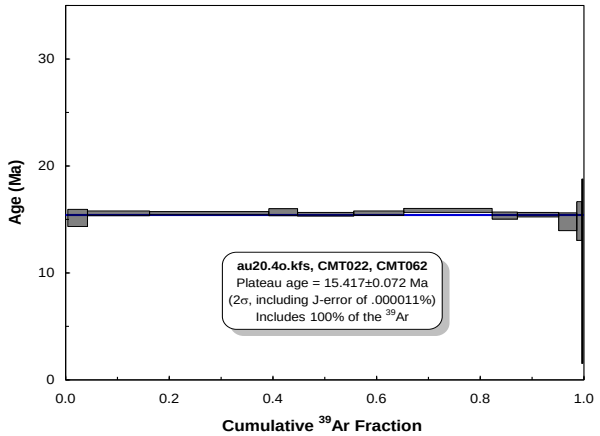

Fig. 49. Release spectra for adularia crystals separated from vein material from Trade Dollar (CMT062). “b” is inferred to be reflective of the earliest crystallization ages for adularia. See appendix 3 for single crystal total fusion and incremental heating data.

a.

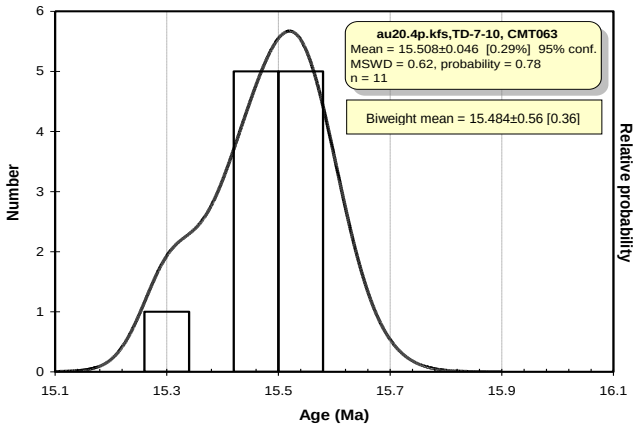

b.

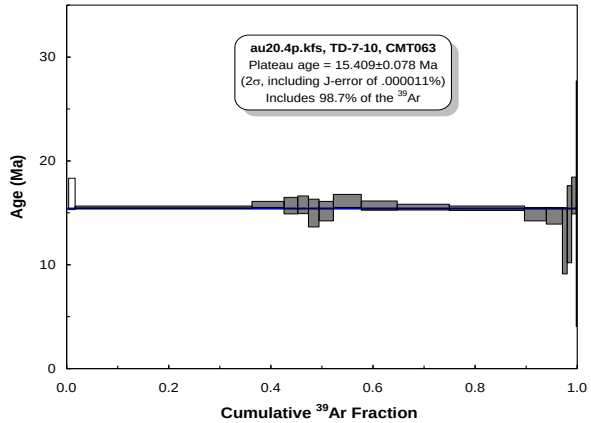

Fig. 50. Release spectra for adularia crystals separated from vein material from Trade Dollar (CMT063). “a” is inferred to be reflective of the earliest crystallization ages for adularia. See appendix 3 for single crystal total fusion and incremental heating data.

CMT064 to CMT067: These samples were collected proximal to each other (i.e the summit of War Eagle Mountain). Age dates range between 15.447±0.090 and 15.92±0.23 Ma and were calculated for adularia collected from vein material (Fig. 51-52). The variance in ages may be indicative of multiple episodes of adularia crystallization/vein formation events within a constrained spatial spread. Samples that underwent incremental heating analyses produced optimal $^{39}Ar_K$ (100%) during analysis implying optimal analytical data acquisition integrity. For this reason the incremental heating samples were considered to be the ages of vein formation. Even so, it should be noted that data obtained from single crystal total fusion samples produced age dates that are statistically similar to those that underwent incremental heating.

.

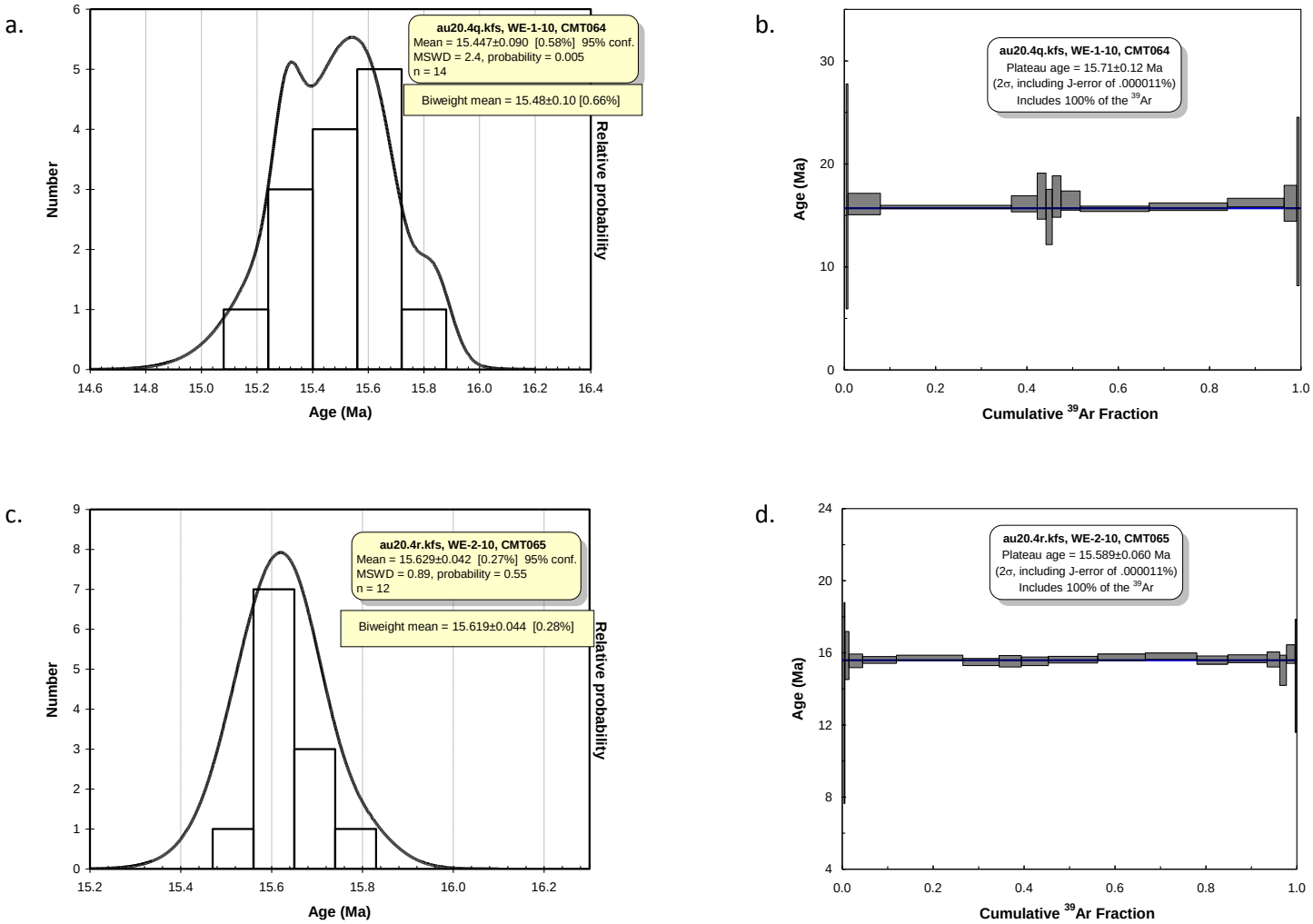

Fig. 51. Release spectra for adularia crystals for Poorman vein CMT064 (a, b) and CMT065 (c, d). b and d are inferred to be reflective of the crystallization ages for adularia. See appendix 3 for single crystal total fusion and incremental heating data.

.

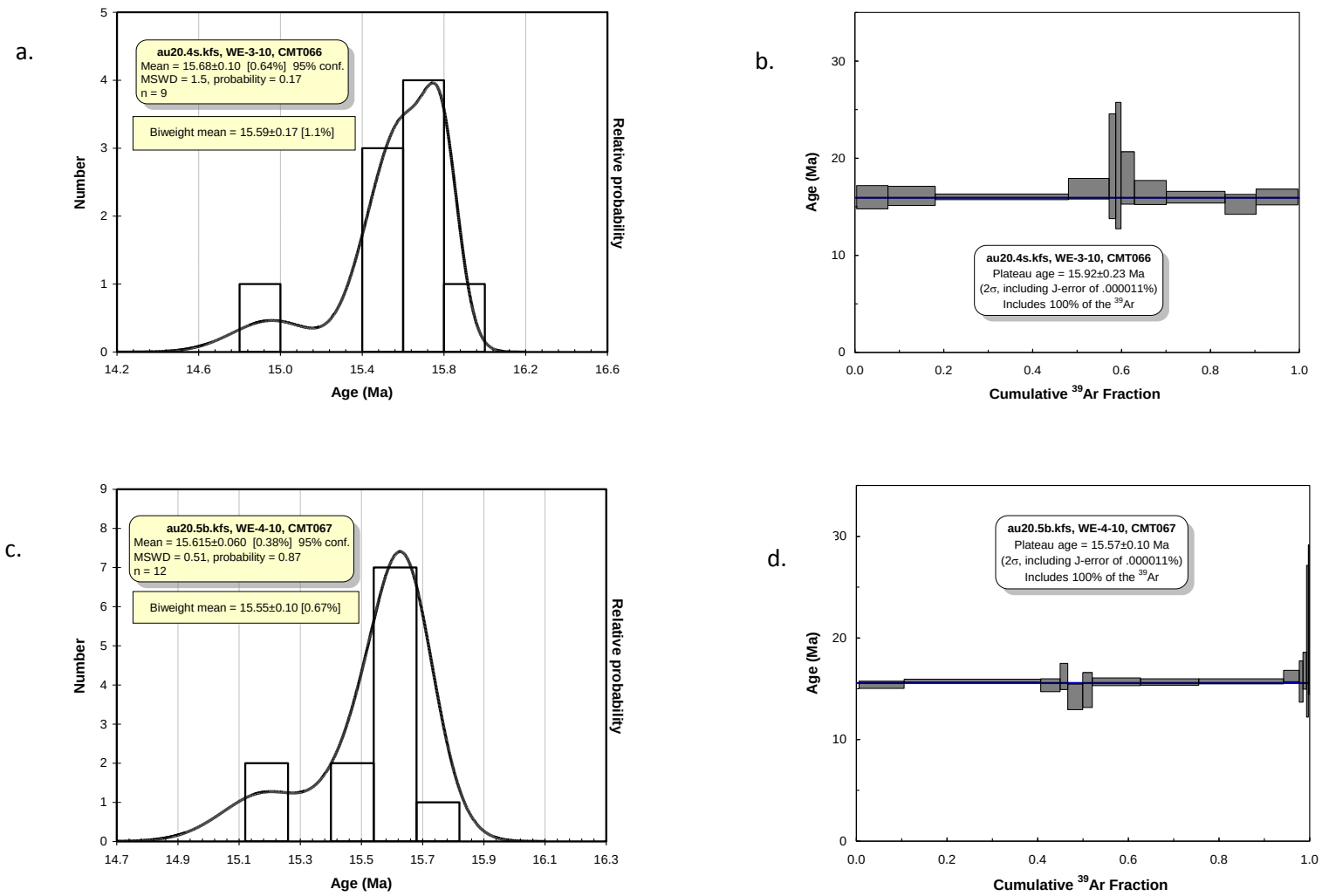

Fig. 52. Release spectra for adularia crystals for Poorman vein CMT066 (a, b) and CMT067 (c, d). b and d are inferred to be reflective of the crystallization ages for adularia. See appendix 3 for single crystal total fusion and incremental heating data.

Interpretation of results: The most striking feature of this study is the agreement of the mineralization and volcanism age dates which coalesce around ~15.5 ± 0.5 Ma (Figs. 39-52; Table 5).However, no obvious spatial hydrothermal trends are evident from the data that could suggest any preferred age variations within the location on the district scale (Fig. 39). This may imply the possible introduction of Au-Ag mineralization as a series of spatially-random, overlapping, but temporally constrained hydrothermal magmatic degassing pulses associated with volcanism.

Taken collectively and on a regional scale, the tecto-magmatic and mineralization events for the Silver City district invariably suggest a temporal nexus of ≈ 15.6 Ma, which falls within the realm of the 16.5 Ma to 15.1 Ma mineralization timeframe of other deposits in the Northern Great basin (Fig. 49; Table 5). However, most of the gold

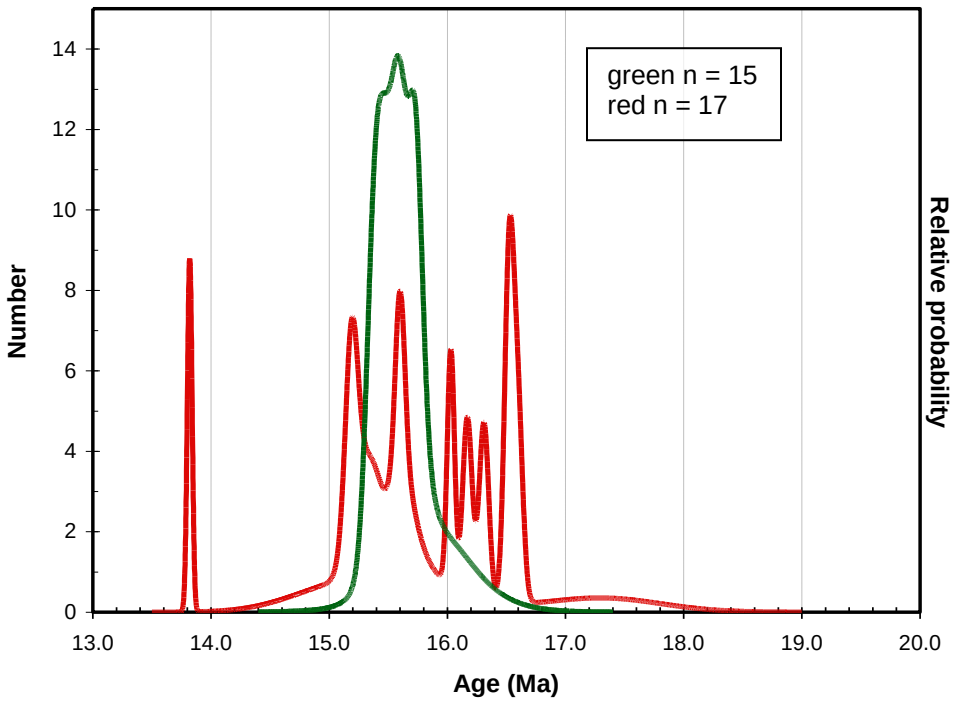

Fig. 53. Composite probability age chart that depicts mineralization ages from this study (green) and previous studies (red) collated from the northern Great Basin.

endowment appears to have been deposited in a brief window between 15.4 Ma and 15.8 Ma. An attempt to rationalize the wide range of Au-Ag mineralization events in the northern Great Basin in relation to the Silver City district's Au-Ag mineralization episode is discussed in detail below. By doing so, this study places important temporal constraints on the genetic link between the nascent Yellowstone Hotspot (circa 17 Ma; John, 2001), and mineralization events in the Silver City district, as well as the northern Great Basin at large.

7. DISCUSSION

An inventory of diagnostic methods that combines geological mapping, geochemistry, and geochronological determinations are used in this research to aid in developing a genetic model for the Silver City district. Areas investigated in this thesis include: (i) the **structural** controls that influence localization of mineralized fluid to form ore bodies, (ii) **transport** mechanisms of mineralized fluids, and meteoric waters; their interaction, and how both these phenomena affects eventual ore and gangue mineral composition and (iii) the **source** and **timing** of Au/Ag epithermal mineralization.

The convergence of structural, geochemical, and geochronological data leads to a proposed model for Au-Ag epithermal mineralization in Silver City district that is in accord with the embryonic Yellowstone hotspot (Saunders et al; 1996, John; 2001; Bruseke et al., 2007).

Regional Structural Controls

The Orofino and Poorman veins occur in open elongate columnar fractures that formed as a result of mid-Miocene extensional tectonics pulling east and west (Panze, 1975). These pull-apart structures are thought to be a consequence of back-arc extension related to the nascent Yellowstone hotspot (Noble et al., 1988; John, 2001; Bruseke et al., 2007). The regional manifestation of this event in the northwestern United States has been tied to the formation of spatially and temporally related low-sulfidation epithermal deposits in the northern Great Basin (John, 2001).

In the Silver City district, faults have three principal orientations: i) north to south, ii) northwest to southeast, and iii) east to west. These structures apparently focused hydrothermal fluid flow and acted as mineralization trap sites. The highest Au and Ag

assays found across a 2.13m vein channel sample correlate with dark altered rhyolite (?), breccias clasts (?), fault gouge (?), associated with the veins' contact zones. This may be due to any one or all three of the following factors: (i) the altered quartz rich rock on the contact zones could be more chemically susceptible or receptive to mineralized hydrothermal fluid alteration; (ii) competency contrast between the quartz vein and the hanging wall and footwall of the granitoid host rock helped to redirect mineralized fluids that pond in the veins contact zones; and (iii) the abrupt release of pressure on mineralized fluid by faulting may have caused brecciation that produced the dark rhyolitic clasts (Fig 26, C). Brecciation resulted in a corresponding increased porosity that helped to provide preferred channels for mineralized fluid conveyance and entrapment. However, veins are only mineralized over a relatively confined vertical extent of ≈ 762m for Orofino vein and ≈ 520m below surface for veins at Florida mountain (Piper and Laney, 1926).

Geochemistry

Both the Orofino and Poorman veins exhibit quartz (SiO_2), calcite ($CaCO_3$) and adularia ($KAlSi_3O_8$) as the dominant gangue mineral assemblage. The pseudomorphic replacement of platy calcite by quartz is of particular importance as it has been shown to be indicative of hydrothermal boiling in epithermal systems (de Ronde and Blattner, 1988; Simmons and Christiansen, 1994). Fluid inclusion temperatures (homogenization) for the two vein sets are assumed to provide an indicator of vein formation entrapment temperatures and pressures. This is because the shallow nature of epithermal deposits renders pressure (lithostatic and hydrostatic) corrections to homogenization temperatures unnecessary (Saunders, pers. commun., 2010). The Poorman and Orofino veins precipitated at a range of temperatures between ≈180°C and 285°C and ≈165°C

and 255°C, respectively.

Combining homogenization temperatures from War Eagle Mountain, DeLamar Mountain (Halsor et al., 1988) and Florida Mountain (Steiner, Unpublished), the central part of the district (Florida Mt.) appears to encompass the highest thermal limit (≈190°C and 310°C) with the flanks recording lower temperatures of ≈ 174°C and 240°C to the west (DeLamar Mt.), and ≈165°C and 255°C to the east at War Eagle Mountain (Fig. 54). It is probable that the central part of the district represents the localized center of the Silver City district's mid-Miocene magmatic plume. This supposition is however complicated by the fact that the fluid inclusions studied herein were selected from samples collected randomly from dump sites that are proximal to the veins of interest. Consequently their in-situ depths and timing of formation cannot be known precisely, especially in such a dynamic system. These data should therefore be used only as a preliminary guide that may direct future detailed studies.

Analyses of measured fluid inclusions show that they are dilute in nature and thus exhibit a strong meteoric (e.g. groundwater) component. Their substantial meteoric fingerprint is consistent with: (i) their low salinities (0.5% - 1% NaCl equivalent), and (ii) laser ablation studies. These studies indicate the measured fluid inclusions consist of either a dilute Ca-Na dominant fluid-type, or a dilute K dominant fluid-type, both of which are correspondingly highly deficient in metal(loid)s.

These meteoric waters are downward percolating fluids that get heated as they progress and in turn mix with upwardly welling acidic volatiles and metal rich solutions sourced from magmas. This enables leaching of major elements (e.g. silica (Si), aluminum (Al), potassium (K), sodium (Na), calcium (Ca) etc.) from host-rocks to produce vein and gangue material such as Quartz (SiO_2), Adularia ($KAlSi_3O_8$) ,Calcite ($CaCo_3$), in near boiling zones.

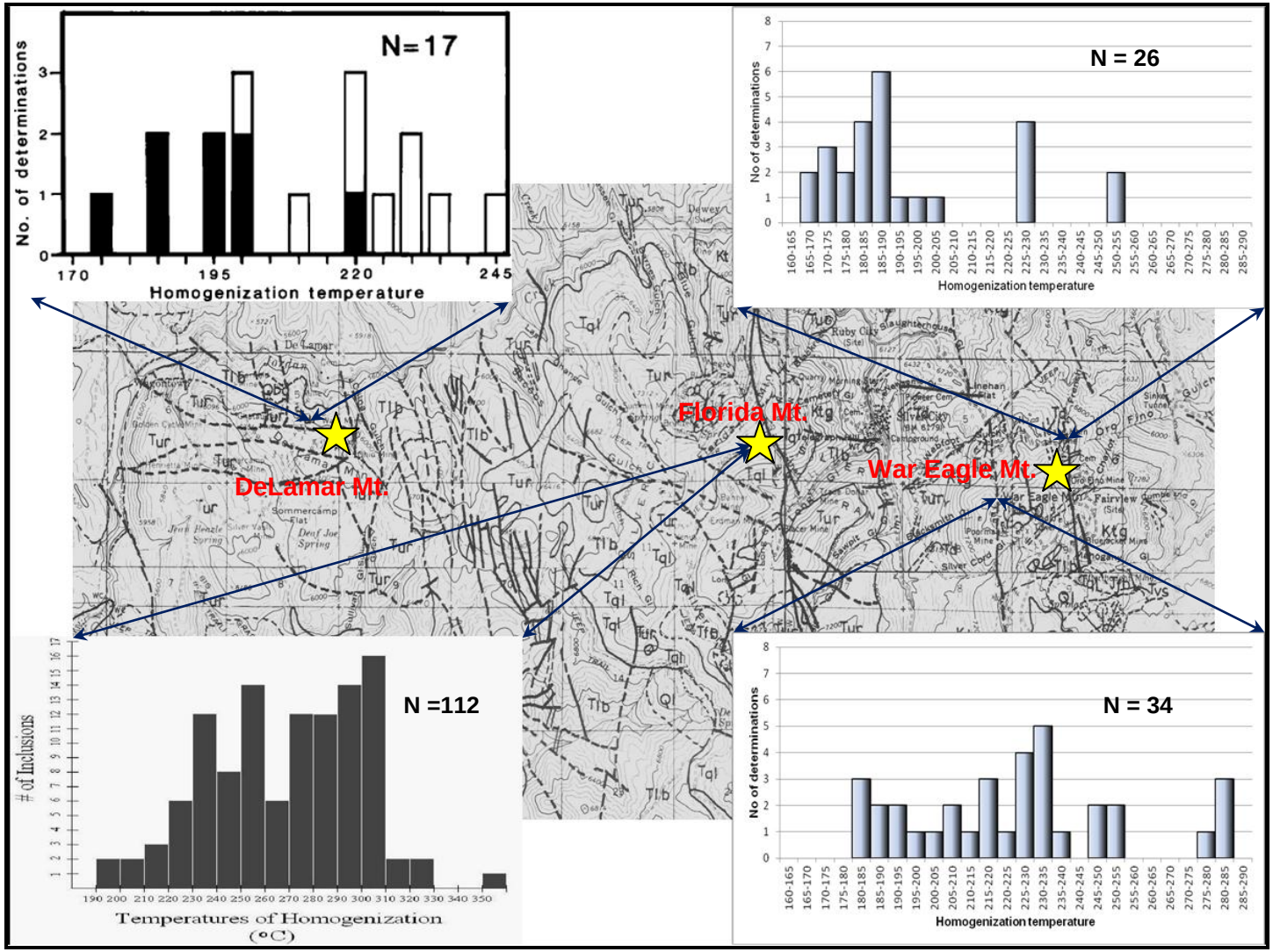

Fig. 54. Map showing a summary of homogenization temperatures for Delamar Mt (Halsor et al., 1988), Florida Mt. (Steiner, Unpublished) and War Eagle Mt.

(Taylor, 2007; Hames et al, 2009). The same meteoric waters dilute fluids containing deep sourced Au/Ag nanoparticles that get entrained into the epithermal environment (Saunders et al., 2008). Consequently, isotopic exchange with surrounding rocks and the titration of Au-bearing fluids into meteoric waters helps to mask the magmatic origin of ascending Au-Ag vapors. The final result is the dominant meteoric signature that typifies the Silver City's mineralization, and many other low sulfidation epithermal deposits worldwide (Simmons et al., 2005). It therefore appears that even though meteoric waters were responsible for precipitation of vein and gangue minerals, they are **not** the source of epithermal Au/Ag mineralization (Saunders et al., 1996, 2008; Heinrich, 2005; Kamenov et al., 2007; Hames et al., 2009).

The debate of an amagmatic or magmatic origin of epithermal Au deposits has persisted for decades. Lindgren (1922, 1933) who is arguably considered the "father" of epithermal deposits, pioneered the thoughts on the possible magmatic origin of metals in epithermal ores. Proponents of the amagmatic model (e.g, Nash et al., 1996, John et al., 2003) hypothesize that Au mineralization being sourced/leached from the crust by heated convectively driven meteoric waters. On the other hand, the magmatic hydrothermal thesis proposes that Au mineralization is derived directly from aqueous magmatic vapors (e.g., Saunders et al., 1996, 2008; Heinrich, 2005; Kamenov et al., 2007; Hames et al., 2009).

Pb isotope data from this and previous studies (Kamenov et al., 2007) yield data that permits a greater understanding of a possible magmatic origin for epithermal precious metals. Pb isotopes alloyed with gold tend to mimic the younger mantle sourced Snake River plain basalts trends observed by Hanan et al. (2008), even though the gold has a more primitive signature. Mid-Miocene Au samples collected from War Eagle Mountain that appear to have interacted with a thinner crust associated with the

Mesozoic accreted terrane, which appear to ultimately originate from the mantle, have been shown here to be more depleted in Pb than both the Cretaceous granitoid and mid-Miocene rhyolites that host them. The disparate isotopic signature of Pb alloyed in Au, and the Pb signatures in the felsic host rocks, implies that gold is not likely to have been leached from the host rocks. In contrast the similarity of isotopic composition for Pb alloyed with Au to Pb signatures of the inferred plume indicates that mafic magmas are most likely the source of Au mineralization. These data therefore further support previous work showing a magmatic connection and demonstrate that primitive basalts are perhaps the primary source of Au (Kamenov et al., 2007).

The fluid type hypothesized for the source of metals in epithermal deposits are low density metal-rich fluids (magmatic aqueous vapors) exsolved directly from magmas or separated from dense saline magmatic fluids at depth (Buchanan, 1981; Heinrich et al., 2004; Heinrich, 2005; Saunders, 2008). Simmons and Brown (2006) demonstrated the existence of appreciable quantities of Au bisulfide complexes for active geothermal solutions from hydrothermal fluids collected from actively forming low sulfidation Au deposits at Luise volcano, Lihir Island, Papua New Guinea. Saunders (1994) proposed that the nucleation at depth (of such low-density magmatic fluids?) results in the formation of Au colloids. However, Au colloid textures are usually only observed in the most high-grade epithermal ores. Even so, they may occur in lower grade ores too but rarely is this textural evidence preserved.

High temperature, low viscosity, and low density metal-rich fluids/vapors upwell rapidly from their source plutons as magmatic degassing progresses, and undergo a rapid decrease in pressure and temperature. The temperature (and pressure?) decrease accompanying fluid rise, apparently triggers Au-Ag colloid nucleation from optimal depths (Obuya., in prep; e.g. Fig. 55). At shallower depths, boiling and mixing with

meteoric waters causes oxidation and pH shifts. A strong decrease in the solubility of Au and Ag eventually ensures that compels ore precipitation and commonly colloid aggregation in the epithermal zone (Saunders,1996; Heinrich et al., 2004; Heinrich, 2005).

Fig. 55 Video-frame capture of a sol (stable suspension) of gold colloids with a diameter 10^{-7}m imaged with a recently invented high-powered optical microscope (after Vainrub et al.,2006. Image used with permission).

Aggregation of Au-Ag nanoparticles in bonanza epithermal ores result in 2 textural forms: (i) self-organized fractal growth dendritic textures (Vikre, 1985; Saunders et al., 1996) and (ii) “sluice box textures” (Saunders, 2008; Unger, 2008). The variance in the two textural forms could be reflective of nanoparticle oxidation states and temperatures that influence metal availability and migration at the time of aggregation (Obuya., in prep). These two factors play a vital role in determining the morphology of Au mineralization. For example, dendritic textures are thought to be consistent with the rapid precipitation from a saturated solution (Unger, 2008). On the other hand “sluice

box textures" that are formed when precious metal colloids are deposited to produce "ginguro" bands (Saunders, 2008), are thought to exemplify the episodic exsolution of low density magmatic volatile phases (Hedenquist and Lowenstein, 1994).

There was a general lack of classic dendritic textural forms in the sample suite used in this study; however Steiner (pers. commun., 2011) reports their presence in the micro scale at Florida Mountain. Equally "sluice box textures" were observed in ores from both the Poorman and Orofino veins (Fig. 22). These textures are possibly a result of an exsolved low density Au/Ag brine from degassing magmas.

Exsolution of the low-density Au-rich fluid from the more saline magmatic base metal rich fluid leaves the deposition and eventual precipitation of base metal rich brines at depth like in a porphyry deposit (Taylor, 2007). The presence of base metals in spoil samples in the southern segments of the Orofino vein may be correlative to the deeper seated portions of the epithermal system. However, base metal occurrence is generally insignificant and when present is usually accompanied by a corresponding decrease in Au and Ag mineralization. This is consistent with separation of base and precious metals, with Au favoring the upper, boiling/gas-rich part of the epithermal system (Buchanan, 1981).

Au occurs mainly in the form of electrum in most epithermal ores including War Eagle Mountain. Calculated bulk Au/Ag ratios suggest an increase in Au proportions eastwards from DeLamar Mountain towards War Eagle Mountain. Silver minerals are generally Se-S bearing and consist of a solid solution continuum of arcanthite (Ag_2S), aguilarite (Ag_4SeS), naumannite (Ag_2Se), and two or more (?) previously undocumented Ag-Se-S phases. The Ag-S-Se solid solution phases were found to be much more common than thought previously (Petruk et al., 1974). The Poorman vein generally shows Ag mineralization that is more similar in composition to aguilarite (Ag_4SeS),

whereas the Orofino's is closer to arcanthite (Ag_2S) in composition. Despite this, their ore assemblage characteristics are generally comparable, indicating that common processes facilitated ore transportation and aggregation. This phenomenon supports the contention of a singular/common magmatic progenitor.

Ag mineral chemistry in the Silver City district and the northern Great Basin at large have recently been proposed to be a product of the volatility of metal(oid)s (Saunders and Bruseke, 2012). Saunders and Bruseke (2012) demonstrated that subduction, partial melting of the mantle, the generation of magma and degassing of the same, could result in the preferential mobilization of volatile elements and compounds.

Haynes (2010) reported that the relative anhydrous volatility of selected metal(loids) follows the following sequence: Hg>As>Se>Te>Tl>>Sb>Pb>Ag>Cu>Au. Given the higher geochemical volatility of Se relative to Te, a general east to west geographic-geochemical zonation of Cenozoic mineralization systems from Te-rich to Se-rich occurs in the western part of the United States of America (Figs. 56-57). Mid-Miocene magmatism triggered by the Yellow Stone hotspot apparently facilitated the distillation events that preferentially segregated Se from the shallow-angle subduction fertile mantle of the Farallon Plate during the Laramide Orogeny (Fig. 57).

Elemental fractionation/magmatic preparation is optimized in this scenario due to a flat-slab subduction (English et al., 2003) interacting with upwelling asthenosphere. This ensures relatively cool temperatures and precludes steep temperature differentials that play a significant role in developing the geographic-geochemical zonation of the Cenozoic deposits in western United States of America. This phenomena result in the significant Se concentrations that supersedes the element's average crustal abundance that Taylor (1964) pegged at ≈ 0.05 ppm.

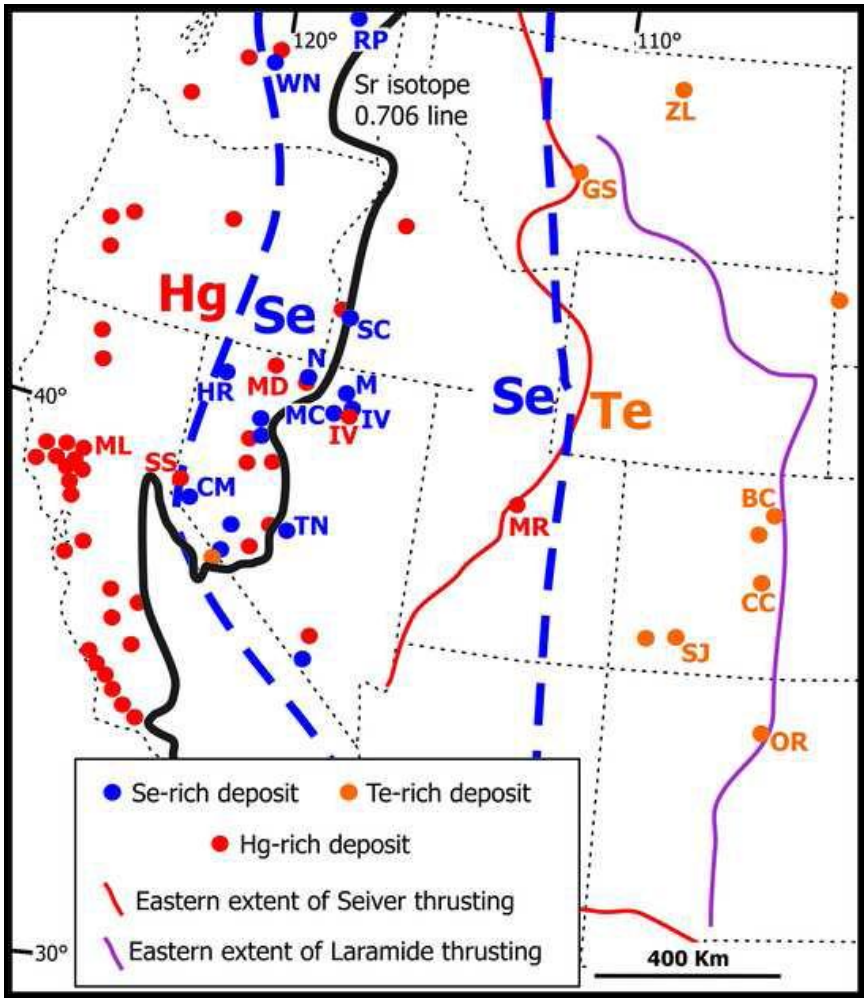

Fig. 56. Map showing the spatial configuration of Hg (not all epithermal), Se and Te enriched Au/Ag epithermal deposits in western USA (Saunders and Bruseke, 2012). **BC**= Boulder County , Kelly and Goddard (1969); Saunders (1986); Saunders (1991) , **CC**=Cripple Creek, Saunders (1986); Saunders (1988); Jensen and Barton (2000); Kelley and Luddington (2002);Unger (2008), **CM**=Comestock, Coats (1936); Vikre (1989);Simon et al. (1997), **GS**= Golden Sunlight, Porter and Ripley (1985); Spry et al. (1996); Mutchler et al. (1997), **HR**= Hog Ranch, Bussey (1996); Vikre (2007a) , **IV** = Ivanhoe/Hollister , Wallace (2003); Unger (2008);Saunders et al. (2011b), **M**= Midas, Goldstrand and Schmidt (2000); Leavitt et al. (2004); Unger (2008); Saunders et al. (2008); Saunders et al. (2011a), **MC**= Mule Canyon , John et al. (2003), **MD**=Mcdermitt , **ML**=McLaughlin, **MR**= Mercur, **N**= National, Vikre (1985); Unger (2008), **OR** = Ortiz, Kay (1986); Mutchler et al. (1997);Kelley and Luddington (2002) **RP**=Republic, Republic , Umpleby (1910); Lindgren (1933);Fifarek et al. (1996); Saunders et al. (2011a), **SC**= Silver City, Halsor et al. (1988); Unger (2008);Saunders et al. (2008), **SJ**= Silverton, Casadevall and Ohmoto (1977);Slack (1980); Unger (2008), **SS**= SteamBoat Springs, **TN**=Tonopah, Umpleby (1910); Spurr (1915); Bastin and Laney (1918); Lindgren (1933), **WN**= Cannon (Wenatchee) Guilbert (1963); Power-Fardy (2009), **ZL**= Zortman-Landusky , Mutchler et al. (1997).

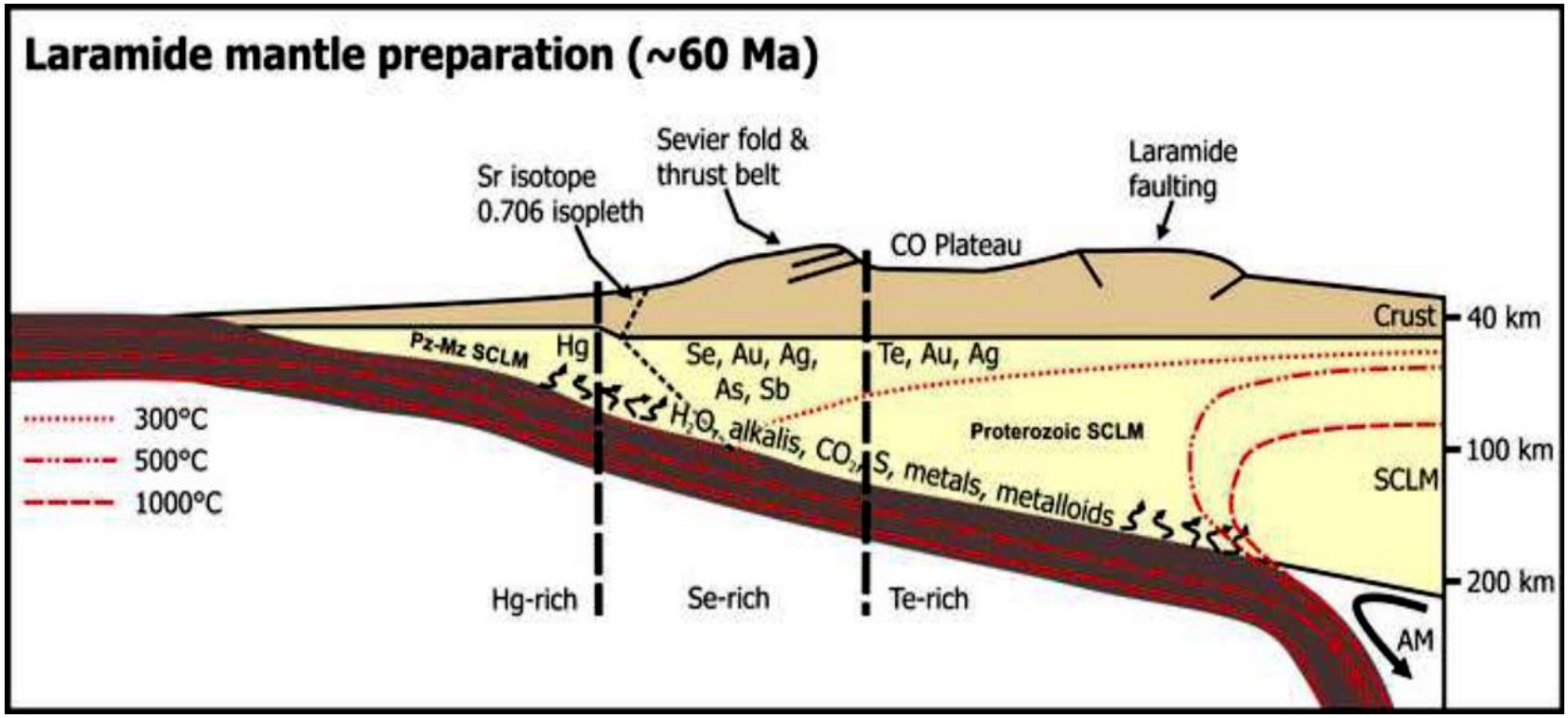

Fig. 57. Profile view of "magamatic mantle preparation" illustrating flat-slab subduction during the Laramide orogeny (modified from Saunders and Bruseke, 2012). Pz-Mz SCLM = Paleozoic- Mesozoic subcontinental lithospheric mantle. AM = Mantle.

Geochronology

$^{40}Ar/^{39}Ar$ geochronological studies have helped to ascertain a temporal nexus (approx 16.1-15.5 Ma) between the hydrothermal mineralization, the nascent Yellowstone hotspot and magmatism of potential source rocks (Hames et al., 2009). Mafic volcanism of the Steens Mountain Basalts and the Santa Rosa Calico Range that are thought to reflect the earliest magmatism of the Yellowstone hotspot occurred from 16.58 ± 0.18 to 15.51 ± 0.28 and 16.73 ± 0.04 to 14.3 ± 0.3 Ma respectively (Bruseke et al.,2007). Age dates of the bimodal volcanism in the study area are consistent with the ages above. Analysis of a rhyolite evaluated from the Silver City districts Trade Dollar mine produced an age date of 15.940 ± 0.097, whereas a basalt sample from the same area produced an age of 16.1 Ma (Hames, pers. commun., 2011). High-grade "bonanza" ores from the district were shown (this study) to have formed at a similar time as both the regional and localized (Silver City district) magmatism. Mineralization ages of these ores range between 15.98 ± 0.33 –15.367 ± 0.061 Ma. However, most of the Au mineralization appears to have been deposited in a brief mineralization window (15.4 Ma -15.8 Ma; Fig. 53). Nevertheless, though the ages in the district are tightly constrained, there is no obvious preferred trend of ore evolution within the location. Discordant hydrothermal conduits and inconsistencies in the paleo-topography may have had a direct bearing on hydrostatic pressure controls and boiling. As a result, irregular distribution of hydrothermal products, including adularia that was used for age dating occurs.

However, a more regional approach that attempts to integrate documented regional chronology of epithermal gold deposits appears to indicate a northeast to southwest advance of epithermal mineralization and volcanic centres (Fig. 58). This is consistent with the tectomagmatism (circa 17 Ma) that occurred as the North American

continent drifted over a relatively fixed magma source or hotspot from east to west (Camp and Ross, 2004). Given that the Yellowstone Hotspot plume has a northeasterly propagation of the trace of its track, generally, the oldest epithermal deposits (i.e. Sleeper and Jumbo) and volcanic centers occupy the western end of the northern Great Basin (Fig 58).

All things considered, the temporal agreement between the early Yellowstone magmatism and low sulfidation epithermal mineralization provides compelling evidence of the connection between the two geological phenomena. $^{40}Ar/^{39}Ar$ dating data therefore helps to infer the temporal link between the Au/Ag ores and a proposed mafic volcanic source (Kamenov et al., 2007) that have invariably been linked to the large scale magmatic episode associated with the nascent Yellowstone hotspot.

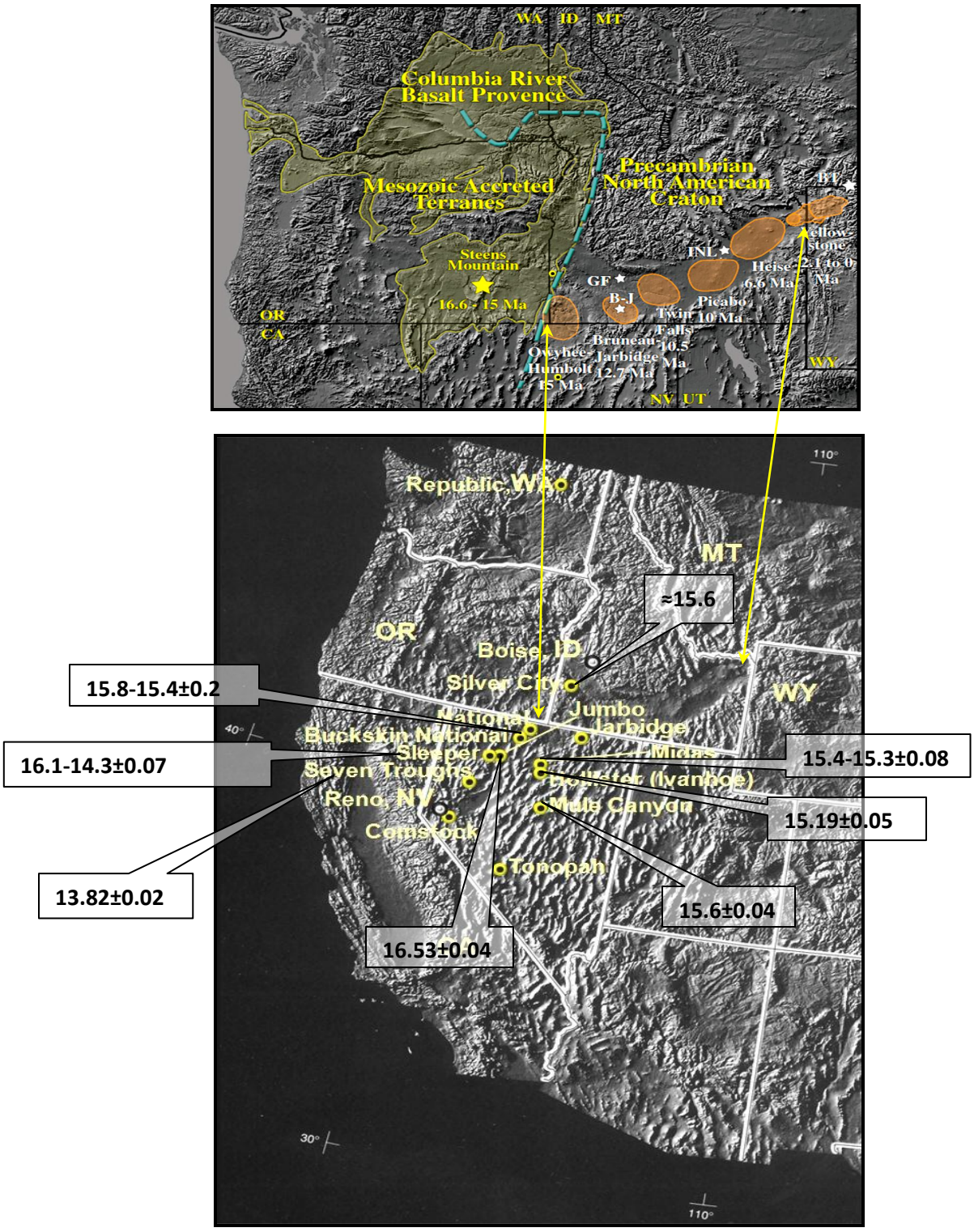

Fig. 58. Top: Shaded relief map (top) modified after Camp and Ross, (2004) showing locations of volcanic centres and corresponding eruption ages at Owyhee Humbolt , Bruneau Jarbidge, Twin Falls, Picabo, Heiss and Yellow Stone. Bottom: Shaded relief map showing low sulfidation epithermal deposit locations and mineralization ages (Ma) in the conterminous western United States, modified after Thelin et al. (1991).

8. CONCLUSIONS

- The geometry of the Orofino and Poorman veins is consistent with elongate, columnar fractures that formed during the mid-Miocene extensional tectonics pulling east and west. The veins are oriented north-south, northwest-southeast and east-west and are mineralized over a relatively confined vertical extent i.e. ≈ 762m below surface for Orofino vein, and ≈ 520m below surface for veins at Florida Mountain (Piper and Laney, 1926).

-Vein depositional temperatures range between 160°C and 285°C and low salinity (0.5% - 1 wt % NaCl equivalent) fluids. Fluid inclusions trapped by quartz adjacent to ore minerals appears to be meteoric and not ore stage.

- Disseminated mineralization is preferentially concentrated on the hanging-wall and footwall of veins due to the following factors:

(i) The altered quartz-rich rock on the veins' contact zones could be more chemically susceptible or receptive to mineralized hydrothermal fluid alteration.

(ii) Competency contrast between the quartz vein and the hanging wall and footwall of the granitoid host rock helped to redirect mineralized fluids that pond in the veins contact zones.

(iii) The abrupt release of pressure on mineralized fluid by faulting may have caused brecciation that produced the dark rhyolitic clasts (Fig. 6; Fig. 26 C). This resulted in a corresponding increase in porosity that help to provide preferred channels for mineralized fluid conveyance and entrapment.

-Two distinct fluids that consist of (i) ascending aqueous magmatic vapors/low density fluid from degassing magmas, and (ii) descending meteoric waters, apparently contribute to the formation of the Au-Ag epithermal deposit at War Eagle Mountain.

However, more work is warranted on this. Other specific conclusions are as follows:

- Downward percolating meteoric waters that get heated as they progress mix with upwardly welling acidic volatiles sourced from magmas. This enables leaching of major elements (e.g. silica (Si), aluminum (Al), potassium (K), sodium (Na), calcium (Ca) etc.) from host-rocks to produce vein and gangue material such as quartz (SiO_2), adularia ($KAlSi_3O_8$) ,calcite ($CaCo_3$), in near boiling zones.

-The fluid type hypothesized for contributing precious metals in epithermal deposits are low density supersaturated Au-Ag nanoparticles (magmatic aqueous vapors) formed at depth that get exsolved/separated directly from deep magmas or deep seated high density (saline) magmatic fluid.

- The disparate Pb chemistry of gold and electrum samples and their Cretaceous granite host rocks implies that the Au is not likely to have been sourced from the felsic rocks. Au is more likely to have emanated from primitive basalts, as proposed by Kamenov et al. (2007).

- Gold mineralization is dominated by electrum (Au-Ag alloy) averaging 59.5:40.5 wt % for the Poorman vein and 53.4:46.6 wt % for the Orofino vein. However, there is a general increase in Au ratios from west (Delamar Mountain) to east (War Eagle Mountain) for the district.

-Silver City district and War Eagle Mountain has a Se-rich system similar to Midas (Goldstrand and Schmidt, 2000) and National (Vikre, 1985) in the northern Great Basin.

- Silver minerals are generally Se-bearing and consist of a solid solution continuum of naumannite (Ag_2Se), aguilarite (Ag_4SeS), acanthite (Ag_2S) and two or more (?) unknown silver selenide and sulfur mineral phases.

-The Poorman vein generally shows that the main Ag mineralization is more similar in composition to aguilarite (Ag_4SeS), whereas the Orofino's is closer to arcanthite (Ag_2S)

in composition. However, the ores are generally comparable. This may be reflective of a common magmatic proginator.

-Ag mineral chemistry in the Silver City district and the northern Great Basin at large is thought to be a product of the volatility of metal(oids) (Saunders and Bruseke, 2012). Elemental fractionation/magmatic preparation (due to a flat slab subduction) results in a general east to west geographic-geochemical zonation of Cenozoic mineralization systems from Te rich to Se rich in the western part of the United States of America.

- Base metals occur in the deeper parts of the epithermal system. A corresponding decrease of Au was detected in these locales. Base metals predate coeval Au-Ag mineralization.

-The most favorable geochemical indicator of a potential epithermal Au/Ag mineralization system in this area would be a coincident gold, silver, zinc, mercury and selenium geochemical anomaly.

-The temporal agreement between the early Yellowstone tecto-magmatism and low sulfidation epithermal mineralization in the Silver City district provides compelling evidence of the connection between the two geological phenomena.

- The complex evolution and spatial overlap of hydrothermal systems precludes any preferred trend of ore evolution within the Silver City district.

-Generally epithermal deposits and volcanic centers in the northern Great Basin display ages that are progressively young northeastwards (Camp and Ross, 2004). When combined together with previous age dates, the data obtained from the Silver City district is consistent with this trend.

9. FUTURE WORK AND IMPLICATIONS FOR EXPLORATION

The Silver City district provides excellent opportunities for both continued academic and commercial research investigations. The discovery of at least 2 previously unknown Ag-Se-S phases should stimulate detailed crystallographic/mineralogical research in future on the Ag-Se (Au) epithermal system. Similarly the presence of an inordinate number of sizeable fluid inclusions in the Orofino and Poorman veins could encourage more detailed studies in the district. Such a study could be driven by the fact that most epithermal systems contain fine-grained silica minerals such as opal, chalcedony, and gels that curtail the formation of sizable fluid inclusions thus discouraging any meaningful analyses (Saunders, 1996; Saunders, 2008). A dual approach that targets both ore and gangue mineral-hosted fluid inclusions could be undertaken. Regular fluid inclusion analyses could be complemented by laser ablation-inductively coupled plasma-mass spectrometry (LA-ICP-MS) and near infrared microscopy that target fluid inclusions hosted by ore minerals that are opaque to visible light. Such a study could contrast the chemical composition of ore-precipitating fluids with meteoric waters and help to trace the source and evolution of mineralized fluids. (Kousmanov et al., 2010). The studies recommended above should take a district-wide approach in order to further constrain the proposed genetic model for the district. Further, a detailed study that attempts to characterize fluid inclusion types could be used to predict the proximity of undiscovered bonanza zones (Moncada et al., 2011). Moncada et al. (2011) demonstrated that fluid inclusions that imply boiling are usually associated with amorphous silica with colloform textures that do not trap primary fluid inclusions. In contrast euhedral quartz with coexisting liquid-rich and vapor-rich inclusions will be precipitated during less intense boiling. A study of fluid inclusions can

therefore be used to determine the presence or absence of boiling which has been demonstrated to control ore metal distribution in Au-Ag epithemal systems. Many epithermal systems are characterized by higher base metal occurrence beneath the boiling horizon and lower (or absent) precious metal grades, whereas above the boiling horizon precious metals are more common. (Buchanan,1981; Hedenquist et al., 2000).

The success of Pb isotope studies in isolating basalts as the source for gold mineralization should form the basis of future works and be tested in other deposits in both the northern Great basin and beyond. However, a definitive answer as to why the Pb isotopic signatures of gold from Midas district consistently display a distinct signature from those of the Silver City district is still lacking. The following ambiguities still remain begging: (i) could the depositional timings and crustal thickness differences in the two districts, be the only primary significant contributing factors to the distinct signatures?, and (ii) was the mantle plume Pb fingerprint changing rapidly over time or was it solely controlled by the SCLM? It is probable that plume magmas in the Silver City district interacted with an ancient SCLM and acquired patterns that are reminiscent of the Snake River Plain basalts. Alternatively, the boundary between the Mesozoic-Paleozoic accreted terranes, and Precambrian North American Craton as suggested by Hanan et al. (2008), requires adjustment westwards around the Silver City district to conform to the Pb in gold isotopic patterns observed in this study.

Several mid to small-budgeted exploration efforts were made in the late 1980s and early 1990s in an attempt to delineate both a bulk minable open pit Au/Ag resource and an extension of narrow high-grade Au/Ag veins, albeit unsuccessfully. For example, an airborne very low frequency electromagnetic (VLF EM), electromagnetic (EM) and magnetics survey carried out on War Eagle Mountain proved inconclusive due to inconsistencies in flight elevation, and the coarse nature of sampling (200 m line

spacing). Furthermore, soil geochemical surveys carried out in some parts of the district proved unreliable due to poor laboratory analytical techniques (Peterson,1991).

One of the few exploration successes recorded during the period was the identification of a mineralized east-west oriented structural lineament that extends from the Poorman vein to the Afterthought mine (Peterson 1991). This accomplishment was achieved from a structural study based on color aerial photographs carried out by Mr. D. Webb (Peterson, 1991). The lineament later identified as the “Hot Zone” was tested by percussion and limited diamond drilling that returned some intermittent mineralized Au-Ag zones (Table 6). However, the true potential of the “Hot Zone” may have been missed given the limited understanding of the structure’s dip direction at the time of drilling (Peterson, 1991). It is likely that the “Hot Zone” is analogous to shear structures believed to be part of a succession of abstruse, east to west oriented (southerly dipping?) shear zones that were first documented as being potentially “viable” by Piper and Laney (1926).

The other exploration success achieved concurrent to the “Hot Zone” discovery was the identification of a previously unknown soil geochemical anomaly in an area south of the Poorman and Orofino veins. This newly identified target was christened “the Cornice Area”. Likewise intermittent mineralized zones were intersected by percussion drilling in this prospect (Table 6).

Given these limited successes, it is clear that the full potential of the Silver City district still remains ambiguous. In order to exhaustively rule out any missed targets, a renewed approach that takes advantage of modern scientific methods must be incorporated into future exploration programs.

The temporally constrained nature of the (Au-Ag) mineralization provides an obvious starting point for future regional exploration targeting. The focus for a low-grade

Hole ID.	Type	Dip°	Azimuth°	From (m)	To (m)	Interval (m)	Ag oz/t	Au oz/t
Cornice Area								
W15	P	90	vertical	21.336	22.86	1.524	0.45	0.616
W23	P	90	vertical	9.144	10.668	1.524	0.24	0.08
W24	P	90	vertical	12.192	13.716	1.524	0.38	0.122
W28	P	90	vertical	1.524	3.048	1.524	0.04	0.456
W73	P	45	270	19.812	21.336	1.524	0.63	0.63
W73	P	45	270	27.432	28.956	1.524	5.81	0.272
Hot Zone								
WE1	DD	90	vertical	145.6944	147.2184	1.524	0.15	0.12
WE3	DD	90	vertical	157.8864	162.4584	4.572	0.11	0.117
WE3	DD	90	vertical	179.2224	180.7464	1.524	0.67	0.284
WE3	DD	90	vertical	185.3184	189.8904	4.572	2.42	0.253
WE4	DD	90	vertical	172.8216	175.8696	3.048	0.39	0.251
WE5	DD	90	vertical	93.2688	94.7928	1.524	0.11	0.118
WE6	DD	90	vertical	94.7928	97.8408	3.048	0.72	0.103
W2	P	90	vertical	56.388	62.484	6.096	1.02	0.282
W3	P	90	vertical	146.304	147.828	1.524	0.44	0.102
W3	P	90	vertical	164.592	167.64	3.048	0.84	0.136
W3	P	90	vertical	175.26	182.88	7.62	5.46	0.197
W4	P	90	vertical	103.632	106.68	3.048	0.29	0.188
W4	P	90	vertical	153.924	156.972	3.048	0.95	0.228
W5	P	90	vertical	97.536	100.584	3.048	0.14	0.186
W6	P	90	vertical	146.304	147.828	1.524	0.42	0.29
W14	P	90	vertical	65.532	67.056	1.524	2.68	0.282
W14	P	90	vertical	131.064	135.636	4.572	8.48	0.55
W14	P	90	vertical	164.592	167.64	3.048	2.27	0.206
W14	P	90	vertical	170.688	173.736	3.048	2.15	0.121
W14	P	90	vertical	184.404	185.928	1.524	2.07	0.162
W14	P	90	vertical	195.072	196.596	1.524	3.62	0.208
W14	P	90	vertical	201.168	205.74	4.572	1.81	0.12
W40	P	-60	270	70.104	73.152	3.048	1.13	0.144
W40	P	-60	270	77.724	91.44	13.716	4.52	0.306
W40	P	-60	270	128.016	132.588	4.572	0.52	0.156
W40	P	-60	270	152.4	155.448	3.048	2.86	0.181
W40	P	-60	270	163.068	176.784	13.716	4.15	0.419
W40	P	-60	270	185.928	195.072	9.144	3.39	0.264
W42	P	-70	90	44.196	47.244	3.048	2.7	0.367

Table 6. Drill log showing selected mineralized zones from the drilling program at Cornice and Hot Zone (Peterson, 1991). The exact UTM coordinates of these drill hole locations could not be established.

bulk open pit mining resource should ideally be the mid-Miocene volcanics that are coeval to mineralization. Exploration efforts should target these formations further along strike, both east and west. Given that the Au-Ag mineralization has been shown to be sympathetic to structural and lithological controls, a detailed geological mapping program that lays an emphasis on a thorough structural investigation is imperative. The limited success at the “Hot Zone” illustrates the need to re-evaluate the structural interpretation for the area. Previous exploration efforts have largely ignored the east to west structures that are orthogonal to the north to south oriented mineralization, yet the district itself is aligned east-west. An investigation of such structural ambiguities within the district and further along strike could help to confirm or disapprove the existence of new targets. To achieve this, intersection lineation’s produced by combining detailed structural mapping of “planer structures” such as faults, joints and bedding, and “linear mineralization structures” such as quartz veins and quartz stringers could be used as a predictive tool for vectoring towards potential Au/Ag mineralization trap sites (Watkins, pers. commun., 2007).

In order to replicate the limited success at the Cornice Area, a well-coordinated regional geochemical soil sampling survey should be conducted for the district. Geochemical soil sampling lines should incorporate both mined areas and pristine ground beyond the known strike length limits of the district. This will help to contrast low-level, regional, secondary dispersion halos that could prove to be potential targets for follow-up work. Going by the strong statistical correlations produced in this study, the most favorable geochemical indicator of a potentially viable epithermal Au/Ag mineralization system would be a coincident Au, Ag, Zn, Hg and Se geochemical anomaly. Broad K anomalies should also be considered as they could reflect potassium enrichment, potassium metasomatism, or perverse hydrothermal alteration, which could

prove useful for vectoring towards Au-Ag mineralization as proposed for Midas, Nevada by Leavitt et al. (2004), and successfully demonstrated by Morrel et al. (2011) for the Waihi-Waitekauri region, New Zealand.

Generally, geophysical methods are acknowledged to have provided limited success in the discovery of epithermal deposits worldwide (Sillitoe 1995; Hedenquist et al., 2000). However, detailed airborne geophysical techniques such as aeromagnetics and airborne radiometric surveys could prove useful in delineating important regional structures and geochemical signals. Aeromagnetic surveys could help to delineate “magnetic quite zones” that may be a reflection of structurally controlled fossil geothermal systems or quartz vein systems (Webster and Henley, 1989). Alternatively radiometric methods could help delineate alteration zones containing elevated K-enrichment associated with Au-Ag mineralization (Webster and Henly, 1989).

REFERENCES

Abbot, M.B., and Wolfe, A.P., 2003, Intensive pre-Incan metallurgy recorded by lake sediments from the Bolivian Andes: Science, v. 301, p. 1893-1895.

Arancibia, G., Matthews, S.J., Cornejo, P., Perez de Arce, C., Zuluaga, J. I.,and Kasanevan, S., 2006, $^{40}Ar/^{39}Ar$ and K-Ar geochronology of magmatic and hydrothermal events in a classic low-sulphidation epithermalbonanza deposit; El Penon, Northern Chile: Mineralium Deposita, v. 41, p. 505-516.

Armstrong, J.T., 1988, Quantitative analysis of silicate and oxide materials: comparison of Monte Carlo, ZAF, and phi-rho-z procedures, in D.E. Newbury, ed., Microbeam Analysis, p. 239-246.

Armstrong, R.L., Taubeneck, W.P., and Hales, P.O., 1977, Rb-Sr and K-Ar geochronology of Mesozoic granitic rocks and their Sr isotopic compositions, Oregon, Washington, and Idaho: Geological Society of America Bulletin, v. 88, p. 397-411.

Asher, R.R., 1968, Geology and mineral resources of a portion of the Silver City region, Owyhee County, Idaho: Idaho Bureau of Mines and Geology Pamphlet 138, p. 106.

Barton, P. B. Jr., and Bethke, P.M., 1986, Chalcopyrite disease in sphalerite: Pathology and epidemiology: American Mineralogist, v 72, p. 451–467.

Bennet, E.H., and Galbraith, J., 1975, Reconnaissance Geology and Geochemistry of the Silver City- South Mountain Region, Owyhee County, Idaho: Idaho Bureau of Mines and Geology, p. 88.

Bethke, P.M., Rye, R.O., Stoffregen, R.E., and Vikre, P.G., 2005, Evolution of the magmatic-hydrothermal acid-sulfate system at Summitville, Colorado: Integration of geological, stable isotope, and fluid inclusion evidence: Chemical Geology, v. 215, p. 281-315.

Bobis, R.E., Jaireth, S., and Morrison, G.W., 1995, The anatomy of a carboniferous epithermal ore shoot at Pajingo, Queensland: setting, zoning, alteration, and fluid conditions: ECONOMIC GEOLOGY, v. 90, p. 1776-1798.

Bonham, H.F., Jr., 1969, Geology and mineral deposits of Washoe and Storey counties, Nevada, with a section on Industrial rock and mineral deposits by K.L. Papke: Nevada Bureau of Mines and Geology Bulletin 70, p.140.

Bonham, H.F., and Garside L.J., 1979, Geology of the Tonopah, Lone Mountain, Klondike, and North Mudlake quadrangles: Nevada Bureau of Mines and Geology Bulletin 92, p. 142, 2 plates.

Bonnichsen B., 1983, Epithermal gold and silver deposits Silver City- De Lamar district, Idaho:Idaho Geological Survey Technical Report 83-84, p. 29.

Bonnichsen, B., and Godchaux, M.M., 2006, Geologic map of the Murphy 30 x 60 quadrangle, Ada, Canyon, Elmore, and Owyhee Counties, Idaho: Idaho Geological Survey DWM-80.

Bruseke, M.E., Heizler, M.T., Hart, W.K., Mertzman, S.K., 2007, Distribution of Oregon Plateau (U.S.A.) flood basalt volcanism: The Steens basalts revisited: Journal of Volcanology and Geothermal Research, v. 161, p. 187-214.

Brueseke, M.E., Hart, W.K., Heizler, M.T., 2008, Chemical and physical diversity of mid-Miocene silicic volcanism in northern Nevada: Bulletin of Volcanology, v. 70, p. 343-360.

Buchanan, L.J., 1981, Precious metal deposits associated with volcanic environments in the southwest: Arizona Geological Society Digest, v. 14, p. 237-262.

Bureau of Land Management News Release, 2009, Reclamation and Sustainable Mineral Development Award Winners (http://www.blm.gov/wo/st/en/info/newsroom/2009/october/NR_10_28_2009.html).

Bussey, S.D., 1996, Gold mineralization and associated rhyolitic volcanism at the Hog Ranch district, northwest Nevada: Geological Society of Nevada, Geology and Ore deposits of the American Cordillera Symposium, Reno-Sparks, Nevada, April 1995, Proceedings, p. 181-207.

Bastin, E.S., and Laney, F.B., 1918, The genesis of the ores at Tonopah, Nevada: U.S. Geological Survey Professional Paper 104, 55 p.

Camp, V.E. and Ross, M.E., 2004, Mantle dynamics and genesis of mafic magmatism in the intermontane Pacific Northwest: Journal of Geophysical Research, v. 109, B08204 DOI:10.1029/2003JB002838.

Camp, V.E and Hanan, B.B., 2008, A plume-triggered delamination origin for the Columbia River Basalt Group: Geosphere, v. 4, p. 480-495.

Carman, G.D., 2003, Geology, mineralization, and hydrothermal evolution of the Ladolam Gold Deposit, Lihir Island, Papua New Guinea, in Simmons, S., and Graham, I., eds., Volcanic, Geothermal, and Ore- Forming Fluids: Rulers and Witnesses of Processes within the Earth: Society of Economic Geologists, Special Publication 10, p. 247-284.

Casadevall, T., and Ohmoto, H., 1977, Sunnyside mine, Eureka mining district, San Juan County, Colorado: Geochemistry of gold and base metal ore deposition in a volcanic environment: ECONOMIC GEOLOGY, v. 72, p. 1285–1320.

Conrad, J.E., and McKee, E.H., 1996, High-precision $^{40}Ar/^{39}Ar$ ages of rhyolitic host rock and mineralized veins at the Sleeper deposit, Humboldt County, Nevada: Geological Society of Nevada, Geology and Ore Deposits of the American Cordillera Symposium, Reno-Sparks, Nevada, April 1995, Proceedings, p. 257-262.

Coats, R.R., 1936, Auguilarite from the Comstock lode, Virginia City, Nevada: American Mineralogist, v. 21, p. 543–534.

Conrad, J.E., McKee, E.H., Rytuba, J.J., Nash, J.T., and Utterback, W.C., 1993, Geochronology of the Sleeper deposit, Humboldt County, Nevada: Epithermal goldsilver mineralization following emplacement of a silicic flow-dome complex: ECONOMIC GEOLOGY, v. 88, p. 81-91.

Corbett G., 2002, Epithermal Gold for Explorationists: The Australian Institute of Geoscientists, p 1-26.

Crafford, E.E.J., and Grauch, V.J.S., 2002, Geologic and geophysical evidence for the influence of deep crustal structures on Paleozoic tectonics and the alignment of world-class gold deposits, northcentral Nevada, USA: Ore Geology Reviews, v. 21, p. 157-184.

Cupp L. B., 1986, War Eagle Mountain Geologic Summary: Pacific Power and Industrial Co., Inc, p.11. (Unpublished).

Cupp, B.L., 1989, Mineralization and volcanism at the DeLamar Silver Mine, Owyhee County, Idaho: Unpublished M.Sc. thesis, Miami University, 95 p.

Dalrymple, G.B., Alexander, E.C., Lanphere, M.A., and Kraker, G.P., 1981, Irradiation of samples for $^{40}Ar/^{39}Ar$ dating using the Geological Survey TRIGA Reactor: USGS Professional Paper 1176, 55 p.

Dalrymple, G.B., and Lanphere, M.A., 1969, Potassium argon dating Principles techniques and applications to geochronology: W.H. Freeman and Company, San Fransisco 258 p.

de Ronde, C.E.J., and Blattner, P., 1988, Hydrothermal alteration, stable isotopes, and fluid inclusions of the Golden Cross epithermal gold-silver deposit, Waihi, New Zealand: ECONOMIC GEOLOGY, v. 83, p. 895-917.

Deyell, C.L., Leonardson, R., Rye, R.O., Thompson, J.F.H., Bissig, T., and Cooke, D.R., 2005, Alunite in the Pascua-Lama high-sulfidation deposit: constraints on alteration and ore deposition using stable isotope geochemistry: ECONOMIC GEOLOGY, v. 100, p. 131-148.

Dickin, A.P., 2005, Radiogenic isotope geology: Cambridge University Press 492p.

Dubé, G., Dunning, G., and Lauziere, K., 1998, Geology of the Hope Brook Mine, Newfoundland, Canada: A preserved Late Proterozoic high-sulfidation epithermal gold deposit and its implications for exploration: ECONOMIC GEOLOGY, v. 93, p. 405-436.

Ekren, E.B., McIntyre, D.H., Bennett, E.H., and Malde, H.E., 1981, Geologic map of Owyhee County, Idaho, west of longitude 116°W: U.S. Geological Survey Map1-1256.

Ekren, E.B., McIntyre, D.H., Bennett, E.H. and Marvin, R.F., 1982, Cenozoic stratigraphy of western Owyhee County, Idaho, in Bonnichsen, B. and Breckenridge, R.M. eds., Cenozoic Geology of Idaho: Idaho Bureau of Mines Geology Bulletin 26, p. 215-235.

English, J.M., Johnston, S.T., and Wang, K., 2003, Thermal modeling of the Laramide Orogeny: Testing the flat-slab subduction hypothesis: Earth and Planetary Science Letters, v. 214, p. 619-632.

Faure, G., 1977, Principles of isotope geology: John Wiley and Sons, New York, 464 p.

Feiss, P.G., Vance, R.K., and Wesolowski, D.J., 1993, Volcanic-rock hosted, gold and base-metal mineralization associated with Neoproterozoic early Paleozoic back-arc extension in the Carolina terrane, southern Appalachian Piedmont: Geology, v. 17, p. 548-551.

Fifarek, R.H., and Rye, R.O., 2005, Stable isotope geochemistry of the Pierina high-sulfidation Au-Ag deposit, Peru: influence of hydrodynamics on SO_4^{2-}-H_2S sulfur isotopic exchange in magmatic-steam and steam-heated environments: Geochemistry of sulfate minerals in high and low temperature environments: Chemical Geology, v. 215, p. 253-279.

Fitton, J.G., James, D., and Leeman, W.P., 1991, Basic magmatism associated with late Cenozoic extension in the western United States: Compositional variations in space and time: Journal of Geophysical Research, v. 96, p. 13,693–13,711.

Frondel, C. and Honea, R.M., 1968, Billingsleyite, a new silver sulfosalt: American Mineralogist, v. 53, p. 1791–1798.

Gillerman, V.S., and Mitchell, V. E., 2005, New developments in a new century for Idaho's precious metal districts, in Rhoden, H.N., Steininger, R.C., and Vikre, P.G., eds., Geological Society of Nevada Symposium 2005: Window to the World, Reno, Nevada, May 2005, p. 663–672.

Goldstrand, P.M., and Schmidt, K.W., 2000, Geology, mineralization, and ore controls at the Ken Snyder gold-silver mine, Elko County, Nevada: Geological Society of Nevada, Geology and Ore Deposits 2000: The Great Basin and Beyond Symposium, May 15-18, 2000, Reno-Sparks, Nevada, Proceedings, p. 265-287.

Goldfarb, R.J., Ayuso, R.A., Miller, M.L., Ebert, S., Marsh, E.E., Petsel, S.A., Miller, L.D., Bradley, D., Johnson, C., and McClelland, W., 2004, The Late Cretaceous Donlin Creek gold deposit, Southwestern Alaska: Controls on epizonal ore formation: ECONOMIC GEOLOGY, v. 99, p. 643-671.

Gosselin, P., and Dubé, B., 2005a, Gold deposits and gold districts of the world: Geological Survey of Canada, Open File 4893, 1 colour poster.

Gosselin, P., and Dubé, B., 2005b, Gold deposits of the world: distribution, geological parameters, and gold content: Geological Survey of Canada, Open File 4895,1 CD-ROM.

Guilbert, J.M., 1963, unpublished report for Day Mines, Inc., cited in Margolis, J., 1989, Arkose-hosted, aquifer-controlled, epithermal Au-Ag mineralization, Wenatchee, Washington: ECONOMIC GEOLOGY, v. 84, p. 1891–1902.

Halsor, S.P., Bornhorst, T.J., Beebe, M., Richardson, K., and Strowd, W., 1988, Geology of the Delamar silver mine, Idaho - A volcanic dome complex and associated hydrothermal system: ECONOMIC GEOLOGY, v. 83, p. 1159-1169.

Hames, W., Unger, D., Saunders, J., Kamenov, G., 2009, Early Yellowstone hotspot magmatism and gold metallogeny: Journal of Volcanology and Geothermal Research v. 188, p. 214 – 224.

Hanan, B.B., Shervais, J.W., Vetter, S.K., 2008. Yellowstone plume-continental lithosphere interaction beneath Snake River Plain. Geology v. 36, p. 51–54.

Hart, W.K., and Carlson, R.W., 1985, Distribution and geochronology of Steens Mountain-type basalts from the northwestern Great Basin: Isochron/West, v. 43, p. 5-10.

Hart, A., 2010 Idaho History: Boise's early railway depots were gateways to the U.S.: Idaho Statesman.com (http://www. Idahostatesman.com/2010/11/14/1418019/boises-early-railway-depots-were.html#xzz1Rt3b7TYN) 05/16/2011.

Hayba, D.O., Bethke, P.M., Heald, P.M., and Foley, N.K., 1985, Geologic, mineralogic, and geochemical characteristics of volcanic-hosted epithermal precious-metal deposits: Reviews in ECONOMIC GEOLOGY, v. 2, p. 129-167.

Haynes, W.M., ed., 2010, Handbook of chemistry and physics: 90th edition: Boca Raton, Chemical Rubber Company, 2804 p.

Hedenquist, J.W., and Lowenstern, J.B., 1994, The role of magmas in the formation of hydrothermal ore deposits: Nature, v. 370, p. 519-527.

Hedenquist, J.W., Arribas, A.R., and Gonzalez-Urien, E., 2000, Exploration for epithermal gold deposits, Chapter 7 in Hagemann, S.G., and Brown, P.E., eds., Gold in 2000: Society of Economic Geologists, Reviews in ECONOMIC GEOLOGY, v. 13, p. 245-277.

Heinrich, C.A., Driesener, T., Stefansson, A., and Seward, T.M., 2004, Magmatic vapor contraction and the transport of gold from the porphyry environment to epithermal ore deposits: Geology, v.32, p. 761-764.

Heinrich, C.A., 2005, The physical and chemical evolution of low-salinity magmatic fluids at the porphyry to epithermal transition: A thermodynamic study: Mineralium Deposita, v. 39, p. 864-889.

Hudson, D.M., John, D.A., and Fleck, R.J., 2006, Geologic setting, geochemistry, and geochronology of epithermal gold-silver deposits in the Seven Troughs District, northwest Nevada: Abstracts with Programs - Geological Society of America, v. 37, no. 7, p. 380.

Huston, D.L., Blewett, R. S., Keillor, B., Standing, J., Smithies, R.H., Marshall, A., Mernagh, T.P., and Kamprad, J., 2002, Lode gold and epithermal deposits of the Mallina Basin, North Pilbara Terrain, Western Australia: ECONOMIC GEOLOGY, v. 97, p. 801-818.

Jensen, E.P., and Barton, M.D., 2000, Gold deposits related to alkaline magmatism: Reviews in economic geology, v. 13, p. 279–313.

John, D.A., 2001 Miocene and early Pliocene epithermal gold silver deposits in the northern Great Basin, western USA: Characteristics, distribution, and relationship to magmatism:ECONOMIC GEOLOGY, v. 96, p.1827-1853.

John, D.A., Hofstra A.H., Theodore T.G., 2003, A special issue devoted to gold deposits in northern Nevada: Part 1. Regional Studies and Epithermal Deposits: ECONOMIC GEOLOGY, v. 98, p.225-234.

Jordan, B.T., Grunder, A.L., Duncan, R.A., and Deino, A.L., 2004, Geochronology of age-progressive volcanism of the Oregon High Lava Plains: Implications for the plume interpretation of Yellowstone: Journal of Geophysical Research, v. 109, B10202 DOI:10.1029/2003JB002776.

Kamenov, G.D., Saunders, J.A, Hames, W.E., and Unger, D.L., 2007, Mafic magmas as sources for gold in middle Miocene epithermal deposits of the northern Great Basin, United States: Evidence from Pb-isotope compositions of native gold: ECONOMIC GEOLOGY, v. 102, p.1191-1195.

Kay, B.D., 1986, Vein and breccia gold mineralization and associated igneous rocks at the Ortiz mine, New Mexico, U.S.A.: Unpublished M.S. thesis, Golden, CO, Colorado School of Mines, 170 p.

Kelly, W.C., and Goddard, E.N., 1969, Telluride ores of Boulder County, Colorado: Geological Society of America Memoir 109, 237 p.

Kelley, K.D., and Ludington, S., 2002, Cripple Creek and other alkaline-related gold deposits in the southern Rocky Mountains, USA: Influence of regional tectonics: Mineralium Deposita, v. 37, p. 38–60.

Kistler, R.W., and Peterman, Z.E., 1978, Reconstruction of crustal California on the basis of initial strontium isotopic compositions of Mesozoic granitic rocks: United States Geological Survey Professional Paper 107, 17p.

Klein, T.L., and Criss, R.E., 1988, An oxygen isotope and geochemical study of meteoric-hydrothermal systems at Pilot Mountain and selected other localities, Carolina Slate Belt: ECONOMIC GEOLOGY, v. 83, p. 801-821.

Kouzmanov,K., Pettke,T., and Heinrich, C.A., 2010, Direct analysis of ore-precipitating fluids: Combined IR microscopy and LA-ICP-MS study of fluid inclusions in opaque ore minerals ECONOMIC GEOLOGY, v. 105, pp. 351–373.

Leavitt, E.D., Spell, T.L., Goldstrand, P.M., and Arehart, G.G., 2004, Geochronology of the Midas low-sulfidation gold-silver deposit, Elko County Nevada: ECONOMIC GEOLOGY, v.99, p. 1665-1686.

Leeman, W.P., Oldow, J.S., and Hart, W.K., 1992, Lithosphere-scale thrusting in the western U.S. Cordillera as constrained by Sr and Nd isotopic transitions in Neogene volcanic rocks: Geology v. 20, p. 63-66.

Lindgren, W., 1898, Hydrothermal potassium feldspar in gold ores from DeLamar, Idaho: American Journal of Science: (Fourth Series) no. 30, p. 418-420.

Lindgren, W., 1900, The gold and silver veins of the Silver City, DeLamar, and other mining districts in Idaho. US geological Survey 20th Annual Report, Part 3, p.65-256.

Lindgren, W., and Drake, N.F., 1904, Description of the Silver City quadrangle: United States Geological Survey Folio 104.

Lindgren, W., 1906, Ore deposition and deep mining: ECONOMIC GEOLOGY v. 1, p. 34-46.

Lindgren, W., 1922, A suggestion for the terminology of certain minerals deposits: ECONOMIC GEOLOGY, v. 17, p. 202-294.

Lindgren, W., 1933, Mineral deposits: New York, McGraw-Hill, 4th ed., 930 p.

Ludwig, K.R., 2003, User‘s manual for Isoplot, v. 3.0, a geochronological tool kit for Microsoft Excel: Berkeley Geochronological Center, Special Publication no. 4.

Marek, J.M., 1991, Reserve Review Report on Delamar and Florida Mountains: Independent Mining Consultants, INC. 32 p.

Megrue, G.H., 1973, Spatial distribution of $^{40}Ar/^{39}Ar$ ages in lunar breccias 14 301: Journal of Geophysics Research, v. 78, p. 3216-3221.

Morrel, A.E., Locke, C.A., Cassidy, J., and Mauk, J.L., Geophysical characteristics of Adularia-sericite epithermal gold-silver deposits in the Waihi-Waitekauri region, New Zealand: ECONOMIC GEOLOGY, v. 106, p. 1031-1041.

Monchada, D., Mutchler, S., Nieto A., Reynolds, T.J., Rimstidt, J.D., Bodnar, R.J., 2011, Mineral textures and fluid inclusion petrographyof the epithermal Ag-Au deposits at Guanajuato, Mexico: Application to exploration: Journal of Geochemical Exploration v., p.16.

Mutchler, F.E., Larson, E.E., and Ross, M.L., 1997, Potential for alkaline igneous rock-related gold deposits in the Colorado Plateau laccolithic centers: U.S. Geological Survey Bulletin 2158, p. 233–252.

Mueller, P.J., and Frost, C.D., 2006, The Wyoming Province: A distinctive Archean craton in Laurentian North America: Canadian Journal of Earth Sciences, v. 43, p. 1391–1397, doi: 10.1139/E06–075.

Naden, J., Kilias, S.P., and Darbyshire, D.P.F., 2005, Active geothermal systems with entrained seawater as modern analogs for transitional volcanic- hosted massive sulfide and continental magmato-hydrothermal mineralization: the example of Milos Island, Greece: Geology, v. 33, p. 541-544.

Nash, J.T., Utterback, W.C., and Trudel, W.S., 1995, Geology and geochemistry of tertiary volcanic host rocks, sleeper gold-silver deposit, Humboldt County, Nevada: United States Geological Survey Bulletin 2090.

Noble, D.C., McCormack, J.K., McKee, E.H., Silberman, M.L., and Wallace, A.B., 1988, Time of mineralization of the evolution of the McDermitt caldera complex, Nevada- and the relation of middle Miocene mineralization in the northern Great Basin to coeval regional basaltic magmatic activity: ECONOMIC GEOLOGY, v. 83, p. 859-863.

O'Brien, S.J., Dube, B., and O'Driscoll, C.F., 1999, High-sulphidation, epithermal-style hydrothermal systems in late Neoproterozoic Avalonian rocks on the Burin Peninsula, Newfoundland: Implications for gold exploration, in Current Research: Newfoundland Geological Survey, Newfoundland Department of Mines and Energy, Report 99-1, p. 275-296.

Obuya, E.A., (Unpublished) Multi-purpose use of electrospun TiO_2 nanostructures for greener chemical transformations and environmental remediation: PhD Dissertation Binghamton University.

Pansze, A.J., 1972, K-Ar ages of plutonism, volcanism, and mineralization, Silver City region, Owyhee County, Idaho: Isochron/West, n.4, p. 1-4.

Pansze, A.J., 1975, Geology and ore deposits of the Silver City-DeLamar-Flint region, OwyheeCounty, Idaho: Idaho Bureau of Mines and Geology Pamphlet 161, 79 p.

Patersen, D.B., 1991, Report on the War Eagle Mountain property Owyhee County, Idaho: War Eagle Mining, Inc., 25 p. (Unpublished).

Panteleyev, A.,1996a, Hot-Spring Au-Ag (H03), in Lefebure, D.V., and Hoy, T., eds., Selected British Columbia mineral deposit profiles, v. 2 – Metallic Deposits: Ministry of Employment and Investment, Open File1996-13, p. 33-36.

Panteleyev, A.,1996b, Epithermal Au-Ag-Cu high sulphidation (H04), in Lefebure, D.V., and Hoy, T., eds., Selected British Columbia mineral deposit profiles, v. 2 – Metallic Deposits, Ministry of Employment and Investment, Open File 1996-13, p. 37-39.

Panteleyev, A.,1996c, Epithermal Au-Ag-Cu low sulphidation (H05), in Lefebure, D.V., and Hoy, T., eds., Selected British Columbia mineral deposit profiles, v. 2 Metallic Deposits, Ministry of Employment and Investment, Open File 1996-13, p.41-44.

Panteleyev, A.,2005a, Epithermal Au-Ag-Cu: High sulphidation: British Columbia Mineral Deposit Profiles, British Columbia Geological Survey, Report H04, modified for Yukon by A. Fonseca, Yukon Geological Survey.

Panteleyev, A., 2005b, Epithermal Au-Ag-Cu: Low sulphidation: British Columbia Mineral Deposit Profiles, British Columbia Geological Survey, Report H05, modified for Yukon by A. Fonseca, Yukon Geological Survey.

Peppard, B., 2002, Geology and geochemistry of the Ivanhoe vein system, Elko, Nevada:Unpublished M.S. thesis, Ann Arbor, University of Michigan, 49 p.

Petruk, W.,Owens, D.R., Stewart, J.M., Murray, E.J., 1974, Observations on acanthite, aguilarite and naumannite: Canadian Mineralogist v. 12, p. 365-369.

Porter, E.W., and Ripley, E., 1985, Petrologic and stable isotope study of the gold-bearing breccia pipe at the Golden Sunlight deposit, Montana: ECONOMIC GEOLOGY, v. 80, p. 1689–1706.

Poulsen, K.H., 1996, Lode gold, in Eckstrand, O.R., Sinclair, W.D., and Thorpe, R.I., eds., Geology of Canadian Mineral Deposit Types: Geological Survey of Canada, Geology of Canada, No. 8, p. 323-328(also Geological Society of America, The Geology of North America, v. P-1).

Poulsen, K.H., Robert, F., and Dube, B., 2000, Geological Classification of Canadian Gold Deposits: Geological Survey of Canada, Bulletin 540, 106 p.

Power-Fardy, D., 2009, A technical review of the “D” reef (formerly the Lovitt-Day gold mine), Wenatchee, Washington USA for Lovitt Resources, Inc., Unpublished report, Watts Griffis, and McOuat Ltd., 107 p.

Piper, A. M., and Laney, F.B., 1926, Geology and metalliferous resources of the region about Silver City, Idaho: Idaho Bureau of Mines and geology Bulletin 11, 165 p.

Renne, P.R., Swisher, C.C., Deino, A.L., Karner, D.B., Owens, T.L., DePaolo, D.J., 1998, Intercalibration of standards, absolute ages, and uncertainties in $^{40}Ar/^{39}Ar$ Dating: Chemical Geology 145, 117–152.

Roedder, E., 1984, Fluid Inclusions: Minerological Society of America, Reviews in miner ology, v. 12, 643p.

Rodgers L. J., and Nicewander, W. A., 1988, Thirteen ways to look at the correlation coefficient : American Statistical Association, The American Statistician, v. 42, no. 1, p. 59-66.

Saunders, J.A.,1988, Textural and geochemical characteristics of gold mineralization from the Cresson mine, Cripple Creek district, Colorado, U.S.A.: Institution of Mining and Metallurgy (London) Transactions, v. 97, p. B36–B39.

Saunders, J.A.,1991, Gold deposits of the Boulder County gold district, Colorado: U.S. Geological Survey Bulletin 1857-I, p. 137–148.

Saunders, J.A., 1993, Supergene oxidation of bonanza Au-Ag veins at the Sleeper Deposit, Nevada, USA: implications for hydrogeochemical exploration in the Great Basin: Journal of Geochemical Exploration, v. 47, p. 359-375.

Saunders, J.A., and May, E.R., 1986, Bessie G: A high-grade epithermal gold telluride deposit, La Plata County, Colorado, in Macdonald, A.J., ed., GOLD'86, An International Symposium on the Geology of Gold, Toronto, 1986, p. 436–444.

Saunders, J.A., Schoenly, P.A., and Cook, R.B., 1996, Electrum disequilibrium crystallization textures in volcanic-hosted bonanza epithermal gold deposits: Proceedings of the International Symposium on the Geology and Ore Deposits of the America Cordillera: (Reno, NV) p. 173-179.

Saunders, J.A., Unger, D.L., Kamenov, G.D., Hames, W.E., and Utterback, W.C., 2008, Genesis of mid-Miocene Yellowstone hotspot-related bonanza epithermal Au-Ag deposits, northern Great Basin region, USA: Mineralium Deposita, 43 p.715-734.

Saunders, J.A., 2010, Retracing Waldemar Lindgren's footsteps: Perspective from an epithermalist celebrating Lindgren's 150th Birthday. SEG Newsletter, No 83, p.26-27.

Saunders, J.A., Kamenov, G.D., Hofstra, A.H., Unger, D.L., Creaser, R.A., and Barra, F., 2011a, "Forensic" geochemical approaches to constrain the source of Au-Ag in low-sulfidation epithermal ores, in Steininger, R., and Pennell, W., eds., Great Basin evolution and metallogeny: Geological Society of Nevada 2010 Symposium, Reno, Nevada, May 14–22, 2010, p. 693–700.

Saunders, J.A., Vikre, P., Unger, D.L., and Beasley, L., 2011b, Colloidal and physical transport textures exhibited by electrum and naumannite in bonanza epithermal veins from western USA, and their significance, in Steininger, R., and Pennell, W., eds., Great Basin evolution and metallogeny: Geological Society of Nevada 2010 Symposium, May 14–22, 2010, p. 825–832.

Saunders, J.A., and Bruseke, M.E., 2012, Volatility of Se and Te during subduction-related distillation and the geochemistry of epithermal ores of the western United States: Economic Geology, v. 107, p. 165–172.

Sawkins, F.J., O'Neil, J.R., and Thompson, J.M., 1979, Fluid inclusion and geochemical studies of vein gold deposits, Baguio district, Philipines: ECONOMIC GEOLOGY, v. 74, p. 1420-1434.

Shervais, J.W., Schuman, M.M.S., and Hanan, B.B., 2005, The Stonyford Volcanic Complex: A forearc seamount in the Northern California Coast Ranges: Journal of Petrology, v. 46, p. 2091–2128, doi: 10.1093/petrology/egi048.

Shimizu, T., Matsueda, H., Ishiyama, D., and Matsubaya, O., 1998, Genesis of epithermal Au-Ag mineralization of the Koryu Mine, Hokkaido Japan: ECONOMIC GEOLOGY v. 93, p. 303-325.

Sillitoe, R.H., 1989, Gold deposits in western Pacific island arcs; the magmatic connection: ECONOMIC GEOLOGY Monographs 6, 274–291.

Sillitoe, R.H.,1992, Giant and bonanza gold deposits, in Whiting, B.H., Mason, R., and Hodgson, C.J. eds., Epithermal and Sub-volcanic Settings, Giant Ore Deposits, p. 231-238.

Sillitoe, R.H., 1993, Epithermal models: genetic types, geometrical controls and shallow features, in Kirkham, R.V., Sinclair, W.D., Thorpe, R.I., and Duke, J.M. eds., Mineral Deposit Modeling: Geological Association of Canada, Special Paper 40, p. 403-417.

Sillitoe, R.H., 1995, Exploration and Discovery of base and precious-metal deposits in the Circum-Pacific Region During the Last 25 years: Resource Geology, Special Issue 19,119 p.

Sillitoe, R.H., Hannington, M.D., and Thompson, J.F.H., 1996, High-sulfidation deposits in the volcanogenic massive sulfide environment: ECONOMIC GEOLOGY, v. 91, p. 204-212.

Sillitoe, R.H., 1997, Characteristics and controls of the largest porphyry coppergold and epithermal gold deposits in the circum-Pacific region: Australian Journal of Earth Sciences, v. 44, p. 373-388.

Sillitoe, R.H., and Hedenquist, J.W., 2003, Linkages between volcanotectonic settings, ore fluid compositions and epithermal precious metal deposits: Society of Economic Geologists Special Publication 10, p. 315-343.

Simmons, S. F., and Brown, K.L., 2006, Gold in magmatic hydrothermal solutions and the rapid formation of a giant gold deposit: Science, v. 314, p. 288-291.

Simmons, S.F., Christensen, B.W., 1994, Origins of calcite in a boiling geothermal System: American Journal of Science, v. 294, p. 361–400.

Simmons, F.S., White N.C., and John, D.A., 2005, Geological characteristics of epithermal precious and base metal deposits: ECONOMIC GEOLOGY 100th anniversary volume p. 485-522.

Simon, G., Kesler, S.E., and Essene, E.J., 1997, Phase relations among selenides, sulfides, tellurides, and oxides: II. Applications to selenide-bearing ore deposits: ECONOMIC GEOLOGY, v. 92, p. 468–484.

Singer, D.A., 1995, World class base and precious metal deposits-a quantitative analysis: ECONOMIC GEOLOGY, v. 90, p. 88-104.

Slack, J.F., 1980, Multistage vein ores of the Lake City district, western San Juan Mountains, Colorado: ECONOMIC GEOLOGY, v. 75, p. 963–991.

Spry, P.G., Paredes, M.M., Foster, F., Truckle, J.S., and Chadwick, T.H., 1996, Evidence for a genetic link between gold-silver telluride and porphyry molybdenum mineralization at the Golden Sunlight deposit, Whitehall, Montana: Fluid inclusion and stable isotope studies: ECONOMIC GEOLOGY, v. 91, p. 507–526.

Spurr, J.E., 1915, Geology and ore deposition at Tonopah, Nevada: ECONOMIC GEOLOGY, v. 10, p. 713–769.

Statham, W., Statham, W., Statham, R., 2003, War Eagle mountain field trip: Owyhee County Historical Society, p. 37.

Sugaki, A., Kitakaze, A. and Isobe, K. (1986) Silver mineralization of the Karuizawa Mine, Fukushima Prefecture, Japan. Mining Geology, v. 36, p. 535-544.

Taylor, B.E., 2007, Epithermal gold deposits, in Goodfellow, W.D., ed., Mineral Deposits of Canada: A synthesis of major deposit-types, district metallogeny, the evolution of geological provinces, and exploration methods: Geological Association of Canada, Mineral Deposits Division, Special Publication No. 5, p. 113-139.

Taylor, S.R., 1964, Abundance of chemical elements in the continental crust: a new Table: Geochemica et Cosmochimica Acta 1964, v. 28, p. 1273-1285.

Thelin G.P., Pike, R.J., 1991, Landforms of the conterminous United States- A digital Shaded relief portrayal: U.S. Department of the Interior, U.S. Geological Survey, 16p.

Tingley J.V., 1998, Mining districts of Nevada: Nevada Bureau Of Mines And Geology Report 47 Second Edition in collaboration with Mackey School of Mines University of Nevada, Reno, p.329.

Turner, W.A., Heaman, L.M., and Creaser, R.A., 2003, Sm-Nd fluorite dating of Proterozoic low-sulfidation epithermal Au-Ag deposits and U-Pb zircon dating of host rocks at Mallery Lake, Nunavut, Canada: Canadian Journal of Earth Sciences, v. 40, p. 1789-1804.

Umpleby, J.B., 1910, Geology and ore deposits of Republic mining district: Washington Geological Survey Bulletin 1, 65 p.

Unger, D.L., 2008, Geochemistry, geochronology and ore petrology of low-sulfidation Au-Ag ores in the northern Great Basin region of Nevada-Idaho: MS thesis Auburn University 152 p.

United States Department of Agriculture Natural Resources Conservation Service, 2011, Geospatial Data Gateway (http://datagateway.nrcs.usda.gov).

Vikre, P.G., 1985, Precious metal vein systems in the National district, Humboldt County, Nevada: ECONOMIC GEOLOGY, v. 80, p. 360-393.

Vikre, P.G., 1989, Fluid-mineral relations in the Comstock Lode: ECONOMIC GEOLOGY, v. 84, p. 1574–1613.

Vikre, P.G.,2007a, Au-Ag-Se deposits in the western US [abs.]: Geological Society of America Abstracts with Programs, v. 39, no. 6, p. 197.

Vikre, P.G., 2007b, Sinter-vein correlations at Buckskin Mountain, National district, Humboldt County, Nevada: Economic Geology, v. 102, p. 193-224.

Vainrub, A., Pustovyy, O., and Vodyanoy, V., 2006, Resolution of 90 nm (λ/5) in an . optical transmission microscope with an annular condenser: Optic Letters, v. 31, no. 19, p. 2855-2857

Wallace, A.R., 2003, Geology of the Ivanhoe Hg-Au district, northern Nevada: Influence of Miocene volcanism, lakes, and active faulting on epithermal mineralization: ECONOMIC GEOLOGY, v. 98, p. 409–424.

Webster, S.S., and Henly, R.W., 1989, Application of high resolution airborne geophysics to epithermal gold exploration in northeast Queensland and Cormandel New Zealand: Exploration Geophysics, v.20, p. 99-102.

Wells, W. W., 1963, Gold camps and silver cities: Idaho B'Jr. Mines and Geol. Bull. 22, 86 p.

Wooden, J.L., and Mueller, P.A., 1988, Pb, Sr, Nd isotopic compositions of a suite of late Archean, igneous rocks, eastern Beartooth Mountains: Implications for crust-mantle evolution : Earth and Planetary Science Letters, v. 87, p. 59–72, doi: 10.1016/0012–821X(88)90064–7.

Worthington, J.E., and Kiff, I.T., 1970, A suggested Volcanogenic Origin for Certain Gold Deposits in the Slate Belt of the North Carolina Piedmont, ECONOMIC GEOLOGY, v. 65, p 529-537.

Yeager, D.A., and Ikona C.K., 1984, A preliminary report on the War Eagle Mines: War Eagle Resources, 37 p. (Unpublished).

Yeager, D.A., and Ikona C.K., 1986, A preliminary report on the War Eagle Mines: War Eagle Resources, 25 p. (Unpublished).

York, D., Hall, C.M., Yanase, Y., hanes, J.A. and Kenyon, W.J., 1981, $^{40}Ar/^{39}Ar$ dating Of terrestrial minerals with a continous laser: Geophysical research letters, v. 8, p 1136-1138.

Appendix 1

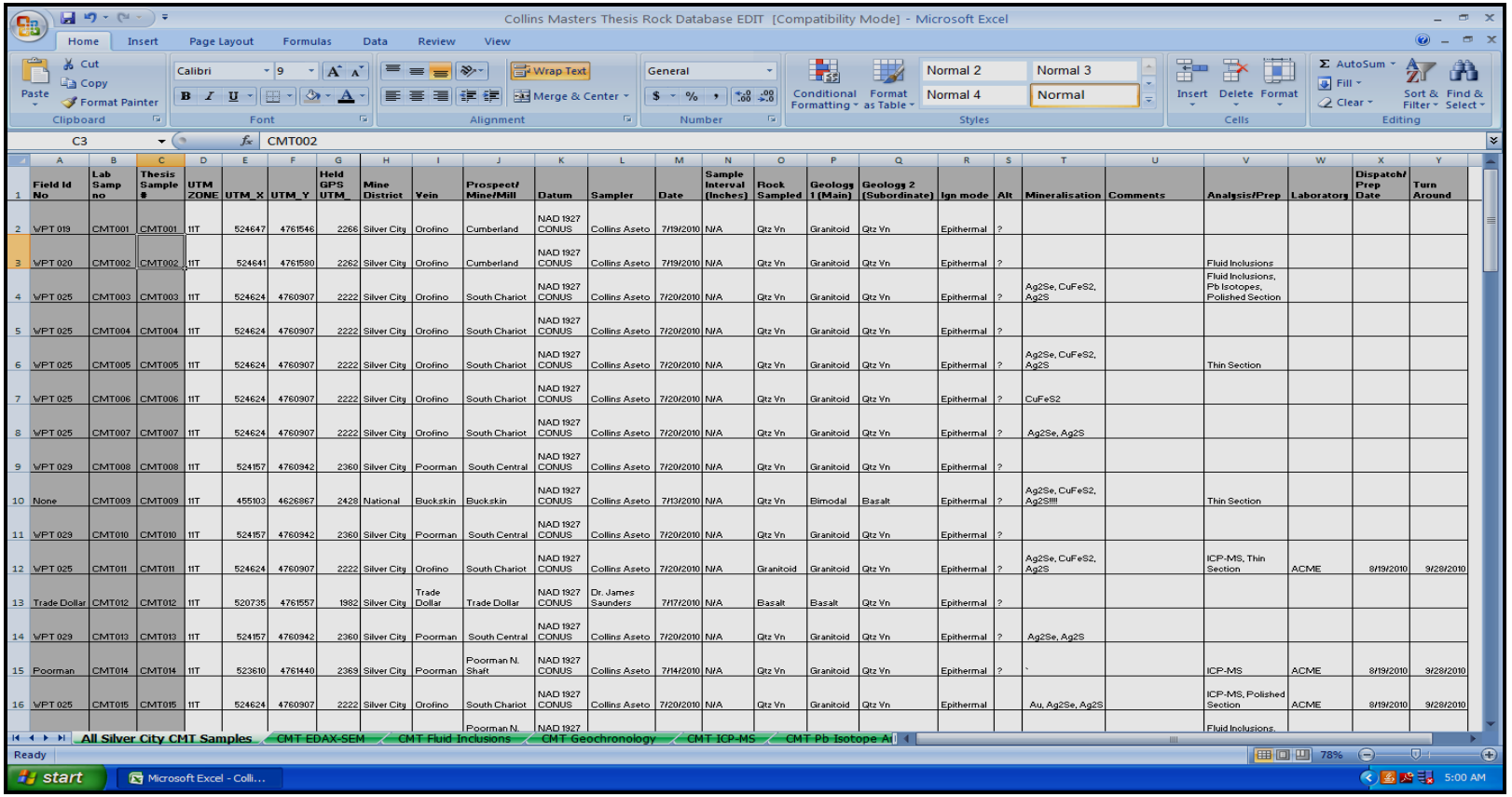

	Field Id No	Lab Samp no	Thesis Sample #	UTM ZONE	UTM_X	UTM_Y	Held GPS UTM_	Mine District	Yein	Prospect/ Mine/Mill	Datum	Sampler	Date	Sample Interval (Inches)	Rock Sampled	Geology 1 (Main)	Geology 2 (Subordinate)	Ign mode	Alt	Mineralisation	Comments	Analysis/Prep	Laboratory	Dispatch/ Prep Date	Turn Around
2	WPT 019	CMT001	CMT001	11T	524647	4761546	2266	Silver City	Orofino	Cumberland	NAD 1927 CONUS	Collins Aseto	7/19/2010	N/A	Qtz Vn	Granitoid	Qtz Vn	Epithermal	?						
3	WPT 020	CMT002	CMT002	11T	524641	4761580	2262	Silver City	Orofino	Cumberland	NAD 1927 CONUS	Collins Aseto	7/19/2010	N/A	Qtz Vn	Granitoid	Qtz Vn	Epithermal	?			Fluid Inclusions			
4	WPT 025	CMT003	CMT003	11T	524624	4760907	2222	Silver City	Orofino	South Chariot	NAD 1927 CONUS	Collins Aseto	7/20/2010	N/A	Qtz Vn	Granitoid	Qtz Vn	Epithermal	?	Ag2Se, CuFeS2, Ag2S		Fluid Inclusions, Pb Isotopes, Polished Section			
5	WPT 025	CMT004	CMT004	11T	524624	4760907	2222	Silver City	Orofino	South Chariot	NAD 1927 CONUS	Collins Aseto	7/20/2010	N/A	Qtz Vn	Granitoid	Qtz Vn	Epithermal	?						
6	WPT 025	CMT005	CMT005	11T	524624	4760907	2222	Silver City	Orofino	South Chariot	NAD 1927 CONUS	Collins Aseto	7/20/2010	N/A	Qtz Vn	Granitoid	Qtz Vn	Epithermal	?	Ag2Se, CuFeS2, Ag2S		Thin Section			
7	WPT 025	CMT006	CMT006	11T	524624	4760907	2222	Silver City	Orofino	South Chariot	NAD 1927 CONUS	Collins Aseto	7/20/2010	N/A	Qtz Vn	Granitoid	Qtz Vn	Epithermal	?	CuFeS2					
8	WPT 025	CMT007	CMT007	11T	524624	4760907	2222	Silver City	Orofino	South Chariot	NAD 1927 CONUS	Collins Aseto	7/20/2010	N/A	Qtz Vn	Granitoid	Qtz Vn	Epithermal	?	Ag2Se, Ag2S					
9	WPT 029	CMT008	CMT008	11T	524157	4760942	2360	Silver City	Poorman	South Central	NAD 1927 CONUS	Collins Aseto	7/20/2010	N/A	Qtz Vn	Granitoid	Qtz Vn	Epithermal	?						
10	None	CMT009	CMT009	11T	455103	4626867	2428	National	Buckskin	Buckskin	NAD 1927 CONUS	Collins Aseto	7/13/2010	N/A	Qtz Vn	Bimodal	Basalt	Epithermal	?	Ag2Se, CuFeS2, Ag2S!!!!		Thin Section			
11	WPT 029	CMT010	CMT010	11T	524157	4760942	2360	Silver City	Poorman	South Central	NAD 1927 CONUS	Collins Aseto	7/20/2010	N/A	Qtz Vn	Granitoid	Qtz Vn	Epithermal	?						
12	WPT 025	CMT011	CMT011	11T	524624	4760907	2222	Silver City	Orofino	South Chariot	NAD 1927 CONUS	Collins Aseto	7/20/2010	N/A	Granitoid	Granitoid	Qtz Vn	Epithermal	?	Ag2Se, CuFeS2, Ag2S		ICP-MS, Thin Section	ACME	8/19/2010	9/28/2010
13	Trade Dollar	CMT012	CMT012	11T	520735	4761557	1982	Silver City	Trade Dollar	Trade Dollar	NAD 1927 CONUS	Dr. James Saunders	7/17/2010	N/A	Basalt	Basalt	Qtz Vn	Epithermal	?						
14	WPT 029	CMT013	CMT013	11T	524157	4760942	2360	Silver City	Poorman	South Central	NAD 1927 CONUS	Collins Aseto	7/20/2010	N/A	Qtz Vn	Granitoid	Qtz Vn	Epithermal	?	Ag2Se, Ag2S					
15	Poorman	CMT014	CMT014	11T	523610	4761440	2369	Silver City	Poorman	Poorman N. Shaft	NAD 1927 CONUS	Collins Aseto	7/14/2010	N/A	Qtz Vn	Granitoid	Qtz Vn	Epithermal	?	`		ICP-MS	ACME	8/19/2010	9/28/2010
16	WPT 025	CMT015	CMT015	11T	524624	4760907	2222	Silver City	Orofino	South Chariot	NAD 1927 CONUS	Collins Aseto	7/20/2010	N/A	Qtz Vn	Granitoid	Qtz Vn	Epithermal		Au, Ag2Se, Ag2S		ICP-MS, Polished Section	ACME	8/19/2010	9/28/2010
										Poorman N.	NAD 1927											Fluid Inclusions,			

A screen shot of the rock database used in this study is shown below. A copy of this database is contained in the compact disc accompanying this thesis, and contains the following data as worksheets : All Silver City CMT samples, CMT EDAX-SEM, CMT Fluid inclusions, CMT Geochronology, CMT ICP-MS, CMT Pb Isotope analyses, CMT Polished Sections, CMT Thin sections, CMT Waypoints 27UTMCONUS.

Appendix 2

Selected scanning electron microscope-energy dispersive spectrometry (SEM_EDAX) data.

War Eagle Mountain-Orofino Vein 16/08/2011 17:18:06

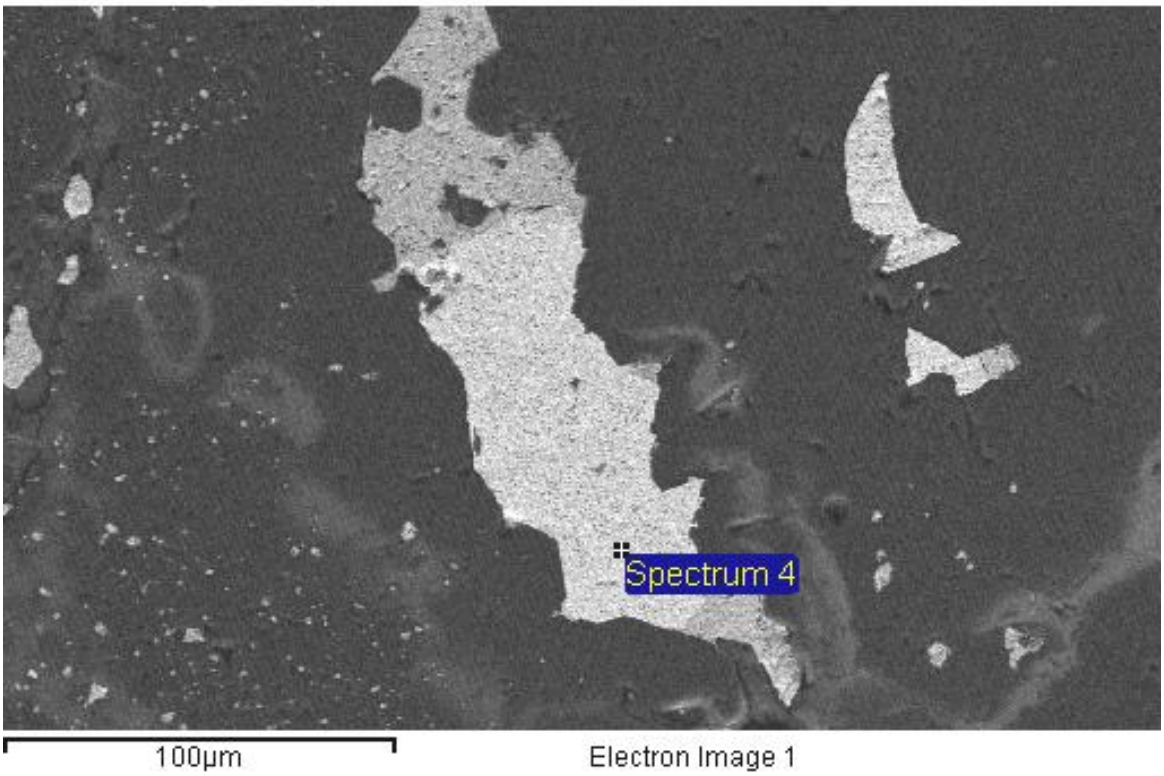

Element	Weight%	Atomic%
Ag L	40.64	55.56
Au M	59.36	44.44
Totals	100.00	

inca

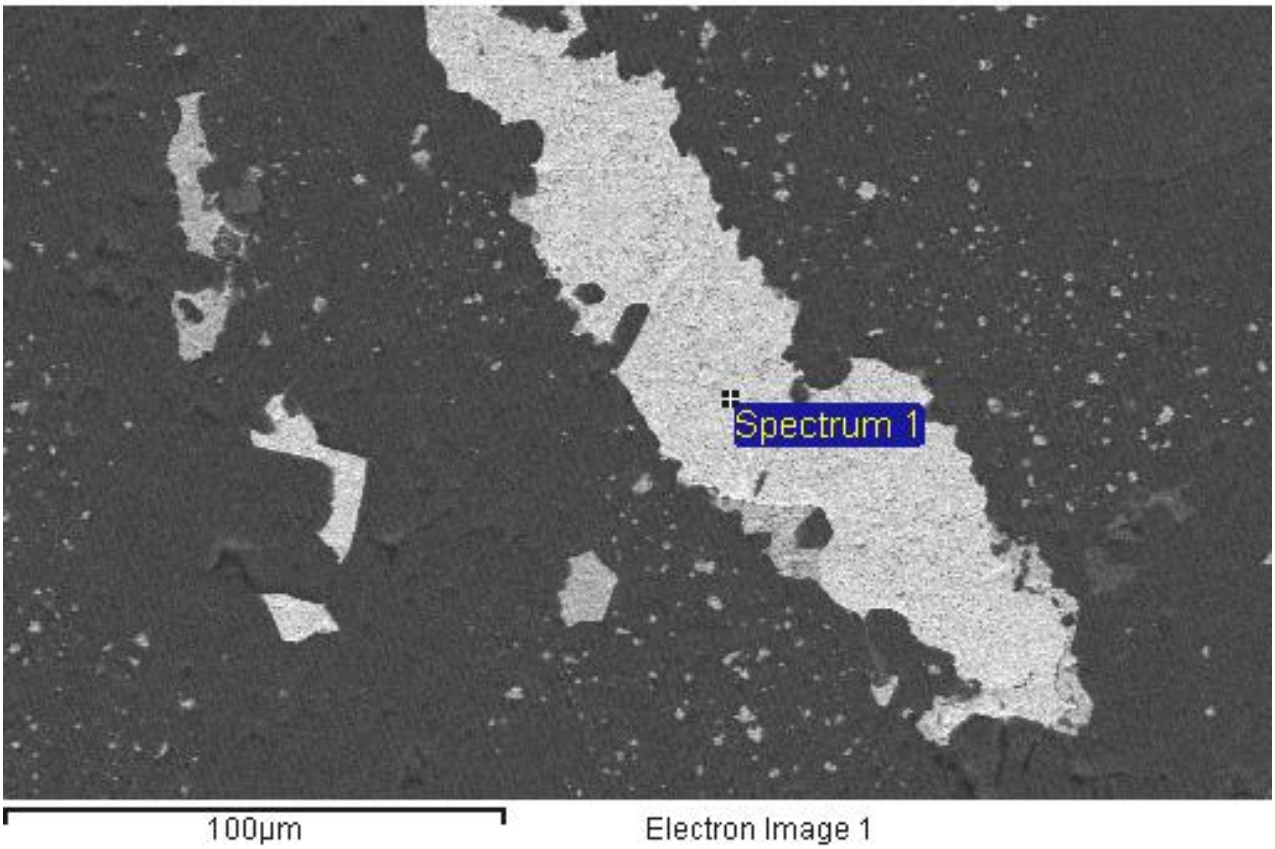

Element	Weight%	Atomic%
Ag L	39.70	54.59
Au M	60.30	45.41
Totals	100.00	

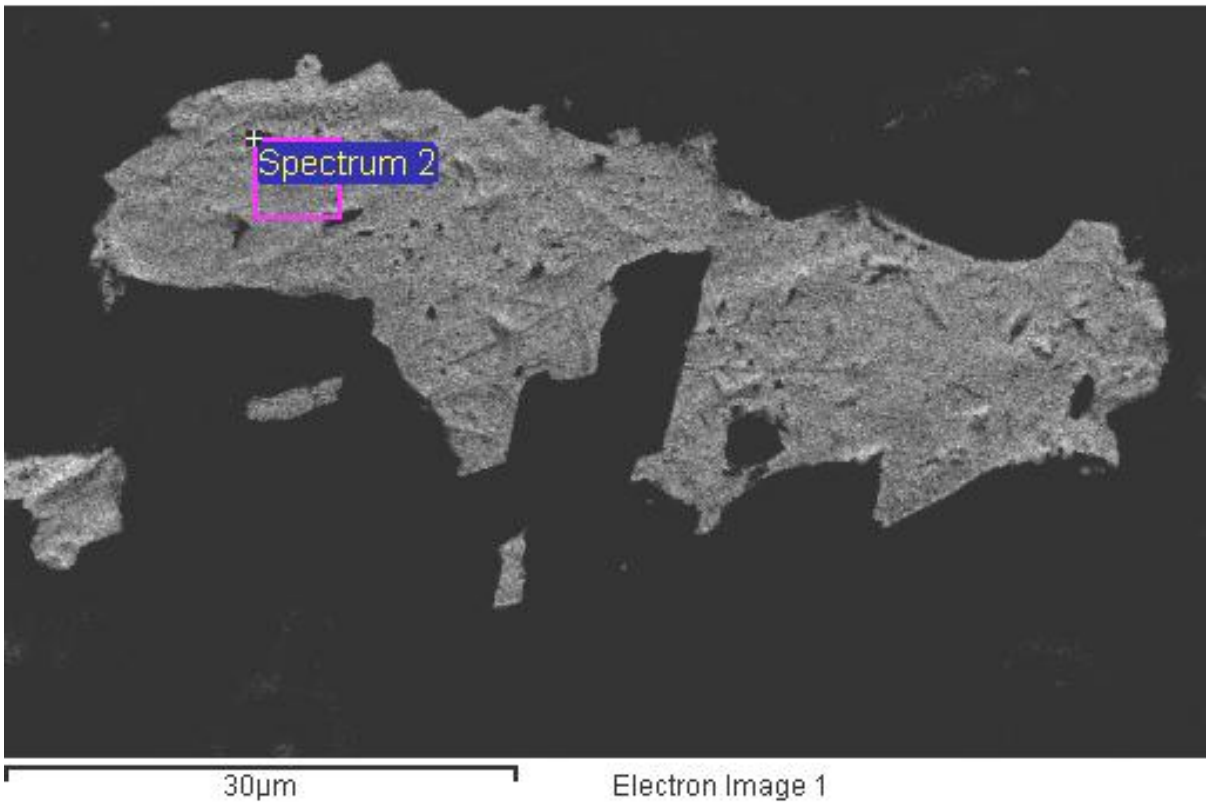

Element	Weight%	Atomic%
S K	11.58	30.03
Se L	6.48	6.82
Ag L	81.94	63.14
Totals	100.00	

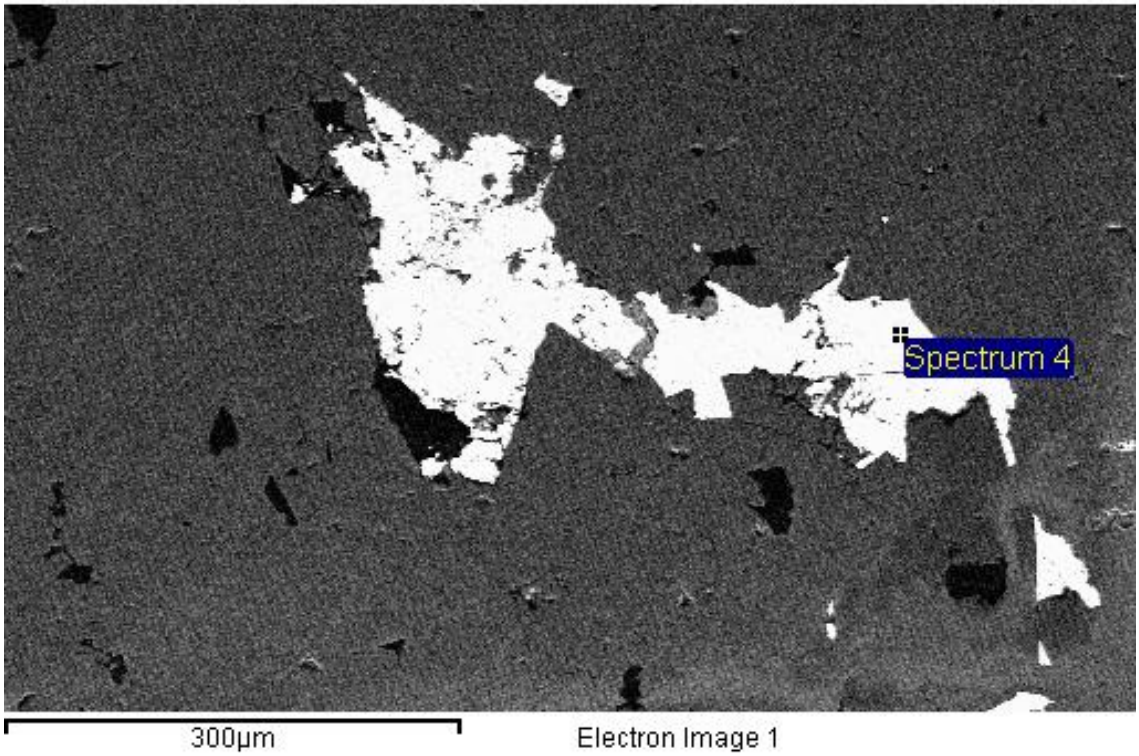

Element	Weight%	Atomic%
S K	14.87	35.79
Se L	12.70	12.41
Ag L	72.43	51.80
Totals	100.00	

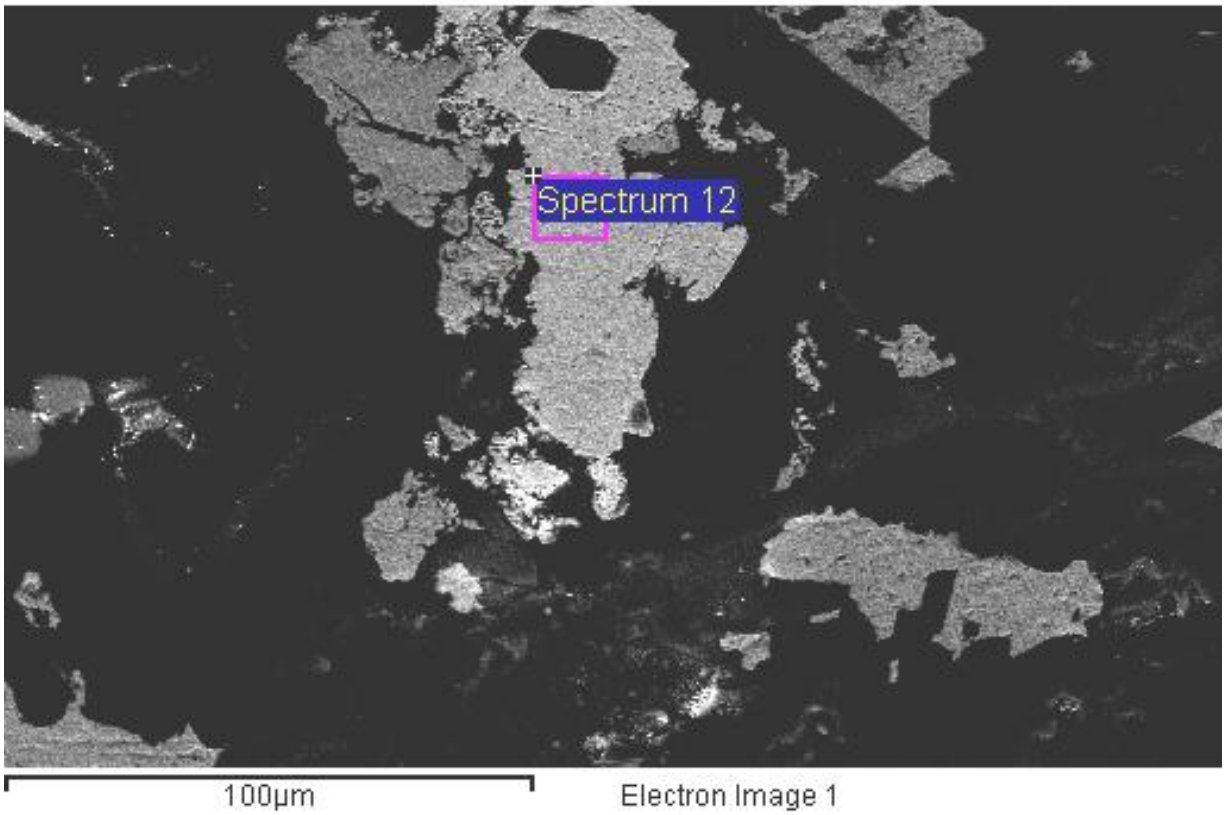

Element	Weight%	Atomic%
Ag L	44.76	59.67
Au M	55.24	40.33
Totals	100.00	

Appendix 3

Single crystal total fusion (SCTF) and Incremental heating (IH) data for War Eagle Mountain. Irradiation file name, field name and thesis sample number are indicated on the top left corner of each chart. SCTF data always precedes IH data where applicable. Samples were irradiated with cadmium shielding in either the US Geological Survey TRIGA reactor in Denver, CO (13 samples, with prefix 'au20'), or in the McMaster Nuclear reactor at Hamilton University in Ontario, Canada (2 samples with prefix 'au15'). Synthetic CaF_2 was included with the irradiation to determine calcium production factors, and Fish Canyon sanidine (from an aliquot prepared at New Mexico Tech) was used to monitor production of $39Ar_K$, with an assigned age of 28.02 Ma (Renne et al., 1998). Radial variations in J-value for the McMaster reactor can be significant, and as a result, the J-values for the two samples irradiated at McMaster in the present study have a standard deviation of 0.5%. Radial variations in J-value for the samples irradiated in the USGS Denver TRIGA were found to be negligible, with the result that monitors for four positions in each layer of the irradiation package were averaged to determine the J-values (with a standard deviation of 0.2%). Aliquots of air from an air pipette were measured daily to evaluate mass discrimination, and procedural blanks were measured following every five analyses of unknowns. Samples were analyzed following gas extraction with a CO_2 laser using an automated extraction line, with data collection on an electron multiplier detector. Dates presented are in volts unless otherwise indicated, and are corrected for backgrounds, mass discrimination, and decay of short-lived isotopes.

au15.3j.kfs, MB07-01 - SCTF Analyses																								
%P	40Ar V			39Ar V			38Ar V			37Ar V			36Ar V			Moles 40Ar*	%Rad	R	Age (Ma)		
16	0.92902	±	0.00116	0.29191	±	0.00055	0.00360	±	0.00006	0.00560	±	0.00030	0.000324	±	0.000018	5.04E-15	89.7%	2.85618	15.30	±	0.10
16	1.99104	±	0.00181	0.60907	±	0.00098	0.00744	±	0.00008	0.00981	±	0.00033	0.000683	±	0.000021	1.08E-14	89.9%	2.93905	15.76	±	0.06
16	1.13037	±	0.00087	0.36208	±	0.00063	0.00439	±	0.00005	0.00640	±	0.00031	0.000159	±	0.000030	6.14E-15	95.9%	2.99387	16.05	±	0.14
16	0.74604	±	0.00077	0.23985	±	0.00067	0.00285	±	0.00004	0.00333	±	0.00018	0.000171	±	0.000015	4.05E-15	93.3%	2.90084	15.56	±	0.11
16	1.41808	±	0.00080	0.41460	±	0.00072	0.00542	±	0.00009	0.00706	±	0.00027	0.000681	±	0.000020	7.70E-15	85.9%	2.93656	15.75	±	0.08
16	0.82300	±	0.00096	0.24852	±	0.00058	0.00311	±	0.00007	0.00444	±	0.00023	0.000277	±	0.000016	4.47E-15	90.1%	2.98378	16.00	±	0.11
16	0.50124	±	0.00098	0.15020	±	0.00038	0.00182	±	0.00003	0.00260	±	0.00018	0.000173	±	0.000015	2.72E-15	89.9%	2.99898	16.08	±	0.16
16	0.83799	±	0.00056	0.24131	±	0.00063	0.00288	±	0.00004	0.00460	±	0.00016	0.000428	±	0.000017	4.55E-15	84.9%	2.94977	15.82	±	0.12
16	1.04683	±	0.00158	0.34114	±	0.00091	0.00411	±	0.00006	0.00724	±	0.00022	0.000080	±	0.000017	5.68E-15	97.8%	3.00106	16.09	±	0.09
16	0.55908	±	0.00107	0.16748	±	0.00052	0.00202	±	0.00005	0.00234	±	0.00018	0.000195	±	0.000016	3.03E-15	89.7%	2.99551	16.06	±	0.17
16	0.36729	±	0.00070	0.10268	±	0.00036	0.00111	±	0.00005	0.00168	±	0.00019	0.000302	±	0.000023	1.99E-15	75.7%	2.70836	14.53	±	0.36
16	2.08265	±	0.00258	0.65948	±	0.00097	0.00793	±	0.00009	0.01559	±	0.00032	0.000532	±	0.000025	1.13E-14	92.5%	2.92182	15.67	±	0.07
16	0.90687	±	0.00154	0.25197	±	0.00055	0.00305	±	0.00007	0.00528	±	0.00020	0.000631	±	0.000024	4.92E-15	79.5%	2.86106	15.34	±	0.16
16	2.38633	±	0.00249	0.76048	±	0.00187	0.00922	±	0.00006	0.01370	±	0.00037	0.000485	±	0.000024	1.30E-14	94.0%	2.95113	15.82	±	0.07

au15.3j.kfs, MB07-01 - IH Analysis																								
%P	40Ar V			39Ar V			38Ar V			37Ar V			36Ar V			Moles 40Ar*	%Rad	R	Age (Ma)		
5	0.17997	±	0.00042	0.04645	±	0.00026	0.00048	±	0.00005	0.00063	±	0.00023	0.000240	±	0.000024	9.77E-16	60.6%	2.34646	12.59	±	0.85
5.5	0.26919	±	0.00042	0.08531	±	0.00041	0.00103	±	0.00004	0.00089	±	0.00014	0.000088	±	0.000025	1.46E-15	90.4%	2.85223	15.30	±	0.46
6	0.53494	±	0.00135	0.16888	±	0.00052	0.00200	±	0.00005	0.00291	±	0.00020	0.000183	±	0.000025	2.90E-15	90.0%	2.84945	15.28	±	0.25
6.5	0.22714	±	0.00070	0.07335	±	0.00026	0.00085	±	0.00005	0.00080	±	0.00021	0.000058	±	0.000025	1.23E-15	92.5%	2.86508	15.36	±	0.56
6.9	0.83779	±	0.00079	0.27017	±	0.00052	0.00322	±	0.00004	0.00346	±	0.00012	0.000154	±	0.000024	4.55E-15	94.6%	2.93368	15.73	±	0.14
7.3	0.43447	±	0.00061	0.14343	±	0.00052	0.00166	±	0.00005	0.00194	±	0.00020	0.000042	±	0.000024	2.36E-15	97.2%	2.94406	15.79	±	0.27
7.6	0.50583	±	0.00068	0.15755	±	0.00044	0.00184	±	0.00006	0.00249	±	0.00021	0.000187	±	0.000024	2.75E-15	89.1%	2.86075	15.34	±	0.25
7.9	0.08046	±	0.00022	0.02591	±	0.00014	0.00025	±	0.00003	0.00052	±	0.00023	0.000111	±	0.000031	4.37E-16	59.2%	1.83698	9.87	±	1.88
8.2	0.37013	±	0.00067	0.12164	±	0.00028	0.00153	±	0.00004	0.00248	±	0.00013	0.000112	±	0.000025	2.01E-15	91.1%	2.77309	14.87	±	0.32
8.5	0.05126	±	0.00034	0.01633	±	0.00008	0.00026	±	0.00004	0.00026	±	0.00017	-0.000016	±	0.000034	2.78E-16	109.1%	3.14084	16.84	±	3.31
9	0.02002	±	0.00030	0.00666	±	0.00009	0.00010	±	0.00004	0.00012	±	0.00020	0.000044	±	0.000024	1.09E-16	35.0%	1.05286	5.66	±	5.79
10	0.07450	±	0.00034	0.02464	±	0.00020	0.00032	±	0.00003	0.00031	±	0.00018	-0.000061	±	0.000030	4.04E-16	124.4%	3.02440	16.21	±	1.91
11	0.02117	±	0.00037	0.00701	±	0.00011	0.00012	±	0.00003	0.00008	±	0.00009	-0.000014	±	0.000018	1.15E-16	119.7%	3.01893	16.19	±	4.11
12	0.01648	±	0.00024	0.00489	±	0.00004	0.00007	±	0.00003	0.00009	±	0.00024	-0.000020	±	0.000017	8.95E-17	135.7%	3.37442	18.08	±	5.38
13	0.00800	±	0.00019	0.00231	±	0.00005	0.00005	±	0.00002	0.00021	±	0.00016	0.000005	±	0.000016	4.34E-17	80.6%	2.78462	14.93	±	11.08
15	0.01503	±	0.00031	0.00412	±	0.00005	0.00009	±	0.00002	0.00018	±	0.00022	-0.000008	±	0.000016	8.16E-17	116.0%	3.65248	19.56	±	6.12

au15.3j.kfs, MB07-01 - IH Analysis																								
%P	40Ar V			39Ar V			38Ar V			37Ar V			36Ar V			Moles 40Ar*	%Rad	R	Age (Ma)		
5	0.98058	±	0.00143	0.07266	±	0.00037	0.00130	±	0.00004	0.00119	±	0.00015	0.002636	±	0.000025	5.32E-15	20.6%	2.77575	14.89	±	0.73
5.5	0.22451	±	0.00040	0.07051	±	0.00029	0.00087	±	0.00003	0.00138	±	0.00021	0.000003	±	0.000029	1.22E-15	99.7%	3.17397	17.01	±	0.66
6	0.06335	±	0.00033	0.01953	±	0.00014	0.00024	±	0.00003	0.00056	±	0.00018	0.000027	±	0.000018	3.44E-16	87.6%	2.84258	15.24	±	1.45
6.5	0.26997	±	0.00042	0.08396	±	0.00031	0.00109	±	0.00004	0.00228	±	0.00012	0.000074	±	0.000018	1.47E-15	92.0%	2.95884	15.86	±	0.35
6.9	0.28971	±	0.00050	0.08646	±	0.00049	0.00107	±	0.00004	0.00212	±	0.00028	0.000100	±	0.000019	1.57E-15	89.8%	3.01046	16.14	±	0.36
7.3	0.24998	±	0.00024	0.06994	±	0.00025	0.00083	±	0.00003	0.00203	±	0.00018	0.000145	±	0.000019	1.36E-15	82.9%	2.96407	15.89	±	0.44
7.6	0.72261	±	0.00087	0.21757	±	0.00047	0.00266	±	0.00006	0.00503	±	0.00026	0.000356	±	0.000042	3.92E-15	85.5%	2.83930	15.23	±	0.31
8	0.39109	±	0.00097	0.12208	±	0.00045	0.00154	±	0.00003	0.00357	±	0.00024	0.000113	±	0.000018	2.12E-15	91.5%	2.93262	15.73	±	0.25
8.5	1.69151	±	0.00150	0.54353	±	0.00057	0.00666	±	0.00008	0.01180	±	0.00025	0.000265	±	0.000020	9.18E-15	95.4%	2.96967	15.92	±	0.06
9	0.59134	±	0.00102	0.19087	±	0.00066	0.00232	±	0.00004	0.00451	±	0.00015	0.000094	±	0.000016	3.21E-15	95.4%	2.95452	15.84	±	0.15
10	0.55508	±	0.00082	0.17578	±	0.00060	0.00214	±	0.00005	0.00405	±	0.00023	0.000073	±	0.000014	3.01E-15	96.2%	3.03685	16.28	±	0.14
11	0.23565	±	0.00030	0.07331	±	0.00036	0.00090	±	0.00003	0.00150	±	0.00022	0.000056	±	0.000013	1.28E-15	93.1%	2.99097	16.04	±	0.29
12	0.05322	±	0.00179	0.01470	±	0.00012	0.00021	±	0.00002	0.00017	±	0.00025	0.000024	±	0.000016	2.89E-16	86.5%	3.13138	16.79	±	1.86
13.5	0.06955	±	0.00037	0.02039	±	0.00018	0.00027	±	0.00003	0.00062	±	0.00011	0.000007	±	0.000013	3.78E-16	97.1%	3.31040	17.74	±	1.06

au15.3j.kfs, MB07-01 - IH Analysis																								
%P	40Ar V			39Ar V			38Ar V			37Ar V			36Ar V			Moles 40Ar*	%Rad	R	Age (Ma)		
5	0.21067	±	0.00029	0.06247	±	0.00037	0.00087	±	0.00004	0.00157	±	0.00023	0.000207	±	0.000029	1.14E-15	71.1%	2.39738	12.87	±	0.75
5.5	0.19761	±	0.00031	0.05961	±	0.00017	0.00074	±	0.00004	0.00127	±	0.00016	0.000140	±	0.000028	1.07E-15	79.1%	2.62374	14.08	±	0.76
6	0.24245	±	0.00035	0.07332	±	0.00045	0.00087	±	0.00004	0.00155	±	0.00031	0.000190	±	0.000029	1.32E-15	76.9%	2.54364	13.65	±	0.64
6.5	0.69052	±	0.00086	0.21357	±	0.00068	0.00268	±	0.00004	0.00373	±	0.00012	0.000264	±	0.000029	3.75E-15	88.8%	2.87002	15.39	±	0.22
6.9	0.32818	±	0.00069	0.10785	±	0.00045	0.00129	±	0.00004	0.00186	±	0.00012	0.000108	±	0.000030	1.78E-15	90.3%	2.74748	14.74	±	0.44
7.3	0.27401	±	0.00065	0.08831	±	0.00047	0.00107	±	0.00003	0.00074	±	0.00014	0.000043	±	0.000015	1.49E-15	95.4%	2.95947	15.87	±	0.29
7.6	0.44937	±	0.00098	0.14397	±	0.00050	0.00173	±	0.00005	0.00185	±	0.00018	0.000088	±	0.000016	2.44E-15	94.2%	2.94128	15.77	±	0.19
8	0.31960	±	0.00063	0.10556	±	0.00033	0.00128	±	0.00002	0.00145	±	0.00015	0.000097	±	0.000027	1.73E-15	91.1%	2.75784	14.79	±	0.41
8.5	0.54922	±	0.00115	0.18152	±	0.00044	0.00221	±	0.00004	0.00257	±	0.00018	0.000040	±	0.000017	2.98E-15	97.9%	2.96181	15.88	±	0.15
9	0.61490	±	0.00106	0.20542	±	0.00073	0.00251	±	0.00006	0.00275	±	0.00019	0.000019	±	0.000017	3.34E-15	99.1%	2.96701	15.91	±	0.15
10	0.20791	±	0.00027	0.06919	±	0.00044	0.00086	±	0.00004	0.00094	±	0.00021	0.000000	±	0.000016	1.13E-15	100.0%	3.00597	16.12	±	0.39
11	0.01389	±	0.00020	0.00445	±	0.00008	0.00003	±	0.00003	-0.00019	±	0.00013	-0.000035	±	0.000016	7.54E-17	175.5%	3.11669	16.71	±	5.72

au15.4g.kfs, NV-8-09 IH Analysis																								
%P	40Ar V			39Ar V			38Ar V			37Ar V			36Ar V			Moles 40Ar*	%Rad	R	Age (Ma)		
5	2.59843	±	0.00167	0.08691	±	0.00032	0.00261	±	0.00004	-0.00015	±	0.00019	0.008087	±	0.000072	1.41E-14	8.0%	2.40096	12.88	±	1.54
5.5	0.27613	±	0.00051	0.08621	±	0.00039	0.00106	±	0.00004	0.00009	±	0.00020	0.000072	±	0.000016	1.50E-15	92.3%	2.95729	15.86	±	0.30
6	0.40363	±	0.00069	0.13268	±	0.00052	0.00160	±	0.00004	0.00002	±	0.00016	0.000005	±	0.000027	2.19E-15	99.6%	3.03038	16.25	±	0.33
6.4	0.35542	±	0.00096	0.12005	±	0.00041	0.00140	±	0.00003	-0.00025	±	0.00013	-0.000012	±	0.000017	1.93E-15	101.0%	2.96048	15.87	±	0.23
6.8	0.36015	±	0.00071	0.12294	±	0.00052	0.00152	±	0.00004	-0.00013	±	0.00018	-0.000014	±	0.000016	1.95E-15	101.2%	2.92944	15.71	±	0.21
7.2	2.35963	±	0.00259	0.60539	±	0.00110	0.00819	±	0.00013	-0.00027	±	0.00023	0.002125	±	0.000026	1.28E-14	73.4%	2.86021	15.34	±	0.08
7.5	0.42193	±	0.00060	0.12849	±	0.00027	0.00159	±	0.00004	-0.00057	±	0.00016	0.000191	±	0.000016	2.29E-15	86.6%	2.84468	15.26	±	0.20
7.8	0.57502	±	0.00064	0.17585	±	0.00056	0.00213	±	0.00004	-0.00019	±	0.00021	0.000237	±	0.000015	3.12E-15	87.8%	2.87087	15.40	±	0.15
8.1	0.36307	±	0.00102	0.10630	±	0.00042	0.00142	±	0.00004	-0.00030	±	0.00025	0.000162	±	0.000014	1.97E-15	86.8%	2.96581	15.90	±	0.23
8.5	0.60275	±	0.00054	0.12276	±	0.00040	0.00164	±	0.00003	-0.00081	±	0.00013	0.000791	±	0.000023	3.27E-15	61.2%	3.00462	16.11	±	0.31
9	1.01823	±	0.00168	0.30861	±	0.00113	0.00392	±	0.00006	0.00019	±	0.00024	0.000480	±	0.000022	5.53E-15	86.1%	2.83980	15.23	±	0.14
10	1.35812	±	0.00094	0.37764	±	0.00079	0.00480	±	0.00007	0.00007	±	0.00007	0.000932	±	0.000023	7.37E-15	79.7%	2.86709	15.38	±	0.11
11	1.66888	±	0.00165	0.46348	±	0.00094	0.00585	±	0.00006	0.00027	±	0.00018	0.001108	±	0.000024	9.06E-15	80.4%	2.89443	15.52	±	0.09
13	0.73019	±	0.00103	0.19818	±	0.00063	0.00239	±	0.00003	0.00005	±	0.00018	0.000508	±	0.000022	3.96E-15	79.4%	2.92646	15.69	±	0.19
15	0.14233	±	0.00030	0.03425	±	0.00017	0.00049	±	0.00003	-0.00005	±	0.00013	0.000176	±	0.000022	7.72E-16	63.5%	2.63681	14.15	±	1.04

au15.4g.kfs, NV-8-09 IH Analysis																								
%P	40Ar V			39Ar V			38Ar V			37Ar V			36Ar V			Moles 40Ar*	%Rad	R	Age (Ma)		
5	1.68183	±	0.00130	0.24077	±	0.00057	0.00360	±	0.00005	0.00017	±	0.00012	0.003270	±	0.000031	9.13E-15	42.5%	2.97147	15.93	±	0.23
5.5	0.39229	±	0.00090	0.13607	±	0.00043	0.00167	±	0.00004	0.00014	±	0.00015	0.000009	±	0.000018	2.13E-15	99.4%	2.86453	15.36	±	0.22
6	0.70116	±	0.00094	0.24252	±	0.00068	0.00290	±	0.00007	0.00024	±	0.00021	0.000042	±	0.000018	3.81E-15	98.2%	2.84010	15.23	±	0.13
6.4	1.11373	±	0.00182	0.37910	±	0.00115	0.00459	±	0.00006	0.00012	±	0.00012	0.000079	±	0.000018	6.04E-15	97.9%	2.87622	15.42	±	0.09
6.8	0.42778	±	0.00080	0.14386	±	0.00044	0.00180	±	0.00004	-0.00005	±	0.00015	0.000056	±	0.000018	2.32E-15	96.1%	2.85771	15.33	±	0.21
7.2	0.41336	±	0.00091	0.13677	±	0.00059	0.00162	±	0.00003	0.00050	±	0.00050	0.000037	±	0.000019	2.24E-15	97.3%	2.94209	15.78	±	0.23
7.5	0.32351	±	0.00089	0.08422	±	0.00026	0.00103	±	0.00003	-0.00034	±	0.00022	0.000284	±	0.000019	1.76E-15	74.0%	2.84285	15.25	±	0.37
7.8	1.10135	±	0.00099	0.37134	±	0.00079	0.00452	±	0.00007	-0.00040	±	0.00014	0.000088	±	0.000016	5.98E-15	97.6%	2.89562	15.53	±	0.08
8.1	0.43449	±	0.00083	0.14468	±	0.00037	0.00199	±	0.00007	-0.00039	±	0.00015	0.000000	±	0.000017	2.36E-15	100.0%	3.00198	16.10	±	0.19
8.5	0.44957	±	0.00049	0.15285	±	0.00070	0.00201	±	0.00003	-0.00042	±	0.00020	0.000025	±	0.000018	2.44E-15	98.3%	2.89226	15.51	±	0.20
9	0.35058	±	0.00048	0.11955	±	0.00039	0.00139	±	0.00003	0.00041	±	0.00017	0.000022	±	0.000018	1.90E-15	98.2%	2.87906	15.44	±	0.24
10	0.68044	±	0.00089	0.22365	±	0.00040	0.00278	±	0.00005	0.00034	±	0.00017	0.000106	±	0.000017	3.69E-15	95.4%	2.90190	15.56	±	0.12
11	0.46824	±	0.00113	0.15752	±	0.00065	0.00193	±	0.00003	0.00051	±	0.00023	0.000041	±	0.000018	2.54E-15	97.4%	2.89618	15.53	±	0.19
13	0.25767	±	0.00031	0.08594	±	0.00040	0.00107	±	0.00004	0.00032	±	0.00021	0.000048	±	0.000019	1.40E-15	94.5%	2.83223	15.19	±	0.36
15	0.05393	±	0.00025	0.01830	±	0.00012	0.00024	±	0.00003	0.00015	±	0.00018	0.000018	±	0.000019	2.93E-16	89.9%	2.64989	14.21	±	1.68

au15.4g.kfs, NV-9-09 IH Analysis																								
%P	40Ar V			39Ar V			38Ar V			37Ar V			36Ar V			Moles 40Ar*	%Rad	R	Age (Ma)		
5	0.35850	±	0.00069	0.02738	±	0.00009	0.00053	±	0.00003	0.00020	±	0.00012	0.000932	±	0.000019	1.95E-15	23.2%	3.03321	16.26	±	1.16
5.5	0.18003	±	0.00031	0.05670	±	0.00039	0.00068	±	0.00004	-0.00016	±	0.00011	0.000025	±	0.000014	9.77E-16	96.0%	3.04649	16.33	±	0.42
6	0.24248	±	0.00038	0.07571	±	0.00040	0.00093	±	0.00003	-0.00010	±	0.00019	0.000073	±	0.000016	1.32E-15	91.1%	2.91697	15.64	±	0.35
6.4	0.21918	±	0.00037	0.04591	±	0.00022	0.00063	±	0.00004	-0.00020	±	0.00024	0.000294	±	0.000014	1.19E-15	60.4%	2.88210	15.46	±	0.49
6.8	0.24070	±	0.00033	0.08102	±	0.00021	0.00098	±	0.00005	-0.00010	±	0.00018	0.000023	±	0.000015	1.31E-15	97.2%	2.88658	15.48	±	0.30
7.2	0.56845	±	0.01310	0.18842	±	0.00703	0.00249	±	0.00005	-0.00016	±	0.00016	-0.000009	±	0.000015	3.09E-15	100.5%	3.01686	16.17	±	0.72
7.5	0.47739	±	0.00063	0.16110	±	0.00072	0.00200	±	0.00006	0.00008	±	0.00018	0.000001	±	0.000015	2.59E-15	99.9%	2.96093	15.88	±	0.17
7.8	0.32431	±	0.00057	0.10919	±	0.00061	0.00133	±	0.00003	0.00001	±	0.00013	0.000002	±	0.000016	1.76E-15	99.8%	2.96487	15.90	±	0.25
8.1	0.67529	±	0.00069	0.22435	±	0.00073	0.00273	±	0.00004	-0.00020	±	0.00016	-0.000016	±	0.000026	3.67E-15	100.7%	3.00993	16.14	±	0.19
8.5	0.47988	±	0.00089	0.16015	±	0.00051	0.00195	±	0.00003	0.00022	±	0.00012	0.000027	±	0.000016	2.60E-15	98.4%	2.94711	15.80	±	0.17
8.5	0.10508	±	0.00058	0.03402	±	0.00026	0.00050	±	0.00005	0.00018	±	0.00023	0.000067	±	0.000022	5.70E-16	81.3%	2.51043	13.47	±	1.06
9	0.18437	±	0.00039	0.05942	±	0.00018	0.00083	±	0.00005	-0.00024	±	0.00013	0.000071	±	0.000024	1.00E-15	88.6%	2.74976	14.75	±	0.63
10	0.66175	±	0.00091	0.21812	±	0.00063	0.00278	±	0.00007	0.00032	±	0.00022	0.000077	±	0.000022	3.59E-15	96.6%	2.93002	15.71	±	0.17
11	0.77202	±	0.00100	0.24829	±	0.00056	0.00323	±	0.00007	0.00001	±	0.00018	0.000121	±	0.000023	4.19E-15	95.4%	2.96544	15.90	±	0.15
12	0.64544	±	0.00055	0.20703	±	0.00048	0.00264	±	0.00006	0.00078	±	0.00029	0.000151	±	0.000023	3.50E-15	93.1%	2.90306	15.57	±	0.18
15	0.31266	±	0.00029	0.09921	±	0.00048	0.00135	±	0.00005	0.00021	±	0.00019	0.000107	±	0.000024	1.70E-15	89.9%	2.83331	15.19	±	0.40

au15.4g.kfs, NV-9-09 IH Analysis																								
%P	40Ar V			39Ar V			38Ar V			37Ar V			36Ar V			Moles 40Ar*	%Rad	R	Age (Ma)		
5	0.51047	±	0.00095	0.10069	±	0.00029	0.00137	±	0.00004	-0.00004	±	0.00017	0.000704	±	0.000021	2.77E-15	59.2%	3.00291	16.10	±	0.35
5.5	0.26540	±	0.00043	0.08884	±	0.00043	0.00108	±	0.00004	-0.00024	±	0.00019	-0.000017	±	0.000018	1.44E-15	101.9%	2.98702	16.02	±	0.33
6	0.21909	±	0.00030	0.07311	±	0.00020	0.00093	±	0.00004	-0.00018	±	0.00016	-0.000022	±	0.000015	1.19E-15	102.9%	2.99658	16.07	±	0.34
6.4	0.27934	±	0.00038	0.09300	±	0.00047	0.00114	±	0.00004	0.00021	±	0.00015	0.000037	±	0.000016	1.52E-15	96.1%	2.88537	15.47	±	0.29
6.8	0.61718	±	0.00117	0.20719	±	0.00038	0.00256	±	0.00004	-0.00023	±	0.00018	0.000022	±	0.000017	3.35E-15	98.9%	2.94726	15.80	±	0.13
7.2	1.45772	±	0.00105	0.48119	±	0.00105	0.00597	±	0.00006	0.00009	±	0.00019	0.000128	±	0.000017	7.91E-15	97.4%	2.95076	15.82	±	0.07
7.5	1.28804	±	0.00085	0.42404	±	0.00081	0.00548	±	0.00010	0.00019	±	0.00024	0.000118	±	0.000017	6.99E-15	97.3%	2.95555	15.85	±	0.07
7.8	0.49389	±	0.00055	0.16208	±	0.00042	0.00199	±	0.00006	-0.00007	±	0.00022	0.000032	±	0.000016	2.68E-15	98.1%	2.98899	16.03	±	0.16
8.1	0.29967	±	0.00043	0.09866	±	0.00048	0.00118	±	0.00004	0.00023	±	0.00018	0.000023	±	0.000014	1.63E-15	97.7%	2.96750	15.91	±	0.25
8.5	0.31608	±	0.00053	0.10267	±	0.00034	0.00125	±	0.00004	-0.00003	±	0.00017	0.000038	±	0.000016	1.72E-15	96.5%	2.96991	15.92	±	0.26
9	0.19777	±	0.00035	0.06460	±	0.00017	0.00068	±	0.00004	-0.00008	±	0.00020	0.000013	±	0.000016	1.07E-15	98.0%	3.00114	16.09	±	0.40
10	0.47373	±	0.00112	0.15442	±	0.00054	0.00195	±	0.00005	-0.00008	±	0.00019	0.000008	±	0.000014	2.57E-15	99.5%	3.05330	16.37	±	0.16
11	0.51867	±	0.00091	0.17096	±	0.00057	0.00203	±	0.00003	0.00014	±	0.00013	-0.000006	±	0.000016	2.82E-15	100.3%	3.03393	16.27	±	0.16
13	0.58907	±	0.00107	0.19432	±	0.00048	0.00234	±	0.00004	-0.00017	±	0.00011	-0.000007	±	0.000015	3.20E-15	100.3%	3.03132	16.25	±	0.13
15	0.62515	±	0.00113	0.20519	±	0.00045	0.00233	±	0.00004	-0.00129	±	0.00024	0.000040	±	0.000013	3.39E-15	98.1%	2.98834	16.02	±	0.11
6.4	0.33090	±	0.00035	0.10063	±	0.00046	0.00132	±	0.00005	-0.00016	±	0.00013	0.000195	±	0.000024	1.80E-15	82.6%	2.71457	14.56	±	0.39
6.8	0.99632	±	0.00153	0.33642	±	0.00072	0.00417	±	0.00007	0.00000	±	0.00017	0.000103	±	0.000024	5.41E-15	97.0%	2.87123	15.40	±	0.12
7.2	0.67223	±	0.00102	0.22640	±	0.00063	0.00276	±	0.00006	-0.00009	±	0.00013	0.000040	±	0.000015	3.65E-15	98.2%	2.91685	15.64	±	0.11
7.5	0.16255	±	0.00061	0.05439	±	0.00032	0.00062	±	0.00003	-0.00015	±	0.00020	0.000037	±	0.000018	8.82E-16	93.3%	2.78928	14.96	±	0.53
7.8	0.20253	±	0.00038	0.05743	±	0.00034	0.00070	±	0.00004	0.00015	±	0.00025	0.000116	±	0.000016	1.10E-15	83.0%	2.92833	15.70	±	0.45
8.1	0.16881	±	0.00022	0.05556	±	0.00014	0.00064	±	0.00004	-0.00026	±	0.00017	0.000014	±	0.000016	9.16E-16	97.5%	2.96153	15.88	±	0.47
8.5	0.37611	±	0.00109	0.11946	±	0.00065	0.00147	±	0.00004	-0.00016	±	0.00024	0.000058	±	0.000015	2.04E-15	95.4%	3.00453	16.11	±	0.23

au15.4g.kfs, NV-9-09 IH Analysis																								
%P	40Ar V			39Ar V			38Ar V			37Ar V			36Ar V			Moles 40Ar*	%Rad	R	Age (Ma)		
5	0.47069	±	0.00060	0.05639	±	0.00032	0.00087	±	0.00004	-0.00077	±	0.00019	0.001022	±	0.000021	2.55E-15	35.9%	2.99200	16.04	±	0.66
5.5	0.36153	±	0.00097	0.11885	±	0.00054	0.00148	±	0.00003	-0.00084	±	0.00011	0.000009	±	0.000015	1.96E-15	99.2%	3.01801	16.18	±	0.22
6	0.27348	±	0.00036	0.09160	±	0.00024	0.00118	±	0.00005	-0.00097	±	0.00019	-0.000037	±	0.000016	1.48E-15	104.0%	2.98469	16.00	±	0.29
6.4	0.22384	±	0.00031	0.07496	±	0.00028	0.00092	±	0.00003	-0.00058	±	0.00021	-0.000031	±	0.000016	1.21E-15	104.0%	2.98536	16.01	±	0.34
6.8	0.71623	±	0.00149	0.23925	±	0.00065	0.00293	±	0.00004	-0.00072	±	0.00022	-0.000065	±	0.000031	3.89E-15	102.7%	2.99335	16.05	±	0.21
7.2	0.43602	±	0.00103	0.14569	±	0.00045	0.00179	±	0.00005	-0.00037	±	0.00023	0.000006	±	0.000015	2.37E-15	99.6%	2.98071	15.98	±	0.18
7.5	0.23960	±	0.00040	0.08035	±	0.00024	0.00095	±	0.00004	0.00006	±	0.00028	-0.000029	±	0.000023	1.30E-15	103.6%	2.98201	15.99	±	0.47
7.8	0.38485	±	0.00103	0.12785	±	0.00048	0.00151	±	0.00004	-0.00022	±	0.00019	-0.000004	±	0.000016	2.09E-15	100.3%	3.01004	16.14	±	0.21
8.1	1.57426	±	0.00148	0.51779	±	0.00106	0.00633	±	0.00008	0.00013	±	0.00017	0.000097	±	0.000015	8.54E-15	98.2%	2.98514	16.01	±	0.06
8.5	0.21216	±	0.00035	0.06996	±	0.00036	0.00083	±	0.00003	0.00019	±	0.00020	-0.000023	±	0.000025	1.15E-15	103.2%	3.03284	16.26	±	0.56
9	0.12486	±	0.00032	0.04136	±	0.00028	0.00055	±	0.00005	0.00009	±	0.00014	-0.000010	±	0.000014	6.78E-16	102.4%	3.01923	16.19	±	0.56
10	0.15095	±	0.00028	0.04933	±	0.00026	0.00064	±	0.00004	-0.00079	±	0.00026	0.000004	±	0.000016	8.19E-16	99.3%	3.03760	16.29	±	0.53
11	0.64017	±	0.00095	0.20806	±	0.00068	0.00254	±	0.00003	-0.00028	±	0.00030	0.000023	±	0.000015	3.47E-15	98.9%	3.04413	16.32	±	0.13
13	0.72161	±	0.00134	0.23384	±	0.00043	0.00304	±	0.00008	-0.00014	±	0.00014	0.000068	±	0.000015	3.92E-15	97.2%	2.99992	16.08	±	0.11
15	0.66788	±	0.00117	0.21817	±	0.00062	0.00268	±	0.00004	-0.00021	±	0.00014	0.000038	±	0.000014	3.62E-15	98.3%	3.00917	16.13	±	0.11

au15.4g.kfs, NV-9-09 IH Analysis																									
%P	40Ar V			39Ar V			38Ar V			37Ar V			36Ar V			Moles 40Ar*	%Rad	R	Age (Ma)		
5	0.21962	±	0.00045	0.07354	±	0.00026	0.00088	±	0.00003	-0.00027	±	0.00029	0.000080	±	0.000028	1.19E-15	89.2%	2.66329	14.29	±	0.60
5.5	0.30160	±	0.00047	0.05391	±	0.00026	0.00078	±	0.00003	0.00009	±	0.00019	0.000526	±	0.000027	1.64E-15	48.5%	2.71139	14.54	±	0.80
6	0.75790	±	0.00131	0.25752	±	0.00072	0.00320	±	0.00005	0.00003	±	0.00016	0.000099	±	0.000024	4.11E-15	96.1%	2.82959	15.17	±	0.16
9	0.62502	±	0.00145	0.20730	±	0.00059	0.00254	±	0.00004	0.00026	±	0.00032	0.000011	±	0.000014	3.39E-15	99.5%	2.99981	16.08	±	0.12
10	0.34383	±	0.00029	0.11258	±	0.00020	0.00147	±	0.00005	-0.00020	±	0.00017	0.000005	±	0.000015	1.87E-15	99.6%	3.04064	16.30	±	0.22
11	0.41481	±	0.00054	0.14027	±	0.00050	0.00169	±	0.00005	-0.00024	±	0.00013	-0.000016	±	0.000014	2.25E-15	101.2%	2.95713	15.86	±	0.17
12	0.32676	±	0.00050	0.11054	±	0.00029	0.00121	±	0.00007	0.00005	±	0.00008	-0.000072	±	0.000024	1.77E-15	106.5%	2.95605	15.85	±	0.35
15	0.29134	±	0.00046	0.09758	±	0.00056	0.00118	±	0.00005	0.00012	±	0.00017	-0.000007	±	0.000012	1.58E-15	100.7%	2.98574	16.01	±	0.22

au20.4i.kfs, BJK BLK Jk, CMT056 SCTF Analyses																								
%P	40Ar V			39Ar V			38Ar V			37Ar V			36Ar V			Moles 40Ar*	%Rad	R	Age (Ma)		
16	4.22064	±	0.00190	2.41187	±	0.00120	0.03261	±	0.00015	0.00322	±	0.00009	0.00212	±	0.00002	2.96E-14	85.18%	1.49068	16.00	±	0.03
16	3.40840	±	0.00217	2.08745	±	0.00206	0.02828	±	0.00011	0.00013	±	0.00004	0.00122	±	0.00002	2.39E-14	89.44%	1.46036	15.67	±	0.04
16	3.58014	±	0.00210	2.32057	±	0.00377	0.03103	±	0.00012	0.00012	±	0.00008	0.00083	±	0.00001	2.51E-14	93.17%	1.43745	15.43	±	0.03
16	3.97302	±	0.00732	2.64454	±	0.00452	0.03526	±	0.00012	0.00006	±	0.00005	0.00060	±	0.00002	2.78E-14	95.52%	1.43502	15.40	±	0.05
16	3.76830	±	0.00437	2.52408	±	0.00326	0.03378	±	0.00016	0.00010	±	0.00007	0.00046	±	0.00002	2.64E-14	96.37%	1.43881	15.44	±	0.03
16	1.41804	±	0.00205	0.89630	±	0.00082	0.01205	±	0.00008	0.00008	±	0.00005	0.00042	±	0.00001	9.93E-15	91.35%	1.44518	15.51	±	0.06
16	2.84229	±	0.00294	1.89236	±	0.00346	0.02514	±	0.00011	0.00013	±	0.00005	0.00037	±	0.00002	1.99E-14	96.13%	1.44379	15.49	±	0.04
16	4.33989	±	0.00348	2.65718	±	0.00511	0.03554	±	0.00016	0.00015	±	0.00006	0.00168	±	0.00003	3.04E-14	88.58%	1.44676	15.53	±	0.05
16	3.57260	±	0.00328	2.23633	±	0.00248	0.03014	±	0.00015	0.00011	±	0.00008	0.00120	±	0.00002	2.50E-14	90.08%	1.43906	15.44	±	0.04
16	2.19882	±	0.00207	1.32411	±	0.00191	0.01783	±	0.00009	-0.00003	±	0.00005	0.00099	±	0.00002	1.54E-14	86.74%	1.44034	15.46	±	0.05
16	4.21713	+	0.00383	2.41187	+	0.00120	0.03252	+	0.00014	0.00322	+	0.00009	0.00211	+	0.00003	2.95338E-14	85.24%	1.49043	15.99	±	0.04
16	3.39128	+	0.00329	2.07989	+	0.00177	0.02818	+	0.00011	0.00013	+	0.00004	0.00121	+	0.00003	2.37502E-14	89.47%	1.45884	15.65	±	0.05
16	3.94999	+	0.00558	2.62135	+	0.00499	0.03516	+	0.00012	0.00006	+	0.00005	0.00060	+	0.00002	2.7663E-14	95.49%	1.43892	15.44	±	0.04
16	3.56546	+	0.00282	2.31117	+	0.00256	0.03093	+	0.00012	0.00012	+	0.00008	0.00083	+	0.00001	2.497E-14	93.14%	1.43695	15.42	±	0.03
16	3.71853	+	0.00987	2.49482	+	0.00589	0.03369	+	0.00016	0.00010	+	0.00007	0.00052	+	0.00003	2.6042E-14	95.87%	1.42889	15.33	±	0.07
16	1.40047	+	0.00336	0.88754	+	0.00175	0.01195	+	0.00007	0.00008	+	0.00005	0.00042	+	0.00001	9.8079E-15	91.24%	1.43964	15.45	±	0.08
16	2.81088	+	0.00616	1.87525	+	0.00372	0.02504	+	0.00010	0.00013	+	0.00005	0.00037	+	0.00002	1.96854E-14	96.08%	1.44021	15.46	±	0.05
16	4.29991	+	0.00788	2.63323	+	0.00525	0.03544	+	0.00016	0.00015	+	0.00006	0.00168	+	0.00003	3.01136E-14	88.47%	1.44473	15.50	±	0.06
16	3.56019	+	0.00270	2.22336	+	0.00279	0.03004	+	0.00015	0.00011	+	0.00008	0.00120	+	0.00002	2.49331E-14	90.05%	1.44188	15.47	±	0.04
16	2.18386	+	0.00286	1.31557	+	0.00189	0.01774	+	0.00009	-0.00003	+	0.00005	0.00094	+	0.00003	1.52942E-14	87.35%	1.44999	15.56	±	0.08

au20.4i.kfs, BJK BLK, CMT056 IH Analysis

%P	40Ar V			39Ar V			38Ar V			37Ar V			36Ar V			Moles 40Ar*	%Rad	R	Age (Ma)	-	
3.5	0.27911	+	0.00095	0.18033	+	0.00058	0.00248	+	0.00004	-0.00007	+	0.00008	0.00008	+	0.00002	1.95467E-15	91.95%	1.42309	15.27	±	0.30
4.5	1.74480	+	0.00388	1.18384	+	0.00380	0.01604	+	0.00009	-0.00012	+	0.00005	0.00012	+	0.00002	1.22194E-14	98.00%	1.44442	15.50	±	0.08
4.8	2.54860	+	0.00431	1.72212	+	0.00341	0.02309	+	0.00012	-0.00005	+	0.00007	0.00022	+	0.00002	1.78486E-14	97.44%	1.44209	15.48	±	0.05
5	0.10659	+	0.00112	0.07109	+	0.00020	0.00093	+	0.00003	-0.00009	+	0.00008	-0.00005	+	0.00003	7.46492E-16	112.94%	1.49920	16.09	±	1.20
5.3	0.08335	+	0.00107	0.05533	+	0.00025	0.00078	+	0.00003	-0.00013	+	0.00005	0.00003	+	0.00002	5.83715E-16	88.67%	1.33564	14.34	±	1.04
5.5	1.26919	+	0.00609	0.83599	+	0.00464	0.01112	+	0.00011	-0.00004	+	0.00005	0.00022	+	0.00002	8.8885E-15	94.76%	1.43868	15.44	±	0.13
5.8	0.89659	+	0.00197	0.60269	+	0.00156	0.00801	+	0.00008	0.00002	+	0.00005	0.00009	+	0.00002	6.27912E-15	96.88%	1.44123	15.47	±	0.10
6	0.56015	+	0.00111	0.37253	+	0.00123	0.00494	+	0.00007	0.00013	+	0.00005	0.00008	+	0.00001	3.92289E-15	95.93%	1.44242	15.48	±	0.14
7	0.79886	+	0.00178	0.53127	+	0.00161	0.00701	+	0.00006	-0.00006	+	0.00006	0.00004	+	0.00002	5.59468E-15	98.68%	1.48380	15.92	±	0.14
8	0.58269	+	0.00109	0.38920	+	0.00116	0.00517	+	0.00004	-0.00012	+	0.00006	0.00008	+	0.00002	4.08077E-15	95.86%	1.43514	15.40	±	0.14
9	0.45829	+	0.00094	0.30881	+	0.00079	0.00410	+	0.00005	0.00001	+	0.00005	0.00005	+	0.00001	3.20955E-15	96.62%	1.43385	15.39	±	0.16
10	0.24567	+	0.00106	0.16857	+	0.00028	0.00220	+	0.00004	0.00001	+	0.00006	0.00003	+	0.00002	1.72052E-15	96.46%	1.40578	15.09	±	0.32
11	0.13111	+	0.00105	0.08916	+	0.00017	0.00118	+	0.00003	0.00002	+	0.00006	0.00004	+	0.00001	9.18206E-16	91.87%	1.35089	14.50	±	0.54
13	0.14758	+	0.00111	0.09948	+	0.00019	0.00124	+	0.00003	-0.00032	+	0.00008	0.00000	+	0.00002	1.03357E-15	99.14%	1.47057	15.78	±	0.53
15	0.11481	+	0.00111	0.07399	+	0.00029	0.00096	+	0.00003	-0.00012	+	0.00005	0.00002	+	0.00002	8.04047E-16	96.06%	1.49044	15.99	±	0.72
16	0.00138	+	0.00124	0.00084	+	0.00009	- 0.00004	+	0.00003	0.00003	+	0.00004	0.00002	+	0.00002	9.66792E-18	- 361.22%	- 5.92946	-65.06	±	-62.70

au20.4j.kfs, CA-1-10, CMT057 IH Analysis																								
%P	40Ar V			39Ar V			38Ar V			37Ar V			36Ar V			Moles 40Ar*	%Rad	R	Age (Ma)		
3.5	0.01676	+	0.00118	0.00374	+	0.00008	0.00009	+	0.00004	-0.00005	+	0.00004	0.00001	+	0.00002	1.17342E-16	75.49%	3.38516	36.12	±	14.59
4	0.97410	+	0.00250	0.60790	+	0.00175	0.00815	+	0.00007	0.00017	+	0.00005	0.00025	+	0.00002	6.82189E-15	92.49%	1.48213	15.90	±	0.11
4.5	6.07222	+	0.01025	4.11006	+	0.00781	0.05507	+	0.00022	0.00048	+	0.00006	0.00036	+	0.00002	4.25256E-14	98.25%	1.45148	15.58	±	0.04
4.8	2.84754	+	0.00797	1.89548	+	0.00627	0.02559	+	0.00019	0.00034	+	0.00006	0.00023	+	0.00003	1.99422E-14	97.58%	1.46600	15.73	±	0.09
5	0.09106	+	0.00115	0.05657	+	0.00025	0.00080	+	0.00004	0.00011	+	0.00005	0.00000	+	0.00002	6.37695E-16	98.52%	1.58591	17.01	±	1.08
5.3	0.58493	+	0.00133	0.36970	+	0.00105	0.00501	+	0.00005	0.00006	+	0.00006	0.00013	+	0.00002	4.09644E-15	93.40%	1.47775	15.86	±	0.16
5.5	0.60168	+	0.00153	0.38987	+	0.00140	0.00511	+	0.00005	0.00008	+	0.00008	0.00006	+	0.00002	4.21376E-15	96.83%	1.49443	16.03	±	0.16
5.8	0.23298	+	0.00094	0.14774	+	0.00060	0.00191	+	0.00004	0.00005	+	0.00006	0.00004	+	0.00002	1.63164E-15	94.65%	1.49258	16.02	±	0.34
6	0.11499	+	0.00102	0.07372	+	0.00030	0.00094	+	0.00004	0.00009	+	0.00005	0.00000	+	0.00002	8.05338E-16	100.94%	1.56000	16.74	±	0.75
7	0.02252	+	0.00115	0.01645	+	0.00015	0.00022	+	0.00003	-0.00015	+	0.00009	-0.00008	+	0.00002	1.57696E-16	208.05%	1.36809	14.68	±	3.99
8	0.03253	+	0.00114	0.01853	+	0.00013	0.00026	+	0.00003	-0.00004	+	0.00006	-0.00001	+	0.00002	2.27799E-16	105.18%	1.75482	18.81	±	2.95
9	0.01539	+	0.00118	0.00699	+	0.00009	0.00013	+	0.00003	-0.00001	+	0.00007	0.00001	+	0.00002	1.07752E-16	72.38%	1.59206	17.08	±	7.51
10	0.00784	+	0.00120	0.00312	+	0.00009	0.00002	+	0.00004	0.00000	+	0.00007	-0.00003	+	0.00002	5.48878E-17	229.51%	2.51052	26.86	±	16.12
11	0.03167	+	0.00115	0.00399	+	0.00010	0.00006	+	0.00004	0.00006	+	0.00009	0.00010	+	0.00002	2.21823E-16	9.56%	0.75818	8.15	±	14.07
13	0.03039	+	0.00112	0.00989	+	0.00007	0.00018	+	0.00004	0.00002	+	0.00004	0.00004	+	0.00002	2.12836E-16	60.63%	1.86387	19.98	±	5.99
15	0.03169	+	0.00122	0.01505	+	0.00009	0.00028	+	0.00002	0.00006	+	0.00004	0.00004	+	0.00001	2.21963E-16	58.53%	1.23290	13.24	±	3.28
16	0.01643	+	0.00119	0.00911	+	0.00010	0.00012	+	0.00002	0.00014	+	0.00003	0.00001	+	0.00001	1.15063E-16	77.92%	1.40548	15.08	±	4.94

au20.4j.kfs,CA-1-10, CMT058 SCTF Analyses																						
%P	40Ar V			39Ar V			38Ar V			37Ar V			36Ar V			Moles 40Ar*	%Rad	R	Age (Ma)		
16	1.95642	±	0.00216	0.82905	±	0.00098	0.01144	±	0.00010	0.00302	±	0.00008	0.00252	±	0.00002	1.37E-14	61.95%	1.46191	15.69	±	0.10
16	1.06614	±	0.00106	0.48049	±	0.00075	0.00650	±	0.00008	0.00274	±	0.00005	0.00124	±	0.00003	7.47E-15	65.74%	1.45872	15.65	±	0.18
16	1.05107	±	0.00139	0.55506	±	0.00082	0.00755	±	0.00007	0.00195	±	0.00008	0.00082	±	0.00002	7.36E-15	76.91%	1.45645	15.63	±	0.12
16	3.30024	±	0.00375	1.88997	±	0.00216	0.02562	±	0.00008	0.00034	±	0.00005	0.00191	±	0.00003	2.31E-14	82.94%	1.44825	15.54	±	0.06
16	0.34519	±	0.00054	0.14524	±	0.00033	0.00201	±	0.00006	0.00174	±	0.00006	0.00044	±	0.00002	2.42E-15	62.60%	1.48786	15.97	±	0.38
16	1.88055	±	0.00306	1.13194	±	0.00144	0.01548	±	0.00014	0.00032	±	0.00004	0.00077	±	0.00002	1.32E-14	87.97%	1.46154	15.68	±	0.06
16	1.20763	±	0.00125	0.45557	±	0.00098	0.00650	±	0.00006	0.00062	±	0.00006	0.00191	±	0.00002	8.46E-15	53.34%	1.41398	15.18	±	0.18
16	0.43718	±	0.00062	0.15038	±	0.00062	0.00212	±	0.00003	0.00245	±	0.00009	0.00073	±	0.00002	3.06E-15	50.76%	1.47558	15.83	±	0.50
16	2.46990	±	0.00231	1.20024	±	0.00079	0.01645	±	0.00010	0.00067	±	0.00005	0.00245	±	0.00002	1.73E-14	70.64%	1.45376	15.60	±	0.07
16	0.64503	±	0.00082	0.14156	±	0.00034	0.00216	±	0.00004	0.00148	±	0.00008	0.00149	±	0.00002	4.52E-15	31.66%	1.44268	15.48	±	0.53
16	1.94908	±	0.00153	0.83124	±	0.00180	0.01144	±	0.00010	0.00302	±	0.00008	0.00248	±	0.00005	1.37E-14	62.39%	1.46301	15.70	±	0.19
16	1.05991	±	0.00105	0.47716	±	0.00070	0.00650	±	0.00010	0.00274	±	0.00005	0.00124	±	0.00003	7.42E-15	65.54%	1.45587	15.62	±	0.18
16	1.04169	±	0.00164	0.54938	±	0.00113	0.00755	±	0.00010	0.00195	±	0.00008	0.00082	±	0.00002	7.30E-15	76.70%	1.45443	15.61	±	0.12
16	3.28156	±	0.00380	1.87654	±	0.00277	0.02562	±	0.00010	0.00034	±	0.00005	0.00191	±	0.00003	2.30E-14	82.84%	1.44867	15.55	±	0.06
16	0.34289	±	0.00071	0.14500	±	0.00033	0.00201	±	0.00010	0.00174	±	0.00006	0.00044	±	0.00002	2.40E-15	62.35%	1.47448	15.82	±	0.39
16	1.86534	±	0.00302	1.13169	±	0.00144	0.01517	±	0.00010	0.00032	±	0.00004	0.00077	±	0.00002	1.31E-14	87.87%	1.44841	15.54	±	0.06
16	1.19800	±	0.00166	0.45243	±	0.00074	0.00650	±	0.00010	0.00062	±	0.00006	0.00191	±	0.00002	8.39E-15	52.97%	1.40252	15.05	±	0.18
16	0.43294	±	0.00068	0.14850	±	0.00044	0.00212	±	0.00010	0.00245	±	0.00009	0.00073	±	0.00002	3.03E-15	50.27%	1.46568	15.73	±	0.50
16	2.45898	±	0.00211	1.19444	±	0.00114	0.01645	±	0.00010	0.00067	±	0.00005	0.00245	±	0.00002	1.72E-14	70.51%	1.45167	15.58	±	0.07
16	0.63984	±	0.00084	0.14132	±	0.00034	0.00216	±	0.00010	0.00148	±	0.00008	0.00149	±	0.00002	4.48E-15	31.11%	1.40843	15.12	±	0.53

au20.4k.kfs, CD-1-10, CMT058 SCTF Analyses																								
%P	40Ar V			39Ar V			38Ar V			37Ar V			36Ar V			Moles 40Ar*	%Rad	R	Age (Ma)		
16	4.74464	±	0.00511	2.79620	±	0.00117	0.03778	±	0.00013	0.00021	±	0.00006	0.00229	±	0.00003	3.32E-14	85.74%	1.45477	15.61	±	0.04
16	2.17405	±	0.00202	1.40116	±	0.00213	0.01863	±	0.00010	0.00015	±	0.00005	0.00045	±	0.00002	1.52E-14	93.91%	1.45718	15.64	±	0.05
16	3.09653	±	0.00169	1.91525	±	0.00195	0.02553	±	0.00009	0.00021	±	0.00007	0.00101	±	0.00003	2.17E-14	90.40%	1.46151	15.68	±	0.05
16	3.97464	±	0.00331	2.40352	±	0.00220	0.03296	±	0.00022	0.00042	±	0.00006	0.00161	±	0.00003	2.78E-14	88.05%	1.45607	15.63	±	0.04
16	2.97840	±	0.00336	1.85929	±	0.00155	0.02529	±	0.00016	-0.00010	±	0.00005	0.00097	±	0.00002	2.09E-14	90.40%	1.44809	15.54	±	0.04
16	2.27572	±	0.00299	1.19010	±	0.00116	0.01661	±	0.00016	0.00010	±	0.00005	0.00188	±	0.00002	1.59E-14	75.58%	1.44518	15.51	±	0.07
16	2.40831	±	0.00204	1.43591	±	0.00157	0.01919	±	0.00012	0.00019	±	0.00007	0.00106	±	0.00003	1.69E-14	86.94%	1.45809	15.65	±	0.06
16	3.67839	±	0.00400	2.16812	±	0.00123	0.02923	±	0.00009	0.00020	±	0.00006	0.00182	±	0.00002	2.58E-14	85.40%	1.44894	15.55	±	0.04
16	2.34926	±	0.00245	1.53579	±	0.00129	0.02042	±	0.00009	0.00021	±	0.00006	0.00029	±	0.00002	1.65E-14	96.36%	1.47403	15.82	±	0.05
16	4.11702	±	0.00343	2.61491	±	0.00185	0.03521	±	0.00009	0.00026	±	0.00004	0.00102	±	0.00002	2.88E-14	92.66%	1.45889	15.66	±	0.03
16	4.74265	±	0.00513	2.79602	±	0.00117	0.03778	±	0.00013	0.00021	±	0.00006	0.00229	±	0.00003	3.32E-14	85.73%	1.45415	15.60	±	0.04
16	2.15828	±	0.00296	1.38971	±	0.00242	0.01863	±	0.00010	0.00015	±	0.00005	0.00050	±	0.00003	1.51E-14	93.11%	1.44610	15.52	±	0.08
16	3.07352	±	0.00433	1.90023	±	0.00304	0.02553	±	0.00009	0.00021	±	0.00007	0.00106	±	0.00004	2.15E-14	89.79%	1.45237	15.59	±	0.07
16	3.94480	±	0.00583	2.39015	±	0.00277	0.03220	±	0.00018	0.00042	±	0.00006	0.00166	±	0.00003	2.76E-14	87.55%	1.44490	15.51	±	0.06
16	2.95898	±	0.00388	1.84500	±	0.00284	0.02489	±	0.00011	-0.00010	±	0.00005	0.00102	±	0.00003	2.07E-14	89.78%	1.43994	15.45	±	0.06
16	2.25363	±	0.00430	1.17733	±	0.00251	0.01621	±	0.00011	0.00010	±	0.00005	0.00194	±	0.00003	1.58E-14	74.61%	1.42823	15.33	±	0.11
16	2.39874	±	0.00186	1.42533	±	0.00216	0.01919	±	0.00012	0.00019	±	0.00007	0.00103	±	0.00005	1.68E-14	87.35%	1.46999	15.77	±	0.12
16	3.65748	±	0.00428	2.15256	±	0.00305	0.02923	±	0.00009	0.00020	±	0.00006	0.00187	±	0.00003	2.56E-14	84.87%	1.44213	15.48	±	0.06
16	2.33016	±	0.00365	1.52194	±	0.00273	0.02042	±	0.00009	0.00021	±	0.00006	0.00029	±	0.00002	1.63E-14	96.33%	1.47490	15.83	±	0.06
16	4.09299	±	0.00474	2.60072	±	0.00286	0.03521	±	0.00009	0.00026	±	0.00004	0.00102	±	0.00002	2.87E-14	92.62%	1.45761	15.64	±	0.03

au20.4l.kfs, CM-5, CMT059 SCTF Analyses																						
%P	40Ar V			39Ar V			38Ar V			37Ar V			36Ar V			Moles 40Ar*	%Rad	R	Age (Ma)		
1.6	2.32605	±	0.00313	1.51681	±	0.00224	0.01989	±	0.00007	0.00019	±	0.00006	0.00041	±	0.00002	1.63E-14	94.81%	1.45388	15.60	±	0.05
1.6	2.85362	±	0.00254	1.90937	±	0.00243	0.02523	±	0.00011	0.00019	±	0.00004	0.00027	±	0.00002	2.00E-14	97.17%	1.45228	15.59	±	0.04
1.6	2.62077	±	0.00327	1.72250	±	0.00158	0.02346	±	0.00018	0.00033	±	0.00008	0.00034	±	0.00002	1.84E-14	96.16%	1.46299	15.70	±	0.04
1.6	0.62119	±	0.00055	0.38822	±	0.00062	0.00518	±	0.00006	0.00075	±	0.00006	0.00016	±	0.00002	4.35E-15	92.21%	1.47550	15.83	±	0.13
1.6	6.60587	±	0.00308	2.89834	±	0.00355	0.04018	±	0.00015	0.00012	±	0.00010	0.00823	±	0.00004	4.63E-14	63.18%	1.44006	15.45	±	0.06
1.6	1.31861	±	0.00416	0.20288	±	0.00095	0.00345	±	0.00006	0.00080	±	0.00007	0.00364	±	0.00005	9.23E-15	18.54%	1.20484	12.94	±	0.88
1.6	3.29873	±	0.00900	1.49470	±	0.00434	0.02093	±	0.00024	0.00015	±	0.00006	0.00386	±	0.00003	2.31E-14	65.46%	1.44457	15.50	±	0.12
1.6	2.03800	±	0.00420	0.81664	±	0.00254	0.01156	±	0.00006	0.00068	±	0.00007	0.00287	±	0.00002	1.43E-14	58.44%	1.45841	15.65	±	0.14
1.6	0.96587	±	0.00249	0.33476	±	0.00111	0.00470	±	0.00006	0.00049	±	0.00008	0.00163	±	0.00002	6.76E-15	50.13%	1.44627	15.52	±	0.23
1.6	2.31405	±	0.00319	1.50077	±	0.00332	0.01992	±	0.00007	0.00051	±	0.00006	0.00045	±	0.00002	1.62E-14	94.22%	1.45276	15.59	±	0.07
1.6	2.82516	±	0.00622	1.88270	±	0.00534	0.02526	±	0.00011	0.00051	±	0.00004	0.00025	±	0.00004	1.98E-14	97.34%	1.46066	15.67	±	0.08
1.6	2.58533	±	0.00765	1.69530	±	0.00536	0.02284	±	0.00015	0.00065	±	0.00008	0.00038	±	0.00001	1.81E-14	95.70%	1.45948	15.66	±	0.08
1.6	0.61831	±	0.00104	0.38226	±	0.00121	0.00521	±	0.00006	0.00108	±	0.00006	0.00020	±	0.00001	4.33E-15	90.51%	1.46400	15.71	±	0.13

au20.4k.kfs,CD-1-10 CMT058 IH Analysis

%P	40Ar V			39Ar V			38Ar V			37Ar V			36Ar V			Moles 40Ar*	%Rad	R	Age (Ma)		
3.5	0.12512	+	0.00098	0.07454	+	0.00014	0.00100	+	0.00003	0.00019	+	0.00005	0.00008	+	0.00001	8.76273E-16	82.03%	1.37686	14.78	±	0.59
4	0.50402	+	0.00118	0.32260	+	0.00128	0.00426	+	0.00004	0.00013	+	0.00006	0.00009	+	0.00001	3.5298E-15	94.56%	1.47735	15.85	±	0.16
4.5	0.63149	+	0.00139	0.43140	+	0.00140	0.00602	+	0.00010	0.00006	+	0.00006	0.00005	+	0.00002	4.4225E-15	97.73%	1.43060	15.35	±	0.18
4.8	2.10207	+	0.00378	1.40467	+	0.00334	0.01871	+	0.00007	0.00039	+	0.00007	0.00020	+	0.00002	1.47214E-14	97.16%	1.45396	15.60	±	0.06
5	2.02006	+	0.00404	1.33752	+	0.00370	0.01796	+	0.00015	0.00022	+	0.00011	0.00021	+	0.00002	1.41471E-14	97.00%	1.46501	15.72	±	0.07
5.3	1.96353	+	0.00454	1.31094	+	0.00381	0.01762	+	0.00014	0.00016	+	0.00006	0.00007	+	0.00003	1.37512E-14	98.97%	1.48236	15.91	±	0.09
5.5	0.60640	+	0.00118	0.39653	+	0.00129	0.00528	+	0.00007	0.00006	+	0.00007	0.00008	+	0.00002	4.24682E-15	96.05%	1.46891	15.76	±	0.16
5.8	1.62036	+	0.00331	1.04516	+	0.00278	0.01389	+	0.00009	0.00014	+	0.00004	0.00026	+	0.00002	1.13479E-14	95.18%	1.47570	15.83	±	0.08
6	1.40787	+	0.00292	0.93678	+	0.00261	0.01247	+	0.00009	0.00018	+	0.00005	0.00011	+	0.00002	9.85971E-15	97.71%	1.46844	15.76	±	0.09
7	1.73209	+	0.00395	1.14368	+	0.00328	0.01518	+	0.00009	0.00037	+	0.00009	0.00017	+	0.00002	1.21303E-14	97.02%	1.46940	15.77	±	0.08
8	1.22239	+	0.00299	0.81884	+	0.00299	0.01092	+	0.00008	0.00016	+	0.00007	0.00008	+	0.00002	8.56077E-15	98.09%	1.46438	15.71	±	0.10
9	1.49236	+	0.00246	0.99978	+	0.00235	0.01312	+	0.00020	0.00017	+	0.00006	0.00010	+	0.00002	1.04515E-14	98.06%	1.46367	15.71	±	0.07
10	0.88841	+	0.00121	0.58744	+	0.00241	0.00782	+	0.00008	0.00007	+	0.00007	0.00004	+	0.00002	6.22182E-15	98.70%	1.49275	16.02	±	0.12
11	0.45806	+	0.00125	0.30696	+	0.00094	0.00407	+	0.00005	0.00020	+	0.00007	0.00001	+	0.00002	3.20792E-15	99.29%	1.48164	15.90	±	0.21
13	0.77408	+	0.00229	0.51164	+	0.00159	0.00691	+	0.00010	-0.00003	+	0.00005	0.00012	+	0.00003	5.42115E-15	95.24%	1.44090	15.46	±	0.18
15	0.44003	+	0.00103	0.26469	+	0.00066	0.00355	+	0.00005	-0.00006	+	0.00006	0.00019	+	0.00002	3.08168E-15	87.57%	1.45583	15.62	±	0.21
16	0.05323	+	0.00134	0.03515	+	0.00015	0.00041	+	0.00005	0.00000	+	0.00004	0.00001	+	0.00002	3.72815E-16	95.78%	1.45061	15.57	±	1.72

au20.4l.kfs, CM-5, CMT059 SCTF Analyses

%P	40Ar V			39Ar V			38Ar V			37Ar V			36Ar V			Moles 40Ar*	%Rad	R	Age (Ma)		
1.6	2.32605	±	0.00313	1.51681	±	0.00224	0.01989	±	0.00007	0.00019	±	0.00006	0.00041	±	0.00002	1.63E-14	94.81%	1.45388	15.60	±	0.05
1.6	2.85362	±	0.00254	1.90937	±	0.00243	0.02523	±	0.00011	0.00019	±	0.00004	0.00027	±	0.00002	2.00E-14	97.17%	1.45228	15.59	±	0.04
1.6	2.62077	±	0.00327	1.72250	±	0.00158	0.02346	±	0.00018	0.00033	±	0.00008	0.00034	±	0.00002	1.84E-14	96.16%	1.46299	15.70	±	0.04
1.6	0.62119	±	0.00055	0.38822	±	0.00062	0.00518	±	0.00006	0.00075	±	0.00006	0.00016	±	0.00002	4.35E-15	92.21%	1.47550	15.83	±	0.13
1.6	6.60587	±	0.00308	2.89834	±	0.00355	0.04018	±	0.00015	0.00012	±	0.00010	0.00823	±	0.00004	4.63E-14	63.18%	1.44006	15.45	±	0.06
1.6	1.31861	±	0.00416	0.20288	±	0.00095	0.00345	±	0.00006	0.00080	±	0.00007	0.00364	±	0.00005	9.23E-15	18.54%	1.20484	12.94	±	0.88
1.6	3.29873	±	0.00900	1.49470	±	0.00434	0.02093	±	0.00024	0.00015	±	0.00006	0.00386	±	0.00003	2.31E-14	65.46%	1.44457	15.50	±	0.12
1.6	2.03800	±	0.00420	0.81664	±	0.00254	0.01156	±	0.00006	0.00068	±	0.00007	0.00287	±	0.00002	1.43E-14	58.44%	1.45841	15.65	±	0.14
1.6	0.96587	±	0.00249	0.33476	±	0.00111	0.00470	±	0.00006	0.00049	±	0.00008	0.00163	±	0.00002	6.76E-15	50.13%	1.44627	15.52	±	0.23
1.6	2.31405	±	0.00319	1.50077	±	0.00332	0.01992	±	0.00007	0.00051	±	0.00006	0.00045	±	0.00002	1.62E-14	94.22%	1.45276	15.59	±	0.07
1.6	2.82516	±	0.00622	1.88270	±	0.00534	0.02526	±	0.00011	0.00051	±	0.00004	0.00025	±	0.00004	1.98E-14	97.34%	1.46066	15.67	±	0.08
1.6	2.58533	±	0.00765	1.69530	±	0.00536	0.02284	±	0.00015	0.00065	±	0.00008	0.00038	±	0.00001	1.81E-14	95.70%	1.45948	15.66	±	0.08
1.6	0.61831	±	0.00104	0.38226	±	0.00121	0.00521	±	0.00006	0.00108	±	0.00006	0.00020	±	0.00001	4.33E-15	90.51%	1.46400	15.71	±	0.13

au20.4l.kfs, CM5, CMT059 IH Analysis

%P	40Ar V			39Ar V			38Ar V			37Ar V			36Ar V			Moles 40Ar*	%Rad	R	Age (Ma)		
3.5	0.27146	+	0.00121	0.16501	+	0.00077	0.00224	+	0.00005	0.00001	+	0.00006	0.00012	+	0.00002	1.9011E-15	87.20%	1.43441	15.39	±	0.36
4	1.70109	+	0.00427	1.11791	+	0.00355	0.01523	+	0.00012	-0.00004	+	0.00009	0.00029	+	0.00003	1.19133E-14	95.00%	1.44557	15.51	±	0.10
4.5	0.12148	+	0.00116	0.07688	+	0.00035	0.00096	+	0.00005	-0.00011	+	0.00008	0.00002	+	0.00002	8.50729E-16	95.86%	1.51442	16.25	±	0.81
4.8	0.33934	+	0.00105	0.20743	+	0.00054	0.00275	+	0.00004	0.00000	+	0.00005	0.00015	+	0.00002	2.3765E-15	87.13%	1.42542	15.30	±	0.27
5	0.56246	+	0.00111	0.34635	+	0.00031	0.00464	+	0.00009	0.00005	+	0.00008	0.00020	+	0.00002	3.9391E-15	89.30%	1.45025	15.56	±	0.18
5.3	0.66402	+	0.00134	0.40017	+	0.00108	0.00527	+	0.00003	-0.00001	+	0.00005	0.00026	+	0.00002	4.65035E-15	88.52%	1.46880	15.76	±	0.15
5.5	0.30156	+	0.00107	0.19491	+	0.00030	0.00251	+	0.00005	-0.00007	+	0.00005	0.00006	+	0.00002	2.11193E-15	94.43%	1.46101	15.68	±	0.31
5.8	0.11487	+	0.00112	0.07481	+	0.00043	0.00099	+	0.00004	-0.00008	+	0.00004	0.00005	+	0.00002	8.04437E-16	87.45%	1.34263	14.41	±	0.81
6	0.04530	+	0.00131	0.02938	+	0.00013	0.00045	+	0.00002	0.00016	+	0.00006	0.00003	+	0.00002	3.1724E-16	77.63%	1.19681	12.85	±	1.72
7	0.14573	+	0.00099	0.09377	+	0.00038	0.00123	+	0.00003	0.00007	+	0.00004	0.00002	+	0.00003	1.02059E-15	96.16%	1.49444	16.03	±	0.89
8	0.01388	+	0.00127	0.00893	+	0.00010	0.00010	+	0.00002	-0.00001	+	0.00003	0.00004	+	0.00001	9.72098E-17	20.65%	0.32092	3.46	±	5.08
9	0.00349	+	0.00127	0.00254	+	0.00011	0.00003	+	0.00003	0.00005	+	0.00006	0.00000	+	0.00002	2.44334E-17	64.61%	0.88860	9.55	±	20.72
10	0.00029	+	0.00127	0.00042	+	0.00010	0.00000	+	0.00004	0.00006	+	0.00006	-0.00002	+	0.00002	2.00104E-18	2232.2%	0.68907	7.41	±	126.24
11	-0.00943	+	0.00114	0.00018	+	0.00010	0.00001	+	0.00003	-0.00015	+	0.00005	-0.00003	+	0.00001	-6.60756E-17	-3.07%	-51.1872	-658.46	±	-611.84
13	-0.00605	+	0.00114	0.00235	+	0.00009	0.00005	+	0.00004	-0.00006	+	0.00006	-0.00001	+	0.00002	-4.23703E-17	36.51%	-2.57888	-28.01	±	-21.71
15	0.00188	+	0.00109	0.00747	+	0.00010	0.00014	+	0.00003	-0.00004	+	0.00006	-0.00005	+	0.00003	1.3163E-17	895.81%	0.25098	2.70	±	10.96
16	-0.00903	+	0.00115	0.00018	+	0.00009	0.00002	+	0.00003	-0.00003	+	0.00003	-0.00001	+	0.00001	-6.32301E-17	83.49%	-50.9752	-655.17	±	-457.10

au20.4m.kfs., CM-6, CMT060 SCTF Analyses																								
%P	40Ar V			39Ar V			38Ar V			37Ar V			36Ar V			Moles 40Ar*	%Rad	R	Age (Ma)		
16	9.35327	±	0.01547	5.79268	±	0.01098	0.07770	±	0.00022	0.00022	±	0.00005	0.00295	±	0.00003	6.55E-14	90.68%	1.46413	15.71	±	0.05
16	7.46181	±	0.02580	4.52826	±	0.01413	0.06079	±	0.00023	0.00737	±	0.00009	0.00285	±	0.00002	5.23E-14	88.70%	1.46165	15.68	±	0.08
16	4.71541	±	0.01385	2.86245	±	0.00898	0.03862	±	0.00026	0.00028	±	0.00010	0.00181	±	0.00003	3.30E-14	88.64%	1.46025	15.67	±	0.08
16	7.28301	±	0.02115	4.28826	±	0.01306	0.05792	±	0.00018	0.00030	±	0.00008	0.00350	±	0.00003	5.10E-14	85.79%	1.45707	15.64	±	0.08
16	5.77179	±	0.01539	3.15750	±	0.00956	0.04284	±	0.00024	0.00024	±	0.00005	0.00417	±	0.00004	4.04E-14	78.67%	1.43809	15.43	±	0.09
16	6.46383	±	0.01466	3.58375	±	0.00926	0.04852	±	0.00019	0.00018	±	0.00013	0.00423	±	0.00003	4.53E-14	80.64%	1.45447	15.61	±	0.07
16	6.16530	±	0.01624	3.33702	±	0.00978	0.04530	±	0.00023	0.00030	±	0.00013	0.00450	±	0.00006	4.32E-14	78.42%	1.44892	15.55	±	0.10
16	3.69446	±	0.01211	1.84981	±	0.00757	0.02532	±	0.00017	0.00025	±	0.00006	0.00354	±	0.00005	2.59E-14	71.68%	1.43152	15.36	±	0.15
16	2.59792	±	0.00766	1.55772	±	0.00550	0.02112	±	0.00016	0.00004	±	0.00006	0.00107	±	0.00002	1.82E-14	87.83%	1.46487	15.56	±	0.09
16	4.98463	±	0.01911	2.14165	±	0.00835	0.02991	±	0.00020	0.00062	±	0.00004	0.00641	±	0.00004	3.49E-14	61.98%	1.44262	15.48	±	0.15
16	5.25116	±	0.00132	3.52793	±	0.00180	0.04734	±	0.00017	0.00024	±	0.00008	0.00027	±	0.00003	3.68E-14	98.48%	1.46587	15.73	±	0.03
16	9.53900	±	0.01569	6.15424	±	0.01017	0.08237	±	0.00025	0.00059	±	0.00008	0.00186	±	0.00002	6.68E-14	94.23%	1.46051	15.67	±	0.04

au20.4m.kfs, CM-6, CMT060 IH Analysis																								
%P	40Ar V			39Ar V			38Ar V			37Ar V			36Ar V			Moles 40Ar*	%Rad	R	Age (Ma)		
3.5	0.27276	±	0.00104	0.03715	±	0.00016	0.00061	±	0.00004	0.00013	±	0.00006	0.00075	±	0.00002	1.91E-15	19.15%	1.40607	15.09	±	1.44
4	0.36920	±	0.00107	0.23813	±	0.00069	0.00316	±	0.00005	0.00053	±	0.00008	0.00005	±	0.00002	2.59E-15	95.76%	1.48464	15.93	±	0.23
4.5	1.34029	±	0.00283	0.89783	±	0.00263	0.01190	±	0.00007	0.00012	±	0.00006	0.00007	±	0.00002	9.39E-15	98.36%	1.46839	15.76	±	0.09
4.8	1.78639	±	0.00429	1.19889	±	0.00349	0.01596	±	0.00009	0.00009	±	0.00009	0.00008	±	0.00002	1.25E-14	98.64%	1.46976	15.77	±	0.09
5	1.63762	±	0.00402	1.09755	±	0.00336	0.01501	±	0.00017	0.00017	±	0.00007	0.00009	±	0.00001	1.15E-14	98.41%	1.46838	15.76	±	0.07
5.3	0.68379	±	0.00152	0.45675	±	0.00139	0.00600	±	0.00007	0.00002	±	0.00014	0.00006	±	0.00002	4.79E-15	97.35%	1.45736	15.64	±	0.12
5.5	0.10377	±	0.00114	0.06977	±	0.00050	0.00088	±	0.00003	-0.00005	±	0.00012	0.00006	±	0.00002	7.27E-16	82.48%	1.22666	13.17	±	1.15
5.8	0.31475	±	0.00105	0.20498	±	0.00063	0.00263	±	0.00005	0.00006	±	0.00011	0.00005	±	0.00002	2.20E-15	94.98%	1.45850	15.65	±	0.26
6	0.29235	±	0.00102	0.19424	±	0.00069	0.00256	±	0.00003	0.00007	±	0.00006	-0.00001	±	0.00003	2.05E-15	101.49%	1.50512	16.15	±	0.45
7	0.37208	±	0.00106	0.24918	±	0.00053	0.00329	±	0.00005	0.00003	±	0.00006	0.00003	±	0.00001	2.61E-15	97.94%	1.46248	15.69	±	0.17
8	2.00129	±	0.00444	1.33412	±	0.00372	0.01787	±	0.00013	0.00006	±	0.00004	0.00019	±	0.00003	1.40E-14	97.13%	1.45700	15.63	±	0.09
9	0.87570	±	0.00239	0.58563	±	0.00192	0.00771	±	0.00008	0.00001	±	0.00007	-0.00002	±	0.00003	6.13E-15	100.81%	1.49531	16.04	±	0.18
10	0.46679	±	0.00102	0.31430	±	0.00096	0.00429	±	0.00006	-0.00005	±	0.00005	0.00003	±	0.00001	3.27E-15	98.05%	1.45623	15.63	±	0.16
11	0.29118	±	0.00104	0.19435	±	0.00067	0.00264	±	0.00004	-0.00010	±	0.00003	0.00003	±	0.00002	2.04E-15	97.16%	1.45562	15.62	±	0.28
13	0.19782	±	0.00129	0.13506	±	0.00037	0.00187	±	0.00003	0.00003	±	0.00009	0.00000	±	0.00002	1.39E-15	99.92%	1.46354	15.70	±	0.38
15	0.07964	±	0.00117	0.05291	±	0.00018	0.00069	±	0.00003	-0.00005	±	0.00007	0.00004	±	0.00002	5.58E-16	84.40%	1.27037	13.64	±	1.34
16	0.02212	±	0.00128	0.01480	±	0.00012	0.00019	±	0.00003	-0.00007	±	0.00005	0.00007	±	0.00002	1.55E-16	7.42%	0.11055	1.19	±	5.10

au20.4n.kfs, CM-10, CMT061 SCTF Analyses

%P	40Ar V			39Ar V			38Ar V			37Ar V			36Ar V			Moles 40Ar*	%Rad	R	Age (Ma)		
								-			-			-						-	
16	3.63104	±	0.00839	2.25444	±	0.00621	0.03031	±	0.00015	0.00018	±	0.00006	0.00136	±	0.00002	2.54E-14	88.93%	1.43232	15.37	±	0.07
16	5.63231	±	0.01471	3.52870	±	0.01015	0.04729	±	0.00021	0.00075	±	0.00004	0.00186	±	0.00003	3.94E-14	90.26%	1.44067	15.46	±	0.07
16	13.90894	±	0.03593	4.50904	±	0.01299	0.06476	±	0.00023	0.00137	±	0.00007	0.02599	±	0.00022	9.74E-14	44.78%	1.38142	14.83	±	0.21
16	9.77761	±	0.03031	5.46836	±	0.01703	0.07426	±	0.00023	0.00118	±	0.00009	0.00657	±	0.00004	6.85E-14	80.15%	1.43308	15.38	±	0.09
16	5.95610	±	0.01995	3.33800	±	0.01117	0.04501	±	0.00016	0.08955	±	0.00044	0.00414	±	0.00003	4.17E-14	79.57%	1.41978	15.24	±	0.10
16	6.63616	±	0.01546	3.93667	±	0.01002	0.05319	±	0.00021	0.00124	±	0.00012	0.00337	±	0.00003	4.65E-14	84.98%	1.43246	15.37	±	0.07
16	4.67362	±	0.01398	3.00655	±	0.00930	0.04017	±	0.00019	0.00028	±	0.00005	0.00120	±	0.00002	3.27E-14	92.39%	1.43619	15.41	±	0.07
16	6.85126	±	0.01823	3.05081	±	0.00910	0.04235	±	0.00016	0.00346	±	0.00008	0.00883	±	0.00009	4.80E-14	61.94%	1.39098	14.93	±	0.14
16	4.60668	±	0.01415	2.93004	±	0.00939	0.03937	±	0.00017	0.64249	±	0.00175	0.00170	±	0.00002	3.23E-14	90.11%	1.41698	15.21	±	0.08
16	7.84863	±	0.02240	4.12994	±	0.01241	0.05626	±	0.00016	0.00314	±	0.00016	0.00650	±	0.00004	5.50E-14	75.52%	1.43526	15.40	±	0.09
16	2.62579	±	0.00754	1.65137	±	0.00578	0.02225	±	0.00013	0.00717	±	0.00024	0.00087	±	0.00002	1.84E-14	90.21%	1.43434	15.39	±	0.09
																	-	-	-		
16	0.31075	±	0.00088	0.00588	±	0.00018	0.00013	±	0.00003	5.78009	±	0.02241	0.00277	±	0.00003	2.18E-15	26.85%	55.4550	725.96	±	-61.46
16	5.07854	±	0.01272	3.37367	±	0.00957	0.04517	±	0.00017	0.00084	±	0.00011	0.00075	±	0.00002	3.56E-14	95.62%	1.43940	15.45	±	0.06

au20.4n.kfs, CM-10, CMT061 IH Analysis																						
%P	40Ar V			39Ar V			38Ar V			37Ar V			36Ar V			Moles 40Ar*	%Rad	R	Age (Ma)		
3.5	0.05925	±	0.00174	0.04081	±	0.00027	0.00054	±	0.00003	0.00017	±	0.00004	0.00001	±	0.00001	4.15E-16	97.12%	1.41010	15.13	±	1.15
4	2.38375	±	0.00471	1.58267	±	0.00366	0.02100	±	0.00014	0.00232	±	0.00006	0.00041	±	0.00002	1.67E-14	94.94%	1.42988	15.35	±	0.06
4.5	1.78607	±	0.00422	1.17548	±	0.00356	0.01575	±	0.00011	0.00027	±	0.00007	0.00036	±	0.00001	1.25E-14	94.05%	1.42908	15.34	±	0.07
4.8	0.92151	±	0.00227	0.59463	±	0.00176	0.00783	±	0.00005	0.00008	±	0.00006	0.00021	±	0.00002	6.45E-15	93.20%	1.44433	15.50	±	0.11
5	0.50018	±	0.00161	0.31255	±	0.00113	0.00407	±	0.00009	0.00007	±	0.00007	0.00019	±	0.00002	3.50E-15	88.56%	1.41720	15.21	±	0.19
5.3	0.27749	±	0.00127	0.16472	±	0.00050	0.00219	±	0.00003	0.00007	±	0.00006	0.00017	±	0.00001	1.94E-15	81.48%	1.37262	14.73	±	0.29
5.5	0.30987	±	0.00125	0.16466	±	0.00054	0.00225	±	0.00003	0.00007	±	0.00005	0.00025	±	0.00001	2.17E-15	76.02%	1.43057	15.35	±	0.29
5.8	0.31722	±	0.00123	0.20050	±	0.00038	0.00271	±	0.00005	0.00008	±	0.00004	0.00010	±	0.00001	2.22E-15	90.76%	1.43602	15.41	±	0.21
6	1.00359	±	0.00227	0.62785	±	0.00152	0.00849	±	0.00006	0.00016	±	0.00005	0.00037	±	0.00002	7.03E-15	89.14%	1.42479	15.29	±	0.10
7	1.40519	±	0.00314	0.91659	±	0.00284	0.01228	±	0.00009	0.00018	±	0.00006	0.00031	±	0.00001	9.84E-15	93.38%	1.43165	15.36	±	0.08
8	2.32164	±	0.00505	1.49384	±	0.00408	0.02040	±	0.00027	0.00008	±	0.00007	0.00056	±	0.00002	1.63E-14	92.86%	1.44311	15.49	±	0.07
9	0.11455	±	0.00134	0.07544	±	0.00030	0.00099	±	0.00004	0.00002	±	0.00006	0.00003	±	0.00002	8.02E-16	91.12%	1.38354	14.85	±	0.77
10	0.05902	±	0.00147	0.03820	±	0.00023	0.00046	±	0.00004	-0.00002	±	0.00005	0.00002	±	0.00002	4.13E-16	90.01%	1.39077	14.93	±	1.55
11	0.00463	±	0.00151	0.00372	±	0.00023	-0.00001	±	0.00003	-0.00006	±	0.00005	0.00000	±	0.00001	3.24E-17	70.39%	0.87451	9.40	±	13.21
13	0.00687	±	0.00148	0.00512	±	0.00023	0.00004	±	0.00004	-0.00016	±	0.00008	-0.00003	±	0.00002	4.81E-17	220.67%	1.33951	14.38	±	10.83
16	0.00093	±	0.00138	0.00048	±	0.00019	-0.00001	±	0.00003	0.00007	±	0.00005	-0.00002	±	0.00001	6.48E-18	815.90%	1.92604	20.64	±	113.41
15	0.01672	±	0.00132	0.01073	±	0.00019	0.00011	±	0.00002	0.00004	±	0.00005	0.00001	±	0.00001	1.17E-16	90.06%	1.40352	15.06	±	4.47

au20.4o.kfs, CMT022, CMT062 SCTF Analyses																							
%P	40Ar V			39Ar V			38Ar V			37Ar V			36Ar V			Moles 40Ar*	%Rad	R	Age (Ma)		
16	3.42048	±	0.00767	2.01570	±	0.00543	0.02723	±	0.00018	0.00036	±	0.00012	0.00183	±	0.00003	2.40E-14	84.22%	1.42908	15.34	±	0.08
16	1.77779	±	0.00503	1.08928	±	0.00386	0.01454	±	0.00007	0.00010	±	0.00007	0.00067	±	0.00002	1.25E-14	88.85%	1.45009	15.56	±	0.10
16	3.79073	±	0.01027	2.42433	±	0.00694	0.03248	±	0.00018	0.00040	±	0.00010	0.00102	±	0.00002	2.65E-14	92.03%	1.43908	15.44	±	0.07
16	2.62594	±	0.00715	1.46710	±	0.00439	0.01983	±	0.00012	0.00072	±	0.00007	0.00175	±	0.00002	1.84E-14	80.26%	1.43655	15.42	±	0.09
16	2.01502	±	0.00537	1.00579	±	0.00294	0.01384	±	0.00013	0.10707	±	0.00104	0.00195	±	0.00002	1.41E-14	71.77%	1.43801	15.43	±	0.11
16	1.81024	±	0.00435	0.82284	±	0.00236	0.01133	±	0.00009	0.00268	±	0.00020	0.00217	±	0.00003	1.27E-14	64.57%	1.42060	15.25	±	0.13
16	1.51939	±	0.00374	0.76649	±	0.00219	0.01031	±	0.00008	-0.00012	±	0.00018	0.00139	±	0.00002	1.06E-14	72.93%	1.44570	15.51	±	0.13
16	0.98054	±	0.00253	0.58063	±	0.00154	0.00786	±	0.00007	0.00006	±	0.00004	0.00040	±	0.00003	6.87E-15	87.95%	1.48530	15.94	±	0.18
16	4.54505	±	0.01098	2.08183	±	0.00502	0.02887	±	0.00013	0.01292	±	0.00017	0.00559	±	0.00007	3.18E-14	63.69%	1.39040	14.92	±	0.13
16	3.05492	±	0.00921	1.21332	±	0.00402	0.01696	±	0.00009	0.01043	±	0.00033	0.00448	±	0.00003	2.14E-14	56.65%	1.42639	15.31	±	0.15
16	6.91849	±	0.02739	4.12758	±	0.01626	0.05577	±	0.00025	0.07221	±	0.00050	0.00329	±	0.00003	4.85E-14	86.02%	1.44180	15.47	±	0.10
16	5.55095	±	0.00862	3.56107	±	0.00614	0.04793	±	0.00020	0.00201	±	0.00007	0.00144	±	0.00002	3.89E-14	92.34%	1.43944	15.45	±	0.04

au20.4o.kfs, CMT022, CMT062 IH Analysis																							
%P	40Ar V			39Ar V			38Ar V			37Ar V			36Ar V			Moles 40Ar*	%Rad	R	Age (Ma)		
3.5	0.00527	±	0.00128	0.00327	±	0.00013	0.00009	±	0.00003	0.00007	±	0.00005	-0.00001	±	0.00001	3.69E-17	167.58%	1.61280	17.30	±	15.14
4	0.29573	±	0.00100	0.20118	±	0.00049	0.00269	±	0.00004	0.00006	±	0.00005	0.00005	±	0.00003	2.07E-15	95.10%	1.39790	15.00	±	0.40
4.5	0.96510	±	0.00194	0.63906	±	0.00198	0.00858	±	0.00005	0.00003	±	0.00007	0.00016	±	0.00002	6.76E-15	95.13%	1.43669	15.42	±	0.11
4.8	1.88006	±	0.00425	1.22232	±	0.00361	0.01648	±	0.00011	0.00020	±	0.00005	0.00042	±	0.00002	1.32E-14	93.44%	1.43726	15.42	±	0.08
5	0.44513	±	0.00105	0.29825	±	0.00064	0.00405	±	0.00005	0.00006	±	0.00009	0.00005	±	0.00001	3.12E-15	96.90%	1.44625	15.52	±	0.17
5.3	0.92287	±	0.00186	0.57807	±	0.00138	0.00781	±	0.00010	-0.00005	±	0.00003	0.00033	±	0.00001	6.46E-15	89.55%	1.42969	15.34	±	0.09
5.5	0.77493	±	0.00182	0.51684	±	0.00165	0.00694	±	0.00008	0.00004	±	0.00007	0.00011	±	0.00001	5.43E-15	95.82%	1.43669	15.42	±	0.10
5.8	1.34471	±	0.00262	0.90340	±	0.00229	0.01209	±	0.00010	0.00012	±	0.00006	0.00008	±	0.00002	9.42E-15	98.25%	1.46249	15.69	±	0.10
6	0.38956	±	0.00095	0.26210	±	0.00084	0.00361	±	0.00006	0.00003	±	0.00008	0.00006	±	0.00001	2.73E-15	95.40%	1.41794	15.22	±	0.17
7	0.62048	±	0.00118	0.42522	±	0.00098	0.00563	±	0.00006	0.00016	±	0.00007	0.00005	±	0.00001	4.35E-15	97.64%	1.42475	15.29	±	0.11
8	0.27067	±	0.00095	0.18345	±	0.00043	0.00255	±	0.00006	0.00000	±	0.00008	0.00007	±	0.00002	1.90E-15	92.32%	1.36213	14.62	±	0.42
9	0.07461	±	0.00122	0.05087	±	0.00021	0.00074	±	0.00004	-0.00006	±	0.00008	0.00002	±	0.00001	5.23E-16	93.42%	1.37013	14.71	±	0.91
10	0.01823	±	0.00128	0.01231	±	0.00012	0.00014	±	0.00003	-0.00004	±	0.00006	0.00002	±	0.00002	1.28E-16	62.82%	0.92955	9.99	±	4.33
11	0.01398	±	0.00127	0.00671	±	0.00014	0.00014	±	0.00003	0.00000	±	0.00004	0.00003	±	0.00002	9.79E-17	32.02%	0.66751	7.18	±	8.24
13	0.00456	±	0.00129	0.00153	±	0.00015	0.00005	±	0.00003	-0.00008	±	0.00005	0.00002	±	0.00001	3.19E-17	-61.52%	-1.83276	-19.86	±	-31.78
15	0.00139	±	0.00126	0.00031	±	0.00013	0.00003	±	0.00004	-0.00007	±	0.00006	0.00006	±	0.00002	9.73E-18	-11.7	-52.1669	-673.73	±	-423.74
16	0.00028	±	0.00125	0.00009	±	0.00014	-0.00003	±	0.00003	-0.00012	±	0.00007	-0.00002	±	0.00001	1.96E-18	1888.2%	3.00900	32.14	±	1075.21

au20.4p.kfs, TD-7-10, CMT063 SCTF Analyses																								
%P	40Ar V			39Ar V			38Ar V			37Ar V			36Ar V			Moles 40Ar*	%Rad	R	Age (Ma)		
16	5.16842	±	0.01192	3.21944	±	0.00938	0.04329	±	0.00021	0.00017	±	0.00017	0.00176	±	0.00002	3.62E-14	89.96%	1.44427	15.50	±	0.07
16	9.62323	±	0.03233	5.68397	±	0.01874	0.07654	±	0.00036	0.00013	±	0.00016	0.00492	±	0.00004	6.74E-14	84.90%	1.43737	15.43	±	0.09
16	6.31984	±	0.01876	3.85521	±	0.01257	0.05177	±	0.00026	0.00023	±	0.00016	0.00246	±	0.00003	4.43E-14	88.52%	1.45111	15.57	±	0.08
16	6.30471	±	0.01936	4.22254	±	0.01411	0.05622	±	0.00015	0.00085	±	0.00011	0.00065	±	0.00002	4.42E-14	96.97%	1.44788	15.54	±	0.07
16	3.84882	±	0.01059	2.49090	±	0.00843	0.03366	±	0.00032	0.00007	±	0.00010	0.00079	±	0.00002	2.70E-14	93.92%	1.45115	15.57	±	0.08
16	3.67515	±	0.00865	2.13416	±	0.00527	0.02916	±	0.00035	0.00047	±	0.00015	0.00205	±	0.00002	2.57E-14	83.56%	1.43888	15.44	±	0.07
16	3.23296	±	0.00812	1.81661	±	0.00536	0.02448	±	0.00008	0.00002	±	0.00021	0.00210	±	0.00002	2.26E-14	80.79%	1.43780	15.43	±	0.08
16	3.49906	±	0.00983	1.77287	±	0.00563	0.02466	±	0.00019	0.00027	±	0.00012	0.00321	±	0.00002	2.45E-14	72.85%	1.43781	15.43	±	0.10
16	3.74917	±	0.00879	2.23442	±	0.00601	0.03052	±	0.00021	0.00014	±	0.00012	0.00175	±	0.00002	2.63E-14	86.24%	1.44697	15.53	±	0.07
16	5.26026	±	0.01137	3.51479	±	0.00811	0.04689	±	0.00016	-0.00006	±	0.00009	0.00056	±	0.00002	3.68E-14	96.85%	1.44943	15.55	±	0.05
0	4.63181	±	0.00679	2.82435	±	0.00461	0.03794	±	0.00023	0.00009	±	0.00011	0.00205	±	0.00002	3.24E-14	86.93%	1.42564	15.30	±	0.05

au20.4p.kfs, TD-7-10, CMT063 IH Analysis																								
%P	40Ar V			39Ar V			38Ar V			37Ar V			36Ar V			Moles 40Ar*	%Rad	R	Age (Ma)		
3.5	0.12366	±	0.00104	0.07277	±	0.00026	0.00095	±	0.00003	-0.00018	±	0.00004	0.00004	±	0.00002	8.66E-16	91.56%	1.55564	16.69	±	0.76
4	2.95611	±	0.00487	1.98425	±	0.00347	0.02650	±	0.00013	0.00017	±	0.00007	0.00036	±	0.00002	2.07E-14	96.44%	1.43670	15.42	±	0.05
4.5	0.54298	±	0.00130	0.35771	±	0.00120	0.00473	±	0.00005	-0.00004	±	0.00007	0.00007	±	0.00002	3.80E-15	96.15%	1.45951	15.66	±	0.15
4.8	0.25658	±	0.00093	0.15404	±	0.00047	0.00201	±	0.00005	-0.00005	±	0.00006	0.00011	±	0.00002	1.80E-15	87.00%	1.44921	15.55	±	0.40
5	0.22007	±	0.00103	0.11944	±	0.00033	0.00158	±	0.00004	0.00006	±	0.00006	0.00016	±	0.00002	1.54E-15	79.12%	1.45786	15.64	±	0.43
5.3	0.18908	±	0.00102	0.12095	±	0.00027	0.00167	±	0.00004	0.00000	±	0.00005	0.00007	±	0.00003	1.32E-15	88.42%	1.38224	14.84	±	0.67
5.5	0.24349	±	0.00121	0.15731	±	0.00031	0.00205	±	0.00005	0.00003	±	0.00005	0.00008	±	0.00002	1.71E-15	90.45%	1.39992	15.02	±	0.48
5.8	0.46712	±	0.00113	0.31074	±	0.00066	0.00403	±	0.00006	-0.00006	±	0.00004	0.00001	±	0.00003	3.27E-15	99.24%	1.49177	16.01	±	0.31
6	0.61220	±	0.00158	0.40906	±	0.00113	0.00551	±	0.00005	0.00001	±	0.00006	0.00006	±	0.00003	4.29E-15	96.93%	1.45068	15.57	±	0.22
7	0.87692	±	0.00177	0.57899	±	0.00159	0.00770	±	0.00005	-0.00009	±	0.00008	0.00015	±	0.00002	6.14E-15	94.83%	1.43625	15.41	±	0.14
8	1.26773	±	0.00227	0.84496	±	0.00193	0.01117	±	0.00010	0.00015	±	0.00005	0.00022	±	0.00002	8.88E-15	94.94%	1.42443	15.29	±	0.10
9	0.36260	±	0.00098	0.24231	±	0.00060	0.00318	±	0.00006	0.00002	±	0.00006	0.00010	±	0.00002	2.54E-15	91.71%	1.37227	14.73	±	0.32
10	0.27389	±	0.00104	0.18443	±	0.00061	0.00237	±	0.00006	0.00015	±	0.00008	0.00008	±	0.00002	1.92E-15	91.35%	1.35667	14.56	±	0.41
11	0.07102	±	0.00120	0.04798	±	0.00024	0.00059	±	0.00006	0.00002	±	0.00005	0.00006	±	0.00002	4.97E-16	76.26%	1.12866	12.12	±	1.61
13	0.07837	±	0.00109	0.05320	±	0.00026	0.00064	±	0.00006	-0.00003	±	0.00008	0.00003	±	0.00003	5.49E-16	86.83%	1.27889	13.73	±	1.87
15	0.07708	±	0.00113	0.05002	±	0.00021	0.00069	±	0.00003	-0.00010	±	0.00005	0.00000	±	0.00001	5.40E-16	100.27%	1.54067	16.53	±	0.89
16	0.01062	±	0.00128	0.00705	±	0.00010	0.00011	±	0.00003	0.00002	±	0.00009	0.00000	±	0.00001	7.44E-17	97.43%	1.46685	15.74	±	5.94

au20.4q.kfs, WE-1-10, CMT064 SCTF Analyses																								
%P	40Ar V			39Ar V			38Ar V			37Ar V			36Ar V			Moles 40Ar*	%Rad	R	Age (Ma)		
16	2.49777	±	0.00590	1.32048	±	0.00383	0.01794	±	0.00011	0.00040	±	0.00015	0.00198	±	0.00003	1.75E-14	76.59%	1.44880	15.55	±	0.11
16	3.96420	±	0.01024	1.80552	±	0.00528	0.02507	±	0.00019	0.00043	±	0.00013	0.00472	±	0.00007	2.78E-14	64.85%	1.42391	15.28	±	0.15
16	2.78988	±	0.00693	1.37413	±	0.00420	0.01897	±	0.00016	-0.00020	±	0.00015	0.00275	±	0.00003	1.95E-14	70.87%	1.43876	15.44	±	0.11
16	2.50867	±	0.00625	1.29805	±	0.00401	0.01773	±	0.00013	0.00007	±	0.00018	0.00217	±	0.00003	1.76E-14	74.38%	1.43752	15.43	±	0.11
16	2.23666	±	0.00585	1.33797	±	0.00418	0.01801	±	0.00016	0.00009	±	0.00007	0.00100	±	0.00003	1.57E-14	86.82%	1.45140	15.58	±	0.10
16	1.75361	±	0.00464	0.89338	±	0.00275	0.01233	±	0.00008	0.00014	±	0.00006	0.00155	±	0.00002	1.23E-14	73.96%	1.45169	15.58	±	0.12
16	0.56761	±	0.00135	0.31608	±	0.00105	0.00430	±	0.00005	0.00086	±	0.00004	0.00040	±	0.00002	3.98E-15	78.93%	1.41745	15.21	±	0.18
16	1.47545	±	0.00342	0.68267	±	0.00201	0.00935	±	0.00011	0.00021	±	0.00007	0.00170	±	0.00002	1.03E-14	65.88%	1.42377	15.28	±	0.14
16	1.08082	±	0.00264	0.63169	±	0.00193	0.00842	±	0.00009	0.00041	±	0.00006	0.00059	±	0.00002	7.57E-15	83.91%	1.43564	15.41	±	0.12
16	4.10711	±	0.01021	2.38352	±	0.00605	0.03230	±	0.00013	0.00024	±	0.00006	0.00212	±	0.00003	2.88E-14	84.72%	1.45988	15.67	±	0.07
0	4.63114	±	0.00681	2.82412	±	0.00461	0.03794	±	0.00011	0.00023	±	0.00006	0.00204	±	0.00002	3.24E-14	86.97%	1.42617	15.31	±	0.05
16	3.00635	±	0.00484	2.02496	±	0.00442	0.02697	±	0.00016	-0.00009	±	0.00007	0.00006	±	0.00003	2.11E-14	99.41%	1.47582	15.84	±	0.06
16	3.15515	±	0.02132	1.83861	±	0.01248	0.02473	±	0.00013	-0.00004	±	0.00008	0.00165	±	0.00004	2.21E-14	84.51%	1.45023	15.56	±	0.19
16	2.12385	±	0.00642	1.29931	±	0.00438	0.01779	±	0.00018	0.00002	±	0.00011	0.00080	±	0.00002	1.49E-14	88.84%	1.45213	15.58	±	0.09

au20.4q.kfs, WE-1-10, CMT064 IH Analysis																								
%P	40Ar V			39Ar V			38Ar V			37Ar V			36Ar V			Moles 40Ar*	%Rad	R	Age (Ma)		
3.5	0.02375	±	0.00115	0.00722	±	0.00010	0.00012	±	0.00004	0.00012	±	0.00005	0.00004	±	0.00001	1.66E-16	47.42%	1.55938	16.73	±	5.50
4	0.22778	±	0.00095	0.15302	±	0.00046	0.00205	±	0.00003	0.00011	±	0.00006	-0.00005	±	0.00003	1.60E-15	106.99%	1.48862	15.97	±	0.53
4.5	0.92528	±	0.00186	0.60690	±	0.00146	0.00820	±	0.00004	0.00004	±	0.00009	0.00013	±	0.00001	6.48E-15	95.86%	1.46141	15.68	±	0.08
4.8	0.18734	±	0.00095	0.12103	±	0.00037	0.00164	±	0.00005	-0.00031	±	0.00013	0.00002	±	0.00001	1.31E-15	96.27%	1.49005	15.99	±	0.39
5	0.06433	±	0.00113	0.04088	±	0.00010	0.00059	±	0.00002	0.00001	±	0.00006	0.00000	±	0.00001	4.51E-16	99.22%	1.56125	16.75	±	1.13
5.3	0.04517	±	0.00113	0.02887	±	0.00015	0.00039	±	0.00003	0.00006	±	0.00007	0.00002	±	0.00001	3.16E-16	87.52%	1.36955	14.70	±	1.34
5.5	0.06805	±	0.00115	0.04049	±	0.00018	0.00056	±	0.00003	-0.00009	±	0.00005	0.00002	±	0.00001	4.77E-16	92.68%	1.55738	16.71	±	1.02
5.8	0.15043	±	0.00106	0.08758	±	0.00023	0.00124	±	0.00004	-0.00013	±	0.00007	0.00006	±	0.00001	1.05E-15	88.50%	1.51985	16.31	±	0.46
6	0.49556	±	0.00096	0.32109	±	0.00087	0.00433	±	0.00006	0.00008	±	0.00008	0.00011	±	0.00001	3.47E-15	93.46%	1.44247	15.48	±	0.13
7	0.54966	±	0.00159	0.36401	±	0.00101	0.00480	±	0.00011	-0.00013	±	0.00006	0.00006	±	0.00002	3.85E-15	96.98%	1.46435	15.71	±	0.19
8	0.39743	±	0.00107	0.26295	±	0.00072	0.00350	±	0.00005	0.00004	±	0.00011	0.00001	±	0.00002	2.78E-15	99.25%	1.50018	16.10	±	0.21
9	0.08814	±	0.00103	0.05896	±	0.00020	0.00082	±	0.00003	0.00002	±	0.00006	-0.00001	±	0.00002	6.17E-16	103.31%	1.49493	16.04	±	0.87
10	0.01846	±	0.00122	0.01221	±	0.00012	0.00016	±	0.00004	0.00007	±	0.00006	-0.00002	±	0.00002	1.29E-16	134.25%	1.51179	16.22	±	4.12
11	0.00235	±	0.00118	0.00167	±	0.00011	0.00003	±	0.00002	0.00008	±	0.00006	-0.00002	±	0.00002	1.65E-17	367.52%	1.40664	15.10	±	34.19
13	0.00157	±	0.00119	0.00082	±	0.00012	-0.00002	±	0.00003	0.00011	±	0.00006	-0.00001	±	0.00002	1.10E-17	307.93%	1.91260	20.50	±	64.00
15	0.00535	±	0.00115	0.00345	±	0.00009	0.00007	±	0.00003	-0.00006	±	0.00007	-0.00002	±	0.00002	3.75E-17	200.12%	1.54797	16.61	±	14.77
16	0.00033	±	0.00115	0.00017	±	0.00010	0.00002	±	0.00002	-0.00006	±	0.00005	-0.00001	±	0.00002	2.28E-18	640.46%	1.84661	19.79	±	295.27

au20.4r.kfs, WE-2-10, CMT065 SCTF Analyses																								
%P	40Ar V			39Ar V			38Ar V			37Ar V			36Ar V			Moles 40Ar*	%Rad	R	Age (Ma)		
16	4.98125	±	0.01092	2.69715	±	0.00770	0.03660	±	0.00014	0.00036	±	0.00005	0.00362	±	0.00003	3.49E-14	78.52%	1.45011	15.56	±	0.08
16	5.37674	±	0.01460	3.27512	±	0.00943	0.04386	±	0.00017	0.00049	±	0.00006	0.00208	±	0.00002	3.77E-14	88.58%	1.45425	15.61	±	0.07
16	3.39106	±	0.00906	2.22299	±	0.00671	0.03025	±	0.00021	0.00032	±	0.00006	0.00056	±	0.00002	2.37E-14	95.11%	1.45080	15.57	±	0.07
16	4.12638	±	0.01175	2.78297	±	0.00851	0.03751	±	0.00025	0.00024	±	0.00008	0.00011	±	0.00003	2.89E-14	99.23%	1.47135	15.79	±	0.07
16	4.85151	±	0.01343	3.11228	±	0.00934	0.04173	±	0.00021	0.00023	±	0.00015	0.00113	±	0.00002	3.40E-14	93.09%	1.45113	15.57	±	0.07
16	3.97289	±	0.00875	2.52499	±	0.00569	0.03385	±	0.00014	0.00029	±	0.00008	0.00098	±	0.00002	2.78E-14	92.74%	1.45916	15.66	±	0.06
16	8.88267	±	0.02667	3.66737	±	0.01225	0.05133	±	0.00021	0.00035	±	0.00016	0.01200	±	0.00004	6.22E-14	60.09%	1.45543	15.62	±	0.13
16	6.14645	±	0.01900	3.92766	±	0.01290	0.05256	±	0.00019	0.00064	±	0.00010	0.00148	±	0.00002	4.30E-14	92.90%	1.45373	15.60	±	0.08
16	2.92943	±	0.00847	1.93613	±	0.00666	0.02584	±	0.00021	0.00024	±	0.00015	0.00034	±	0.00002	2.05E-14	96.60%	1.46164	15.68	±	0.08
16	5.22213	±	0.01350	2.86917	±	0.00829	0.03868	±	0.00021	0.00020	±	0.00021	0.00364	±	0.00005	3.66E-14	79.42%	1.44550	15.51	±	0.09
16	13.35236	±	0.03317	8.57873	±	0.02151	0.11524	±	0.00043	0.00105	±	0.00008	0.00278	±	0.00003	9.35E-14	93.84%	1.46063	15.67	±	0.06
16	6.32263	±	0.01856	4.15739	±	0.01374	0.05565	±	0.00023	0.00022	±	0.00011	0.00091	±	0.00002	4.43E-14	95.73%	1.45585	15.62	±	0.07

au20.4r.kfs, WE-2-10, CMT065 IH Analysis																								
%P	40Ar V			39Ar V			38Ar V			37Ar V			36Ar V			Moles 40Ar*	%Rad	R	Age (Ma)		
3.5	0.02839	±	0.00112	0.01820	±	0.00009	0.00021	±	0.00003	0.00005	±	0.00005	0.00002	±	0.00002	1.99E-16	78.35%	1.22257	13.13	±	2.81
4	0.10440	±	0.00105	0.06879	±	0.00023	0.00093	±	0.00004	0.00005	±	0.00006	0.00001	±	0.00001	7.31E-16	96.91%	1.47087	15.78	±	0.67
4.5	0.36319	±	0.00088	0.24534	±	0.00081	0.00337	±	0.00005	-0.00002	±	0.00004	0.00003	±	0.00001	2.54E-15	97.45%	1.44258	15.48	±	0.19
4.8	0.92407	±	0.00188	0.62328	±	0.00171	0.00836	±	0.00008	0.00011	±	0.00005	0.00007	±	0.00001	6.47E-15	97.68%	1.44820	15.54	±	0.09
5	2.09913	±	0.00426	1.20117	±	0.00288	0.01624	±	0.00007	0.00015	±	0.00005	0.00117	±	0.00002	1.47E-14	83.48%	1.45889	15.66	±	0.07
5.3	1.00548	±	0.00260	0.65619	±	0.00190	0.00880	±	0.00008	0.00003	±	0.00010	0.00021	±	0.00002	7.04E-15	93.80%	1.43735	15.43	±	0.10
5.5	0.65880	±	0.00164	0.40046	±	0.00146	0.00535	±	0.00005	0.00007	±	0.00006	0.00028	±	0.00002	4.61E-15	87.59%	1.44094	15.46	±	0.16
5.8	0.76514	±	0.00195	0.49410	±	0.00158	0.00666	±	0.00007	0.00005	±	0.00007	0.00018	±	0.00002	5.36E-15	93.08%	1.44142	15.47	±	0.12
6	1.33007	±	0.00417	0.89892	±	0.00262	0.01196	±	0.00008	0.00011	±	0.00006	0.00009	±	0.00002	9.31E-15	98.01%	1.45023	15.56	±	0.09
7	1.25933	±	0.00321	0.85460	±	0.00275	0.01143	±	0.00008	0.00012	±	0.00004	0.00003	±	0.00002	8.82E-15	99.20%	1.46174	15.69	±	0.09
8	1.38195	±	0.00269	0.93872	±	0.00241	0.01252	±	0.00008	0.00006	±	0.00006	0.00001	±	0.00002	9.68E-15	99.73%	1.46818	15.75	±	0.09
9	0.83073	±	0.00228	0.55703	±	0.00158	0.00737	±	0.00007	0.00002	±	0.00006	0.00008	±	0.00002	5.82E-15	97.08%	1.44784	15.54	±	0.11
10	1.07027	±	0.00347	0.71516	±	0.00238	0.00942	±	0.00007	0.00013	±	0.00008	0.00010	±	0.00002	7.50E-15	97.16%	1.45401	15.60	±	0.11
11	0.34311	±	0.00102	0.23134	±	0.00072	0.00304	±	0.00005	0.00023	±	0.00007	0.00003	±	0.00001	2.40E-15	97.83%	1.45099	15.57	±	0.21
13	0.17381	±	0.00103	0.11859	±	0.00036	0.00155	±	0.00004	0.00010	±	0.00008	0.00003	±	0.00002	1.22E-15	95.11%	1.39399	14.96	±	0.42
15	0.23727	±	0.00093	0.15792	±	0.00042	0.00212	±	0.00005	-0.00001	±	0.00005	0.00001	±	0.00001	1.66E-15	98.44%	1.47904	15.87	±	0.26
16	0.04041	±	0.00115	0.02733	±	0.00016	0.00038	±	0.00003	-0.00006	±	0.00006	0.00001	±	0.00001	2.83E-16	92.36%	1.36553	14.66	±	1.58

au20.4s.kfs, WE-3-10, CMT066 SCTF Analyses																								
%P	40Ar V			39Ar V			38Ar V			37Ar V			36Ar V			Moles 40Ar*	%Rad	R	Age (Ma)		
16	4.19959	±	0.00993	1.75891	±	0.00494	0.02456	±	0.00012	0.00023	±	0.00006	0.00560	±	0.00003	2.94E-14	60.58%	1.44633	15.52	±	0.11
16	4.33525	±	0.01223	1.60927	±	0.00509	0.02281	±	0.00012	0.00044	±	0.00005	0.00708	±	0.00007	3.04E-14	51.73%	1.39350	14.96	±	0.19
16	4.51439	±	0.01317	1.66705	±	0.00544	0.02362	±	0.00015	0.00029	±	0.00006	0.00713	±	0.00004	3.16E-14	53.34%	1.44443	15.50	±	0.15
16	0.82412	±	0.00233	0.00916	±	0.00027	0.00069	±	0.00004	0.00117	±	0.00008	0.00281	±	0.00003	5.77E-15	-0.64%	-0.57666	-6.23	±	-41.00
16	2.87726	±	0.00768	1.73011	±	0.00468	0.02307	±	0.00014	0.00030	±	0.00005	0.00113	±	0.00002	2.02E-14	88.40%	1.47011	15.77	±	0.08
16	2.00427	±	0.00519	1.03238	±	0.00263	0.01398	±	0.00006	-0.00003	±	0.00004	0.00165	±	0.00002	1.40E-14	75.61%	1.46790	15.75	±	0.11
16	3.71587	±	0.01205	2.13258	±	0.00725	0.02886	±	0.00013	0.00022	±	0.00006	0.00207	±	0.00003	2.60E-14	83.55%	1.45574	15.62	±	0.10
16	1.96845	±	0.00620	1.23170	±	0.00433	0.01695	±	0.00022	0.00000	±	0.00006	0.00066	±	0.00004	1.38E-14	90.16%	1.44094	15.46	±	0.12
16	1.32387	±	0.00281	0.87936	±	0.00245	0.01175	±	0.00016	-0.00011	±	0.00005	0.00010	±	0.00002	9.27E-15	97.86%	1.47326	15.81	±	0.08
16	2.54748	±	0.01158	1.56862	±	0.00733	0.02108	±	0.00012	0.00032	±	0.00007	0.00088	±	0.00002	1.78E-14	89.81%	1.45851	15.65	±	0.12

au20.4s.kfs, WE-3-10, CMT066 IH Analysis

%P	40Ar V			39Ar V			38Ar V			37Ar V			36Ar V			Moles 40Ar*	%Rad	R	Age (Ma)		
3.5	0.00520	±	0.00117	0.00348	±	0.00011	0.00005	±	0.00003	0.00005	±	0.00007	0.00004	±	0.00002	3.64E-17	-99.08%	-1.47760	-16.00	±	-14.65
4	0.18922	±	0.00087	0.12755	±	0.00018	0.00172	±	0.00005	-0.00005	±	0.00009	0.00002	±	0.00001	1.33E-15	96.72%	1.43475	15.40	±	0.32
4.5	1.44708	±	0.00284	0.96790	±	0.00298	0.01297	±	0.00006	0.00012	±	0.00005	0.00015	±	0.00001	1.01E-14	96.91%	1.44893	15.55	±	0.07
4.8	1.17734	±	0.00219	0.77684	±	0.00230	0.01036	±	0.00009	0.00019	±	0.00003	0.00019	±	0.00001	8.25E-15	95.20%	1.44288	15.48	±	0.08
5	0.34820	±	0.00094	0.23123	±	0.00068	0.00306	±	0.00007	0.00009	±	0.00007	0.00007	±	0.00001	2.44E-15	94.29%	1.41989	15.24	±	0.21
5.5	1.98212	±	0.00399	1.27326	±	0.00361	0.01708	±	0.00009	0.00014	±	0.00006	0.00038	±	0.00002	1.39E-14	94.36%	1.46891	15.76	±	0.07
6	0.40980	±	0.00108	0.27621	±	0.00086	0.00365	±	0.00007	0.00020	±	0.00005	0.00002	±	0.00002	2.87E-15	98.79%	1.46574	15.73	±	0.20
7	0.10340	±	0.00099	0.06890	±	0.00017	0.00083	±	0.00005	0.00011	±	0.00013	0.00005	±	0.00002	7.24E-16	85.97%	1.29013	13.85	±	0.73
8	0.00565	±	0.00118	0.00378	±	0.00009	0.00007	±	0.00003	0.00008	±	0.00007	0.00002	±	0.00002	3.96E-17	3.95%	0.05899	0.64	±	15.03
9	0.00005	±	0.00119	0.00030	±	0.00011	0.00004	±	0.00003	0.00021	±	0.00008	0.00005	±	0.00002	3.61E-19	-29376%	-49.7045	-635.59	±	-366.36
11	0.00580	±	0.00115	0.00383	±	0.00012	0.00001	±	0.00002	0.00019	±	0.00013	0.00004	±	0.00002	4.06E-17	-85.41%	-1.29332	-13.99	±	-17.55
13	0.00143	±	0.00111	0.00081	±	0.00011	-0.00001	±	0.00002	0.00010	±	0.00012	0.00003	±	0.00002	1.00E-17	483.33%	-8.51964	-94.24	±	-93.06
16	0.00088	±	0.00114	0.00055	±	0.00012	0.00000	±	0.00002	0.00019	±	0.00006	-0.00002	±	0.00001	6.19E-18	663.74%	-1.61901	-17.37	±	88.22

au20.4s.kfs, WE-3-10, CMT066 IH Analysis																					
%P	**40Ar V**			**39Ar V**			**38Ar V**			**37Ar V**			**36Ar V**			**Moles 40Ar***	**%Rad**	**R**	**Age (Ma)**		
3.5	0.00529	±	0.00111	0.00326	±	0.00010	0.00002	±	0.00002	0.00000	±	0.00008	0.00007	±	0.00003	3.70E-17	-304.14%	-4.93036	-53.94	±	-31.95
4	0.12697	±	0.00093	0.08599	±	0.00024	0.00116	±	0.00003	0.00006	±	0.00006	0.00000	±	0.00002	8.89E-16	100.60%	1.47657	15.84	±	0.61
4.5	0.19393	±	0.00092	0.13027	±	0.00031	0.00176	±	0.00003	0.00000	±	0.00007	-0.00005	±	0.00002	1.36E-15	107.54%	1.48862	15.97	±	0.50
4.8	0.58691	±	0.00121	0.36718	±	0.00108	0.00491	±	0.00006	-0.00007	±	0.00007	0.00015	±	0.00002	4.11E-15	92.64%	1.48069	15.89	±	0.15
5	0.20209	±	0.00087	0.11274	±	0.00036	0.00151	±	0.00005	-0.00009	±	0.00005	0.00009	±	0.00002	1.42E-15	86.95%	1.55860	16.72	±	0.54
5.3	0.03279	±	0.00108	0.01845	±	0.00010	0.00029	±	0.00003	-0.00013	±	0.00004	0.00000	±	0.00002	2.30E-16	100.05%	1.77700	19.05	±	2.71
5.5	0.02533	±	0.00105	0.01418	±	0.00008	0.00016	±	0.00002	-0.00013	±	0.00004	-0.00001	±	0.00001	1.77E-16	108.26%	1.78508	19.14	±	3.27
5.8	0.06411	±	0.00093	0.03604	±	0.00011	0.00044	±	0.00002	-0.00006	±	0.00006	0.00001	±	0.00002	4.49E-16	93.57%	1.66439	17.85	±	1.36
6	0.15251	±	0.00083	0.08765	±	0.00028	0.00114	±	0.00003	-0.00010	±	0.00007	0.00006	±	0.00002	1.07E-15	87.46%	1.52188	16.33	±	0.62
7	0.27662	±	0.00083	0.16252	±	0.00042	0.00218	±	0.00004	-0.00006	±	0.00007	0.00012	±	0.00002	1.94E-15	86.79%	1.47719	15.85	±	0.31
8	0.14993	±	0.00078	0.08558	±	0.00021	0.00121	±	0.00003	0.00010	±	0.00004	0.00010	±	0.00001	1.05E-15	80.37%	1.40806	15.11	±	0.52
9	0.20173	±	0.00085	0.11537	±	0.00036	0.00159	±	0.00004	0.00013	±	0.00007	0.00011	±	0.00001	1.41E-15	84.56%	1.47863	15.87	±	0.40
10	0.00465	±	0.00102	0.00268	±	0.00010	0.00005	±	0.00003	0.00001	±	0.00007	-0.00005	±	0.00002	3.26E-17	447.47%	1.73626	18.62	±	26.69
11	0.00325	±	0.00105	0.00135	±	0.00007	0.00000	±	0.00003	-0.00001	±	0.00005	0.00001	±	0.00001	2.28E-17	-31.87%	-0.76645	-8.28	±	-35.72
13	0.00581	±	0.00099	0.00285	±	0.00007	0.00003	±	0.00003	0.00001	±	0.00006	0.00001	±	0.00001	4.07E-17	64.18%	1.30546	14.02	±	14.63
15	0.00046	±	0.00104	0.00013	±	0.00008	-0.00006	±	0.00002	-0.00012	±	0.00006	0.00002	±	0.00001	3.21E-18	-10.8	-38.5397	-472.08	±	-491.99
16	0.00223	±	0.00106	0.00024	±	0.00008	-0.00004	±	0.00003	-0.00006	±	0.00004	0.00001	±	0.00001	1.57E-17	-86.10%	-7.94917	-87.77	±	-192.02

au20.5b.kfs, WE-4-10, CMT067 SCTF Analyses																								
%P	40Ar V			39Ar V			38Ar V			37Ar V			36Ar V			Moles 40Ar*	%Rad	R	Age (Ma)		
16	11.52032	±	0.02461	4.43170	±	0.01180	0.06246	±	0.00030	0.00186	±	0.00005	0.01751	±	0.00012	8.07E-14	55.08%	1.43185	15.21	±	0.13
16	3.81668	±	0.01039	2.25947	±	0.00734	0.03040	±	0.00016	0.00009	±	0.00005	0.00165	±	0.00002	2.67E-14	87.20%	1.47302	15.64	±	0.08
16	3.26310	±	0.01011	1.61589	±	0.00584	0.02287	±	0.00036	0.00053	±	0.00005	0.00305	±	0.00003	2.29E-14	72.38%	1.46156	15.52	±	0.12
16	3.48965	±	0.01007	1.57694	±	0.00524	0.02210	±	0.00029	0.00029	±	0.00006	0.00396	±	0.00003	2.44E-14	66.43%	1.47015	15.61	±	0.12
16	2.78233	±	0.00688	1.45693	±	0.00435	0.01975	±	0.00011	0.00000	±	0.00007	0.00217	±	0.00003	1.95E-14	76.93%	1.46913	15.60	±	0.10
16	2.78233	±	0.00688	1.45693	±	0.00435	0.01975	±	0.00011	0.00000	±	0.00007	0.00217	±	0.00003	1.95E-14	76.93%	1.46913	15.60	±	0.10
16	3.78392	±	0.00505	1.12272	±	0.00129	0.01635	±	0.00011	0.00030	±	0.00006	0.00738	±	0.00005	2.65E-14	42.34%	1.42695	15.16	±	0.14
16	3.06595	±	0.00703	1.45919	±	0.00391	0.02017	±	0.00013	-0.00009	±	0.00008	0.00311	±	0.00002	2.15E-14	70.00%	1.47088	15.62	±	0.10
16	2.06386	±	0.00418	1.20750	±	0.00349	0.01613	±	0.00013	-0.00002	±	0.00005	0.00096	±	0.00002	1.45E-14	86.31%	1.47525	15.67	±	0.08
16	2.67496	±	0.00554	1.19321	±	0.00257	0.01637	±	0.00010	-0.00009	±	0.00006	0.00317	±	0.00003	1.87E-14	64.97%	1.45640	15.47	±	0.10
16	1.64270	±	0.00391	0.98458	±	0.00335	0.01329	±	0.00008	0.00002	±	0.00004	0.00063	±	0.00002	1.15E-14	88.72%	1.48031	15.72	±	0.10
16	8.88418	±	0.03085	5.16324	±	0.01892	0.06983	±	0.00024	0.00123	±	0.00011	0.00437	±	0.00003	6.22E-14	85.48%	1.47086	15.62	±	0.09

au20.5b.kfs, WE-4-10, CMT067 IH Analyses																								
%P	40Ar V			39Ar V			38Ar V			37Ar V			36Ar V			Moles 40Ar*	%Rad	R	Age (Ma)		
3.5	0.01928	±	0.00114	0.01159	±	0.00009	0.00012	±	0.00003	0.00005	±	0.00009	0.00004	±	0.00003	1.35E-16	45.30%	0.75379	8.02	±	8.63
4	0.89422	±	0.00199	0.58802	±	0.00170	0.00783	±	0.00005	-0.00008	±	0.00008	0.00017	±	0.00003	6.26E-15	94.30%	1.43403	15.23	±	0.17
4.5	3.03308	±	0.00347	1.78854	±	0.00209	0.02405	±	0.00010	0.00005	±	0.00004	0.00135	±	0.00004	2.12E-14	86.82%	1.47241	15.64	±	0.07
4.8	0.53873	±	0.00224	0.25734	±	0.00170	0.00348	±	0.00005	-0.00013	±	0.00008	0.00058	±	0.00002	3.77E-15	68.37%	1.43136	15.20	±	0.31
5	0.19458	±	0.00089	0.09839	±	0.00044	0.00133	±	0.00003	-0.00007	±	0.00004	0.00015	±	0.00002	1.36E-15	76.54%	1.51360	16.07	±	0.65
5.3	0.41028	±	0.00099	0.19841	±	0.00052	0.00265	±	0.00005	-0.00008	±	0.00005	0.00050	±	0.00004	2.87E-15	63.88%	1.32102	14.03	±	0.63
5.5	0.31480	±	0.00102	0.12031	±	0.00062	0.00164	±	0.00004	-0.00004	±	0.00010	0.00050	±	0.00003	2.20E-15	53.01%	1.38698	14.73	±	0.87
5.8	1.26478	±	0.00326	0.63315	±	0.00211	0.00865	±	0.00009	-0.00014	±	0.00006	0.00115	±	0.00003	8.86E-15	73.25%	1.46315	15.54	±	0.19
6	1.30526	±	0.00294	0.75900	±	0.00232	0.01033	±	0.00007	-0.00005	±	0.00005	0.00067	±	0.00003	9.14E-15	84.94%	1.46072	15.51	±	0.15
7	2.10109	±	0.00493	1.11510	±	0.00307	0.01524	±	0.00008	-0.00007	±	0.00006	0.00158	±	0.00003	1.47E-14	77.84%	1.46658	15.57	±	0.12
8	0.38811	±	0.00088	0.20040	±	0.00089	0.00270	±	0.00004	-0.00009	±	0.00006	0.00028	±	0.00002	2.72E-15	78.40%	1.51845	16.12	±	0.28
9	0.10012	±	0.00109	0.05063	±	0.00021	0.00064	±	0.00006	-0.00010	±	0.00005	0.00009	±	0.00002	7.01E-16	74.16%	1.46634	15.57	±	1.02
10	0.09770	±	0.00099	0.04909	±	0.00023	0.00064	±	0.00006	-0.00008	±	0.00004	0.00007	±	0.00001	6.84E-16	78.77%	1.56755	16.64	±	0.91
11	0.03695	±	0.00107	0.02004	±	0.00010	0.00024	±	0.00002	0.00003	±	0.00006	-0.00002	±	0.00002	2.59E-16	115.66%	1.84408	19.56	±	3.76
13	0.02778	±	0.00111	0.01356	±	0.00010	0.00016	±	0.00003	-0.00006	±	0.00007	-0.00002	±	0.00002	1.95E-16	115.99%	2.04744	21.71	±	3.70
15	0.00547	±	0.00112	0.00292	±	0.00010	0.00008	±	0.00003	0.00003	±	0.00006	0.00002	±	0.00002	3.83E-17	-24.33%	-0.45596	-4.87	±	-18.00
16	0.00799	±	0.00113	0.00363	±	0.00011	0.00004	±	0.00003	0.00003	±	0.00005	0.00002	±	0.00002	5.59E-17	35.08%	0.77184	8.21	±	14.87